UNIVERSITY OF ALBERTA

Rayleigh Backscattering Impact on Fiber Optic Transmission Systems

by

PING WAI WAN ©

A thesis submitted to the Faculty of Graduate Studies and Research in partial fulfillment of the requirements for the degree of DOCTOR OF PHILOSOPHY

Department of Electrical Engineering

Edmonton, Alberta
Fall 1996

National Library of Canada
Acquisitions and Bibliographic Services Branch
395 Wellington Street
Ottawa, Ontario
K1A 0N4

Bibliothèque nationale du Canada
Direction des acquisitions et des services bibliographiques
395, rue Wellington
Ottawa (Ontario)
K1A 0N4

Your file Votre référence

Our file Notre référence

The author has granted an irrevocable non-exclusive licence allowing the National Library of Canada to reproduce, loan, distribute or sell copies of his/her thesis by any means and in any form or format, making this thesis available to interested persons.

The author retains ownership of the copyright in his/her thesis. Neither the thesis nor substantial extracts from it may be printed or otherwise reproduced without his/her permission.

L'auteur a accordé une licence irrévocable et non exclusive permettant à la Bibliothèque nationale du Canada de reproduire, prêter, distribuer ou vendre des copies de sa thèse de quelque manière et sous quelque forme que ce soit pour mettre des exemplaires de cette thèse à la disposition des personnes intéressées.

L'auteur conserve la propriété du droit d'auteur qui protège sa thèse. Ni la thèse ni des extraits substantiels de celle-ci ne doivent être imprimés ou autrement reproduits sans son autorisation.

ISBN 0-612-18125-1

Canada

UNIVERSITY OF ALBERTA
LIBRARY RELEASE FORM

NAME OF AUTHOR:	**Ping Wai Wan**
TITLE OF THESIS:	**Rayleigh Backscattering Impact on Fiber Optic Transmission Systems**
DEGREE:	**Doctor of Philosophy**
YEAR THIS DEGREE GRANTED:	**Fall 1996**

Permission is hereby granted to the University of Alberta Library to reproduce single copies of this thesis and to lend or sell such copies for private, scholarly, or scientific research purposes only.

The author reserves all other publication and other rights in association with the copyright in the thesis, and except as hereinbefore provided, neither the thesis nor any substantial portion thereof may be printed or otherwise reproduced in any material form whatever without the author's prior written permission.

1105 Hensen Close
Edmonton, Alberta, Canada
T6R 2M2

DATE: Aug. 29, 96

UNIVERSITY OF ALBERTA

FACULTY OF GRADUATE STUDIES AND RESEARCH

The undersigned certify that they have read, and recommend to the Faculty of Graduate Studies and Research for acceptance, a thesis entitled

"Rayleigh Backscattering on Fiber Optic Transmission Systems"

submitted by PING WAI WAN in partial fulfillment of the requirements for the degree of DOCTOR OF PHILOSOPHY.

Jan Conradi
Dr. Jan Conradi
Supervisor

Dave Irvine-Halliday
Dr. David Irvine-Halliday
U. of Calgary

Dr. Pawel Gburzynski
Comp. Sci.

Dr. Wayne Grover
Elec. Eng.

Jm McMullin
Dr. Jim McMullin
Elec. Eng.

DATE: August 28/96

DEDICATION

To my father, brothers and sisters,
for their love, encouragement and support.

In memory of my mother,
her love, patience and tenderness were unforgettable.

ABSTRACT

By modeling the Rayleigh scattering coefficient along the fiber as a circular complex Gaussian random variable, this dissertation derives a general and accurate expression which describes the intrinsic noise generated by Rayleigh backscattering. The expression is so general that it can be applied to systems with an arbitrary magnitude of source coherence. After experimental verification, this expression has been applied to directly and externally modulated cable television systems, which use Amplitude Modulated-Subcarrier Multiplexed (AM-SCM) format. In doing this the system performance in relation to fiber length, source coherence and number of optical amplifiers has been analyzed.

To avoid the amplified noise generated by Rayleigh backscattering in optically amplified Intensity Modulated-Direct Detection (IM-DD) digital systems, isolators can be placed in front and after the in-line amplifiers. However, isolators in the transmission link will restrict the direction to be one-way and therefore, it may not be the most cost-effective method to use in bi-directional transmission systems. This dissertation discusses various kinds of optically amplified bi-directional transmission configurations. In particular, a series of bi-directional transmission experiments have demonstrated that systems with a single link and no isolators show the greatest potential in minimizing the number of components in providing long distance bi-directional transmission.

Furthermore, a derivation of the power penalty expression due to both the effects of Rayleigh backscattering of the Amplified Spontaneous Emission (ASE) and the signal in optically amplified IM-DD digital systems, as well as its experimental verification, have been included. Using this expression a theoretical study of systems with a single link and no isolators has been performed. Finally, the theoretical study is extended to include systems utilizing high scattering fiber amplifiers, such as the Praseodymium-Doped Fluoride Fiber Amplifiers (PDFFAs) or distributed Erbium-Doped Fiber Amplifiers (EDFAs).

ACKNOWLEDGEMENTS

It is a great pleasure for me to express my sincere thanks to my supervisor Professor Dr. Jan Conradi for the guidance and excellent facilities that were provided throughout the course of this work. Furthermore, I would like to thank other members of my examining committee, Dr. Irvine-Halliday, Dr. Gburzynski, Dr. Grover and Dr. McMullin for reviewing and commenting this thesis.

I would like to acknowledge the technical support and advice of David Clegg and Jason Lamont. Without their help, this project would surely take another year to finish. Dean Michaels is also thanked for his computer help, particularly for the time he spent on networking my PC.

I wish to thank my colleagues at *TRL*abs for their companion and useful discussions during this work, particularly Sheldon Walkin, Mike Sieben, Dave Moore, Rainer Iraschko, Ashish Duggal, Danny Li, Danial Sze, Vipul Rawat and Demetrious Stamatelakis. In addition, ex-colleagues, such as Dobby Lam, Steve Lai, Tom Young, Ben Chan, Jeremy Sewall, Caroline Delisle and Yimin Hua are thanked for frequent discussions in many areas. In particular, Tom Young, Dave Moore, Steve Lai, Ben Chan, Rainer Iraschko, Sheldon Walkin, Dean Michaels and Mike Sieben are also thanked for numerous hours on playing poker and bridge with me.

I would like to thank every member in my family and Dominica Cheng for their encouragement and endurance.

For financial assistance, I am indebted to the Natural Sciences and Engineering Research Council of Canada, Bell-Northern Research, and TR*Labs* for supporting this work through the NSERC/BNR/TR*Labs* Industrial Chair in Fiber Optic Communications at the University of Alberta.

TABLE OF CONTENTS

CHAPTER 1 INTRODUCTION 1

1.1. PREVIOUS RESEARCH ON RAYLEIGH BACKSCATTERING 1

1.2. OBJECTIVES AND ORGANIZATION 3

1.2.1. Organization of the Dissertation 4

CHAPTER 2 DRB NOISE THEORY 6

2.1. DRB NOISE INTENSITY 7

2.2. AUTOCORRELATIONS OF DRB NOISE INTENSITY 11

2.3. DEPOLARIZATION AND SPECTRAL DENSITY OF DRB NOISE 17

CHAPTER 3 DRB NOISE IN AM-SCM SYSTEMS 19

3.1. OVERVIEW OF CATV SYSTEMS 19

3.1.1. Architecture 19

3.1.2. CATV Signal Format 22

3.1.2.1. Non-Uniform DRB Noise Spectrum in CNR Calculations 25

3.1.3. Operating Windows 25

3.2. EXPERIMENTAL VERIFICATION 26

3.2.1. Source Electric Field of General AM-SCM Signal 26

3.2.2. Experimental Setup 28

3.2.3. Spectrum of the DRB Noise 30

3.2.4. Fiber Length Dependence of DRB Noise 33

3.3. DRB NOISE IN AM-SCM SYSTEMS 34

3.3.1. Large Chirping in Directly Modulated Systems 34

3.3.1.1. Comparison of DRB Noise in 1310 nm and 1550 nm Systems 40

3.3.1.2. Reduction of DRB Impact by Putting Isolators in Link 41

3.3.1.3. Spectrum of DRB noise 43

3.3.1.4. Carrier to Noise Ratio Degradation 47

3.3.1.4.1. Systems without Optical Amplifiers 47

3.3.1.4.2. Systems Utilizing Optical Amplifiers 55
3.3.1.4.2.1. Noises of Optical Amplifiers 56
3.3.1.4.2.2. CNR Degradation 58
3.3.2. Chirpless External Modulation Systems 62
3.3.2.1. Carrier to Noise Ratio Degradation 68
3.3.2.1.1. Systems without Optical Amplifiers 68
3.3.2.1.2. Non-Uniform Modulation Indices 75
3.3.2.1.3. Systems Utilizing Optical Amplifiers 77
CHAPTER 4 DRB NOISE IN DIGITAL IM-DD SYSTEMS 80
4.1. DERIVATION OF POWER PENALTY 82
4.1.1. DRB Noise of Signal 82
4.1.1.1. Single In-Line Optical Amplifier 82
4.1.1.2. Open Cascade of Optical Amplifiers 85
4.1.2. Increase in ASE 89
4.1.2.1. Total Direct Traveling ASE Power 89
4.1.2.2. Added ASE due to SRB 90
4.1.2.3. Added ASE due to DRB 93
4.1.2.4. Added ASE due to SRB and DRB 95
4.1.3. Noise Analysis 96
4.2. EXAMINATION OF OPEN CASCADE SYSTEMS 100
4.2.1. Power Penalty 100
4.2.2. Total Amplifier Gain 103
4.2.3. End-To-End Bit Error Ratio 105
4.3. EXPERIMENTAL VERIFICATION 109
4.3.1. Experimental Setup 109
4.3.1.1. Optical Transmitter 109
4.3.1.2. Optical Receiver 111
4.3.2. Receiver Sensitivity Measurement 112
4.3.3. Receiver Power Penalty Measurements 117

4.3.3.1. Single In-line EDFA 119
4.3.3.1.1. Approximation to Extinction Ratio 122
4.3.3.1.2. Theoretical and Experimental Comparison 124
4.3.3.1.3. Reduced Extinction Ratio 125
4.3.3.1.4. Discussion of These Experiments 128
4.3.3.2. Multiple In-line EDFAs 129
4.3.3.2.1. Two In-line EDFAs 129
4.3.3.2.2. Three In-line EDFAs 134
4.3.3.2.3. Discussion of These Multiple In-line EDFA Experiments 139
4.3.4. End-to-End BER Measurement 140
4.3.5. Experiment Summary 144
4.4. BI-DIRECTIONAL TRANSMISSION 144
4.4.1. Types of Bi-directional Transmission Systems 145
4.4.1.1. Two Fiber link Bi-directional 145
4.4.1.2. One Fiber Link with Bi-directional Amplifiers 145
4.4.2 Bi-directional Transmission Experiments 151
4.4.2.1. Experimental Arrangement 151
4.4.2.2. Experimental Results 154
4.5. IMPACT BY INTERNAL AMPLIFIER RAYLEIGH BACKSCATTERING 156
4.5.1. Penalty Derivation due to Internal DRB 157
4.5.2. Theoretical Results 161
CHAPTER 5 CONCLUSIONS 165
5.1. SUMMARY OF THE RESULTS ON ANALOG SYSTEMS 165
5.2. SUMMARY OF RESULTS ON DIGITAL SYSTEMS 166
5.3. FUTURE RESEARCH 167
APPENDIX A: DERIVATION OF EQN. (2.22) 176
APPENDIX B: PARAMETER MEASUREMENTS 177
B.1. Rayleigh Backscattering Reflectance 177

B.2. Laser Linewidth Measurement 178
B.3. Laser Chirp Measurement 180
APPENDIX C: DERIVATION OF EQN. (3.14) 184
APPENDIX D: DETERMINATION OF THE WORST CNR CHANNEL 186
APPENDIX E: ACCOUNT FOR THE SIGNAL DEPENDENCE 188
APPENDIX F: DERIVATION OF THE POWER PENALTY 190

LIST OF TABLES

Table 3.1: Parameters involved in the experiments and calculations. 30

Table 3.2: Summary of fibers used in the experiments..33

Table 3.3: Parameters involved in the CNR calculations. 50

Table 4.1: List of parameter values used in the calculation of the BER. 108

Table 4.2: Summary of fibers used in the experiments...119

Table 4.3: 1 in-line EDFA measurement results. 121

Table 4.4: The modification and parameters involved in the calculation of the penalty...125

Table 4.5: 1 in-line EDFA measurement results for the signal with a smaller eye opening..127

Table 4.6. Measurement results for the 2 in-line EDFA configuration. 133

Table 4.7: Measurement results for the 3 in-line EDFA configuration. 138

Table 4.8: Parameters involved in the experiment and theoretical calculation. 143

Table 4.9: Link budgets and component counts for various bi-directional system configurations...156

LIST OF FIGURES

Figure 2.1: A simple DRB illustration 7

Figure 3.1: Tree-and-branch architecture of a typical CATV network 20

Figure 3.2: A basic HFC design 21

Figure 3.3: Spectrum of a subcarrier multiplexed AM-VSB signal 22

Figure 3.4: Magnitude spectra of a received TV channel before and after VSB filtering in receivers 23

Figure 3.5: Laser optical output power and diode current characteristic 27

Figure 3.6: Experimental setup for measuring DRB noise 29

Figure 3.7: DRB RIN for various small total rms modulation indices 32

Figure 3.8: The measured and calculated DRB RIN at 10 MHz and 25 MHz for various fiber lengths 34

Figure 3.9: The ratio of the DRB noises in 1310 nm to that in 1550 nm systems 41

Figure 3.10: Transmission links: without and with isolators 42

Figure 3.11: DRB noise reduction for 1310 nm and 1550 nm systems with the use of isolators 43

Figure 3.12: Calculated RIN of DRB generated from a 50 km long fiber in 1550 nm system using general expression and Gaussian approximation 44

Figure 3.13: DRB RIN versus fiber length for various chirping efficiencies in 1310 nm and 1550 nm systems 47

Figure 3.14: A simple CATV transmission 48

Figure 3.15: CNR for different received powers in 1310 and 1550 nm systems 51

Figure 3.16: CNR of channel 2 versus fiber length for different received powers in 1310 nm and 1550 nm systems 53

Figure 3.17: CNR of channel 2 in 1310 nm and 1550 nm systems versus chirping efficiency 55

Figure 3.18: A simple CATV system diagram utilizing optical amplifiers 56

Figure 3.19: Doubly amplified DRB 56

Figure 3.20: CNR versus fiber length in 1310 nm and 1550 nm systems utilizing optical amplifiers 62

Figure 3.21: A series of Lorentzian-shaped noise spectra at DC and carrier frequencies contributing to the overall DRB noise spectrum 65

Figure 3.22: Theoretical DRB RIN for a 50 km long 1550 nm CATV system, R_{Rb} = -33.2 dB and 250 MHz, 14 MHz, 1 MHz and 100 kHz laser linewidths 67

Figure 3.23: Channel CNR for 1310 nm and 1550 nm externally modulated systems with 1 MHz intrinsic laser linewidth and various received powers 70

Figure 3.24: Channel CNR for 1310 nm and 1550 nm externally modulated systems with 14 MHz intrinsic laser linewidth and various received powers 71

Figure 3.25: Channel CNR for 1310 nm and 1550 nm externally modulated systems with 250 MHz intrinsic laser linewidth and various received powers 72

Figure 3.26: CNRs in 1310 nm and 1550 nm systems versus intrinsic laser linewidth. The channels used for calculation are 2, 12, 22, 32 and 42 74

Figure 3.27: CNR values before and after the non-uniform modulation indices. Also listed are the modulation indices used for obtaining a uniform 76

Figure 3.28: CNR values before and after the non-uniform modulation indices and 0.7 dB increase in optical received power have been applied. Also listed are the modulation indices used for retaining 50 dB CNR 77

Figure 3.29: CNR in channel 2 versus fiber length in 1310 nm and 1550 nm systems utilizing optical amplifiers 79

Figure 4.1: DRB of signal in a system using 1 in-line amplifier and no isolators in link 80

Figure 4.2: SRB and DRB of ASE in a system using 1 in-line amplifier and no isolators in link: SRB of ASE and DRB of ASE 81

Figure 4.3: Different DRB mechanisms in a single in-line amplifier system without using isolators 83

Figure 4.4: Comparison of the contributions due to the three different mechanisms of DRB of a signal in a single in-line amplifier link 85

Figure 4.5: An open cascade system with *N* identical in-line amplifiers and *N*+1 interconnecting fibers 86

Figure 4.6: DRB signal which travels around one amplifier 86

Figure 4.7: DRB signal which travels around two amplifiers 87

Figure 4.8: DRB signal which travels around three amplifiers 87

Figure 4.9: An open cascade of *N* amplifiers showing all the contributions to the direct ASE power at the receiver 90

Figure 4.10: SRB ASE event in a transmission link with one in-line amplifier....... 92

Figure 4.11: All SRB ASE events in a transmission link with two in-line amplifiers....... 92

Figure 4.12: All SRB ASE events in a transmission link with three in-line amplifiers.....92

Figure 4.13: All DRB ASE events in a 3 in-line amplifier transmission link 95

Figure 4.14: Power penalty versus number of amplifiers in an open cascade with $G = 1/IL = 17$ dB, BER=10^{-14}, R_{Rb}=-33 dB and $d = 10$............................101

Figure 4.15: Power penalty versus number of amplifiers in an open cascade with $G\ IL = 0.5$, BER=10^{-14}, $G = 17$ dB, R_{Rb}=-33 dB and $d = 10$....................102

Figure 4.16: Total amplifier gain versus number of amplifiers in link with $G\ IL = 1$. The calculations utilize BER = 10^{-14}, R_{Rb} = -33 dB $d = 10$ and the penalty as a parameter 104

Figure 4.17: Total amplifier gain versus number of amplifiers in link with $G\ IL = 0.5$. The calculations utilize BER = 10^{-14}, R_{Rb} = -33 dB, $d = 10$ and the penalty as a parameter 105

Figure 4.18: BER versus gain-loss product for the system using a cascade of 8 amplifiers, with and without Rayleigh backscattering for interamplifier losses: 14, 17 and 20 dB 108

Figure 4.19: Block diagram of the optical transmitter used in the experiment..............111

Figure 4.20: Block diagram of the optical receiver used in the experiment 112

Figure 4.21: Back to back configuration for the receiver sensitivity 114

Figure 4.22: Averaged eye diagram of the signal 114

Figure 4.23: Component ISI measurement configuration 115

Figure 4.24: Eye diagram for the K&L 2.5 GHz LPF 115

Figure 4.25: Eye diagram for the Veritech amplifier...116

Figure 4.26: Eye diagram for the Mini-Circuit Amplifier...116

Figure 4.27: Sensitivities of the receivers with and without the EDFA 117

Figure 4.28: An EDFA unit with gain measurement capability 118

Figure 4.29: The configuration for 1 in-line EDFA experiment 120

Figure 4.30: Optical signal power levels during spaces and marks...............................123

Figure 4.31: An optical receiver 123

Figure 4.32: Eye diagram for 1 in-line EDFA experiment 124

Figure 4.33: The experimental and theoretical penalties versus the in-line EDFA gain..125

Figure 4.34: Eye of the received signal after adjusting the bias slightly........................126

Figure 4.35: Experimental and theoretical power penalties for the signal with a smaller eye opening 127

Figure 4.36: Both the experimental and theoretical results for the two extinction ratios 129
Figure 4.37: Configuration for 2 in-line EDFA experiment 132
Figure 4.38: Eye diagram of the received signal in the 2 in-line EDFA experiment 133
Figure 4.39: Experimental and theoretical results for the 2 in-line EDFA experiment .. 134
Figure 4.40: Configuration for the 3 in-line EDFA experiment 137
Figure 4.41: Eye diagram of the received signal in the 3 in-line EDFA experiment 138
Figure 4.42: Experimental and theoretical results for the 3 in-line EDFA experiment .. 139
Figure 4.43: Both the experimental and theoretical results for the 1, 2 and 3 in-line amplifier configurations 140
Figure 4.44: Experimental BER on 3 in-line EDFA open cascade systems 142
Figure 4.45: Experimental BER on 3 in-line EDFA systems with isolators 143
Figure 4.46: Conventional 2 fiber link bi-directional system with isolators in each link 145
Figure 4.47: 1 fiber link bi-directional system employing bi-directional amplifiers 146
Figure 4.48: Configuration of a bi-directional amplifier using 2 amplifiers, 2 circulators and 2 BPFs at the signal wavelengths 147
Figure 4.49: Configuration of a bi-directional amplifier using 2 amplifiers, 2 WDMs operating at the signal wavelengths and 4 isolators 148
Figure 4.50: Configuration of a bi-directional amplifier using 2 amplifiers, and 2 directional WDMs operating at the signal wavelengths 149
Figure 4.51: Configuration of a bi-directional amplifier using 1 amplifier, and 4 directional WDM devices 150
Figure 4.52: Single fiber link bi-directional transmission system employing open cascade amplifiers 150
Figure 4.53: Full duplex bi-directional transmission with a single fiber link and 3 in-line EDFAs 153
Figure 4.54: Bi-directional transmission using 2 links and 4 in-line EDFAs 153
Figure 4.55: BERs of the different links as a function of the link budget for the 1543 nm and 1541 nm transmitters 155
Figure 4.56: Double Rayleigh backscattering of a signal induced inside an optical fiber amplifier 157
Figure 4.57. Power penalty against number of lumped amplifiers for a BER of 10^{-14}, NA of 0.2 and with the Rayleigh scattering loss coefficient as a parameter 162

Figure 4.58: Power penalty against number of lumped amplifiers for a BER of 10^{-14}, NA of 0.4 and with the Rayleigh scattering loss coefficient as a parameter 163

Figure 4.59: Isolator spacing against transmission length for a distributed EDFA system with a BER of 10^{-14}, 1 dB power penalty and two values of Rayleigh backscattering coefficient 164

Figure 4.60: Penalty against isolator spacing for a 9000 km distributed EDFA system with a BER of 10^{-14} and two values of Rayleigh backscattering coefficient 164

LIST OF ABBREVIATIONS

AC	Alternating Current
Amp	Amplifier
AM-SCM	Amplitude Modulated-Subcarrier Multiplexed
APC	Angled-facet Physical Contact
AT&T	American Telegraph and Telephone
ASE	Amplified Spontaneous Emission
BER	Bit Error Ratio
BPF	Bandpass Filter
BNR	Bell-Northern Research
BW	Bandwidth
CATV	Cable Television
CCG	Circular Complex Gaussian
Ch	Channel
CNR	Carrier to Noise Ratio
CSO	Composite Second Order
CTB	Composite Triple Beat
CW	Continuous Wave
dB	Decibel
dBc	Decibel with respect to the Carrier
dBm	Decibel with respect to 1 mW
DC	Direct Current
DFB	Distributed Feedback
DOP	Degree of Polarization
DRB	Double Rayleigh Backscattering
EDF	Erbium-Doped Fiber
EDFA	Erbium-Doped Fiber Amplifier
FM	Frequency Modulation
GPIB	General Purpose Interface Bus
HFC	Hybrid Fiber/Coax
HP	Hewlett Packard
IM-DD	Intensity Modulated-Direct Detection
ISI	Intersymbol Interference

LPF	Lowpass Filter
M. Sc.	Master of Science
NA	Numerical Aperture
NBFM	Narrow Band Frequency Modulation
NRZ	Non Return to Zero
OC	Optical Carrier
PDFFA	Praseodymium-Doped Fluoride Fiber Amplifier
Ph. D.	Doctor of Philosophy
PRBS	Pseudo-Random Bit Sequence
Q	Personick's Q Factor
RB	Rayleigh Backscattering
RF	Radio Frequency
RIN	Relative Intensity Noise
rms	Root-Mean-Square
RX	Receiver
SCM	Subcarrier Multiplexed
SNR	Signal to Noise Ratio
SOP	State of Polarization
SRB	Single Rayleigh Backscattering
TV	Television
TR*Labs*	Telecommunications Research Laboratories
TX	Transmitter
VCR	Video Cassette Recorder
VOA	Variable Optical Attenuator
WDM	Wavelength Division Multiplexer
WBFM	Wide Band Frequency Modulation

LIST OF SYMBOLS

$\langle\cdot\rangle$	ensemble average
$\overline{\cdot}$	time average
$*$	complex conjugate
$\otimes$	convolution
$\delta(\cdot)$	the Delta function
$\mathrm{erf}(\cdot)$	the Error function
$\mathrm{Re}[\cdot]$	real part
$\Im[\cdot]$	Fourier transform
A_{eff}	effective area of optical fiber core
α	total intensity attenuation coefficient
α_s	intensity coefficient due to RB
B_e	electrical noise equivalent bandwidth in CATV channel
B_o	receiver optical noise equivalent bandwidth
B_{re}	electrical noise equivalent bandwidth in IM-DD receiver
β	propagation constant
CNR_i	CNR in channel i
D	receiver optimal decision threshold
D_{RB}	receiver optimal decision threshold including RB impact
d	extinction ratio
δP	increase in received power
ΔP	receiver power penalty (dB)
ΔP_{lump}	receiver power penalty due to DRB inside lump amplifier
ΔP_{dist}	receiver power penalty due to DRB inside distributed amplifier
ΔR_{RB_n}	RB reflectance in n^{th} section of fiber
$\Delta \nu$	intrinsic laser linewidth

ΔN	ratio between DRB noises in 1310 nm to 1550 nm
$\Delta\rho_n$	differential RB function in n^{th} section of fiber
Δl	length of fiber sections
$e(t)$	electrical source field
$\varepsilon_s(t)$	complex amplitude of source field
$\varepsilon_{dir}(t,L)$	complex amplitude of directly traveling field at L
$\varepsilon_{DRB}(t,L)$	complex amplitude of total doubly backscattered field at L
f_o	optical frequency
f_i	subcarrier frequency of channel i
f_u	highest CATV channel frequency
f_{inst}	instantaneous frequency
$\phi(t)$	intrinsic laser phase noise
G	gain of optical amplifier
g_{RF}	voltage gain of RF amplifier
$g(z)$	gain coefficient
g_o	average gain coefficient
γ	chirping efficiency
$h\nu$	photon energy
I_p	bias current minus threshold current
$I(t)$	optical intensity
$I_{DRB}(t)$	DRB noise optical intensity
IL	interamplifier loss
I_{DC}	DC current
i_{th}	thermal noise current
i_{shot}	shot noise current
i_{laser}	noise current due to intrinsic laser RIN
i_{sig_sp}	noise current due to signal and ASE beating
$i_{sig\_sp,1}$	noise current due to signal and ASE beating during a mark
$i_{sig\_sp,0}$	noise current due to signal and ASE beating during a space

i_{sp_sp}	noise current due to ASE and ASE beating
$i_{DRB,i}$	DRB induced noise current in channel i
$i_{DRB,i,j}$	DRB induced noise current in channel i generated from j^{th} fiber section
$i_{DRB}^2(f)$	DRB induced square noise current spectral density
$i_{DRB,iso}^2(f)$	DRB induced square noise current spectral density with isolators surrounding in-line amplifiers
$i_{DRB,lump}$	DRB induced noise current from lumped amplifier
$i_{DRB,dist}$	DRB induced noise current from distributed amplifier
L	length of fiber
L_b	fiber length between transmitter and in-line optical amplifier
L_a	fiber length between in-line optical amplifier and receiver
L_s	fiber length between in-line optical amplifiers, or length of isolated distributed fiber
L_l	total length of lumped or distributed amplifier
λ_1	upstream signal wavelength
λ_2	downstream signal wavelength
M	number of optical amplifiers or isolators in AM-SCM system
$m(t)$	AM-SCM modulating signal
m_i	peak modulation index in channel i
μ	rms modulation index
N_{sc}	number of scattering partitions
N_{ch}	number of CATV channels
N	number of in-line optical amplifiers in digital system
N_r	DRB noise reduction
NA	numerical aperture
n_1	refractive index of core
n_2	refractive index of cladding
n_t	polarization state parameter

n_{sp}	spontaneous emission factor of an optical amplifier
$n_{sp,tot}$	effective spontaneous emission factor of a chain of optical amplifiers
P_{re}	average optical power
P_{tx}	transmitter launched power
P_1	directly traveling optical power during a mark
P_0	directly traveling optical power during a space
$P_{dir}(t,L_l)$	directly traveling optical power at output of amplifier
P_{ASE}	ASE power of in-line optical amplifier
$P_{ASE,dir}$	directly traveling ASE power at receiver
$P_{ASE,re}$	total ASE power at receiver
$P_{ASE,DRB}$	ASE generated by DRB at receiver
$P_{ASE,SRB}$	ASE generated by SRB at receiver
$P_{ASE,RB}$	ASE generated by both SRB and DRB at receiver
$P_{DRB}(f)$	DRB noise intensity spectral density
Q	Personick's Q factor
q	electronic charge
θ_i	initial phase of signal in channel *i*
RIN_{sig_sp}	RIN due to signal-ASE beating
RIN_{DRB}	RIN due to DRB noise
RIN_{laser}	intrinsic laser RIN
$R_{I_{DRB}}(\tau)$	time-autocorrelation function of DRB noise intensity
$R_{\varepsilon_{dir}}(\tau)$	time-autocorrelation function of complex amplitude of directly traveling field
R_{Rb}	Rayleigh backscattering reflectance for a infinitely long fiber
$R_{Rb,1310}$	RB reflectance at 1310 nm
$R_{Rb,1550}$	RB reflectance at 1550 nm
R	effective input impedance of RF amplifier
$\Re$	responsivity
S	recapture factor

σ_f	standard deviation of heavily chirped DRB noise spectrum
σ_0^2	total square noise current at receiver during a space
σ_1^2	total square noise current at receiver during a mark
$\sigma_{0,RB}^2$	total square noise current at receiver during a space including RB impact
$\sigma_{1,RB}^2$	total square noise current at receiver during a mark including RB impact
Δt	short period of time
v	group velocity
$V_{p\text{-}p}$	peak-to-peak voltage

Chapter 1

INTRODUCTION

Over the past 30 years, fiber optic communication has evolved from a fundamental laboratory research idea to a proven technology that is used to transmit data, voice and video on a commercial basis. The inherent advantages of using optical fibers over conventional copper wires arise from the properties of optical fiber, such as low loss, vast bandwidth, small size, light weight, immunity to interference, electrical isolation, low cost and an abundance of raw materials in nature. Furthermore, with the advent of fiber amplifiers and wavelength division multiplexing technology, fiber optic technology has advanced to the point where both local loop and transoceanic transmission systems are economically and technically justified. Nevertheless, to implement the most cost-effective systems, apart from taking physical convenience and upgradeability into consideration, it is essential to recognize and understand system intrinsic noises. Rayleigh backscattering generated by fibers is one of these intrinsic noise sources, and this thesis is devoted to theorizing and exploring the impact of Rayleigh backscattering on various fiber optic systems.

1.1. Previous Research on Rayleigh Backscattering

It is known that signals which are multiply reflected, whether by discrete reflections from two or more splices or connectors or by Double Rayleigh Backscattering (DRB), will convert the laser phase noise to amplitude noise through the interference of the backreflected signal with the original signal. This generates one of the fundamental noise sources in fiber optic transmission systems [1-13]. The spectrum of this noise has been calculated for various special cases. For example, if the optical source is unmodulated and the reflections are discrete or undergo Rayleigh backscattering, the noise spectrum assumes the original Lorentzian lineshape of the source laser [1], with a spectral width which is double that of the laser.

Also, Darcie *et al.* [6] and Yonetani *et al.* [12] have shown that if the laser is strongly chirped through direct modulation, the original Lorentzian spectrum is broadened considerably, assuming a Gaussian shape. According to their finding, this broad spectrum has the effect of spreading out the laser phase noise, thereby reducing the noise impact of this multiple reflection on a system. However, if an optical amplifier is positioned between two reflecting sites, one on either side of the amplifier, the reflected signal is doubly amplified [5,11,13], the system impact of this noise can be quite severe. This is independent of whether the reflecting sites are discrete or continuous in the form of the Rayleigh backscattering from fibers. If the amplifier is surrounded by optical isolators, this impact can be substantially reduced.

Gysel and Staubli [14-16] have shown that the interferometric noise power spectral density generated by a singly Rayleigh scattered signal can be determined through the scattering properties of the fiber and the autocorrelation function of the signal electric field. Thus, this method is particularly powerful in that the noise power across the electrical spectrum of the information signal can be determined. Recently, Atlas *et al.* [13] determined the DRB noise impact on an Amplitude Modulated-Subcarrier Multiplexed (AM-SCM) system using a zero chirp external modulator. Their analysis is very similar to the one developed in this thesis, even though both investigations were undertaken independently.

In addition to the aforesaid research on Rayleigh backscatter noise, much research work has been done on other Rayleigh backscatter-related phenomena. One popular example is optical time domain reflectometry, which has been widely employed both in the laboratory and the field to non-destructively measure the spatial dependence of the optical fiber attenuation, splice and connector loss, and fault location. It has also been demonstrated that using the spatial dependence of the polarization state of the Rayleigh backscattered light, optical fibers can be uniquely identified [17]. This method can be used to remotely update the wiring database of an optical fiber network.

Moreover, linewidth reduction and lasing wavelength hopping for a distributed feedback laser diode which is exposed to Rayleigh backscattered light from a single-mode fiber has been investigated [18-19]. Furthermore, it has been shown [20-21] that Rayleigh backscattering within an erbium-doped fiber amplifier imposes an upper limit on its gain and performance.

1.2. Objectives and Organization

Even though extensive research has been done on Rayleigh backscattering, there are still many issues which need to be addressed so that many systems can be implemented cost-effectively. For instance, with isolators surrounding the in-line fiber amplifier to avoid RB, bi-directional transmission requires the use of two separate fiber links, with each carrying signals in one direction, or additional components must be used. That means extra cost and an increase in system complexity in comparison to systems that transmit bi-directionally using no isolators and only one fiber link, with different wavelengths carrying signals in opposite directions. Therefore, one of the main objectives of this work is to investigate how far we can "push" the one fiber link bi-directional transmission in practice before RB will seriously degrade and limit transmission performance.

To achieve this, we first need to derive a general expression which specifies the noise generated by DRB for systems with an arbitrary amount of source coherence and with many in-line amplifiers. As mentioned previously, such an expression was not previously available. Furthermore, since analog transmission is extremely vulnerable to noise, RB impact could play an important role in designing such systems. Therefore, another goal of this work is to study the negative impact of RB on analog transmission systems.

With the intention of providing a better understanding and characterization of RB effects on various forms of transmission systems, the author has constructed several key research objectives for this dissertation:

1) derive a general and accurate expression describing the noise due to RB, including the effect of source phase modulation of arbitrary magnitude.
2) experimentally verify the expression using a source with various amounts of phase modulation.
3) apply the expression to various analog and digital transmission systems to analyze their performance in the presence of RB.
4) investigate digital receiver sensitivity degradation due to RB of the Amplified Spontaneous Emission (ASE) from in-line amplifiers.
5) investigate the impact on systems of the RB that can take place within fiber amplifiers with high scattering coefficients.
6) experimentally demonstrate the feasibility of bi-directional systems using 1 fiber link and no isolators, and compare such systems to conventional 2 fiber link systems.

1.2.1. Organization of the Dissertation

The rest of the dissertation is structured as follows:

- **Chapter 2** presents for the first time a general and accurate analytical expression describing the spectral density of the DRB noise at a receiver in terms of the scattering properties of the fiber and the autocorrelation of the signal electric field. Incorporated into the theory is the effect of Rayleigh scattering induced depolarization and the consequent reduction of DRB noise. This expression has proven most general and useful for the remainder of the text.
- **Chapter 3** discusses the impact of DRB noise on analog systems. It first presents the experimental verification for the general DRB noise expression. This verification is done in a directly modulated AM-SCM system with various amounts of chirp. Then, for easy usage, the expression is simplified for directly modulated AM-SCM systems. In doing this a large amount of chirp has been assumed, a good assumption for directly modulated AM-SCM laser diodes. Using this simplified expression, directly modulated AM-SCM systems with and without the use of optical amplifiers, are

analyzed in the presence of DRB noise. For systems using chirpless external modulators, the general expression is simplified again. This simplified expression is then applied to analyze the performance of systems using chirpless external modulators, with and without optical amplifiers.

- **Chapter 4** derives a receiver power penalty expression which accounts for both the impact of DRB noise and RB of ASE from in-line amplifiers, for optically amplified Intensity Modulated-Direct Detection (IM-DD) digital systems. Using this receiver power penalty expression the system gain budget for systems without isolators in links is studied and the validity of the expression is subsequently experimentally confirmed. Also, bi-directional transmission experiments using conventional 2 fiber link configurations with the use of isolators, as well as single fiber link configurations without the use of isolators are conducted and their results are compared. Finally, the DRB effects inside the fiber amplifiers are also addressed and quantified in terms of the power penalty.
- **Chapter 5** summarizes and concludes this work, and also projects the direction for future research.

Chapter 2

DRB NOISE THEORY

Light propagating along an optical fiber is attenuated due to the combined effects of intrinsic and extrinsic absorption and Rayleigh scattering. Extrinsic absorption results from impurity atoms in the glass material, whereas intrinsic absorption occurs due to the basic constituent atoms of fiber material. Rayleigh scattering results from small scale fluctuations in the refractive index of the fiber due to density and composition variations frozen into the fiber during manufacturing. In modern fibers the loss due to extrinsic absorption has been reduced to a level that is negligible compared to the loss from Rayleigh scattering at the wavelengths used in conventional lightwave transmission systems, thereby leaving the intrinsic absorption and Rayleigh scattering the most dominant intrinsic loss mechanisms [22-23].

In the electric field domain, the signal optical field traveling along an optical fiber is continuously scattered in all directions. The forward scattered field propagates as the signal [24]. A fraction of the backscattered field is scattered within the numerical aperture of the fiber, is recaptured and then travels in the backward direction. This constitutes the Rayleigh backscattered field. This backscattered field can undergo backscattering again. This process is termed Double Rayleigh Backscattering (DRB), and this doubly backscattered field, which travels with the forward propagating signal, beats with the signal field at the receiver, generates DRB relative intensity noise and thus increases the noise level at the receiver. In the rest of this chapter, the primary emphasis is on the fiber scattering model and the derivation of general expressions describing the spectral density of this noise.

2.1. DRB Noise Intensity

Consider a linearly polarized electrical source field $e(t)$

$$e(t) = \mathrm{Re}[\varepsilon_s(t)e^{j2\pi f_o t}] \tag{2.1}$$

with optical carrier frequency f_o and complex amplitude $\varepsilon_s(t)$, which contains the inherent laser phase noise and electrical signal information in the forms of amplitude and/or angle modulation. Re[·] denotes the real part. For mathematical simplicity, we initially assume the state of polarization is preserved during transmission and backscattering along the single mode fiber, but this restriction will be removed later. To determine the total doubly Rayleigh backscattered field, we will partition the fiber into N_{sc} equal scatter sections of Δl along the fiber, and then add up, on a complex amplitude basis, each doubly Rayleigh backscattered field that is generated from two scatter sections along the transmission link as shown in Figure 2.1.

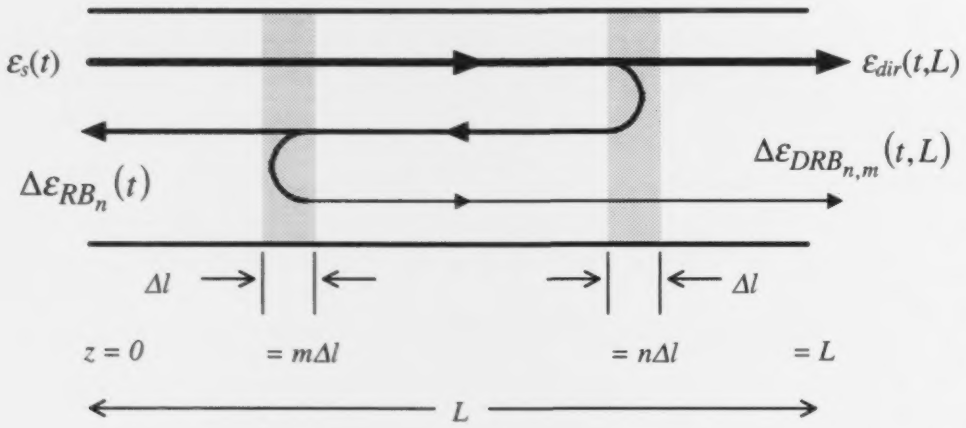
$\varepsilon_s(t)$
$\varepsilon_{dir}(t,L)$
$\Delta\varepsilon_{DRB_{n,m}}(t,L)$
$\Delta\varepsilon_{RB_n}(t)$
Δl
Δl
$z = 0$
$= m\Delta l$
$= n\Delta l$
$= L$
L

Figure 2.1: A simple DRB illustration.

The complex amplitude of the direct traveling field at location z along the link is given by

$$\varepsilon_{dir}(t,z) = \varepsilon_s\left(t - \frac{z}{v}\right)e^{-\left(\frac{\alpha}{2} + j\beta\right)z} \tag{2.2}$$

where v, α and β are the group velocity, total intensity attenuation coefficient and propagation constant. Then, the complex amplitude of the singly Rayleigh backscattered field from the n^{th} scatter section at location $z = n\Delta l$ can be expressed as

$$\Delta\varepsilon_{RB_n}(t) = \varepsilon_s\left(t - \frac{n\Delta l}{v}\right)e^{-\left(\frac{\alpha}{2} + j\beta\right)n\Delta l}\Delta\rho_n \tag{2.3}$$

The differential Rayleigh backscattering function $\Delta\rho_n$ describes the fraction of backscattered field due to Rayleigh backscattering in the n^{th} section of fiber at location $z = n\Delta l$ in relation to the forward traveling field. Also the backscattered optical intensity, defined by the magnitude-squared of the optical field, and the reflectance due to Rayleigh backscattering ΔR_{RB_n} in the n^{th} section of fiber are respectively given by

$$\left|\Delta\varepsilon_{RB_n}(t)\right|^2 = \left|\varepsilon_s\left(t - \frac{n\Delta l}{v}\right)e^{-\frac{\alpha}{2}n\Delta l}\right|^2 \left|\Delta\rho_n\right|^2 \tag{2.4}$$

and

$$\Delta R_{RB_n} = \frac{\left|\Delta\varepsilon_{RB_n}(t)\right|^2}{\left|\varepsilon_s\left(t - \frac{n\Delta l}{v}\right)e^{-\frac{\alpha}{2}n\Delta l}\right|^2} = \left|\Delta\rho_n\right|^2 \tag{2.5}$$

Proceeding in a similar fashion, at the end of a fiber of length L, the doubly Rayleigh backscattered field from the n^{th} and m^{th} sections located respectively at $z = n\Delta l$ and $z = m\Delta l$ as shown in Figure 2.1 can be expressed as

$$\Delta\varepsilon_{DRB_{n,m}}(t,L) = \varepsilon_{dir}\left(t - 2\frac{(n-m)\Delta l}{v}, L\right)e^{-\left(\frac{\alpha}{2}+j\beta\right)2(n-m)\Delta l}\Delta\rho_m\Delta\rho_n \tag{2.6}$$

Combining each contribution described by Eqn. (2.6) yields the total doubly backscattered field $\varepsilon_{DRB}(t,L)$ at the end of the fiber as

$$\varepsilon_{DRB}(t,L) = \sum_{n=1}^{N_{sc}}\sum_{m=1}^{n-1}\varepsilon_{dir}\left(t - 2\frac{(n-m)\Delta l}{v}, L\right)e^{-\left(\frac{\alpha}{2}+j\beta\right)2(n-m)\Delta l}\Delta\rho_m\Delta\rho_n \tag{2.7}$$

where n and m now denote the indices of the summations.

For an Intensity Modulated-Direct Detection (IM-DD) system, the received optical intensity is to be detected and converted to an electrical signal by a photodetector. Any unwanted fluctuations in optical intensity will appear as a noise current or voltage. To consider the impact of DRB on the IM-DD system, the intensity $I(t)$ of the aggregate optical field is obtained as

$$\begin{aligned} I(t) &= \left|\varepsilon_{dir}(t,L) + \varepsilon_{DRB}(t,L)\right|^2 \\ &= \left(\varepsilon_{dir}(t,L) + \varepsilon_{DRB}(t,L)\right)\left(\varepsilon_{dir}(t,L) + \varepsilon_{DRB}(t,L)\right)^* \\ &= \left|\varepsilon_{dir}(t,L)\right|^2 + \left|\varepsilon_{DRB}(t,L)\right|^2 + 2\,\mathrm{Re}\left[\varepsilon_{dir}(t,L)\varepsilon_{DRB}^*(t,L)\right] \end{aligned} \tag{2.8}$$

where $*$ represents the complex conjugate. The first term in Eqn. (2.8) is the desired signal intensity, the second term is the intensity due to doubly Rayleigh backscattered light and the third term is the noise intensity generated by the doubly Rayleigh backscattered field beating with the forward traveling signal field. The magnitude of the second term is negligible compared to the third term due to the low backscattering in conventional fibers. This should be the case even for the event of a space (or logical zero) in a digital system because the direct field is generally not completely extinguished and is still much larger than the DRB field. For example, the DRB field generated in a long fiber with an effective backscattering reflectance of -33 dB is approximately 66 dB smaller than the average direct signal, whereas for an optical transmitter with a typical extinction ratio of 13 dB, the field during a space is only approximately 10 dB smaller than the average direct signal. Therefore, the field during a space is about 56 dB larger than the DRB field. Even if an optical amplifier with 20 dB gain is situated between the backscattering fibers, the field during a space is still 16 dB larger than the DRB field that travels around the amplifier and is thereby doubly amplified. One might expect that if the amplifier gain is increased to 25 dB, the field during a space will only be 6 dB larger than this doubly amplified DRB field; however, we will show through the analysis in Chapter 5 that only optical amplifiers with moderate gain can be employed in transmission links impacted by DRB.

Another justification for the neglect of the DRB light intensity is that other signal-independent noises, such as thermal noise at the receiver and spontaneous to spontaneous beat noise from optical amplifiers, are usually much greater. The DRB noise intensity is now defined by

$$I_{DRB}(t) = 2\,\mathrm{Re}\left[\varepsilon_{dir}(t,L)\varepsilon_{DRB}^{*}(t,L)\right] \tag{2.9}$$

Eqn. (2.9) is an expression for the time-dependent DRB noise intensity in terms of the electric field of the optical signal $\varepsilon_{dir}(t,L)$ and the electric field of the DRB light $\varepsilon_{DRB}(t,L)$. Note that $\varepsilon_{dir}(t,L)$ is the transmitted field and implicitly contains the information signal and any time dependent chirping induced by directly or externally modulating the optical source.

2.2. Autocorrelations of DRB Noise Intensity

To find the DRB noise intensity spectral density one can first determine the ensemble-average of the time-autocorrelation function of the DRB noise intensity

$$R_{I_{DRB}}(\tau) = \overline{I_{DRB}(t) I_{DRB}(t+\tau)} \tag{2.10}$$

and then take its Fourier transform [25,30]. In the above equation, the overbar represents the time-average. The ensemble-average of the time-autocorrelation function, abbreviated as simply the average time-autocorrelation in what follows, can be expressed as

$$\left\langle R_{I_{DRB}}(\tau) \right\rangle = \left\langle \overline{I_{DRB}(t) \cdot I_{DRB}(t+\tau)} \right\rangle \tag{2.11}$$

and $\langle \cdot \rangle$ represents the ensemble-average. If Eqn. (2.9) is inserted into Eqn. (2.11), the average time-autocorrelation becomes

$$\left\langle R_{I_{DRB}}(\tau) \right\rangle = \left\langle \overline{\begin{array}{l} \left\{ \left(\varepsilon_{dir}(t,L) \varepsilon_{DRB}^*(t,L) + \varepsilon_{dir}^*(t,L) \varepsilon_{DRB}(t,L) \right) \cdot \right. \\ \left. \left(\varepsilon_{dir}(t+\tau,L) \varepsilon_{DRB}^*(t+\tau,L) + \varepsilon_{dir}^*(t+\tau,L) \varepsilon_{DRB}(t+\tau,L) \right) \right\} \end{array}} \right\rangle \tag{2.12}$$

After inserting the expression for the total DRB field, Eqn. (2.12) yields

$$\left\langle R_{I_{DRB}}(\tau)\right\rangle =$$

$$\left\langle \overline{\left\{ \left[\begin{pmatrix} \varepsilon_{dir}(t,L)\displaystyle\sum_{n=1}^{N_{sc}}\sum_{m=1}^{n-1}\varepsilon_{dir}^{*}\left(t-2\frac{(n-m)\Delta l}{v},L\right)e^{-\left(\frac{\alpha}{2}-j\beta\right)2(n-m)\Delta l}\Delta\rho_m^{*}\Delta\rho_n^{*}+ \\ \varepsilon_{dir}^{*}(t,L)\displaystyle\sum_{n=1}^{N_{sc}}\sum_{m=1}^{n-1}\varepsilon_{dir}\left(t-2\frac{(n-m)\Delta l}{v},L\right)e^{-\left(\frac{\alpha}{2}+j\beta\right)2(n-m)\Delta l}\Delta\rho_m\Delta\rho_n \end{pmatrix} \cdot \begin{pmatrix} \varepsilon_{dir}(t+\tau,L)\displaystyle\sum_{l=1}^{N_{sc}}\sum_{k=1}^{l-1}\varepsilon_{dir}^{*}\left(t-2\frac{(l-k)\Delta l}{v}+\tau,L\right)e^{-\left(\frac{\alpha}{2}-j\beta\right)2(l-k)\Delta l}\Delta\rho_k^{*}\Delta\rho_l^{*}+ \\ \varepsilon_{dir}^{*}(t+\tau,L)\displaystyle\sum_{l=1}^{N_{sc}}\sum_{k=1}^{l-1}\varepsilon_{dir}\left(t-2\frac{(l-k)\Delta l}{v}+\tau,L\right)e^{-\left(\frac{\alpha}{2}+j\beta\right)2(l-k)\Delta l}\Delta\rho_k\Delta\rho_l \end{pmatrix} \right] \right\}} \right\rangle \tag{2.13}$$

After expanding and using the statistical property that the mean of a product of functions of random independent processes, $(\varepsilon_{dir}\ldots)$ and $(\Delta\rho_n\ldots)$ can be expressed as the product of their means, Eqn (2.13) yields

$$\left\langle R_{I_{DRB}}(\tau)\right\rangle = \begin{pmatrix} \left\langle \overline{\varepsilon_{dir}(t,L)\varepsilon_{dir}(t+\tau,L)\sum\sum\sum\sum\ldots} \right\rangle \left\langle \Delta\rho_m^{*}\Delta\rho_n^{*}\Delta\rho_k^{*}\Delta\rho_l^{*} \right\rangle + \\ \left\langle \overline{\varepsilon_{dir}(t,L)\varepsilon_{dir}^{*}(t+\tau,L)\sum\sum\sum\sum\ldots} \right\rangle \left\langle \Delta\rho_m^{*}\Delta\rho_n^{*}\Delta\rho_k\Delta\rho_l \right\rangle + \\ \left\langle \overline{\varepsilon_{dir}^{*}(t,L)\varepsilon_{dir}(t+\tau,L)\sum\sum\sum\sum\ldots} \right\rangle \left\langle \Delta\rho_m\Delta\rho_n\Delta\rho_k^{*}\Delta\rho_l^{*} \right\rangle + \\ \left\langle \overline{\varepsilon_{dir}^{*}(t,L)\varepsilon_{dir}^{*}(t+\tau,L)\sum\sum\sum\sum\ldots} \right\rangle \left\langle \Delta\rho_m\Delta\rho_n\Delta\rho_k\Delta\rho_l \right\rangle \end{pmatrix} \tag{2.14}$$

This new equation includes terms composed of the averages of the product of differential Rayleigh backscattering coefficients and direct traveling fields.

Before proceeding, the statistics of the Rayleigh backscattering function has to be studied and accurately modeled. Since the correlation distance of refractive index fluctuations in an optical fiber is of the order of molecular dimensions and much smaller than the optical wavelengths used for fiber communications, each section contains many distinct and almost identical scattering centers if the section length Δl is chosen to be in the order of an optical wavelength [14,26]. Then, by the central limit theorem, the backscattered field from the section exhibits circular complex Gaussian (CCG) statistics and $\Delta\rho$ can be modeled by a CCG random variable [14,27]. In addition, since $\Delta\rho$ of different sections are uncorrelated, the following relation can be approximated:

$$\left\langle \Delta\rho_m \Delta\rho_n{}^* \right\rangle = \left\langle \left|\Delta\rho_n\right|^2 \right\rangle \delta(n-m) \tag{2.15}$$

Here $\delta(n)$ is the Delta function with the properties that $\delta(n)=1$ for $n=0$, and $\delta(n)=0$ otherwise. Substituting Eqn. (2.5) into the above equation yields

$$\left\langle \Delta\rho_m \Delta\rho_n{}^* \right\rangle = \left\langle \Delta R_{RB_n} \right\rangle \delta(n-m) \tag{2.16}$$

By equating the average of the Rayleigh backscattering reflectance due to Δl as

$$\left\langle \Delta R_{RB_n} \right\rangle = \alpha_s \, S \, \Delta l \tag{2.17}$$

where α_s and S are the intensity coefficient due to Rayleigh scattering and recapture factor [26,28], respectively, the delta correlation can be rewritten in terms of the measurable quantities as

$$\left\langle \Delta\rho_m \Delta\rho_n{}^* \right\rangle = \alpha_s \, S \, \Delta l \, \delta(n-m) \tag{2.18}$$

The recapture factor is the fraction of scattered power coupled into the fiber in the backward direction. The product of α_s and S describes the total backscattered power per meter, also known as the Rayleigh backscattering coefficient. For standard single-mode fiber, the typical values for this product at 1550 nm are about -70 to -73 dB/m [20].

With the delta correlated CCG assumption for $\Delta\rho$, as shown in Eqn. (2.18), the following relation can be derived [13-14]:

$$\begin{aligned}
&\langle \Delta\rho_m \Delta\rho_n \Delta\rho_k \Delta\rho_l \rangle = 0 \\
&\langle \Delta\rho_m{}^* \Delta\rho_n{}^* \Delta\rho_k{}^* \Delta\rho_l{}^* \rangle = 0 \\
&\langle \Delta\rho_m{}^* \Delta\rho_n{}^* \Delta\rho_k \Delta\rho_l \rangle = \alpha_s{}^2 S^2 \Delta l^2 \left(\delta(n-l)\delta(m-k) + \delta(n-k)\delta(m-l)\right) \\
&\langle \Delta\rho_m \Delta\rho_n \Delta\rho_k{}^* \Delta\rho_l{}^* \rangle = \alpha_s{}^2 S^2 \Delta l^2 \left(\delta(n-l)\delta(m-k) + \delta(n-k)\delta(m-l)\right)
\end{aligned} \tag{2.19}$$

After applying the above relations, the average time-autocorrelation expression in (2.14) becomes

$$\langle R_{I_{DRB}}(\tau) \rangle = 2\,\mathrm{Re}\left[\left\langle \varepsilon_{dir}(t,L)\varepsilon_{dir}{}^*(t+\tau,L) \cdot \sum_{n=1}^{N_{sc}} \sum_{m=1}^{n-1} \begin{matrix} \varepsilon_{dir}{}^*\left(t - 2\dfrac{(n-m)\Delta l}{v}, L\right) \cdot \\ \varepsilon_{dir}\left(t - 2\dfrac{(n-m)\Delta l}{v} + \tau, L\right) e^{-\alpha 2(n-m)\Delta l} \Delta l^2 \end{matrix} \right\rangle \alpha_s{}^2 S^2 \right] \tag{2.20}$$

Due to the very small change in the slowly varying complex field envelope within Δl, the summations in Eqn. (2.20) can be accurately replaced with their corresponding integrals as shown below:

$$\langle R_{I_{DRB}}(\tau) \rangle = 2\,\mathrm{Re}\left[\left\langle \varepsilon_{dir}(t,L)\varepsilon_{dir}{}^*(t+\tau,L) \cdot \int_0^L \int_0^{z_2} \begin{matrix} \varepsilon_{dir}{}^*\left(t - 2\dfrac{z_2 - z_1}{v}, L\right) \cdot \\ \varepsilon_{dir}\left(t - 2\dfrac{z_2 - z_1}{v} + \tau, L\right) e^{-\alpha 2(z_2 - z_1)} dz_1 dz_2 \end{matrix} \right\rangle \alpha_s{}^2 S^2 \right] \tag{2.21}$$

If the following conditions are satisfied:

a) the fiber loss is small within the source field coherence length so that the value of $\varepsilon^*_{dir}(\cdot+\tau,L)\varepsilon_{dir}(\cdot,L)$ changes much faster than that of $e^{-\alpha 2(\cdot)}$, we show in Appendix A that the above autocorrelation can be rewritten as

$$\left\langle R_{I_{DRB}}(\tau)\right\rangle =$$
$$2\,\mathrm{Re}\left[\left\langle \overline{\begin{array}{l}\varepsilon_{dir}(t,L)\varepsilon_{dir}{}^*(t+\tau,L)\cdot \\ \int\limits_0^L\left\{\frac{1}{z_2}\int\limits_0^{z_2}\varepsilon_{dir}{}^*\left(t-2\frac{z_2-z_1}{v},L\right)\varepsilon_{dir}\left(t-2\frac{z_2-z_1}{v}+\tau,L\right)dz_1\cdot\int\limits_0^{z_2}e^{-\alpha 2(z_2-z_1)}dz_1\right\}dz_2\end{array}}\right\rangle\right]\alpha_s{}^2S^2$$

(2.22)

With low attenuation fibers, this condition should be easily satisfied.

b) the source field coherence length is relatively short compared to the fiber length so that with the definition of a time-autocorrelation [29,30] (or with Eqn. (2.10)),

$$R_y(\tau)=\lim_{T\to\infty}\frac{1}{T}\int\limits_{-\frac{T}{2}}^{\frac{T}{2}}y^*(t)y(t+\tau)dt \tag{2.23}$$

the inner integration of $\varepsilon_{dir}{}^*(\cdot+,L)\varepsilon_{dir}(\cdot+\tau,L)$ in Eqn. (2.22) approximates a time-autocorrelation function of the source field. This condition is also satisfied in common transmission systems. Then, Eqn (2.22) becomes

$$\begin{aligned}\left\langle R_{I_{DRB}}(\tau)\right\rangle &= 2\,\mathrm{Re}\left[\left\langle\overline{\varepsilon_{dir}(t,L)\varepsilon_{dir}{}^*(t+\tau,L)\int\limits_0^L R_{\varepsilon_{dir}}(\tau)\cdot\int\limits_0^{z_2}e^{-\alpha 2(z_2-z_1)}dz_1dz_2}\right\rangle\right]\alpha_s{}^2S^2\\ &= 2\,\mathrm{Re}\left[\left\langle\overline{\varepsilon_{dir}(t,L)\varepsilon_{dir}{}^*(t+\tau,L)R_{\varepsilon_{dir}}(\tau)\int\limits_0^L\int\limits_0^{z_2}e^{-\alpha 2(z_2-z_1)}dz_1dz_2}\right\rangle\right]\alpha_s{}^2S^2\end{aligned}$$

(2.24)

where $R_{\varepsilon_{dir}}(\tau)$ is the time-autocorrelation function of the complex amplitude of the directly traveling field. Rearranging the last equation and using Eqn. (2.10) give rise to

$$\left\langle R_{I_{DRB}}(\tau)\right\rangle = 2\,\mathrm{Re}\left[\left\langle R_{\varepsilon_{dir}}{}^{*}(\tau)R_{\varepsilon_{dir}}(\tau)\int_{0}^{L}\int_{0}^{z_2} e^{-\alpha 2(z_2-z_1)}dz_1dz_2\right\rangle\right]\alpha_s{}^2S^2$$

$$= 2\left[\left\langle R_{\varepsilon_{dir}}{}^{*}(\tau)R_{\varepsilon_{dir}}(\tau)\right\rangle\right]\left[\int_{0}^{L}\int_{0}^{z_2} e^{-\alpha 2(z_2-z_1)}dz_1dz_2\right]\alpha_s{}^2S^2$$

$$= 2\frac{\alpha_s{}^2S^2}{4\alpha^2}\left(2\alpha L + e^{-2\alpha L} - 1\right)\left\langle\left|R_{\varepsilon_{dir}}(\tau)\right|^2\right\rangle \tag{2.25}$$

Thus, the average time-autocorrelation function of the noise intensity due to DRB is simply related to the magnitude-squared of the time-autocorrelation function $R_{\varepsilon_{dir}}(\tau)$ of the electric field of the source. Since the total Rayleigh backscattering reflectance R_{Rb} for an infinitely long piece of fiber can be expressed [5] as

$$R_{Rb} = \frac{\alpha_s S}{2\alpha} \tag{2.26}$$

Eqn. (2.25) becomes

$$\left\langle R_{I_{DRB}}(\tau)\right\rangle = 2R_{Rb}{}^2\left(2\alpha L + e^{-2\alpha L} - 1\right)\left\langle\left|R_{\varepsilon_{dir}}(\tau)\right|^2\right\rangle \tag{2.27}$$

Typically, the value of R_{Rb} for standard single-mode fiber at 1550 nm ranges from -33 to -31 dB.

2.3. Depolarization and Spectral density of DRB Noise

To remove the restrictive assumption made earlier on the preservation of the state of polarization of the electric field, one can make use of the results from Deventer [31] on polarization properties of Rayleigh backscattering in single-mode fiber. They simply state that in a standard low birefringence fiber, the singly Rayleigh backscattered light has the same State of Polarization (SOP) as the forward traveling light, with its Degree of Polarization (DOP) equal to 1/3 due to depolarization during backscattering. Thus, 2/3 of the backscattered light has been depolarized and has a random state of polarization.

Similarly, when the singly backscattered light undergoes backscattering again, the doubly backscattered light has the same SOP as the forward traveling light, and its DOP reduces to 1/9. Therefore, at the end of the link, only 5/9 of the doubly backscattered light (1/9 plus half the completely depolarized doubly backscattered light) mixes with the direct signal light and generates DRB noise at the receiver. This differs from the assumption of completely unpolarized doubly Rayleigh backscattered light at the receiver [5]. The DRB noise intensity spectral density is now obtained by taking the Fourier transform of the average time-autocorrelation (Eqn. (2.27)) and multiplying it by 5/9 to account for the birefringence and depolarization effect of the single-mode fiber:

$$P_{DRB}(f)=\frac{10}{9}R_{Rb}{}^{2}\left(2\alpha L+e^{-2\alpha L}-1\right)\Im\left[\left\langle\left|R_{\varepsilon_{dir}}(\tau)\right|^{2}\right\rangle\right] \tag{2.28}$$

where $\Im[\cdot]$ denotes Fourier transformation. Eqn. (2.28) is the general and accurate analytical expression describing the expected noise spectrum due to DRB, and is the most important finding in this chapter. For clarification, this expression is now referred to as the DRB noise expression. Unlike previous analyses of DRB [1-13], the author is dealing with the autocorrelation function of the signal electric field without any assumptions about the form of modulation.

This expression reveals that for the case of a real time-autocorrelation of the source field, DRB noise can be explicitly described by the self convolution of the source field spectrum as

$$P_{DRB}(f)=\frac{10}{9}R_{Rb}{}^{2}\left(2\alpha L+e^{-2\alpha L}-1\right)\left\{\Im\left[R_{\varepsilon_{dir}}(\tau)\right]\otimes\Im\left[R_{\varepsilon_{dir}}(\tau)\right]\right\} \tag{2.29}$$

Since the time-autocorrelation and spectrum of a typical unmodulated DFB laser source are real and Lorentzian [25,68], respectively, and since the self convolution of a Lorentzian lineshape is also Lorentzian, albeit of double width, the DRB noise in this case is also Lorentzian. This conclusion is confirmed by other researchers' work [1,5,7].

Further uses of the DRB noise expression, applying digital or analog modulation, with or without chirp, to the source in various systems, are made in the following chapters.

Chapter 3

DRB Noise in AM-SCM SYSTEMS

A general overview of current cable television systems is presented. For simplicity, cable television is abbreviated as CATV, even though it was historically coined to stand for community antenna television. Prior to employing the previously derived DRB noise expression in various fiber optic CATV systems, the experimental verification of this expression in a fiber optic Amplitude Modulated-Subcarrier Multiplexed (AM-SCM) system is discussed. Simplified expressions are then derived to describe the DRB noise in directly and externally modulated AM-SCM systems, utilizing either 1310 nm or 1550 nm window laser sources. The Carrier to Noise Ratio (CNR) reduction due to the DRB noise in these systems is then investigated.

3.1. Overview of CATV Systems

3.1.1. Architecture

Due to the recent deregulation of information service businesses, the information exchange monopoly will soon be relaxed extensively. The CATV industry is now facing competition from telephone companies providing integrated video and telephone services. On the other hand, the CATV providers can also exploit this opportunity to provide full telephony integration with delivery of broadcast video. Figure 3.1 illustrates the traditional coaxial cable based tree-and-branch architecture which was designed to transport and distribute television programs from the headend office to customers in a one-way direction. The main disadvantage of tree-and-branch topology is the lengthy cascade of RF amplifiers which results in reduced reliability and available bandwidth, and poorer system noise and distortion performance. In addition, this topology lacks bi-directionality and switching capability. In order to provide broadband interactive integrated services, this architecture requires modification, and in some cases a complete system rebuild may be more cost effective.

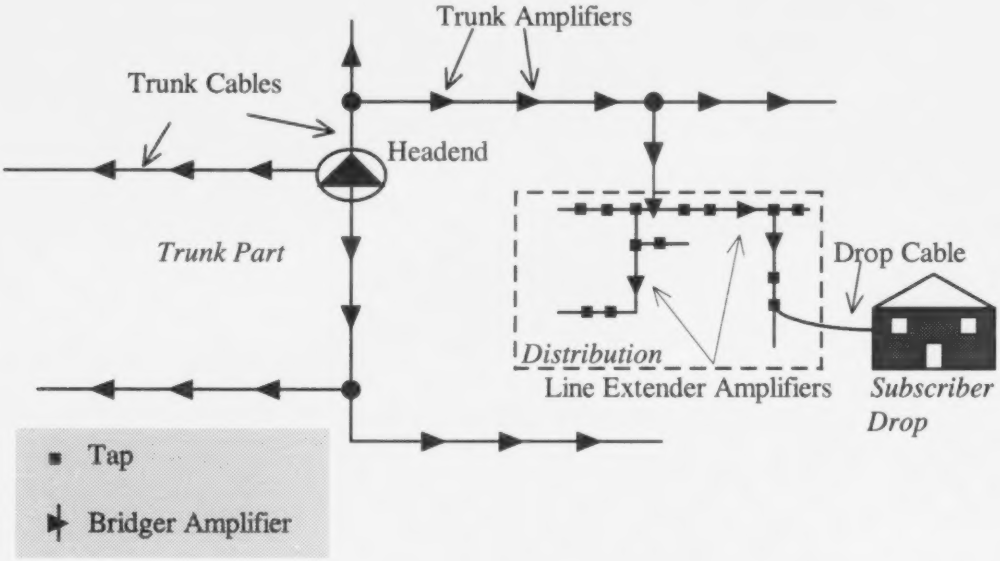
Trunk Amplifiers
Trunk Cables
Headend
Trunk Part
Drop Cable
Distribution
Line Extender Amplifiers
Subscriber Drop
Tap
Bridger Amplifier

Figure 3.1: Tree-and-branch architecture of a typical CATV network.

The most widely studied and deployed architecture for providing broadband interactive integrated services in the past few years is the Hybrid Fiber/Coax (HFC) architecture [32-35]. In a HFC system, as shown in Figure 3.2, the output from an optical transmitter is intensity-modulated with the aggregate signal in the headend and sent via single-mode fibers to a serving node. The optical signal is then converted to an electrical signal by a photodetector and the electrical signal is distributed to the subscribers via the existing coaxial cable network. Replacing the trunk cable with fiber means that there are fewer RF trunk amplifiers in cascade, which improves system reliability, picture quality and bandwidth availability. Since the trunk cable accounts for only about 14% of the total footage in a network [36], replacement of trunk cable with fiber and reuse of the distribution cable and subscriber drop can reduce the upgrade cost.

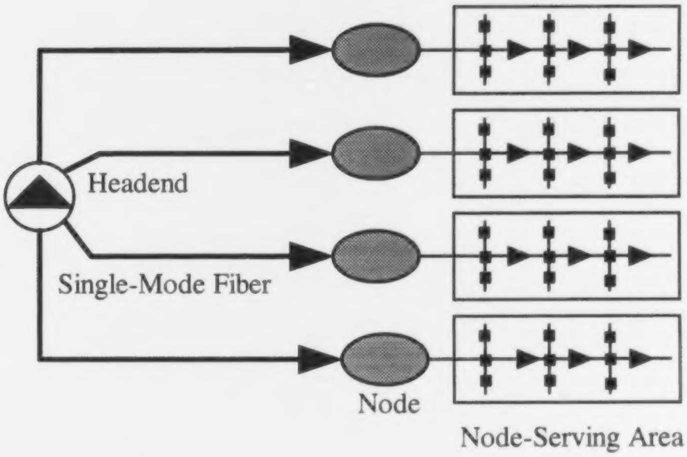

Figure 3.2: A basic HFC design.

The early design of HFC was to deliver one-way broadcast video, thus the laser output at the headend office was split and guided to several nodes serving from a few hundred to several thousand subscribers in order to minimize cost. However, this design lacked the capability of upstream transmission to the headend due to the fact that a large number of subscribers share the common upstream bandwidth spanning 5 to 30 MHz. Currently, the approach used in HFC systems parallels cellular systems in the sense that the size of a node serving area is shrinking. Since the return spectrum spans 5 to 30 MHz, by shrinking the node serving area and limiting the number of subscribers served down to a few hundred, larger return bandwidth per subscriber will be available for interactive services [33-34]. In addition, with the further reduction in the number of amplifiers in cascade, the available bandwidth can exceed 1 GHz [32].

3.1.2. CATV Signal Format

In fiber optic CATV systems, analog AM-Vestigial Sideband (VSB) SCM is used to deliver multichannel video programs to subscribers. To generate an AM-VSB SCM signal, a number of baseband video signals are first frequency up-converted by amplitude modulating various sub-carriers at different RF frequencies, and then each of these up-converted signals passes through a VSB filter to reduce its bandwidth, and finally these filtered signals are combined to modulate the optical transmitter. Figure 3.3 shows the spectrum of the electrical modulating signal.

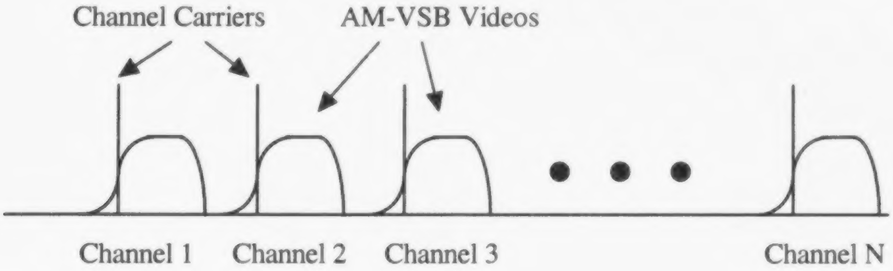

Figure 3.3: Spectrum of a subcarrier multiplexed AM-VSB signal

However, in current CATV systems, instead of a true VSB filter, bandpass filters are used at the transmitter. Then at the receiving end, a single VSB filter is employed at the IF (Intermediate Frequency) stage to give the overall VSB filter characteristics so that the video modulation on the visual VSB TV signal can be recovered without distortion [37]. The spectra of a received video channel before and after VSB filtering are shown in Figure 3.4.

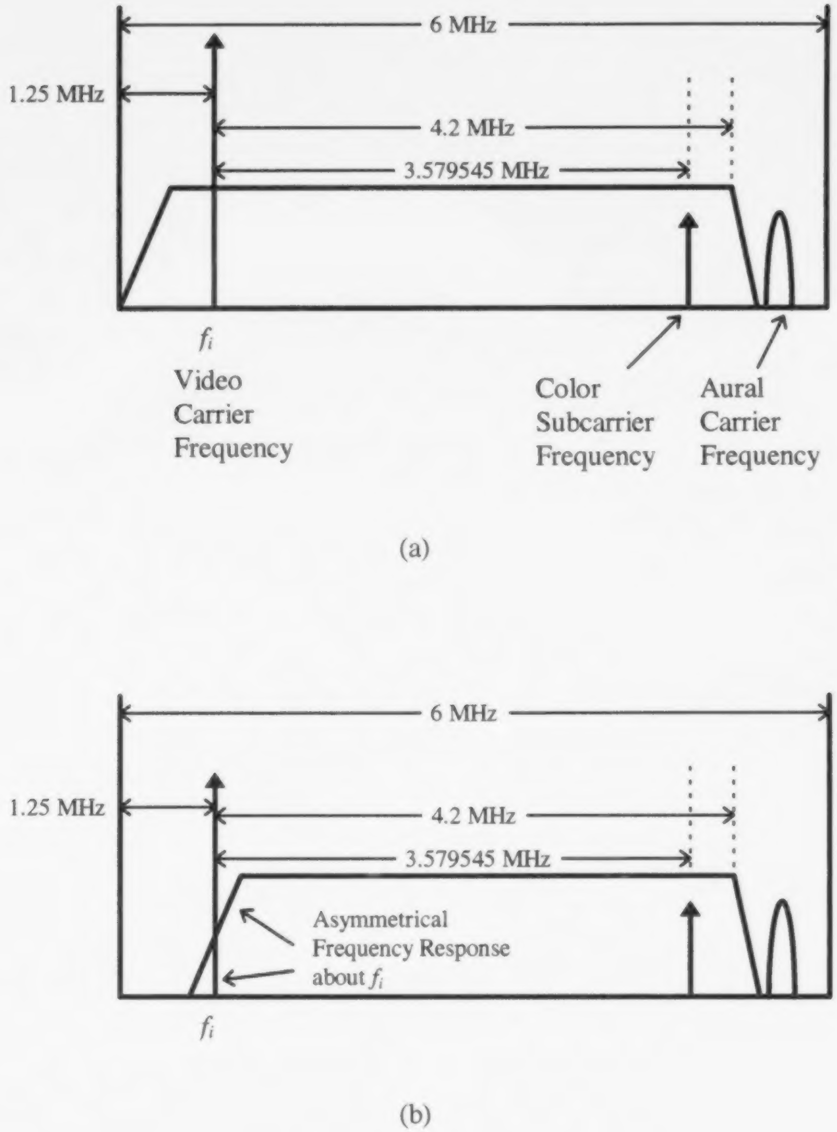
6 MHz
1.25 MHz
4.2 MHz
3.579545 MHz
f_i
Video Carrier Frequency
Color Subcarrier Frequency
Aural Carrier Frequency
(a)
6 MHz
1.25 MHz
4.2 MHz
3.579545 MHz
Asymmetrical Frequency Response about f_i
f_i
(b)

Figure 3.4: Magnitude spectra of a received TV channel (a) before and (b) after VSB filtering in receivers.

The advantages of using AM-VSB format are its bandwidth efficiency, simple hardware requirement, and compatibility with existing TV and VCR units. On the other hand, SCM can also provide an upgradeable and expandable multichannel platform. It is expandable in the sense that more channels can be easily added with minimum added hardware. The upgradeability offered from SCM results from the fact that SCM is independent of the modulation scheme. In this case, other modulation formats, such as FM or high-definition compressed digital video, can be transported with AM-VSB video so as to provide a transition period from the analog system to more robust digital systems. For this reason, this form of digital/analog hybrid system design has been investigated extensively over the past few years, particularly in the areas of digital video signal, using quadrature amplitude modulation [38-40] and multi-level VSB modulation [41-42], employment of linearized external modulator [43-45] and digital signal degradation due to laser clipping distortion [46-48].

Due to the analog nature of the AM-VSB video signal, it is extremely vulnerable to coherent and non-coherent interference. The coherent and non-coherent interference impairments are specified by Composite Second Order (CSO), Composite Triple Beat (CTB), and Carrier to Noise Ratio (CNR). These figures of merit are defined as follows [49]:

- **CSO**: the ratio of the carrier power to the power in the composite second-order intermodulation tone caused by the second order curvature of the non-linear transfer characteristic, which, for the Northern America CATV frequency plan, occurs at the video carrier frequency ±1.25 MHz.
- **CTB**: the ratio of the carrier power to the power in the composite third-order intermodulation tone caused by the third order curvature of the non-linear transfer characteristic, which for the Northern America CATV frequency plan, occurs at the video carrier frequency.
- **CNR**: the ratio of the carrier power for a given channel to the noise power near the carrier, assuming a noise bandwidth of 4 MHz.

For good picture quality, the required values of CSO, CTB and CNR at the subscriber termination are about 55 dBc, 55 dBc and 48 dB, respectively. Therefore, due to added noise and distortion from RF amplifiers in the trunking and distribution network, the required values for these figures before subscriber termination are significantly higher and are dependent of the number of RF amplifiers in the system.

3.1.2.1. Non-Uniform DRB Noise Spectrum in CNR Calculations

In the carrier to noise ratio definition above, the total noise spectral density is assumed to be uniform within a channel so that no integration is needed for calculating the total noise within the channel. However, as we will show later the DRB noise spectral density can be non-uniform within a channel, thus we have to integrate the DRB noise spectral density to calculate its total noise. To achieve this we have to determine the appropriate lower and upper limits in the integral. As shown earlier in Figure 3.4.b, the main detected video signal occupies approximately 4.2 MHz, ranging from the video carrier f_i to f_i + 4.2 MHz. Therefore, the total DRB noise that couples into the signal also has a bandwidth of approximately 4.2 MHz, ranging from f_i to f_i + 4.2 MHz. Since a noise equivalent bandwidth of 4 MHz is normally used for CNR measurements, we will follow this common practice, and thereby use f_i and f_i + 4 MHz as the upper and lower limits, respectively, in integrating the DRB noise in this chapter.

3.1.3. Operating Windows

To date, CATV companies deploying HFC systems have mainly been utilizing 1310 nm technology. The reasons for using this technology are many. First, optoelectronics for analog transmission at this wavelength is considered to be mature and relatively inexpensive. Second, chromatic dispersion is minimized at this wavelength so that dispersion-induced distortion is eliminated to ease the strict CSO requirement. Third, fiber loss at this transmission window is only ~0.35 dB/km. Lastly, transmitters containing high power solid-state lasers at 1310 nm and linearized external modulators can yield a system budget of 17 dB.

However, over the past few years much work has been done in incorporating the benefits of 1550 nm into an HFC environment [50-54]. This is due to the advantages of using 1550 nm such as the commercial availability of Erbium-Doped Fiber Amplifiers

(EDFAs) at that wavelength as well as lower attenuation, i.e. 0.25 dB/km as opposed to 0.35 dB/km at 1310 nm. The benefit of lower attenuation is the ability to utilize the available link budget more efficiently, whether that be in the form of increased optical splitting loss or longer loop lengths. It has been experimentally demonstrated that no considerable CSO degradation was observed in either directly [53-54] or externally [52] modulated systems employing EDFAs. In the directly modulated systems, the dispersion effect from the standard single-mode fiber was equalized out by a dispersion compensating fiber. On the other hand, the systems employing an external modulator could yield a link budget of 25 dB or 100 km. Both of these results suggest the feasibility of using 1550 nm technology in analog transmission to extend the system reach.

Due to the stringent noise performance and trend of using long fiber in the CATV system, DRB noise, which depends on the length of fiber, can be a detrimental factor. Previous research [9,10,12,13], to some extent, has confirmed this degradation. The rest of this chapter strives to complete the investigation of this negative impact on fiber optic CATV systems using 1310 nm and 1550 nm laser sources, with and without utilizing optical amplifiers.

3.2. Experimental Verification

3.2.1. Source Electric Field of General AM-SCM Signal

To verify the DRB noise expression, a generic signal should be used in the experiment. A directly modulated AM-SCM signal is a good candidate and was used in the experiment for this purpose. Its effectiveness is due to its analog nature and the fact that various amounts of phase or frequency modulation [55] can be imposed onto the optical signal. To clarify, in a directly modulated system the laser output is modulated by varying the injection current. A typical laser current-to-power transfer characteristic is depicted in Figure 3.5. Due to the variation of the injection current, the carrier density is varied, which, in addition to modulating the optical output power, in turn yields a change of the refractive index and of the optical lasing frequency as well. This change in optical frequency, often referred to as static chirp, broadens the spectrum of the source electric field and can provide a dispersion limit to the transmission bandwidth in many high speed systems [56-58].

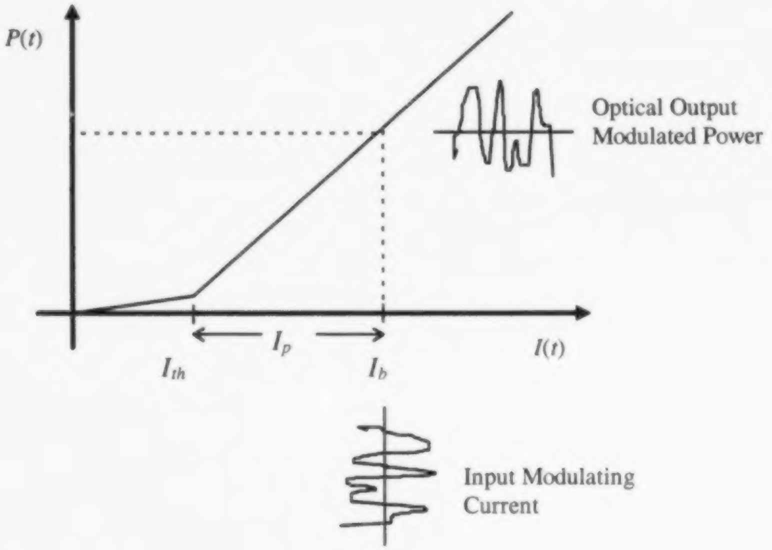

Figure 3.5: Laser optical output power and diode current characteristic.

The time dependent received optical power in a AM-SCM system can be expressed as

$$P(t) = P_{re}(1 + m(t)) \tag{3.1}$$

where P_{re} is the average received optical power, and $m(t)$ is the modulating signal which for an SCM signal format is given by

$$m(t) = \sum_{i=1}^{N_{ch}} m_i \cos(2\pi f_i t + \theta_i) \tag{3.2}$$

where m_i, f_i and θ_i are respectively the peak modulation index, frequency and initial phase of the signal in channel i, and N_{ch} is the number of channels.

Under an assumption of linear chirp [6,9], where the variation of the optical frequency is linearly proportional to the change of injected current, the complex amplitude of the detected electric field is

$$\varepsilon_{dir}(t) = \sqrt{\frac{P_{re}(1+m(t))}{A_{eff}}} \cdot e^{j\phi(t)} \cdot e^{j2\pi\int_0^t \gamma \cdot I_p \cdot m(\zeta)d\zeta} \tag{3.3}$$

where γ is the laser chirping efficiency in MHz/mA, $\phi(t)$ is the intrinsic laser phase noise, I_p is the bias current minus the threshold current, and A_{eff} is the effective area of the fiber core and which is introduced to convert the optical power to optical intensity. The term $e^{j2\pi\int\bullet}$ represents the time dependent phase due to the chirp. This equation and the DRB noise expression (2.28) are utilized in the following paragraphs to calculate theoretical DRB noise spectra, which are then compared to experimental results to confirm the validity of the DRB noise expression.

3.2.2. Experimental Setup

The DRB Relative Intensity Noise (RIN) terms were determined experimentally in a directly modulated 42-channel AM-SCM system, using a fixed length of fiber and different modulation depths. RIN is defined as the detected noise spectral density normalized to the received power. The experimental setup used is shown in Figure 3.6. In order to calculate DRB noise spectra for comparison with experimental results, parameters such as the chirping efficiency, laser linewidth and Rayleigh backreflectance had to be measured as well. The measured values of these parameters are tabulated in Table 3.1, and the measurement details are discussed in Appendix B.

In the experiment, fiber connections were either fusion splices or Angled-facet Physical Contact connectors (APC) to ensure that the dominant backreflection effect was due to the Rayleigh backscattering. The optical source was an analog optical transmitter designed and built by Kinh Pham, a former master of science student at TR*Labs*. The laser diode is a highly linear distributed feedback laser diode developed by FUJITSU for CATV applications. The diode has its peak wavelength at 1543 nm at room temperature and a built-in isolator with better than -25 dB isolation to prevent external reflection. An additional isolator was inserted at the transmitter to further reduce the reflection coupling from the optical fiber, and also at the receiver to stop any reflection from the receiver back into the optical fiber. The CATV receiver is a model 600 RX module from Ipitek, with a bandwidth of 8-600 MHz. The detector inside the module is a 131-D ASTROTEC® long-wavelength PIN photodetector from AT&T. Its specified responsivity at 1550 nm is 1.0 Amp/Watt. Other important parameters involved in the experiment are listed in Table 3.1.

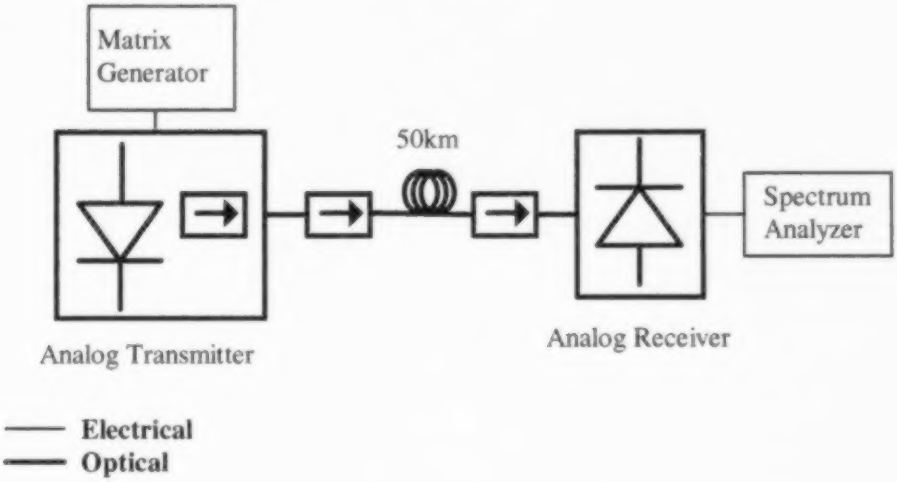
Matrix Generator
50km
Spectrum Analyzer
Analog Transmitter
Analog Receiver
Electrical
Optical

Figure 3.6: Experimental setup for measuring DRB noise.

Northern Telecom fiber	50 km
Total average fiber loss @ and 1.54 μm	0.23 dB/km
Rayleigh backreflectance @ 1.54 μm (R_{Rb})	-33.2 dB
Total average fiber loss @ and 1.31 μm	0.35 dB/km
Rayleigh backreflectance @ 1.31 μm (R_{Rb})	-31.5 dB
Laser	
Threshold current (I_{th})	18.5 mA
Bias current (I_p)	58.5 mA
Measured intrinsic laser linewidth (Δv)	14 MHz
Measured chirping efficiency (γ)	250 MHz/mA

Table 3.1: Parameters involved in the experiments and calculations.

3.2.3. Spectrum of the DRB Noise

The laser current was modulated by 42 RF carriers from a model SX-16 matrix generator from Matrix Test Equipment, Inc. The carrier frequencies are the Northern America CATV channel allocations from 55.25 to 337.25 MHz. The modulation index of each channel was set to 0, 0.24%, 0.43% and 0.86%, which corresponds to a total rms optical modulation index of 0, 1.1%, 2.0% and 3.9%, respectively, according to the following relation between total rms modulation index μ and modulation index per channel m_i :

$$\mu = \sqrt{\sum_{i=1}^{N_{ch}} \frac{m_i^{\,2}}{2}} \tag{3.4}$$

The laser output power when biased at 58.5 mA was 7.0 dBm, and the received power after 13.6 dB loss due to 50 km of single-mode fiber from Northern Telecom and 2 isolators was -6.6 dBm. The measured DRB RIN spectral densities for different total rms optical modulations are shown in Figure 3.7. The noisy curves represent measured DRB RIN, and the numbers beside the curves denote the modulation indices used in the experiment. Since the DRB noise spectral density broadens and reduces as chirp increases, for valid and accurate noise measurements, the total rms modulation indices used in the experiment were limited to only a few percent in order to ensure that the DRB noise was considerably higher than the intrinsic noise floor of the system. The measured results shown in this figure were obtained by subtracting the detected noise power spectral densities measured using a variable optical attenuator to replace the 50 km length of fiber from the noise power spectral densities when the 50 km length of fiber was used and then normalizing the results to the detected signal power. Note that the presence of the first five subcarriers was deleted for clarification. The theoretical values in Figure 3.7 were obtained by inserting Eqn. (3.3) into the general DRB noise expression and then calculating its Fourier transform numerically. The theoretical noise spectral density calculated in this way agrees very well with the experimental values, meaning that the shape of the DRB noise spectrum can be determined accurately by the theory. When the total rms modulation index was set to zero, the spectral density resembled the laser linewidth, which had a Lorentzian lineshape due to the fact that the forward traveling signal and the doubly backscattered signal created a delayed self-homodyne system. However, as the index was increased, the noise power spectrum became flatter and wider because the increasing impact of laser chirp further reduced the correlation of the electric field, causing the effect of intrinsic laser phase noise to be negligible. The results of this experiment, as shown in Figure 3.7, point out clearly the generality of the DRB noise expression by showing the transition between the case when the DRB noise spectrum was determined by intrinsic laser linewidth to the case when the DRB noise spectrum was determined by laser chirping. Therefore, the expression can be applied without the assumption that the source spectrum is either heavily chirped [6,9,12] or chirpless [1,5,7,10,13].

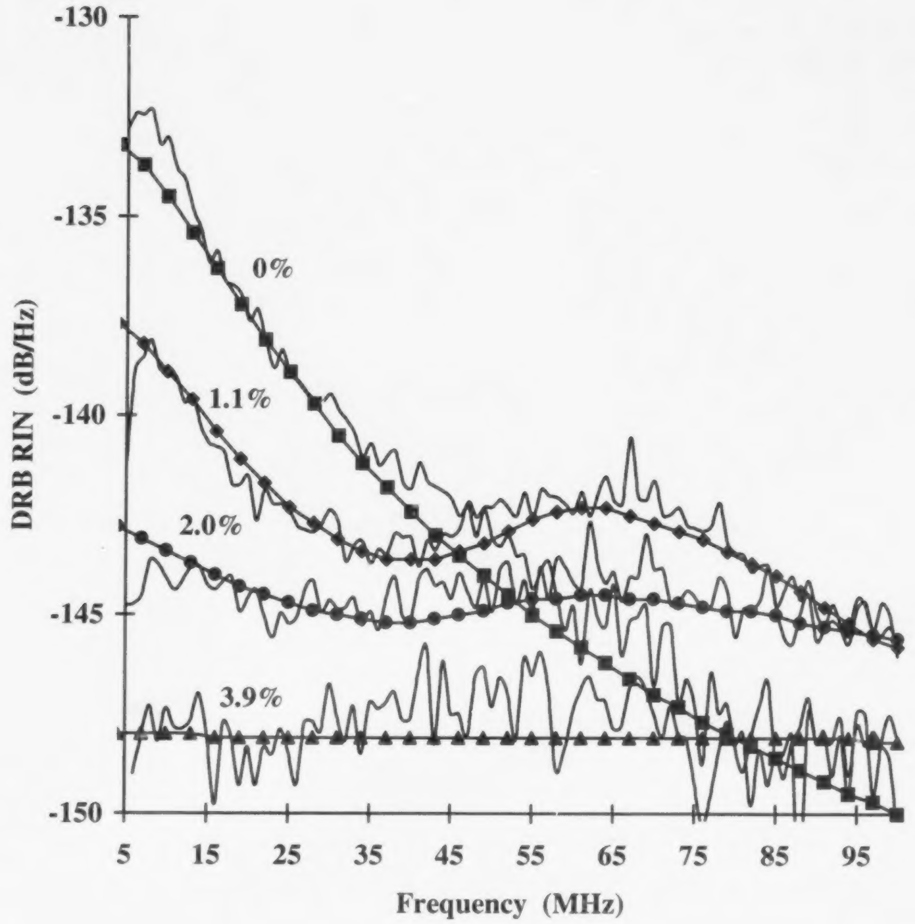

Figure 3.7: DRB RIN for various small total rms modulation indices. The numbers beside the curves denote the indices used in the experiment. The symbolized and noisy curves represent the calculated and measured DRB RIN, respectively.

3.2.4. Fiber Length Dependence of DRB Noise

To verify the length dependence in the DRB noise expression, the DRB RIN spectral densities at 10 and 25 MHz, with the modulation index equal to zero for three different fiber lengths, were measured. The experimental setup was the same as in Figure 3.6. The three fiber lengths were 10 km, 25 km and 50 km, and their fiber losses and Rayleigh backreflectances are different and listed in Table 3.2. Zero modulation index is used to obtain maximum DRB noises at these measured frequencies, as previously indicated in Figure 3.7.

Figure 3.8 indicates that the theoretical values agree very closely with the experimental values, thus completely justifying the validity of the DRB noise expression. It is worth noting that the DRB noise continues to grow with length according to $2\alpha L - 1$. Similar experimental results on length dependence of DRB noise with different operating conditions, in which a directly modulated laser source with 1000 MHz rms of laser chirp was used, has been obtained by Blauvelt *et al.* [9]. However, with that amount of laser chirp, their DRB noise came relatively close to the other noise sources present in the experiment, thereby reducing the resolution of their measurement.

Fiber length (km)	Total Average Fiber Loss (dB/km)	Rayleigh Backreflectance (R_{Rb})
10	0.219	-32.2 dB
25	0.223	-32.5 dB
50	0.244	-33.2 dB

Table 3.2: Summary of fibers used in the experiments.

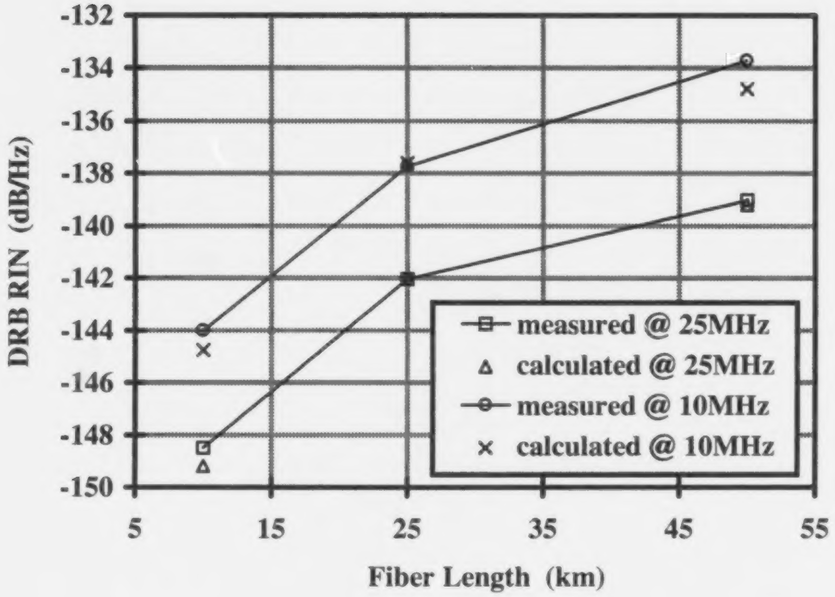

Figure 3.8: **The measured and calculated DRB RIN at 10 MHz and 25 MHz for various fiber lengths.**

3.3. DRB Noise in AM-SCM Systems

Uses of the general DRB noise expression require numerical calculations which can be approximated in some cases so that the expression becomes more convenient for use. In the following sections, the expression is simplified for lightwave AM-SCM systems with directly and externally modulated transmitters. Also discussed are the theoretical studies of CNR degradation on these systems.

3.3.1. Large Chirping in Directly Modulated Systems

For most directly modulated laser diodes in AM-SCM systems, the effects of laser chirp dominate over the intrinsic laser phase noise, as evidenced by the previous experimental results. In this case, the intrinsic laser phase noise $\phi(t)$ can be ignored, and Eqn. (3.3) for the laser complex field amplitude can be simplified to

$$\varepsilon_{dir}(t) = \sqrt{\frac{P_{re}\left(1 + m(t)\right)}{A_{eff}}} \cdot e^{j2\pi \int_0^t \gamma \cdot I_p \cdot m(\zeta) d\zeta} \tag{3.5}$$

After Taylor expanding, this equation becomes

$$\varepsilon_{dir}(t) = \sqrt{\frac{P_{re}}{A_{eff}}} \left(1 + \frac{m(t)}{2} - \frac{m(t)^2}{8} + \cdots \right) e^{j2\pi \int_0^t \gamma \cdot I_p \cdot m(\zeta) d\zeta} \tag{3.6}$$

and the time-autocorrelation function of the field amplitude can be calculated as

$$R_{\varepsilon_{dir}}(\tau) = \frac{P_{re}}{A_{eff}} \overline{\left(1 + \frac{m(t)}{2} - \frac{m(t)^2}{8} + \cdots \right)\left(1 + \frac{m(t+\tau)}{2} - \frac{m(t+\tau)^2}{8} + \cdots \right) e^{j2\pi \int_t^{t+\tau} \gamma \cdot I_p \cdot m(\zeta) d\zeta}} \tag{3.7}$$

In the case where the laser chirp-induced frequency variation is much larger than the highest channel frequency, the time-average of the product of the amplitude variation and frequency variation due to chirp in Eqn. (3.7) can be approximated by the product of the time-average of the amplitude variation and the time-average of the frequency variation. If the second and higher order terms of $m(t)$ are ignored due to the relatively small $m(t)$ in practical systems, the detected DRB noise power spectral density obtained by substituting the time-autocorrelation in Eqn. (3.7) into the general DRB noise expression (2.28) becomes

$$P_{DRB}^2(f)=\frac{10}{9}R_{Rb}^2\left(2\alpha L+e^{-2\alpha L}-1\right)\frac{P_{re}}{A_{eff}^2}{}^2\,\Im\left[\overline{\left(1+\frac{m(t)m(t+\tau)}{4}\right)}^2\,\overline{\left|e^{j2\pi\int_t^{t+\tau}\gamma\cdot I_p\cdot m(\zeta)d\zeta}\right|}^2\right]$$

(3.8)

Recall that the above equation describes the DRB noise intensity spectral density, and thus by multiplying this equation by the squares of the effective area of the core A_{eff} and detector responsivity $\Re$, we obtain the DRB mean square noise current spectral density as

$$i_{DRB}^2(f)=\frac{10}{9}R_{Rb}^2\left(2\alpha L+e^{-2\alpha L}-1\right)P_{re}^2\Re^2\,\Im\left[\overline{\left(1+\frac{m(t)m(t+\tau)}{4}\right)}^2\,\overline{\left|e^{j2\pi\int_t^{t+\tau}\gamma\cdot I_p\cdot m(\zeta)d\zeta}\right|}^2\right]$$

(3.9)

Using the time-average relation below:

$$\overline{\cos\left(2\pi f_i t+\theta_i\right)\cos\left(2\pi f_j(t+\tau)+\theta_j\right)}=\begin{cases}\frac{1}{2}\cos\left(2\pi f_i\tau\right) & \text{if } f_i=f_j\\ 0 & \text{otherwise}\end{cases}\tag{3.10}$$

and the equivalence of multiplication in time domain and convolution in frequency domain, Eqn. (3.9) becomes

$$i_{DRB}^2(f)=\frac{10}{9}R_{Rb}^2\left(2\alpha L+e^{-2\alpha L}-1\right)P_{re}^2\Re^2\begin{pmatrix}\Im\left(\left(1+\frac{1}{8}\sum_i^{N_{ch}}m_i^2\cos\left(2\pi f_i\tau\right)\right)^2\right)\otimes\\ \Im\left(\overline{\left|e^{j2\pi\int_t^{t+\tau}\gamma\cdot I_p\cdot m(\zeta)d\zeta}\right|}^2\right)\end{pmatrix}$$

$$\cong \frac{10}{9} R_{Rb}^{2}\left(2\alpha L + e^{-2\alpha L} - 1\right) P_{re}^{2} \Re^{2} \left(\begin{array}{l} \Im\left(1 + \frac{1}{4} \sum_{i}^{N_{ch}} m_i^{2} \cos\left(2\pi f_i \tau\right)\right) \otimes \\ \Im\left(\left| e^{j2\pi \int_{t}^{t+\tau} \gamma \cdot I_p \cdot m(\zeta) d\zeta} \right|^{2} \right) \end{array} \right) \qquad (3.11)$$

where ⊗ denotes the convolution. Eqn. (3.11) shows that the noise spectrum can be determined by the convolution of two individual spectra. One is the unit impulse at DC plus a series of impulses at carrier frequencies with magnitude $m_i^2 / 4$, and the other is the spectrum generated due to laser chirping, which is described by the exponential term. Since the bandwidth of this chirped spectrum is relatively wide and typically exceeds the highest frequency component of the impulses, these impulses at carrier frequencies can be ignored in calculating the convolution to a good approximation. Then, Eqn. (3.11) can be further simplified to

$$i_{DRB}^{2}(f) = \frac{10}{9} R_{Rb}^{2}\left(2\alpha L + e^{-2\alpha L} - 1\right) P_{re}^{2} \Re^{2} \Im\left(\left| e^{j2\pi \int_{t}^{t+\tau} \gamma \cdot I_p \cdot m(\zeta) d\zeta} \right|^{2} \right) \qquad (3.12)$$

However, for the case of small chirp or chirpless systems, these impulses may have an impact on the calculation and must be included. Their effects will be thoroughly analyzed in a subsequent section dealing with externally modulated systems.

If Eqn. (3.12) is rewritten as

$$i_{DRB}^{2}(f) = \frac{10}{9} R_{Rb}^{2}\left(2\alpha L + e^{-2\alpha L} - 1\right) P_{re}^{2} \Re^{2} \Im\left(\left| \begin{array}{l} \cos\left(2\pi \int_{t}^{t+\tau} \gamma \cdot I_p \cdot m(\zeta) d\zeta\right) + \\ j\sin\left(2\pi \int_{t}^{t+\tau} \gamma \cdot I_p \cdot m(\zeta) d\zeta\right) \end{array} \right|^{2} \right) \qquad (3.13)$$

then the term $\overline{j\sin(\cdot)}$ in the new equation can be shown, as in Appendix C, to be zero, yielding

$$
\begin{aligned}
i_{DRB}^{2}(f) &= \frac{10}{9} R_{Rb}^{2}\left(2\alpha L + e^{-2\alpha L} - 1\right) P_{re}^{2} \Re^{2} \Im\left[\left(\overline{\cos\left(2\pi \int_{t}^{t+\tau} \gamma \cdot I_p \cdot m(\zeta) d\zeta\right)}\right)^{2}\right] \\
&= \frac{10}{9} R_{Rb}^{2}\left(2\alpha L + e^{-2\alpha L} - 1\right) P_{re}^{2} \Re^{2} \cdot \\
&\qquad \Im\left[\overline{\cos\left(2\pi \int_{t}^{t+\tau} \gamma \cdot I_p \cdot m(\zeta) d\zeta\right)}\right] \otimes \Im\left[\overline{\cos\left(2\pi \int_{t}^{t+\tau} \gamma \cdot I_p \cdot m(\zeta) d\zeta\right)}\right]
\end{aligned}
\tag{3.14}
$$

Note that $\overline{\cos(\cdot)}$ in the above DRB noise spectrum equation is similar to a time-autocorrection of a Wide-Band FM (WBFM) signal, and therefore the rationale used for simplifying a WBFM spectrum in [59] can be applied here as follows. The instantaneous frequency of the WBFM field amplitude is determined by its time-derivative of the argument of the cos function as

$$
f_{inst} = \frac{1}{2\pi} \frac{d\left(2\pi \int_{0}^{t} \gamma \cdot I_p \cdot m(\zeta) d\zeta\right)}{dt} = \gamma \cdot I_p \cdot m(t) \tag{3.15}
$$

Due to the large amount of chirping, the frequency at time t, which is proportional to modulating signal $m(t)$, as stated in Eqn. (3.15), does not change radically, and therefore, its phasor completes many revolutions, and contributes some power at that frequency during a short period of time Δt. Therefore, the overall spectral density has approximately the same form as the probability density function of the modulating signal. Since the modulating signal in SCM systems with numerous channels can be approximately described by a zero-mean Gaussian distribution [60,61] with a standard deviation equal to the rms modulation index μ defined by Eqn. (3.4), the shape of the spectral density is also Gaussian, with its standard deviation σ_f given by

$$\sigma_f = \mu \cdot \gamma \cdot I_p \tag{3.16}$$

As a result, Eqn. (3.14) simply becomes

$$\begin{aligned} i_{DRB}{}^2(f) &= \frac{10}{9} R_{Rb}{}^2\left(2\alpha L + e^{-2\alpha L} - 1\right) P_{re}{}^2 \Re^2 \left(\frac{1}{\sigma_f\sqrt{2\pi}} e^{\frac{-f^2}{2\sigma_f{}^2}} \otimes \frac{1}{\sigma_f\sqrt{2\pi}} e^{\frac{-f^2}{2\sigma_f{}^2}} \right) \\ &= \frac{10}{9} R_{Rb}{}^2\left(2\alpha L + e^{-2\alpha L} - 1\right) P_{re}{}^2 \Re^2 \frac{1}{2\sigma_f\sqrt{\pi}} e^{\frac{-f^2}{4\sigma_f{}^2}} \end{aligned} \tag{3.17}$$

With Eqn. (3.17), the DRB mean square noise current spectral density can be easily determined for directly modulated AM-SCM systems. Also, using Eqn. (3.17) the DRB noise can be expressed in the form of RIN. Since RIN is usually expressed as being single-sided, and the density given by Eqn. (3.17) is double-sided, a multiplying factor of two is required in deriving the DRB RIN as follows:

$$\begin{aligned} RIN_{DRB}(f) &= 2\frac{i^2{}_{DRB}(f)}{P_{re}{}^2\Re^2} \\ &= \frac{10}{9} R_{Rb}{}^2\left(2\alpha L + e^{-2\alpha L} - 1\right) \frac{1}{\sigma_f\sqrt{\pi}} e^{\frac{-f^2}{4\sigma_f{}^2}} \end{aligned} \tag{3.18}$$

A similar expression to Eqn. (3.18) can be found in [6], in which the multipath interference noise, due to discrete reflections, was considered. Also, shown in [12] is another similar expression for DRB RIN in terms of the full width half maximum of the laser optical spectrum under modulation.

3.3.1.1. Comparison of DRB Noise in 1310 nm and 1550 nm Systems

It becomes obvious from Eqn. (3.18) that the spectral shapes of DRB induced noises in 1310 nm and 1550 nm laser systems are the same if the operating conditions and the chirping efficiencies of these two systems are identical. However, due to the higher Rayleigh backreflectance and fiber loss at 1310 nm, the noise spectrum in a 1310 nm system is higher than that of a 1550 nm system. To determine the magnitude ratio of a DRB noise spectrum in 1310 nm systems to a DRB noise spectrum in 1550 nm systems, the following relation can be easily established and used:

$$\Delta N = \frac{R_{Rb,1310}{}^{2}\left(2\alpha_{1300}L + e^{-2\alpha_{1300}L} - 1\right)}{R_{Rb,1550}{}^{2}\left(2\alpha_{1550}L + e^{-2\alpha_{1550}L} - 1\right)} \tag{3.19}$$

where the subscripts denote the wavelengths. Using this equation with the backreflectances and fiber losses listed in Table 3.1, Figure 3.9 shows the ratio as a function of fiber length. It can be seen from Figure 3.9 that the ratio can be as large as 8 dB when short fibers are used in these systems. As the fiber lengths increase, the ratio decreases and finally plateaus at about 6 dB. Therefore, 6-8 dB higher DRB noise for 1310 nm systems compared to 1550 nm systems can be used as a good approximation. Note that it can be easily seen in Section (3.32) that this equation is also valid for externally modulated systems.

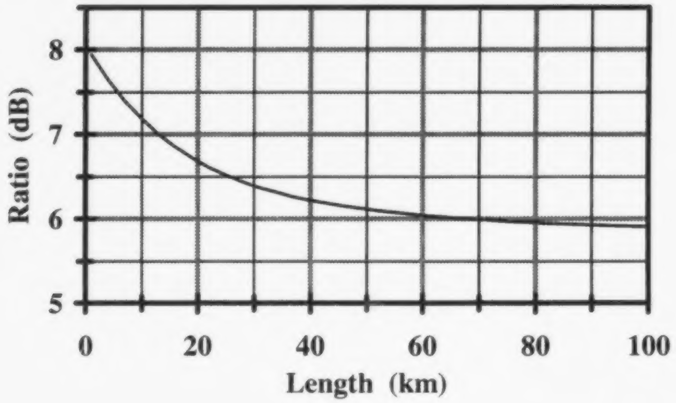

Figure 3.9: The ratio of the DRB noises in 1310 nm to that in 1550 nm systems.

3.3.1.2. Reduction of DRB Impact by Putting Isolators in Link

By breaking down the fiber link into shorter sections with isolators as depicted in Figure 3.10, the DRB impact can be reduced according to the DRB RIN equation (3.18). By comparing a system with M isolators, each separated by a length of L_s, to a system without isolators in link, one can employ Eqn. (3.18) to determine the reduction of DRB noise N_r by the use of isolators as

$$N_r = \frac{(M+1)\left(2\alpha L_s + e^{-2\alpha L_s} - 1\right)}{\left(2\alpha L + e^{-2\alpha L} - 1\right)} \tag{3.20}$$

where L is the total transmission length and which is equal to M+1 times L_s. With this new equation and the losses given in Table 3.1, Figure 3.11 shows the noise reduction versus the total transmission length in 1310 nm and 1550 nm systems with 2, 5 and 8 isolators (or equivalently 3, 6 and 9 isolated sections). This figure indicates that DRB noise can be efficiently reduced by breaking down the fiber with isolators. For example, one can add two isolators into a system to break up the total transmission length into 3 isolated sections. If the total transmission length is 20 km, there will be approximately 2.4

dB and 3.1 dB DRB noise reduction for 1310 nm and 1550 nm systems, respectively. For longer transmission length, more isolators have to be added for the similar noise reduction as shown in Figure 3.11. Note that one must be of course be cognizant of the additional insertion loss of isolators when designing such link.

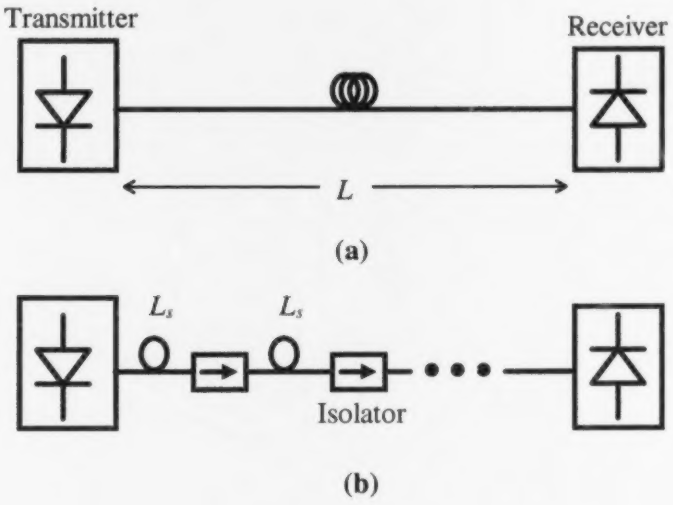

Figure 3.10: Transmission links: (a) without and (b) with isolators.

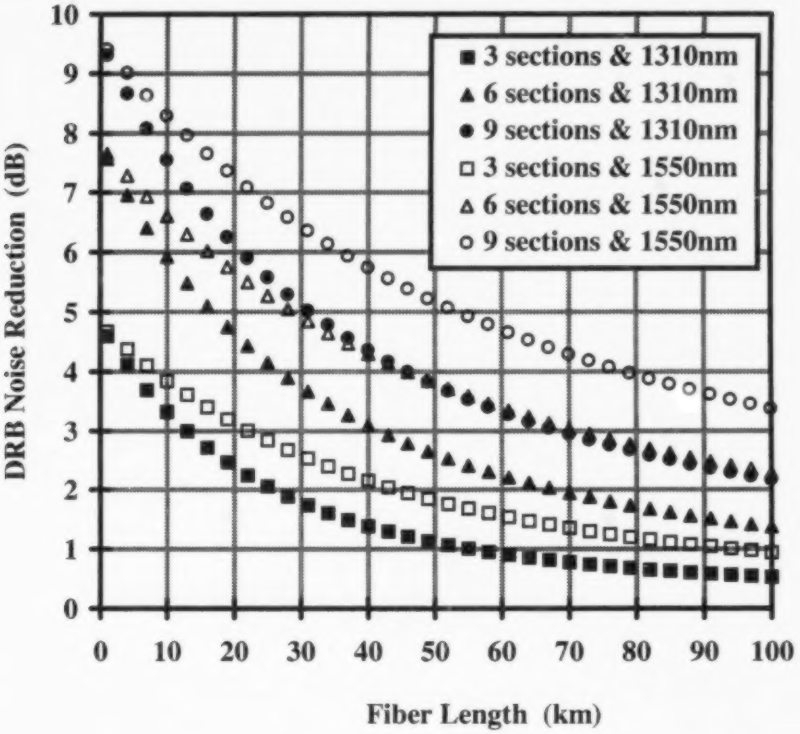

Figure 3.11: DRB noise reduction for 1310 nm and 1550 nm systems with the use of isolators.

3.3.1.3. Spectrum of DRB noise

Using Eqn. (3.18), Figure 3.12 shows the calculated DRB RIN generated from a 50 km fiber in a 42-channel CATV 1550 nm system. Also shown is the corresponding calculated DRB RIN when the general DRB noise expression is used. These calculations use various total rms modulation indices and the parameters tabulated in Table 3.1. The solid lines and symbols denote the calculations using the general DRB noise expression and Gaussian approximation, respectively. With the ratio given in Figure 3.9, the corresponding DRB RIN in a 1310 nm system can be readily deduced from Figure 3.12. For this reason, the DRB RIN in a 1310 nm system is not plotted and can be determined by adding ~6 dB to the results in Figure 3.12. Also note that 23% of the total rms modulation index corresponds to a typical 5% peak modulation index per channel.

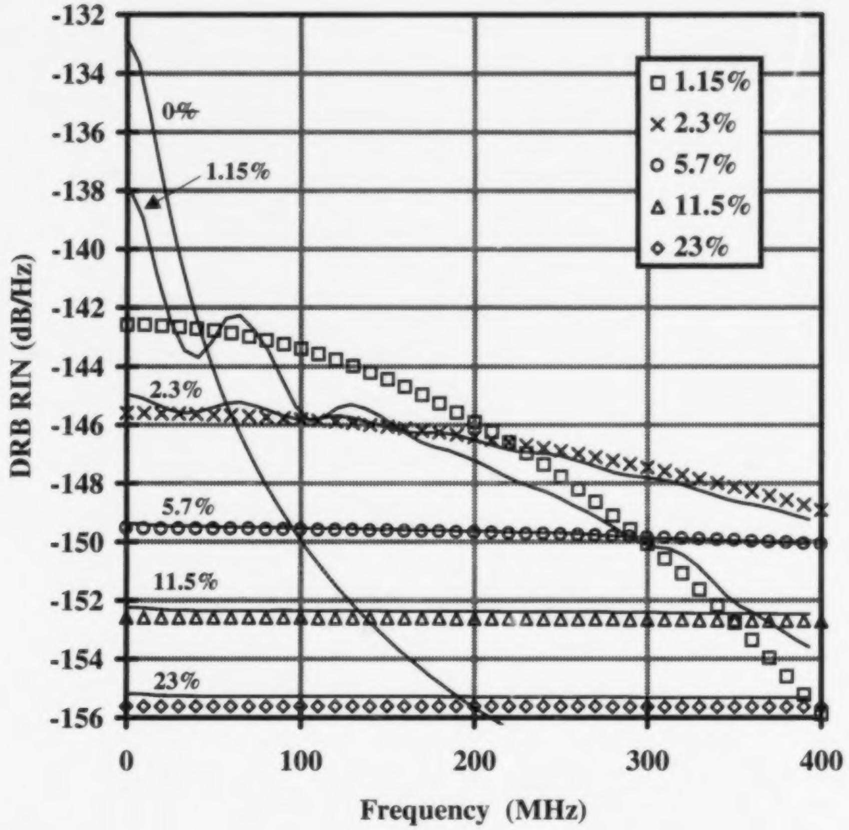

Figure 3.12: Calculated RIN of DRB generated from a 50 km long fiber in 1550 nm system i) using general expression (2.28) denoted by solid lines, ii) using Gaussian approximation (3.18) denoted by symbols. Insets are the total rms modulation indices used in the calculation.

This figure indicates that as one increases the modulation depth, laser chirping will change the noise current spectral density from being determined by the unmodulated laser lineshape to a broad Gaussian shape, and eventually the intrinsic laser phase noise becomes insignificant. It is clear that both the general DRB noise expression and Eqn. (3.18), which has ignored the intrinsic laser phase noise, give essentially the same result for a total rms modulation index larger than about 2.3%, which corresponds to only a 0.5% peak modulation index for each channel in the system under consideration, since these modulation indices provide large enough phase variation due to chirping, as compared to the intrinsic laser phase noise. This figure also indicates that with the chosen parameters, DRB RIN for common lightwave 1310 nm and 1550 nm AM-SCM systems can be as large as -150 dB/Hz and -156 dB/Hz, respectively, which is larger than the intrinsic RIN of many high quality laser diodes in the standard CATV frequency range. In this case, the effect of DRB must be considered when designing such systems. In addition, since the calculated RIN is rather flat over the CATV frequency range, the frequency-dependence on the RIN described by Eqn. (3.18) can be removed, yielding

$$RIN_{DRB} = \frac{10}{9} R_{Rb}{}^{2}\left(2\alpha L + e^{-2\alpha L} - 1\right)\frac{1}{\sigma_f \sqrt{\pi}} \tag{3.21}$$

if the highest CATV channel frequency f_u satisfies the following condition:

$$\frac{f_u}{2\sigma_f} << 1 \tag{3.22}$$

The above simplified equation is frequency-independent and gives less than 0.5 dB difference from the results obtained by applying Eqn. (3.18) and the general DRB noise expression to a typical 42-channel CATV system with 23% rms modulation index, highest CATV channel frequency equal to 337.35 MHz, I_p = 40 mA, and a laser chirp efficiency of only 55 MHz/mA. Therefore, Eqn. (3.18) and (3.21) can be used accurately in most directly modulated AM-SCM systems.

Using the simplified frequency-independent equation with parameters listed in Table 3.1 as well as various chirping efficiencies, Figure 3.13 shows the calculated DRB RIN versus fiber length in 42-channel 1310 nm and 1550 nm systems. These figures illustrate clearly that DRB RIN is strongly dependent on the laser chirping efficiency and fiber length. To prevent DRB from causing serious CNR degradation in CATV systems, the DRB RIN should be as low as -155 dB/Hz; therefore, these figures reveal that the transmission distances for 1310 nm and 1550 nm systems are limited only to 15 km and 45 km, respectively, even though laser diodes with large chirping efficiencies of 200 MHz/mA are used. A detailed study on CNR degradation due DRB noise is presented in the following section.

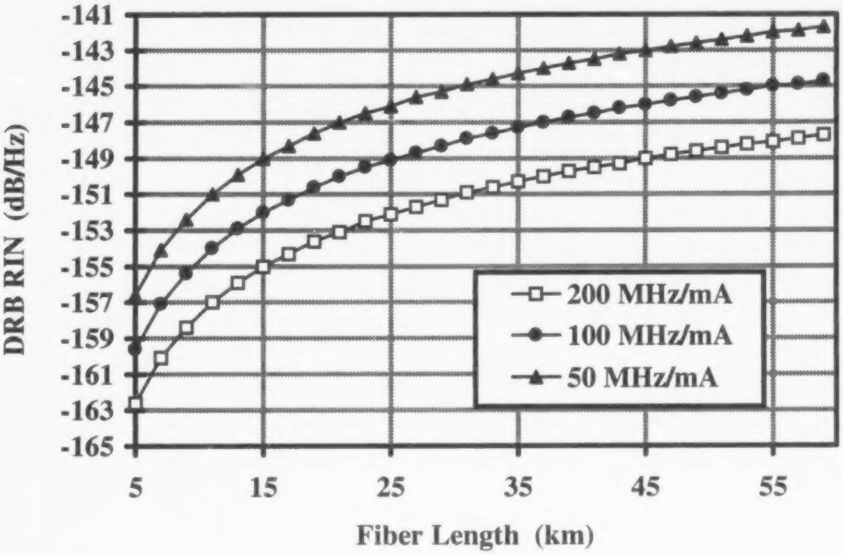

(a)

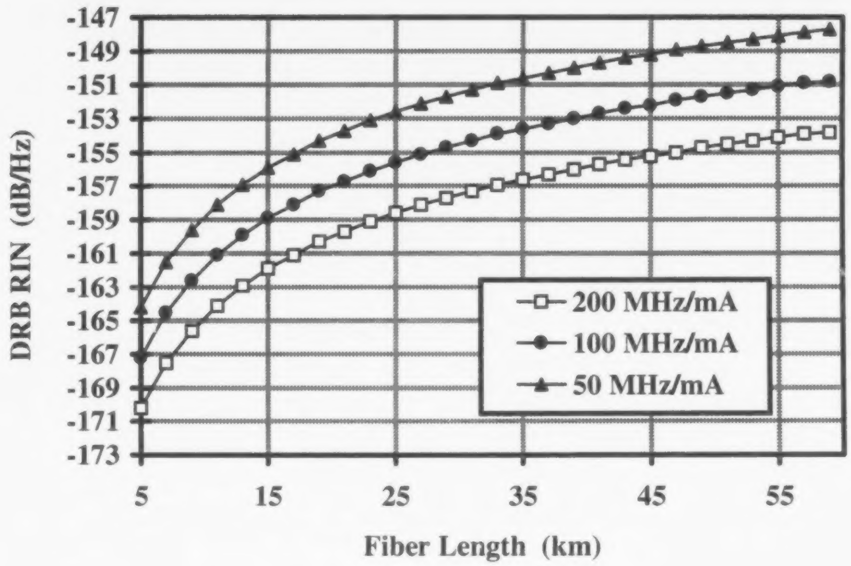

(b)

Figure 3.13: DRB RIN versus fiber length for various chirping efficiencies in (a) 1310 nm and (b) 1550 nm systems.

3.3.1.4. Carrier to Noise Ratio Degradation

3.3.1.4.1. Systems without Optical Amplifiers

Shown in Figure 3.14 is a simple CATV system having one piece of transmission fiber and no optical amplifiers. The CNR expression of channel i for this system, including DRB impact, can be obtained as

$$CNR_i = \frac{0.5(m_i P_{re} \Re)^2}{\langle i_{th}{}^2 \rangle + \langle i_{shot}{}^2 \rangle + \langle i_{laser}{}^2 \rangle + \langle i_{DRB,i}{}^2 \rangle} \tag{3.23}$$

where $\langle i_{th}{}^2 \rangle$, $\langle i_{shot}{}^2 \rangle$, $\langle i_{laser}{}^2 \rangle$ and $\langle i_{DRB,i}{}^2 \rangle$ are the mean square noise currents due to thermal noise, shot noise, intrinsic laser RIN and DRB RIN in channel i, respectively. It should be noted that this CNR expression can also be applied to externally modulated systems without optical amplifiers, which will be discussed later in this chapter.

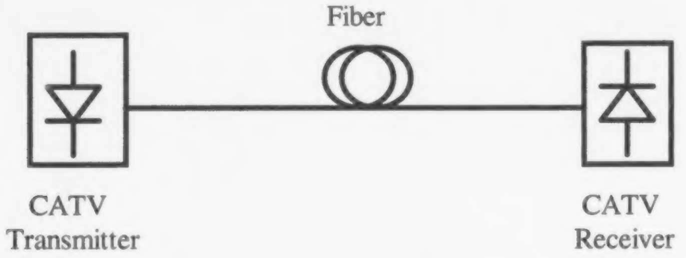

Figure 3.14: A simple CATV transmission.

After integrating Eqn. (3.18), the mean square noise current due to DRB RIN in channel *i* in directly modulated systems with fiber length *L* can be expressed as

$$\begin{aligned}\left\langle i_{DRB,i}{}^2\right\rangle &= P_{re}{}^2\Re^2 \int_{f_i}^{f_i+B_e} RIN_{DRB}(f)df \\ &= P_{re}{}^2\Re^2 \frac{10}{9} R_{Rb}{}^2\left(2\alpha L + e^{-2\alpha L} - 1\right)\left(\operatorname{erf}\left(\frac{f_i + B_e}{2\sigma_f}\right) - \operatorname{erf}\left(\frac{f_i}{2\sigma_f}\right)\right)\end{aligned} \tag{3.24}$$

where $\operatorname{erf}(\cdot)$ is the Error function obtained from integrating the Gaussian spectrum of DRB noise, f_i is the frequency of channel *i*, and B_e is the 4 MHz bandwidth, specified for CNR measurement [49]. Also, the mean square noise currents, due to shot noise and intrinsic laser RIN, can be respectively expressed as

$$\left\langle i_{shot}{}^2\right\rangle = 2q\, P_{re}\, \Re\, B_e \tag{3.25}$$

and

$$\left\langle i_{laser}{}^{2} \right\rangle = RIN_{laser}\, P_{re}{}^{2}\, \Re^{2}\, B_{e} \tag{3.26}$$

where q and RIN_{laser} are the electronic charge and intrinsic laser RIN, respectively. With Eqn. (3.23) to (3.26), the CNR of each channel of a directly modulated system can be determined.

Figure 3.15 depicts the entire CNRs across the CATV spectrum for 50 km fiber systems, employing directly 1310 nm and 1550 nm modulated laser diodes with 50 MHz/mA chirping efficiency, using received optical power as a parameter. The system parameters used in the calculation are tabulated in Table 3.3. This figure illustrates that the CNRs of the directly modulated systems, as earlier revealed in Figure 3.12, are nearly constant, even for a small amount of chirping efficiency. Therefore, results of examination of any one channel should apply to all other channels. However, this may not hold true when more channels are added or when a different CATV frequency allocation plan is used, such that the highest frequency channel is close to the standard deviation σ_f, resulting in the failure of the condition (3.22). Figure 3.15 shows clearly that both systems are degraded by the DRB; however, the 1310 nm system is more seriously affected, due to higher scattering at this wavelength, and cannot satisfy the 50 dB CNR requirement even for large received optical powers, indicating RIN domination. For the 1550 nm system, a received power of about -6 dBm results in approximately 50 dB CNR in the presence of DRB. For instance, using a typical 6 dBm output power laser would yield a system link budget of 12 dB, or equivalently about 50 km.

It should be noted that chirp and chromatic dispersion-induced distortion can limit the transmission lengths in 1550 nm systems, and has not been considered in determining the link budget; however, this distortion can be compensated, by employing either dispersion compensation fiber [53-54] or electronic means [32,62-63]. This distortion can also be made to fall outside the band of interest by upconverting the composite modulating signal to within one octave wide. For illustration, a conventional CATV signal, with channel carriers ranging from 55.25 MHz to 337.25 MHz, can be up-converted by a 400 MHz oscillator to 455.25 MHz to 737.25 MHz. If this new signal is now used to modulate the laser diode, the generated CSO at the receiver will not fall within the signal bandwidth, and therefore can be filtered out by an appropriate bandpass filter. After the filter, the original CSO-free CATV signal can be recovered by down-converting with another 400 MHz oscillator located at the receiver.

Parameters	Symbols	Values
Intrinsic laser RIN	RIN_{laser}	-158 dB/Hz
Chirping efficiency	γ	50 MHz/mA
Receiver noise current density	$\sqrt{\langle i_{th}^2 \rangle} / \sqrt{Hz}$	6 pA/$\sqrt{Hz}$
Responsivity @ 1.54 μm	$\Re$	1.0
Responsivity @ 1.31 μm	$\Re$	0.85
Rayleigh backreflectance @ 1.31 μm	R_{Rb}	-31.5 dB
Rayleigh backreflectance @ 1.54 μm	R_{Rb}	-33.2 dB
Noise bandwidth	B_e	4 MHz
Channel modulation index	m	5%

Table 3.3: Parameters involved in the CNR calculations.

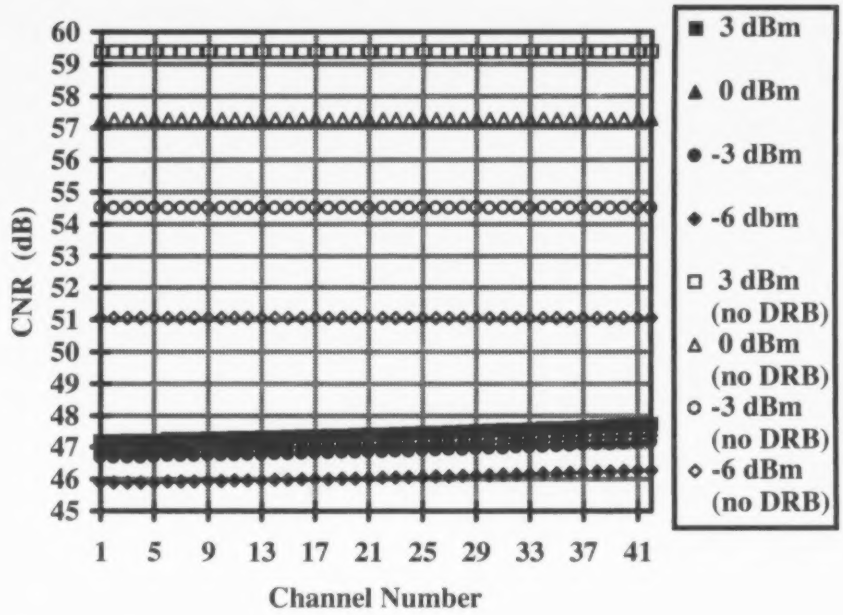

(a)

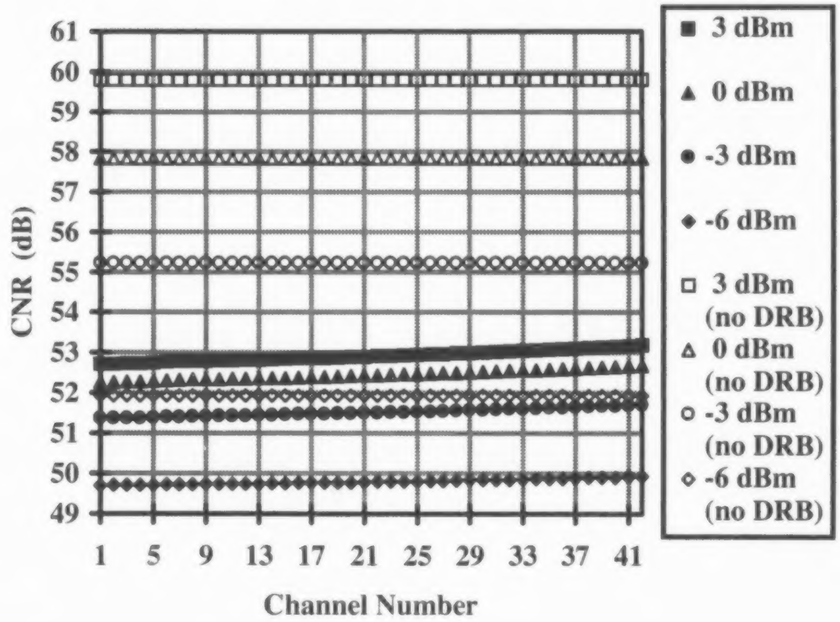

(b)

Figure 3.15: CNR for different received powers in (a) 1310 and (b) 1550 nm systems.

Figure 3.16 depicts the degradation in CNR for channel 2 of 1310 nm and 1550 nm systems in relation to fiber length, using the same chirping efficiency and parameters used in the calculation for Figure 3.15. This figure indicates that at zero fiber length, without any added DRB noise, the CNR at low detected power increases linearly with detected power, thereby indicating shot noise limited detection. At +3 dBm received power, there is a contribution to the total noise from intrinsic laser RIN. As the fiber length increases the system noise becomes more dominated by DRB RIN, as evidenced by progressively smaller improvement in CNR at a fixed distance, as the detected power is allowed to increase from -6 dBm to +3 dBm. Similar to previous results in Figure 3.15, CNRs in 1310 nm are more severely degraded than in 1550 nm. In addition, Figure 3.16 reveals that the 50 dB CNR requirement in 1310 nm systems with short length fibers (10 - 20 km) can be met, which is somewhat confirmed by the existing 1310 nm CATV network.

Recall that this result is calculated for a system without isolators in the link, and since the DRB noise can be reduced by breaking up the total transmission link into isolated sections as shown in Figure 3.11, the CNR, particularly in DRB noise limiting region, can be improved by putting isolators in the link.

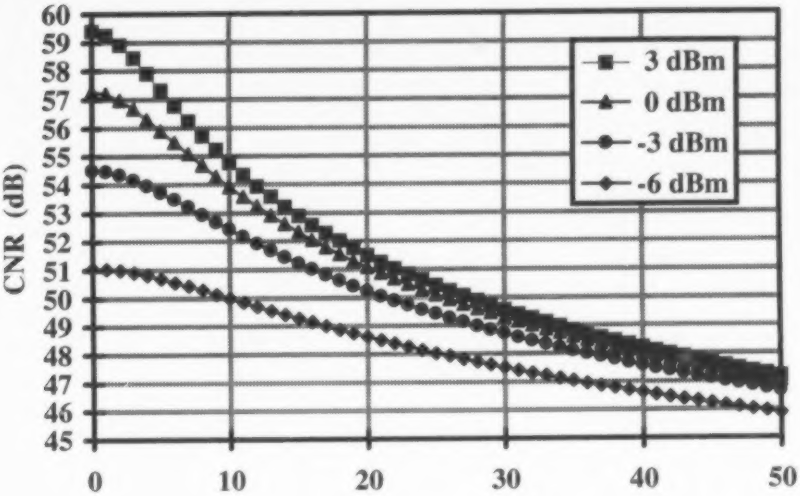

(a)

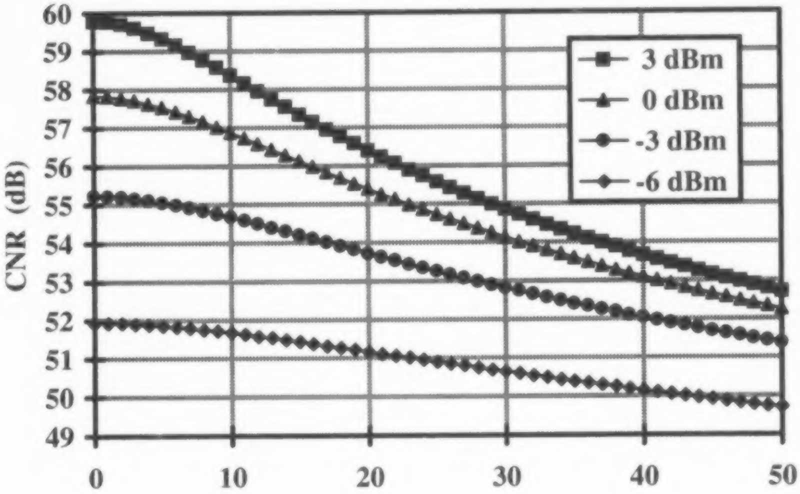

(b)

Figure 3.16: CNR of channel 2 versus fiber length for different received powers in (a) 1310 nm and (b) 1550 nm systems.

Figure 3.17 depicts the effect of chirping efficiency on the CNR of channel 2 for 1310 nm and 1550 nm systems with transmitted fiber length set to 50 km. In this case, the dominant noise source is DRB noise when chirping is small. As chirping increases, the DRB noise spectrum broadens and its spectral density decreases, making its contribution to total system noise negligible. Therefore, instead of employing short fiber to fulfill CNR requirement as mentioned earlier, one can utilize laser diodes with larger chirping efficiencies. For example, by utilizing a laser diode with an approximately 350 MHz/mA chirping efficiency, a detected power of -6 dBm yields 50 dB CNR in a 50 km 1310 nm system, as indicated in Figure 3.17 (a). However, a chirping efficiency of only 70 MHz/mA will be required if the system is operated at 1550 nm.

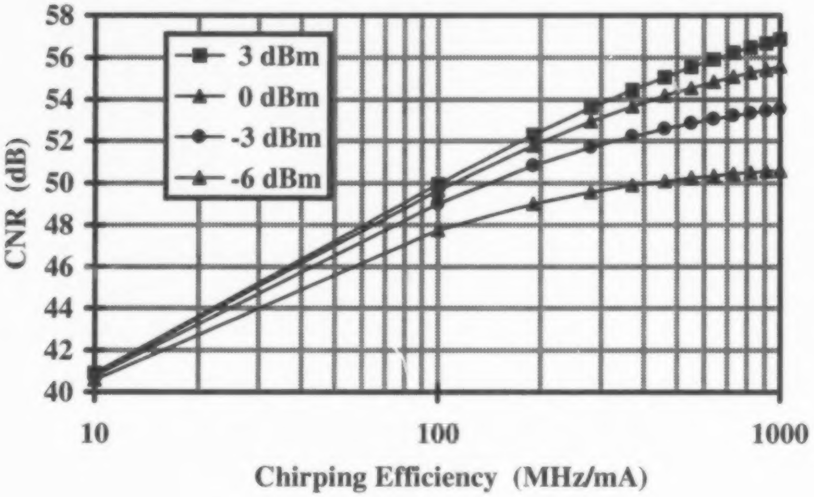

(a)

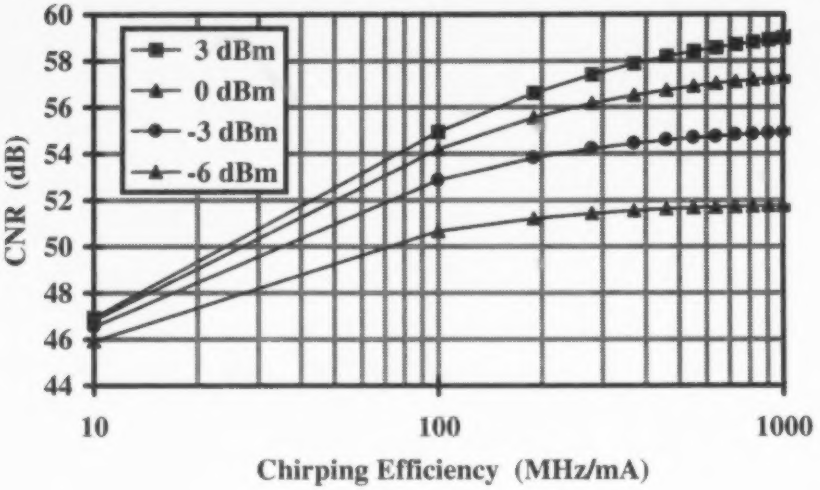

(b)

Figure 3.17: CNR of channel 2 in (a) 1310 nm and (b) 1550 nm systems versus chirping efficiency.

3.3.1.4.2. Systems Utilizing Optical Amplifiers

Uses of optical amplifiers to increase link budgets in 1310 nm [64-65] and 1550 [13,50-54] nm AM-SCM systems have been demonstrated. A typical optically amplified CATV system diagram is shown in Figure 3.18. In this diagram, the system is configured with a post-amplifier and with in-line amplifiers to compensate for the fiber and splitting losses. It is important that uni-directional amplifiers be used to prevent doubly amplified DRB [5,13,66]. Doubly amplified DRB, as shown in Figure 3.19, is similar to DRB within a piece of fiber except that the backscattered signal is now allowed to pass through the amplifier twice and will generate a noise at a receiver which is much larger DRB noise generated within a piece of fiber. With the use of isolators, doubly amplified DRB is eliminated, leaving the system with DRB generated only within isolated fibers. Due to the very stringent CNR requirement in analog CATV applications, the author will only consider amplifiers with isolators; however, amplifiers without isolators will be thoroughly studied and discussed in digital transmission systems in the next chapter.

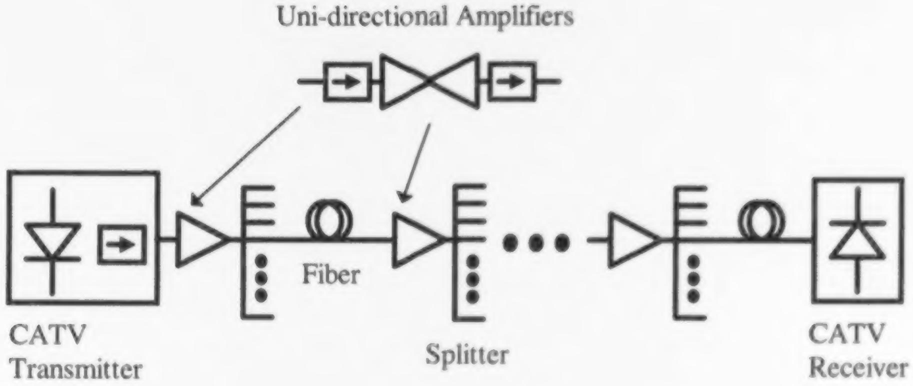
Uni-directional Amplifiers
Fiber
CATV
Transmitter
Splitter
CATV
Receiver

Figure 3.18: A simple CATV system diagram utilizing optical amplifiers.

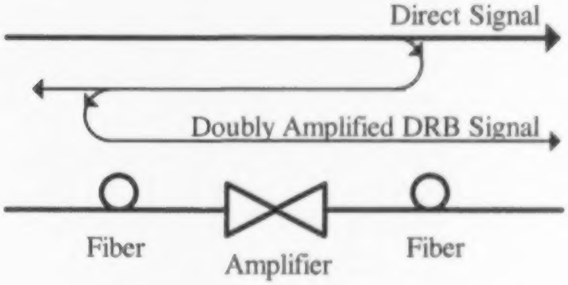
Direct Signal
Doubly Amplified DRB Signal
Fiber
Amplifier
Fiber

Figure 3.19: Doubly amplified DRB.

3.3.1.4.2.1. Noises of Optical Amplifiers

In an optical amplifier, Amplified Spontaneous Emission (ASE) is emitted and its magnitude can be expressed as

$$P_{ASE} = m_t\, n_{sp}\, h\nu (G-1) B_o \tag{3.27}$$

where n_{sp} and G are respectively the spontaneous emission factor and gain of the optical amplifier, m_t is the polarization state parameter, $h\nu$ is the photon energy at the operating wavelength, and B_o is the optical noise equivalent bandwidth. n_{sp} equals 1 for ideal amplifiers, whereas for practical amplifiers it is about 1.3 to 2. m_t equals 1 and 2 for semiconductor and fiber optical amplifiers, respectively. Three inherent noises in receiver will be generated by this ASE. Two of them result from the electric field beating due to the squaring effect of the photodetection. They are known as signal to spontaneous beat noise, which results from the beating of signal and ASE fields, and spontaneous to spontaneous beat noise, which results from the self-beating of ASE field. For receivers without polarizers, the mean square noise currents for signal to spontaneous beat noise and spontaneous to spontaneous beat noise are respectively given by [67,71]

$$\left\langle i_{sig\_sp}{}^2 \right\rangle = \frac{4}{m_t} P_{re}\, P_{ASE,re}\, \Re^2 \frac{B_e}{B_o} \tag{3.28}$$

and

$$\left\langle i_{sp\_sp}{}^2 \right\rangle = \frac{2}{m_t} \left(P_{ASE,re} \right)^2 \Re^2 \frac{B_e}{B_o} \tag{3.29}$$

where $P_{ASE,re}$ is the received ASE power. Another noise generated is the shot noise due to the received ASE power and can be expressed as

$$\left\langle i_{shot}{}^2 \right\rangle = 2\,q\, P_{ASE,re}\, \Re\, B_e \tag{3.30}$$

Note that these noise equations are general and in terms of the received ASE power, and can be applied to any optically amplified systems. For example, in the case of multiple optical amplifier systems, the received power in these equation is replaced by the total accumulated ASE power at the receiver.

In CATV systems, the shot noise due to the received ASE power and noise due to spontaneous to spontaneous beating can be neglected due to the fact that for adequate CNR detection, the required received power needs to be large, making signal to spontaneous beat noise a prominent noise source generated by optical amplifier. In this case, the signal to spontaneous beat noise will only be considered in the following CATV system analysis.

3.3.1.4.2.2. CNR Degradation

CATV systems employing 1310 nm and 1550 nm optical amplifiers will be considered here and both are as depicted in Figure 3.18. In these systems, an optical post-amplifier is employed to boost the signal before transmission. Since the dominant noise in optically amplified CATV systems is the signal to spontaneous beat noise, it is not very beneficial to employ an optical preamplifier in front of the receiver, and therefore, no preamplifiers are included in the analysis. The in-line amplifiers are surrounded by isolators to eliminate the doubly amplified DRB as depicted earlier in Figure 3.19.

The generic CNR expression for CATV systems utilizing M optical amplifiers, can be obtained by modifying the previous CNR expression (3.23) to include the noises added by optical amplifiers and by multiple fiber sections:

$$CNR_i = \frac{0.5\left(m_i P_{re} \Re\right)^2}{\left\langle i_{th}{}^2 \right\rangle + \left\langle i_{shot}{}^2 \right\rangle + \left\langle i_{laser}{}^2 \right\rangle + \left\langle i_{sig\_sp}{}^2 \right\rangle + \sum_{j=1}^{M+1} \left\langle i_{DRB,i,j}{}^2 \right\rangle} \tag{3.31}$$

where $\left\langle i_{DRB,i,j}{}^2 \right\rangle$ is the DRB mean square noise current, due to DRB noise in i channel generated from j^{th} fiber section, and which can be calculated with Eqn. (3.24). It should be mentioned that the amplifiers in this system partition the system fiber L into $M+1$ sections of fiber, each with length $L/(M+1)$; therefore, according to Section (3.3.1.2), the total effect of DRB should be reduced, as compared to a continuous fiber with length L.

If the interstage loss equals the amplifier gain, the total accumulated received ASE power can be calculated as

$$\begin{aligned}P_{ASE,re} &= \Big(m_t\, n_{sp,1}\, hv(G-1)B_o + m_t\, n_{sp,2}\, hv(G-1)B_o + \ldots + \\ &\quad m_t\, n_{sp,M}\, hv(G-1)B_o\Big)\frac{1}{G} \\ &= m_t\left(\sum_{i=1}^{M} n_{sp,i}\right) hv\frac{(G-1)}{G}B_o \\ &= m_t\, n_{sp,tot}\, hv\frac{(G-1)}{G}B_o\end{aligned} \tag{3.32}$$

where $n_{sp,tot}$ is the effective spontaneous emission factor of a chain of amplifiers and is given by the summation of the individual amplifier's spontaneous emission factor. If $G >> 1$, this equation is simplified to

$$P_{ASE,re} = m_t\, n_{sp,tot}\, hv\, B_o \tag{3.33}$$

Then, from Eqn. (3.28) the mean square noise current in the receiver can be expressed as

$$\left\langle {i_{sig\_sp}}^2 \right\rangle = 4P_{re}\, n_{sp,tot}\, hv\, \Re^2 B_e \tag{3.34}$$

From the above equation, it becomes clear that the signal to spontaneous beat noise is independent of the polarization state parameter m_t; therefore the following analysis is applicable to systems utilizing semiconductor optical amplifiers and systems utilizing fiber optical amplifiers.

Using Eqn. (3.34), Eqn. (3.24) to (3.26), and the generic CNR expression (3.31), Figure 3.20 shows the theoretical CNRs in channel 2 versus system fiber length L in 1310 nm and 1550 nm optically amplified CATV systems with received powers of -6 dBm, -3 dBm and 3 dBm and various numbers of amplifiers. In the calculation amplifiers with a spontaneous emission factor of 2 are used and the rest of the parameters are the same as those previously used for the non-amplifier systems, listed in Table 3.3. Also, equal interamplifier fiber length is assumed, giving equal DRB contribution from each section. Several important characteristics can be identified in these figures as follows.

In the absence of DRB noise, i.e. at zero fiber length, by comparing the results for the same received powers, it is quickly realized that CNRs are greatly reduced by introducing amplifiers to the system, indicating a significant contribution from signal to spontaneous beat noise. For a received power of -3 dBm and 50 dB CNR detection, only one amplifier can be used in both the 1310 nm and 1550 nm systems, as indicated by the curves with hollowed squares in this figure; however, by increasing the received power to +3 dBm, 50 dB CNR can be obtained with as many as 4 amplifiers in use. Therefore, in optically amplified systems, with the gain provided from the amplifiers, it is often beneficial to use higher received power to compensate for the additional noise added by the amplifiers in order to obtain the required CNR when no amplifiers are used. In this sense, one can use the total amplifier gain minus the increase in received power to restore that CNR to defines the improvement provided by the amplifiers.

As the fiber length increases, the DRB noise starts to contribute to the total system noise, as evidenced by the decrease in CNR. This degradation is much more severe in the 1310 nm system due to higher scattering at this wavelength. For 1310 nm systems requiring 50 dB CNR, the longest possible transmission fiber length with 3 dBm received power changes from about 27 km when no amplifiers are utilized to about 17 km when 4 amplifiers are in use. This reduction is due to the added noise from the amplifiers which decreases the amount of DRB noise that can be tolerated for a particular CNR. Similar reduction occurs in the 1550 nm system as well. However, the 1550 nm system, even with 4 amplifiers, can have as long as 50 km length of fiber and still satisfy the 50 dB CNR requirement. These figures also indicate that optical amplifiers can be used to extend the system reach and coverage. For instance, for a received power of -6 dBm in the 1310 nm system without the utility of amplifiers, the longest possible fiber length is 10 km to satisfy 50 dB CNR; if 3 amplifiers are used and 3 dBm received power is detected, the transmission length is extended to about 20 km and the remaining power budget increased by the utility of amplifiers can be used to compensate the distribution loss for a larger number of subscribers.

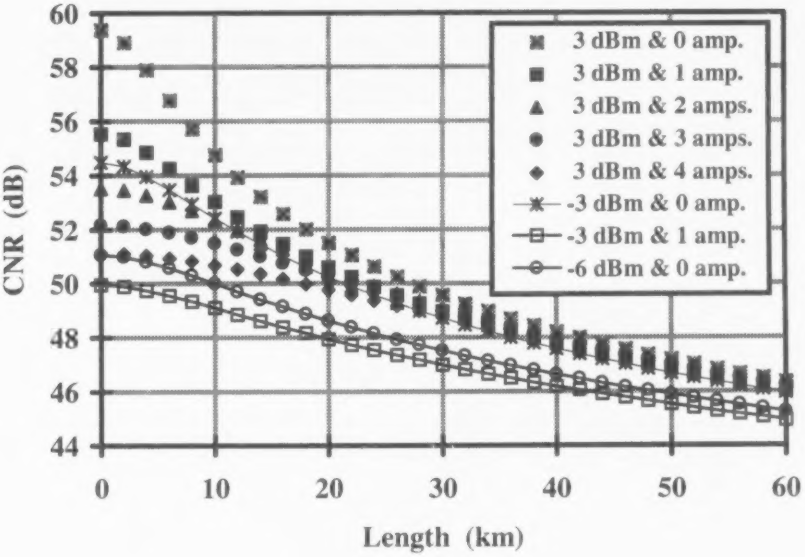

(a)

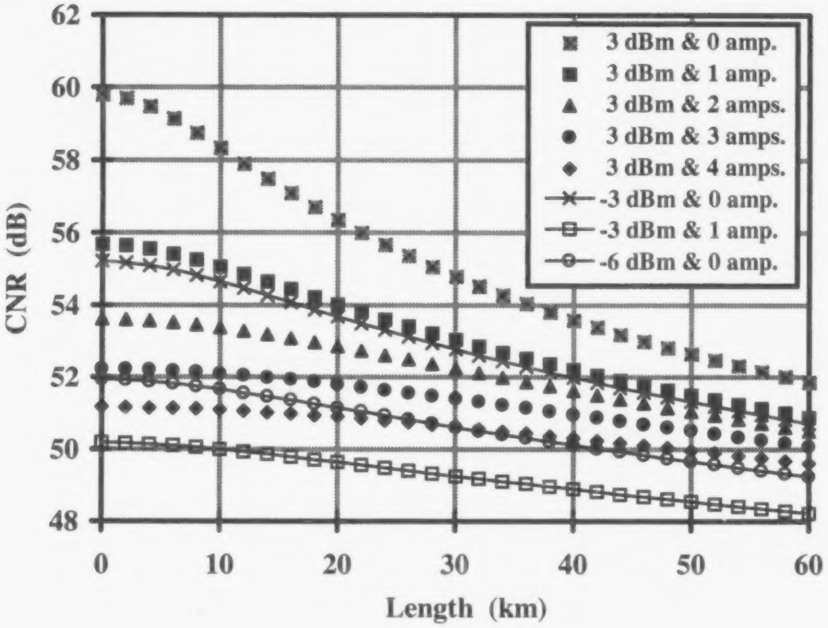

(b)

Figure 3.20: CNR versus fiber length in (a) 1310 nm and (b) 1550 nm systems utilizing optical amplifiers.

3.3.2. Chirpless External Modulation Systems

Now, the DRB impact on systems that employ chirp-free linearized external modulators will be investigated. The analysis here parallels the previous one in direct modulation systems. The DRB noise spectrum will first be derived by applying the general DRB noise expression to externally modulated systems, and then the degradation in CNR will be studied based on this derived noise spectrum. In addition, some practices to combat this DRB harmful effect will also be discussed.

By setting the chirp efficiency $\gamma = 0$ in Eqn. (3.3), the detected normalized electric field amplitude is given by

$$\varepsilon_{dir}(t)=\sqrt{\frac{P_{re}}{A_{eff}}(1+m(t))}\cdot e^{j\phi(t)} \tag{3.35}$$

and after Taylor expanding, the time-autocorrelation function of the laser field can be expressed as

$$R_{\varepsilon_{dir}}(\tau)=\frac{P_{re}}{A_{eff}}\overline{\left(1+\frac{m(t)}{2}-\frac{m(t)^2}{8}+\cdots\right)\left(1+\frac{m(t+\tau)}{2}-\frac{m(t+\tau)^2}{8}+\cdots\right)e^{j2\pi(\phi(t+\tau)-\phi(t))}} \tag{3.36}$$

Since the intrinsic laser phase noise is independent of the signal *m*(*t*), the time average in Eqn. (3.31) can be split, yielding

$$R_{\varepsilon_{dir}}(\tau)=\frac{P_{re}}{A_{eff}}\overline{\left(1+\frac{m(t)}{2}-\frac{m(t)^2}{8}+\cdots\right)\left(1+\frac{m(t+\tau)}{2}-\frac{m(t+\tau)^2}{8}+\cdots\right)}\cdot\overline{e^{j2\pi(\phi(\tau+\tau)-\phi(\tau))}} \tag{3.37}$$

If the second and higher order terms of *m(t)* are ignored due to the small modulation level per channel employed in CATV systems, the detected DRB induced mean square noise current spectral density, obtained by substituting Eqn. (3.37) into the general DRB noise expression (2.28), can be determined in a similar fashion as before, yielding

$$i_{DRB}{}^{2}(f)=\frac{10}{9}R_{Rb}{}^{2}\left(2\alpha L+e^{-2\alpha L}-1\right)P_{re}{}^{2}\Re^{2}\left(\begin{array}{l}\Im\left[1+\frac{1}{4}\sum_{i=1}^{N_{ch}}m_i{}^{2}\cos\left(2\pi f_i\tau\right)\right]\otimes\\ \Im\left[\overline{e^{j2\pi(\phi(t+\tau)-\phi(t))}}\right]\otimes\\ \Im\left[\overline{e^{j2\pi(\phi(t+\tau)-\phi(t))}}\right]\end{array}\right) \tag{3.38}$$

where f_i are the standard Northern America CATV frequencies allocated from 55.25 to 337.25 MHz. Since the Fourier transform of the phase noise term in the above equation resembles the lineshape of the source laser, and since the lineshape of a DFB laser is typically Lorentzian [25,68], the above equation can be expressed as

$$i_{DRB}{}^{2}(f)=\frac{10}{9}R_{Rb}{}^{2}\left(2\alpha L+e^{-2\alpha L}-1\right)P_{re}{}^{2}\Re^{2}\left(\delta(f)+\frac{1}{4}\sum_{i=1}^{N_{ch}}m_i{}^{2}\delta(f-f_i)\right)\otimes\frac{2\Delta v}{\pi\left(\Delta v^{2}+f^{2}\right)} \tag{3.39}$$

where Δv is the intrinsic laser linewidth (full width half maximum). Then the final DRB noise current spectrum and its RIN are given by

$$i_{DRB}{}^{2}(f)=\frac{10}{9}R_{Rb}{}^{2}\left(2\alpha L+e^{-2\alpha L}-1\right)P_{re}\Re^{2}\left(\frac{2\Delta v}{\pi\left(\Delta v^{2}+f^{2}\right)}+\sum_{i=1}^{N_{ch}}\frac{m_i{}^{2}}{4}\frac{2\Delta v}{\pi\left(\Delta v^{2}+\left(f-f_i\right)^{2}\right)}\right) \tag{3.40}$$

and

$$RIN_{DRB}(f) = \frac{10}{9} R_{Rb}{}^{2}\left(2\alpha L + e^{-2\alpha L} - 1\right)\left(\frac{2\Delta\nu}{\pi\left(\Delta\nu^{2} + f^{2}\right)} + \sum_{i=1}^{N_{ch}} \frac{m_i{}^{2}}{4} \frac{2\Delta\nu}{\pi\left(\Delta\nu^{2} + \left(f - f_i\right)^{2}\right)}\right) \tag{3.41}$$

As shown in the above equations, and depicted in Figure 3.21, the detected DRB noise spectrum can be described as a Lorentzian-shaped noise centered at DC, plus a series of Lorentzian-shaped noises centered at the subcarrier frequencies, and scaled by the individual modulation indices of the various channels.

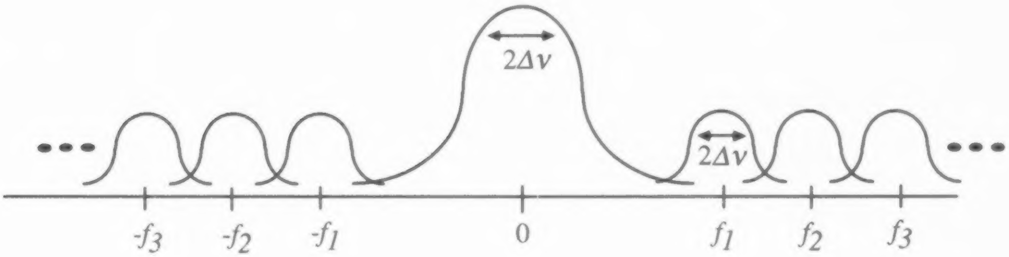

Figure 3.21: A series of Lorentzian-shaped noise spectra at DC and carrier frequencies contributing to the overall DRB noise spectrum.

By summing all the noise contributions from each carrier, Figure 3.22 shows the calculated DRB RIN versus frequency for a 1550 nm system with $L = 50$ km, and various laser linewidths. Using Figure 3.9, located in a previous section dealing with directly modulated systems, the corresponding results for a 1310 nm system can be easily deduced by adding ~6 dB to the calculated DRB RIN in Figure 3.22 in order to account for the higher scattering at this wavelength. Therefore they will not be plotted.

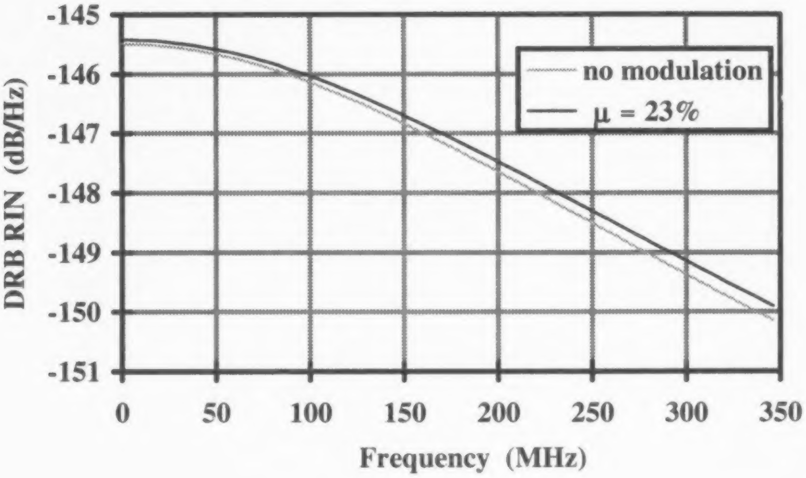

(a) *Δν* = 250 MHz

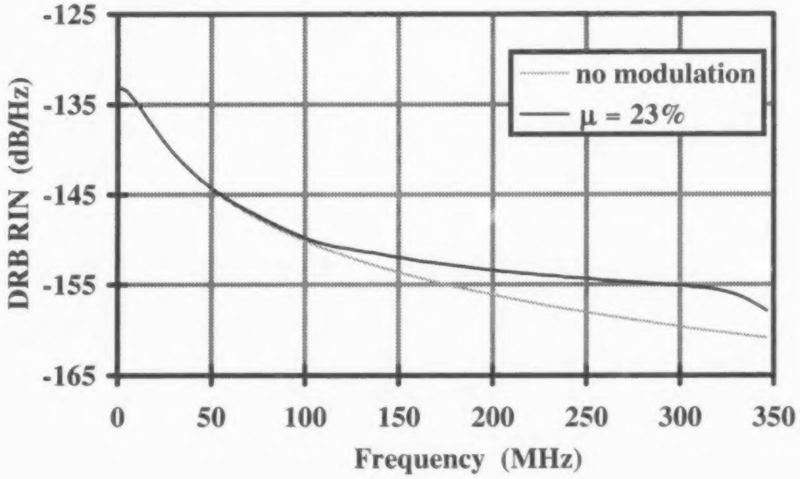

(b) *Δν* =14 MHz

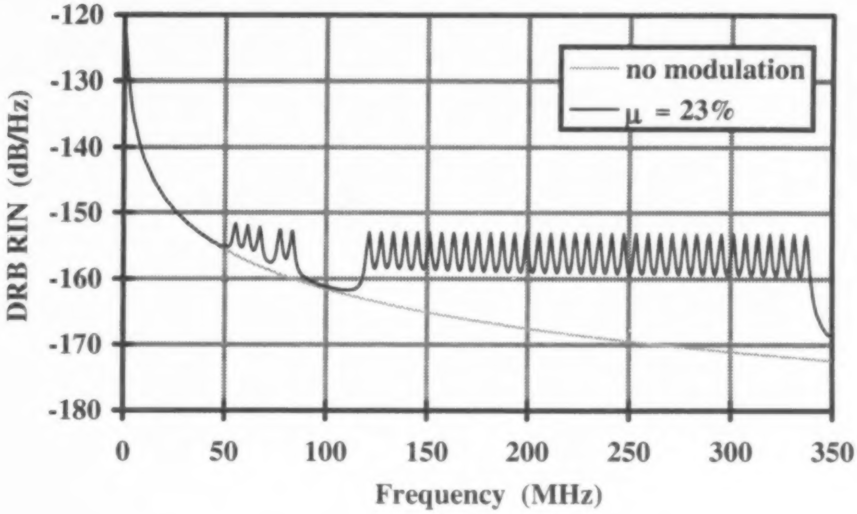

(c) $\Delta\nu$ =1 MHz

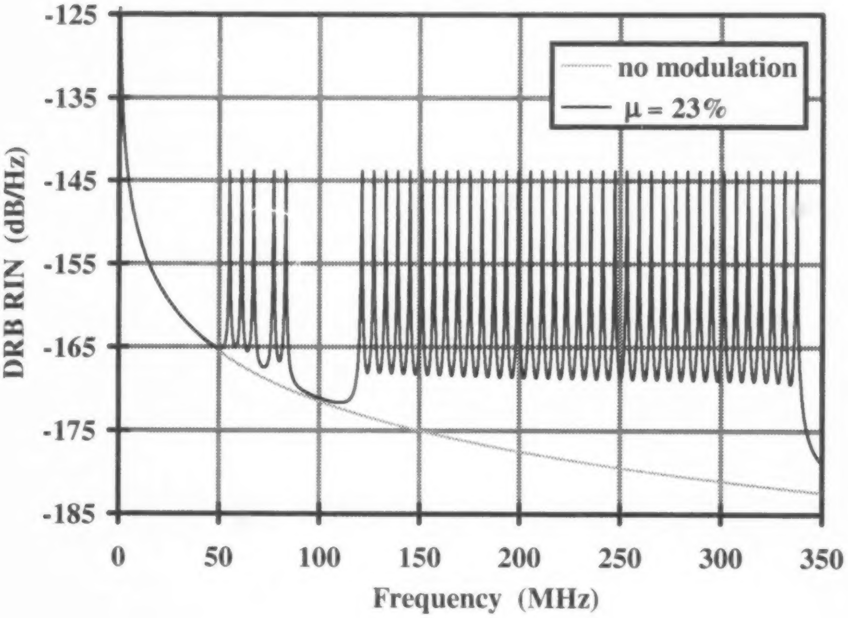

(d) $\Delta\nu$ = 100 kHz

Figure 3.22: Theoretical DRB RIN for a 50 km long 1550 nm CATV system, R_{Rb} = -33.2 dB and a) 250 MHz, b) 14 MHz c) 1 MHz and d) 100 kHz laser linewidths.

This figure indicates that the last term in Eqn. (3.41), i.e. the DRB noise spectrum centered at each subcarrier frequency, contributes significantly to the DRB noise when the source linewidth becomes comparable to or less than the frequency spacing of the CATV carriers. When the linewidth is less than approximately 1 MHz, all of the DRB noise contribution at high channel frequencies comes from the last term. Therefore, depending on the laser linewidth, the Rayleigh backreflectance and the length of fiber, DRB may have a significant impact on systems using chirp-free external modulators and highly coherent lasers, even though the DRB noise centered at DC decays rapidly. This impact in terms of CNR reduction is further explored in the following subsection.

3.3.2.1. Carrier to Noise Ratio Degradation

3.3.2.1.1. Systems without Optical Amplifiers

To determine the performance of an externally modulated AM-SCM system, as depicted in Figure 3.14, which is impacted by DRB, one can calculate the CNR of each channel using the CNR expression (3.23). Similar to previous analyses on directly modulated systems, the DRB noise spectrum in externally modulated systems described by Eqn. (3.40) is integrated over the bandwidth B_e to obtain its contribution to the total system noise, yielding the mean square noise current due to DRB noise in channel i as

$$\left\langle i_{DRB,i}{}^{2}\right\rangle = \frac{10}{9} R_{Rb}{}^{2}\left(2\alpha L + e^{-2\alpha L} - 1\right) P_{re}{}^{2} \Re^{2} \frac{2}{\pi}\left[\tan^{-1}\left(\frac{f}{\Delta\nu}\right) + \sum_{k=1}^{N_{ch}} \frac{m_k{}^{2}}{4} \tan^{-1}\left(\frac{f - f_k}{\Delta\nu}\right)\right]_{f_i}^{f_i + B_e} \tag{3.42}$$

In the above equation, index k is used along with the summation to calculate the DRB contributions from all subcarriers to channel i, and also the DRB noise related to an Arc Tangent function, results from integration of the Lorentzian-shaped DRB noise spectra. By substituting this equation into the CNR expression (3.23), we show in Figure 3.23 the calculated CNRs for 50 km long externally modulated 1310 nm and 1550 nm systems with lasers whose intrinsic linewidth is equal to 1 MHz. Other parameters used for calculation are the same as those of the previous directly modulated system, listed in Table 3.3. Figure 3.24 and Figure 3.25 show the calculated CNR values of the same systems, except that the intrinsic laser linewidth is now increased to 14 MHz and 250 MHz. Also shown in these figures are the CNR values obtained with DRB ignored. From these figures, it becomes clear that the CNR reduction progressively increases as the optical received power increases. Also, with these figures, the following characteristics can be identified.

As seen in Figure 3.23, when the linewidth is narrow and below approximately 1 MHz, CNRs are reduced by DRB noise and are relatively flat across the CATV spectrum except channel 1 to channel 6. This is because as depicted earlier in Figure 3.22.c, the contributions of DRB noise to high channels are similar. This degradation confirms that the up-converted noise spectra, as shown in Figure 3.22.c, are significant and cannot be ignored in determining the CNR. To fulfill the 50 dB CNR requirement for each channel, received powers of about -3 dBm and -6 dBm are needed for the 1310 nm and 1550 nm systems, respectively.

However, as the linewidth in the calculation is increased to 14 MHz and 250 MHz, Figure 3.24 and Figure 3.25 reveal that CNRs are further reduced and that larger reduction occurs at lower channels. This occurs because the DRB noise spectral density centered at DC broadens and contributes most strongly to the low end channels, and this density decreases as the frequency increases, as was previously shown in Figure 3.22.a and b. In this case, the CNRs in lower channels for the 1310 nm system cannot meet the requirement no matter how much received power is used, implying that DRB RIN is both dominating and limiting the CNR. For the 1550 nm system, the CNRs in lower channels can meet the requirement only if a high received power is detected.

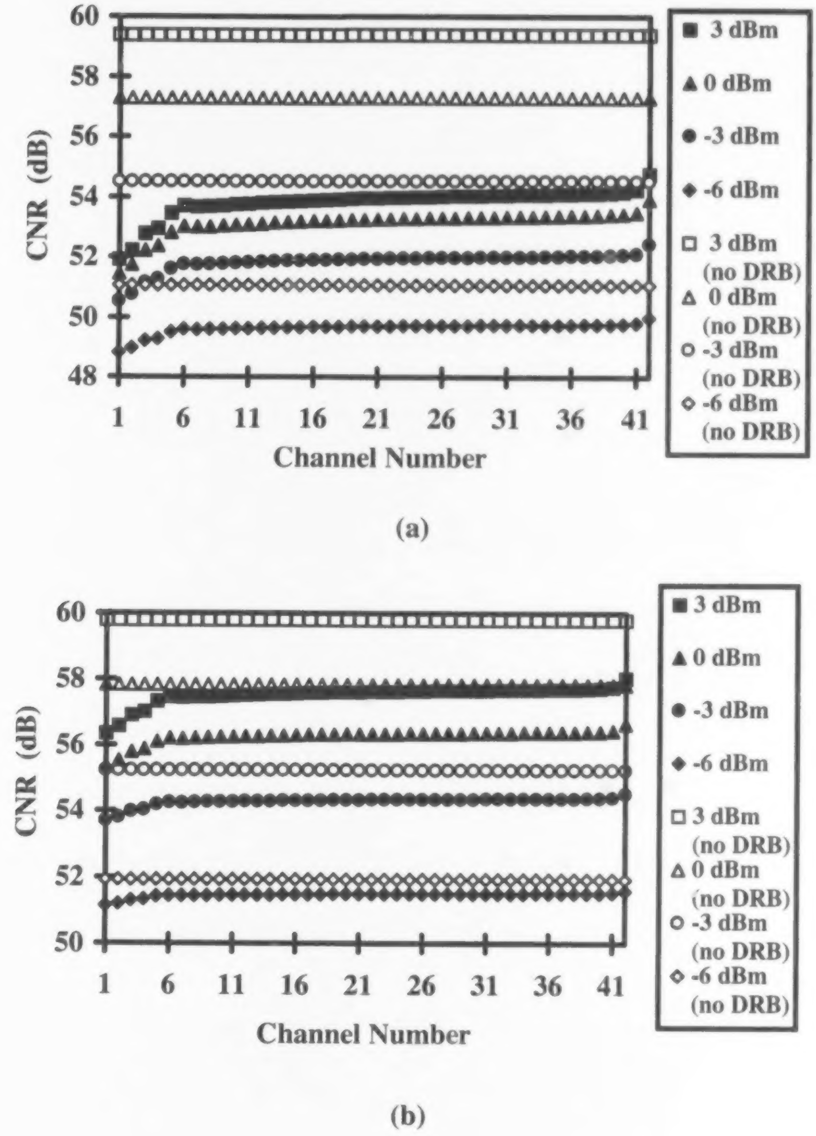

Figure 3.23: Channel CNR for (a) 1310 nm and (b) 1550 nm externally modulated systems with 1 MHz intrinsic laser linewidth and various optical received powers. The solid symbols denote the CNR values with added DRB noise.

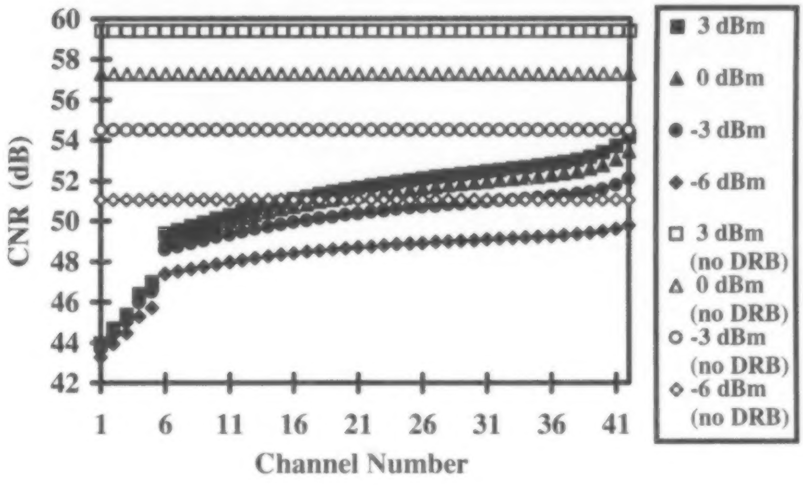

(a)

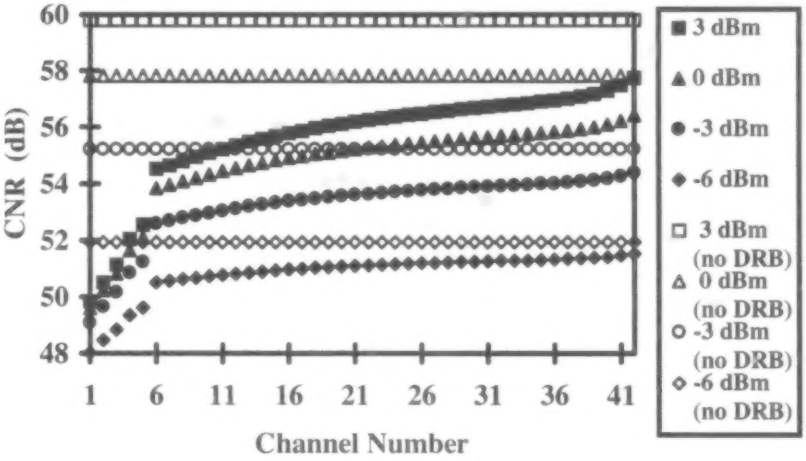

(b)

Figure 3.24: Channel CNR for (a) 1310 nm and (b) 1550 nm externally modulated systems with 14 MHz intrinsic laser linewidth and various optical received powers. The solid symbols denote the CNR values with added DRB noise.

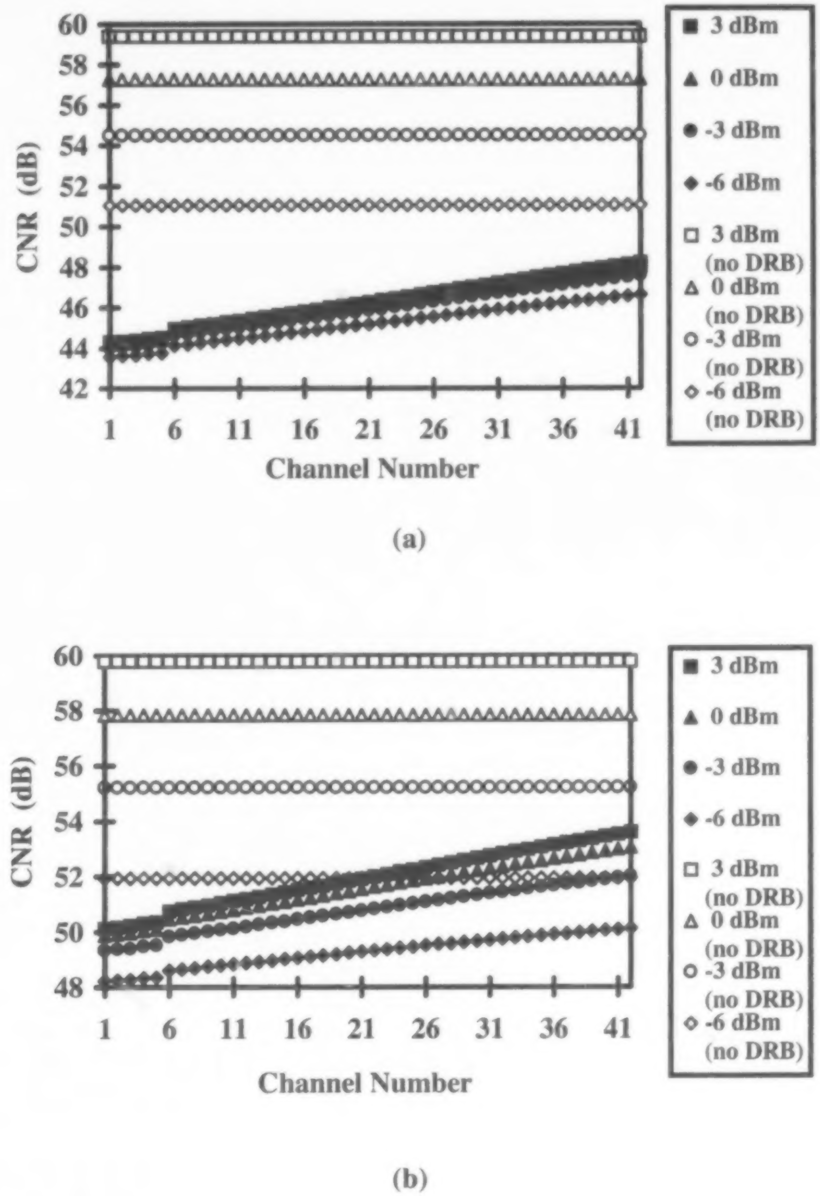

Figure 3.25: Channel CNR for (a) 1310 nm and (b) 1550 nm externally modulated systems with 250 MHz intrinsic laser linewidth and various optical received powers. The solid symbols denote the CNR values with added DRB noise.

To thoroughly examine the CNR in relation to intrinsic laser linewidth, Figure 3.26 shows the calculated CNR values for channels 2, 12, 22, 32 and 42 in 50 km 1310 nm and 1550 nm systems, as the linewidth is allowed to increase from 1 MHz to 10000 MHz. The calculation is done by substituting Eqn. (3.40) into the general CNR expression (3.23) and by using -3 dBm received power. The CNR values obtained with DRB noise ignored are also plotted in this figure. It clearly shows that channels at higher frequencies are less sensitive to DRB noise. In addition, there exists a linewidth value for each channel for minimum CNR, i.e. maximum integrated DRB RIN within the channel. Appendix D shows that by differentiating the DRB noise expression (3.40) to determine the extremities, the minimum value of a CNR occurs when the linewidth is close to its channel carrier frequency. This is further confirmed in this figure. Similar to previous results obtained for directly modulated systems, as the linewidth increases beyond the highest frequency channel, the laser becomes relatively incoherent, which in turn broadens and reduces the DRB noise spectral density, thereby reducing the system degradation due to DRB. To fulfill the 50 dB CNR requirement, the 1310 nm system must use a laser diode with a linewidth less than about 1.5 MHz. On the other hand, the 1550 nm system has less constraint on this linewidth requirement and we can use a laser diode with a linewidth either less than about 10 MHz or larger than about 300 MHz.

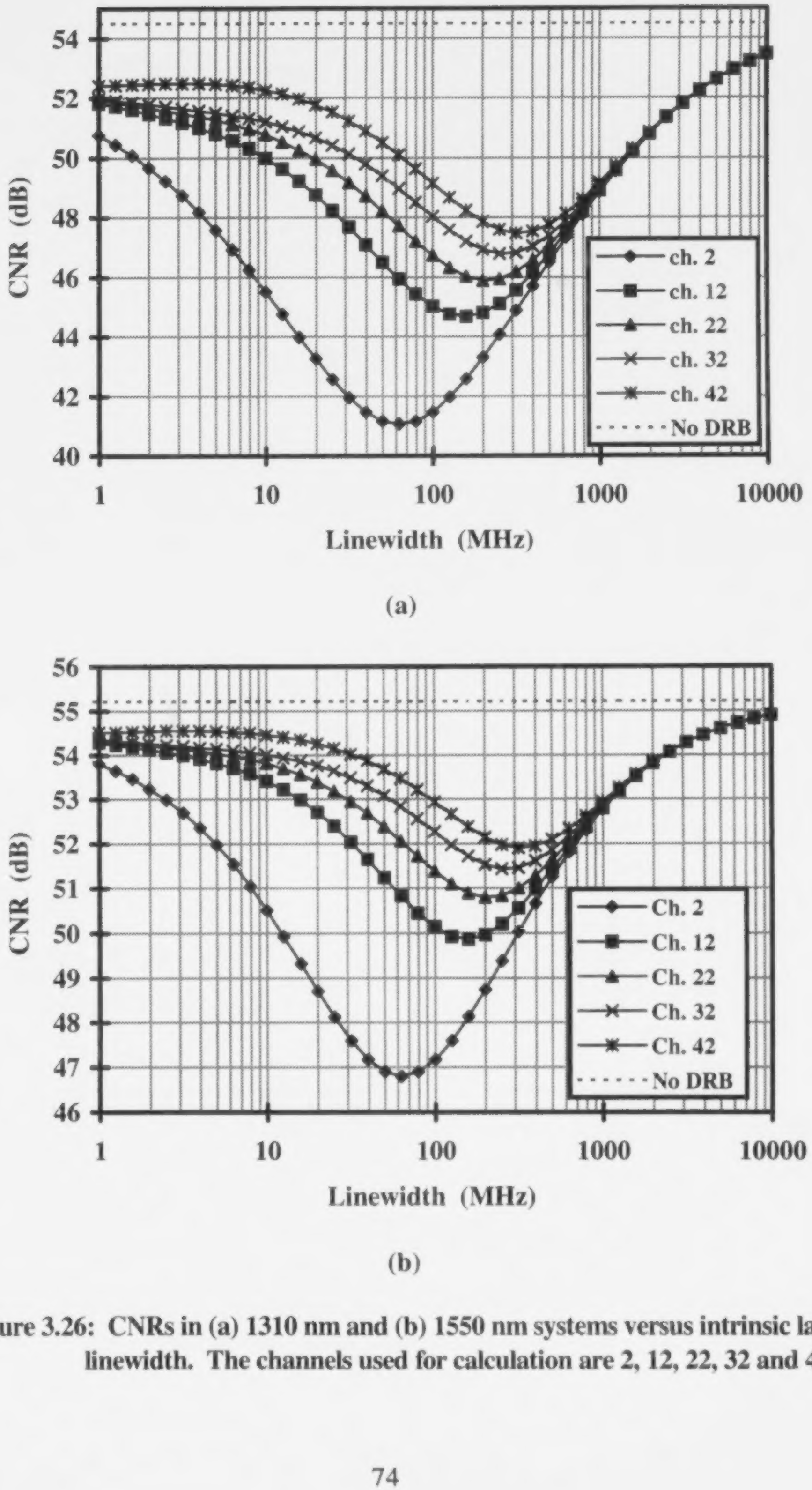

(a)

(b)

Figure 3.26: CNRs in (a) 1310 nm and (b) 1550 nm systems versus intrinsic laser linewidth. The channels used for calculation are 2, 12, 22, 32 and 42.

3.3.2.1.2. Non-Uniform Modulation Indices

As seen in the previous section, for some externally modulated CATV systems, high received powers are required so that the CNRs for low channels can fulfill the requirement. Since the DRB impact is less for high channels, the CNR at high channels will exceed the requirement. In order to reduce the CNR channel dependence caused by DRB, such that the each channel will have the same CNR, one can reduce the coherence of the laser source by using direct modulation, adding a second stage phase modulator [8,70] or applying laser dithering [69-70]. In these cases, by applying the proper amount of phase modulation, the DRB noise spectrum is broadened and reduced across the CATV frequency band.

If chromatic dispersion or distortion induced by the non-flat gain spectrum of the optical amplifier is a limiting factor so that the source coherence cannot be reduced, from an engineering point of view, one can apply non-uniform modulation indices to each channel and use Eqn. (3.23) to obtain the desired overall system CNR. For the previously investigated 1550 nm 42-channel externally modulated CATV system, with an intrinsic laser RIN of -158 dB/Hz, 5% modulation index for each channel (i.e. 23% rms optical modulation index) and a CNR target of 50 dB, the received power required at a 6 $\mathrm{pA}/\sqrt{\mathrm{Hz}}$ noise current density receiver is -7.5 dBm with DRB neglected. If DRB is included, the CNR will be degraded, particularly for the low frequency channels. Figure 3.27 shows the reduced CNR for this system with a fiber length equal to 50 km and a 14 MHz laser linewidth.

To cancel the channel dependence, while keeping the same total rms optical modulation index according to Eqn.(3.4), Eqn. (3.23) can be used in an iterative fashion to determine the required values for m_i for uniform CNRs. Figure 3.27 also shows the determined uniform CNRs and the non-uniform modulation indices m_i after the system has been engineered in this way. This figure indicates that by employing the non-uniform modulation indices, the CNR channel dependence can be completely canceled, and that the overall CNR reduces from 50 dB to 49.2 dB. As expected, the non-uniform modulation indices for low end channels are higher than 5%, whereas the indices for high end channels are lower than 5%.

Similarly, one can use the above engineering method with increased received power to retain original uniform 50 dB CNRs. Figure 3.28 shows the corrected CNRs and the non-uniform modulation indices m_i used to achieve the original uniform 50 dB CNRs. The received power needed to retain the original 50 dB CNRs is determined to be -6.8 dBm, which corresponds to a 0.7 dB increase in optical received power. The above simple example is intended to illustrate that DRB impact on CNRs in external modulation systems can possibly be corrected with non-uniform modulation indices, along with a small amount of power penalty in received optical power.

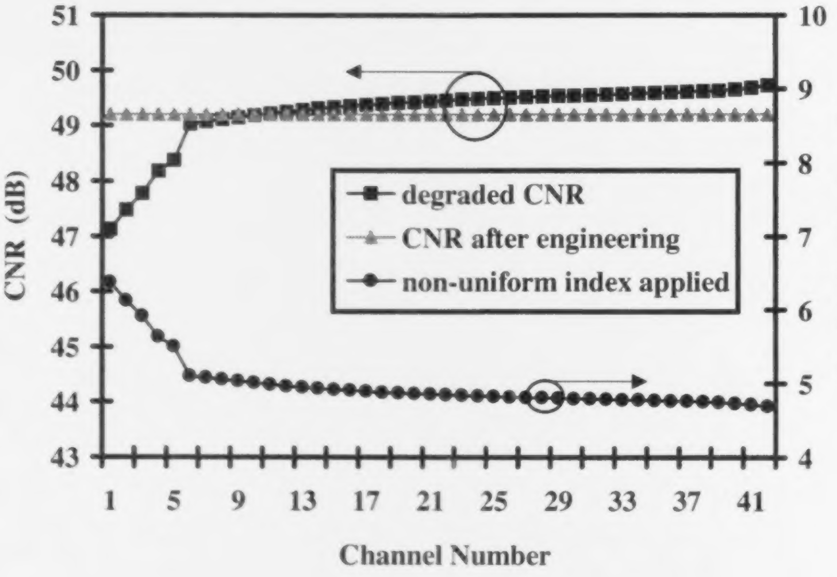

Figure 3.27: **CNR values before and after the non-uniform modulation indices. Also listed are the modulation indices used for obtaining a uniform CNR across the TV spectrum.**

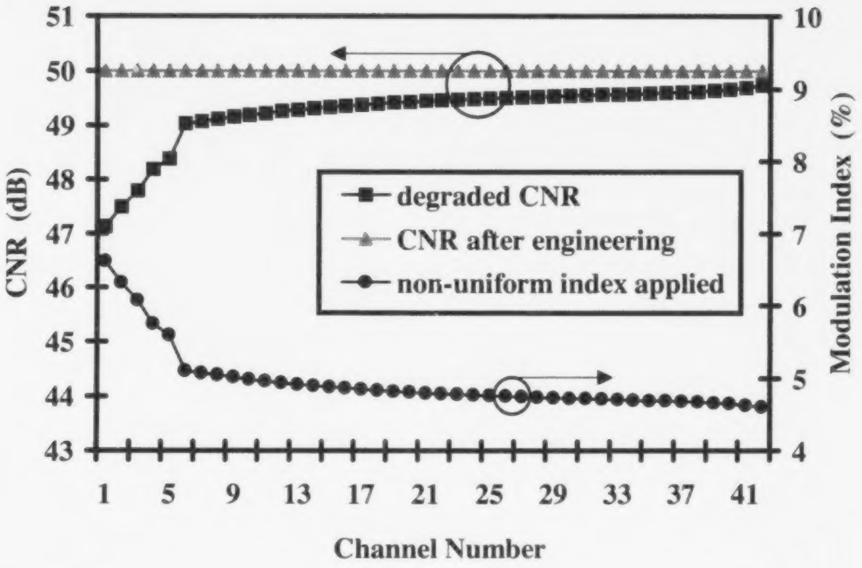

Figure 3.28: CNR values before and after the non-uniform modulation indices and 0.7 dB increase in optical received power have been applied. Also listed are the modulation indices used for retaining 50 dB CNR across the TV spectrum.

3.3.2.1.3. Systems Utilizing Optical Amplifiers

From Figure 3.26, in order to transmit CATV signals in 1300 nm and 1550 nm practically, the intrinsic laser linewidth should be either relatively narrow or relatively wide. To this end, this section will analyze only the impact of DRB on optically amplified externally modulated systems with narrow linewidth laser sources. By substituting the DRB mean square noise current (Eqn. (3.40)) into the generic CNR expression (3.31), the CNR in externally modulated systems, utilizing optical amplifiers as depicted in Figure 3.18, can be calculated. Figure 3.29 shows the calculated CNR for channel 2 as a function of system fiber length in 1310 nm and 1550 nm optically amplified systems with the received power and number of amplifiers as parameters. In the calculation, 1 MHz laser linewidth and n_{sp} of 2 are assumed, and the lowest channel is considered, for it has the worst CNR, as indicated in Figure 3.23.

With zero fiber length, i.e. no DRB, these systems have the same received signal and noises as in the previously analyzed optically amplified directly modulated system. Therefore, as was expected from previous results in Figure 3.20 in the directly modulated systems, the signal to spontaneous beat noise reduces the CNR considerably as revealed in Figure 3.29. In addition, for a received power of -3 dBm and 50 dB CNR detection, only one amplifier can be used in these systems. However, by increasing the received power to +3 dBm, as many as 4 amplifiers can be used.

For 50 dB CNR and 3 dBm received power, the longest possible transmission lengths are about 50 km and more than 60 km for 1310 nm and 1550 nm systems with 3 amplifiers, respectively. Compared to externally modulated systems without amplifiers and with a received power of -6 dBm, these transmission lengths are extended. Therefore, just as the system with direct modulation, optical amplifiers can be used in the system with external modulation to increase its transmission span and distribution coverage.

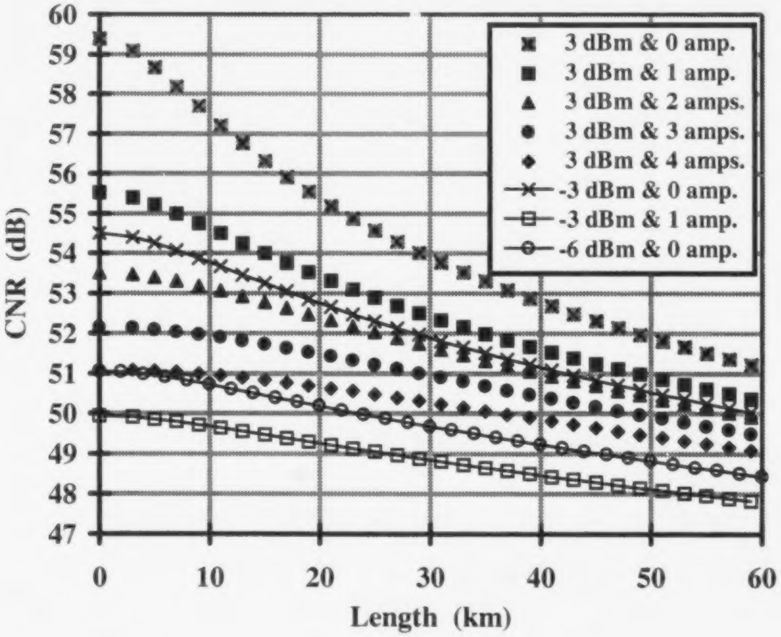

(a)

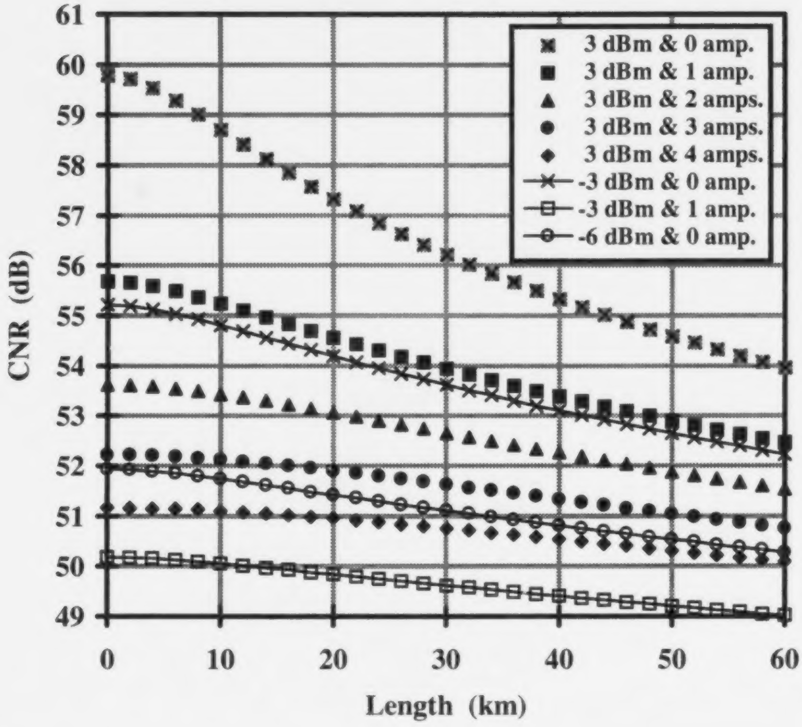

(b)

Figure 3.29: CNR in channel 2 versus fiber length in (a) 1310 nm and (b) 1550 nm systems utilizing optical amplifiers.

Chapter 4

DRB Noise in DIGITAL IM-DD SYSTEMS

Since digital systems can tolerate more noise than analog systems, the DRB effect becomes insignificant in most of the digital systems. However, for systems with an optical amplifier that does not employ any isolators, the noise generated by the doubly amplified DRB of a signal, as shown in Figure 4.1, can be detrimental and limit the usable gain of the amplifier [3,5]. Besides this doubly amplified DRB noise, singly amplified Single Rayleigh Backscattering (SRB) of the backward traveling ASE and doubly amplified DRB of the forward traveling ASE from the optical amplifier also occur as illustrated in Figure 4.2. When systems employ multiple in-line amplifiers, multi-amplified SRB and DRB of ASE and DRB of a signal will also be generated. This occurrence, which increases the total received ASE and noise at a receiver thereby reducing its sensitivity, has not been considered previously.

In conventional uni-directional optically amplified Intensity Modulated-Direct Detection (IM-DD) transmission systems, optical isolators are placed in front and after the amplifiers to restrict the transmission to one direction, so as to eliminate these RB events. However, doing so also makes bi-directional transmission on a single fiber more complicated and involves the implementation of more components.

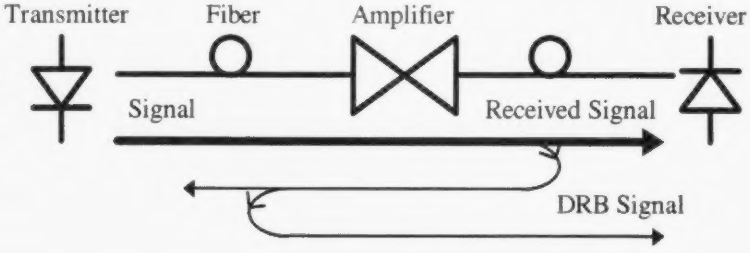

Figure 4.1: DRB of signal in a system using 1 in-line amplifier and no isolators in link.

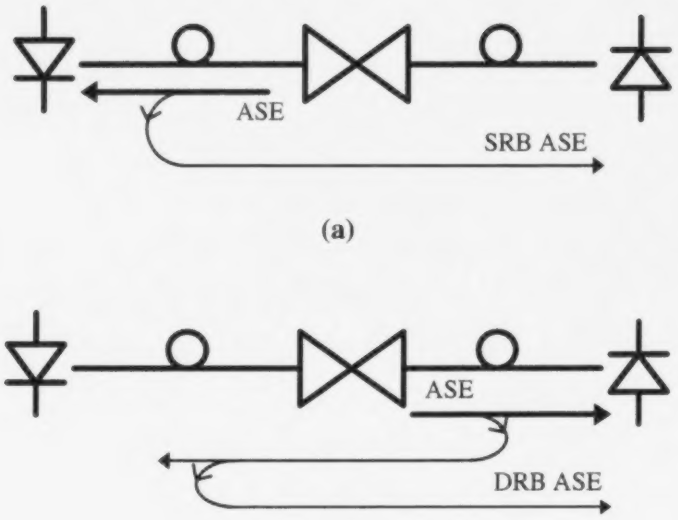

(a)

(b)

Figure 4.2: SRB and DRB of ASE in a system using 1 in-line amplifier and no isolators in link: (a) SRB of ASE and (b) DRB of ASE.

On the other hand, optically amplified systems that do not employ isolators in the link show a potential promise for minimum component requirement and maximum network flexibility. In this chapter, the impact due to Rayleigh scattering on such systems will be investigated thoroughly. To elucidate the context of this writing, the phrase "open cascade of amplifiers" is now used to refer to as a chain of optical amplifiers for which optical isolators are not located between the amplifiers in the chain.

To quantify the detrimental effect due to the multi-amplified SRB and DRB of ASE and DRB of a signal in an open cascade system, a receiver power penalty expression will be derived for the first time. The power penalty, caused by Rayleigh scattering effects, is defined as the relative increase in received optical power that is required to obtain the same Bit Error Ratio (BER) as when Rayleigh scattering is not included in systems. Then, by applying this power penalty equation, BER, total available amplifier gain and power penalty in open cascade systems will be studied. Following this will be a series of OC-48 transmission experiments for the verification of the theoretical work. In addition, to demonstrate the feasibility of bi-directional transmission using an open cascade of optical amplifiers, an experimental comparison of full duplex OC-12 bi-directional transmission open cascade systems to conventional 2 fiber systems is also presented in this chapter. At the end of this chapter, the impact of internal DRB of a signal, which is generated within high scattering optical fiber amplifiers and distributed fiber amplifiers, will also be studied.

4.1. Derivation of Power Penalty

Rayleigh backscattering gives rise to two detrimental effects: (i) DRB noise is referred to as the noise generated by DRB of a signal and, (ii) Rayleigh backscattering of ASE will result in an increase in ASE at the receiver, due to both SRB and DRB of ASE. These two effects are quite different in the sense that DRB noise is a coherent noise, whereas the increase in ASE is incoherent, and can be analyzed on a power basis. This section first determines the total DRB noise in an open cascade system. Secondly, it determines the increase in receiver ASE due to the multi-amplified SRB and DRB of ASE. Finally, by combining these two results, it derives a general receiver power penalty expression accounting for the total impact caused by Rayleigh backscattering. Note that unlike the author's previous work [66], no constraints on the amplifier gain and interamplifier loss will be imposed on the following DRB noise and increase in ASE derivation.

4.1.1. DRB Noise of Signal

4.1.1.1. Single In-Line Optical Amplifier

Consider a simple system with a single in-line amplifier without any optical isolators. There are 3 generic DRB mechanisms in this system as Figure 4.3 illustrates: 1) both backscattering events occur before the amplifier, 2) both backscattering events occur after the amplifier and 3) the first backscattering event occurs after the amplifier and the second occurs before the amplifier. Generally, the third mechanism is the most dominant DRB noise contribution due to the large amplification of the amplifier. By modifying Eqn. (2.7), the doubly amplified doubly Rayleigh backscattered field can be expressed as

$$\varepsilon_{DRB}(t,L) = G \sum_{n=\frac{L_b}{\Delta l}}^{\frac{L}{\Delta l}} \sum_{m=1}^{\frac{L_b}{\Delta l}-1} \varepsilon_{dir}\left(t-2\frac{(n-m)\Delta l}{v},L\right) e^{-\left(\frac{\alpha}{2}+j\beta\right)2(n-m)\Delta l} \Delta\rho_m \Delta\rho_n \qquad (4.1)$$

where G is the net optical power gain of the amplifier, L_b is the fiber length before the optical amplifier and L is the total fiber length.

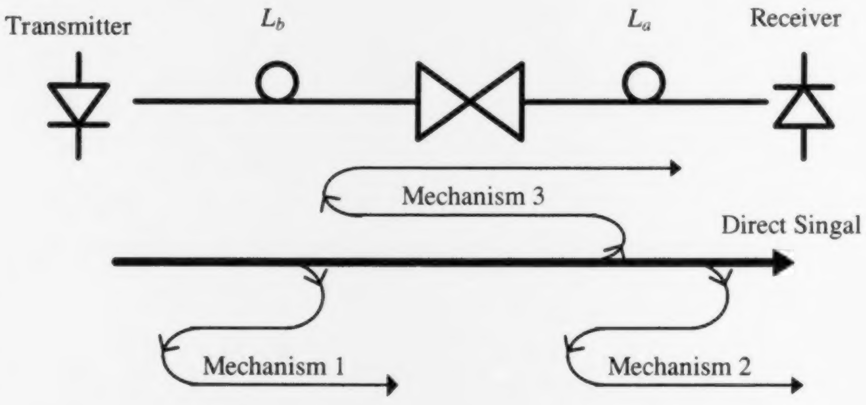

Figure 4.3: Different DRB mechanisms in a single in-line amplifier system without using isolators.

Since the amplifier does not change the statistical properties used previously in deriving DRB noise, the derivation parallels that of chapter 2, yielding the DRB mean square noise current spectral density, including the effects of the backscattering mechanisms 1, 2 and 3:

$$i_{DRB}^2(f) = \frac{10}{9} R_{Rb}^2 \Re^2 A_{eff}^2 \begin{pmatrix} \left(2\alpha L_b + e^{-2\alpha L_b} - 1\right) + \left(2\alpha L_a + e^{-2\alpha L_a} - 1\right) \\ + \left(1 - e^{-2\alpha L_b}\right)\left(1 - e^{-2\alpha L_a}\right) G^2 \end{pmatrix} \Im \left\langle \left| R_{\varepsilon_{dir}}(\tau) \right|^2 \right\rangle \tag{4.2}$$

where L_a is the fiber length after the amplifier. The first two terms inside the bracket are due to the DRB mechanisms 1 and 2, and the last term, which is proportional to the square of the amplifier gain, is derived from mechanism 3. Again, this equation is general and is given in terms of the time-autocorrelation of the received electric field. In the special case where L_b, $L_a \rightarrow \infty$, the source is not modulated and the complete depolarization is assumed, the equation reduces to that of Gimlett *et al.* [5].

To compare the contributions from these three different mechanisms, Figure 4.4 shows the calculated values of the three terms inside the bracket of Eqn. (4.2) as a function of fiber length. In the calculations, L_b and L_a are the same, and both have a typical loss of 0.25 dB/km, and a moderate amplifier gain of 13 dB is utilized. Two important characteristics can be identified. First, all the contributions from Mechanisms 1, 2 and 3 increase substantially at short fiber lengths. However, the effect of mechanism 3 levels off beyond 20 km of fiber. In a typical range of fiber lengths that commonly appear between in-line amplifiers, which is approximately 40 km to 100 km, the contribution due to mechanism 3 is independent of the fiber length and significantly dominates the contributions due to mechanisms 1 and 2. Secondly, for higher amplifier gains, this domination will further strengthen; therefore, one can conclude that in systems utilizing open cascade amplifiers, each with a practical amplifier gain, the effects of mechanisms 1 and 2, and the length dependence, can be neglected to a good approximation, as

$$\begin{aligned} i_{DRB}^2(f) &\approx \frac{10}{9} R_{Rb}^2 \Re^2 A_{eff}^2 \left(1 - e^{-2\alpha L_b}\right)\left(1 - e^{-2\alpha L_a}\right) G^2 \Im \left\langle \left| R_{\varepsilon_{dir}}(\tau) \right|^2 \right\rangle \\ &\approx \frac{10}{9} R_{Rb}^2 \Re^2 A_{eff}^2 G^2 \Im \left\langle \left| R_{\varepsilon_{dir}}(\tau) \right|^2 \right\rangle \end{aligned} \tag{4.3}$$

There is only one significant DRB mechanism in a single in-line amplifier system, and from the above equation, the DRB noise due to this mechanism can be determined by the products of the Rayleigh backscattering reflectance of the fibers (R_{Rb}^2) that have backscattered the signal, and the gain (G^2) that the backscattered signal experiences during the round trip between backscattering. Similarly, the DRB noise generated by each DRB event in a system employing many in-line amplifiers can also be determined. By summing of all these DRB noises, the total DRB noise for such a system can be calculated, as shown in the following subsection.

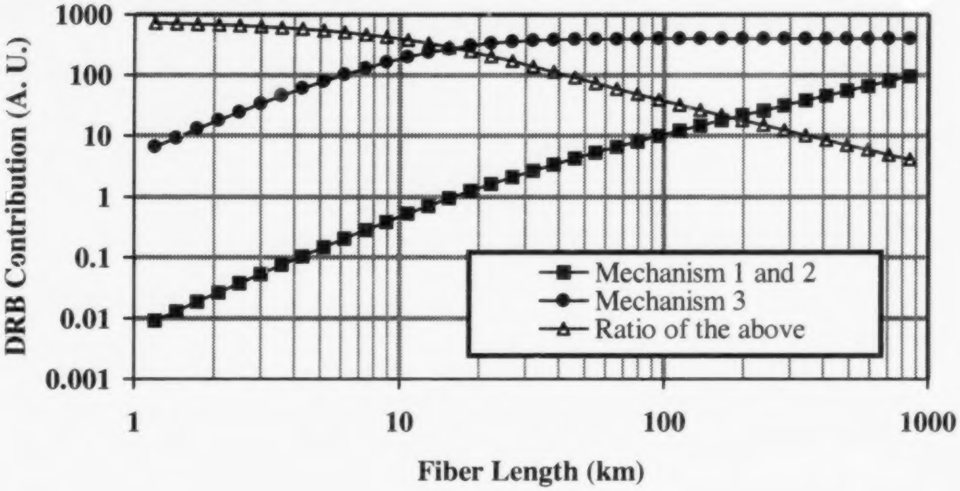

Figure 4.4: Comparison of the contributions due to the three different mechanisms of DRB of a signal in a single in-line amplifier link.

4.1.1.2. Open Cascade of Optical Amplifiers

To derive the total DRB noise for systems with open cascades of multiple optical amplifiers, we consider a system as depicted in Figure 4.5. The system has N identical amplifiers and N+1 fibers, each with the identical Rayleigh backscattering reflectance and fiber loss IL.

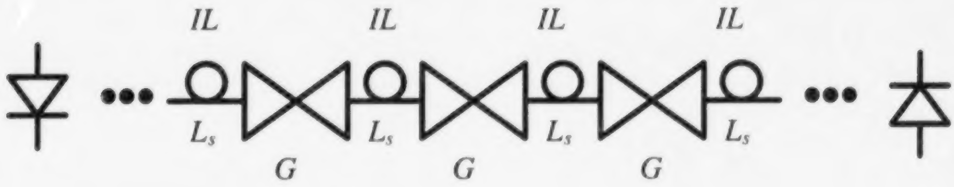

Figure 4.5: An open cascade system with *N* identical in-line amplifiers and *N*+1 interconnecting fibers.

The total DRB noise is composed of *N* contributions that have traveled around one amplifier as depicted in Figure 4.6, plus the *N-1* contributions that have traveled around two amplifiers and one interamplifier loss as depicted in Figure 4.7, plus *N-2* contributions that have traveled around three amplifiers and two interamplifier losses as depicted in Figure 4.8 and so on. This gives rise to the following expression:

$$i_{DRB}{}^2(f) = \frac{10}{9} R_{Rb}{}^2 \Re^2 A_{eff}{}^2 \begin{pmatrix} NG^2 + (N-1)G^4 IL^2 + (N-2)G^6 IL^4 + \cdots + \\ G^{2N}\, IL^{2(N-1)} \end{pmatrix} \Im\left\langle \left| R_{\varepsilon_{dir}}(\tau) \right|^2 \right\rangle$$

$$= \frac{10}{9} R_{Rb}{}^2 \Re^2 A_{eff}{}^2 \left[G^2 \sum_{i=1}^{N} i \left(G\, IL \right)^{2(N-i)} \right] \Im\left\langle \left| R_{\varepsilon_{dir}}(\tau) \right|^2 \right\rangle \tag{4.4}$$

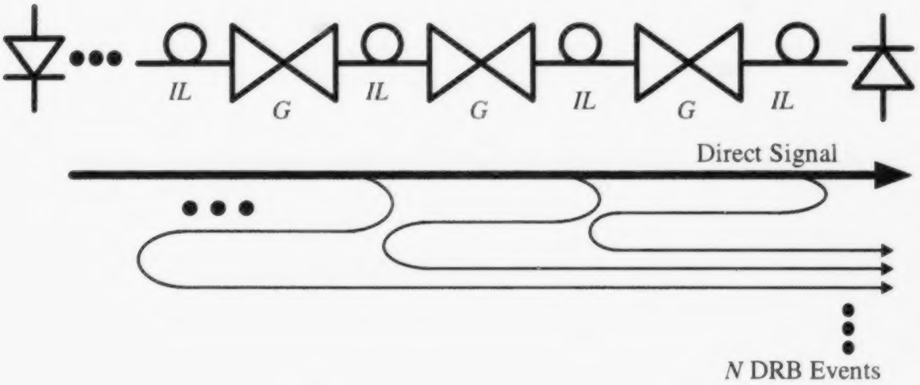

Figure 4.6: DRB signal which travels around *one* amplifier.

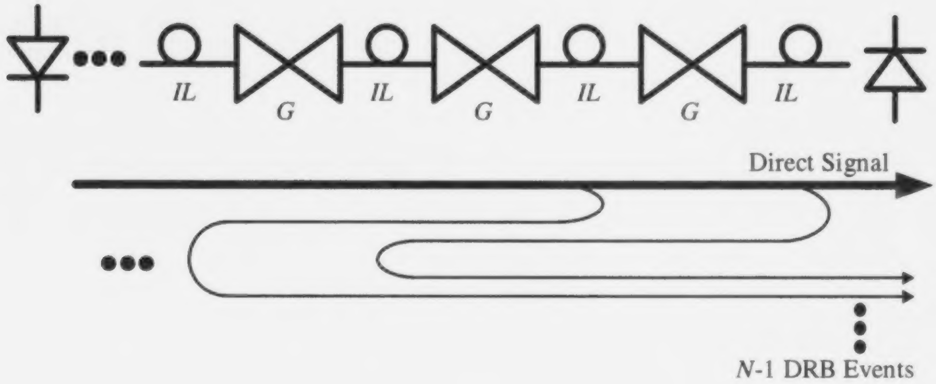

Figure 4.7: DRB signal which travels around *two* amplifiers.

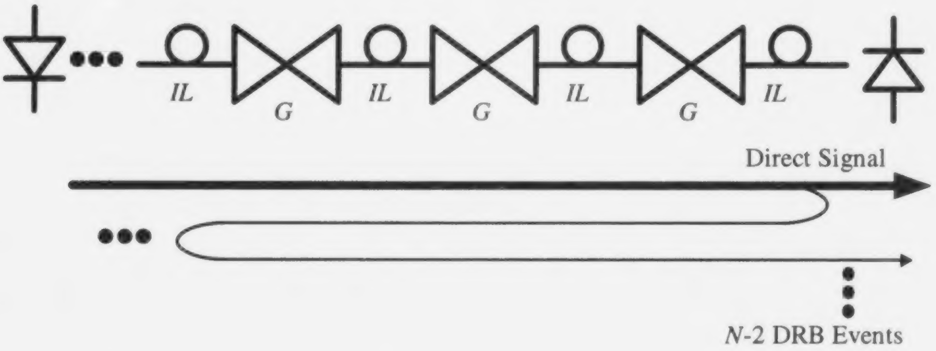

Figure 4.8: DRB signal which travels around *three* amplifiers.

Note that in deriving this equation, the contributions generated within *N+1* fiber sections and the fiber length dependence have been neglected, which is justified by the earlier comparison in Figure 4.4. It becomes clear from this equation that this noise increases not only with the number of amplifiers in link, but also with the product of interamplifier loss and amplifier gain. Therefore, an open cascade link with the amplifier gain being greater than the reciprocal of interamplifier loss resulting in $(G\,IL) > 1$, will enhance DRB noise; thus, such a link configuration should be avoided. On the other hand, a link with the amplifier gain being equal to or even smaller than the reciprocal of interamplifier loss resulting in $(G\,IL) \leq 1$, can have an impact on reduction of the DRB noise. A detailed study of the impact of this gain-loss product on system performance will be presented after the derivation of the penalty power expression.

For common uni-directional transmission systems with optical isolators surrounding each amplifier, the multi-amplified double Rayleigh backscattering is eliminated, and the systems are left only with the cumulative effects of double Rayleigh backscattering within each fiber section between amplifiers:

$$i_{DRB,iso}{}^2(f) = \frac{10}{9} R_{Rb}{}^2 \Re^2 A_{eff}{}^2 (N+1)\left(2\alpha L_s + e^{-2\alpha L_s} - 1\right) \Im\left\langle \left| R_{\varepsilon_{dir}}(\tau)\right|^2 \right\rangle \tag{4.5}$$

where L_s is the fiber length between amplifiers.

In the previous work on analog systems, DRB noise spectral densities have been used to determine its impact. However, for baseband digital IM-DD systems, it is the total received noise power within the receiver bandwidth which determines the BER, rather than the noise spectrum. As long as the digital modulation process does not broaden the DRB noise spectrum beyond the signal bandwidth required for detection, all the DRB noise will fall within the receiver bandwidth. Therefore, by integrating the noise spectral density described by Eqn. (4.4) over frequency, one can calculate the total DRB noise for the open cascade system. Then, substituting the following identity:

$$\int \Im\left\langle \left| R_{\varepsilon_{dir}}(\tau)\right|^2 \right\rangle df = \left\langle \left| R_{\varepsilon_{dir}}(0)\right|^2 \right\rangle = \frac{P_{re}^2}{A_{eff}{}^2} \tag{4.6}$$

into Eqn. (4.4) yields the total DRB noise in the open cascade system as

$$\left\langle i_{DRB}{}^2 \right\rangle = \frac{10}{9} R_{Rb}{}^2 P_{re}{}^2 \Re^2 G^2 \sum_{i=1}^{N} i\left(G\,IL\right)^{2(N-i)} \tag{4.7}$$

Since the noise induced by DRB is due to the beating between the direct traveling signal field and the DRB field, then in an IM-DD binary system, with marks and spaces respectively denoted by large and small signal fields, DRB induced noise during marks will be larger than that during spaces. To account for this signal-dependence, Appendix E shows that the noise given by the last equation can be modified to

$$\left\langle i_{DRB,i}{}^{2}\right\rangle = \frac{10}{9} R_{Rb}{}^{2} P_{re} P_i \Re^2 G^2 \sum_{i=1}^{N} i\left(G\,IL\right)^{2(N-i)} \tag{4.8}$$

where P_i denotes the received optical powers during a space or mark, and as before P_{re} represents the received averaged power. This equation will be used later to derive the general power penalty expression.

4.1.2. Increase In ASE

Here, the direct traveling ASE power and the increase in ASE, due to SRB and DRB in the previously described system is calculated. The direction the signal travels is defined here as forward. For mathematical convenience, the forward traveling ASE and backward traveling ASE that each amplifier emits are assumed to be equal. For bi-directionally pumped fiber amplifiers, this is a very good assumption.

4.1.2.1. Total Direct Traveling ASE Power

Figure 4.9 depicts the contribution from each amplifier to the total received direct ASE power in the open cascade system with N amplifiers. Summing all these contributions yields this power as

$$\begin{aligned} P_{ASE,dir} &= P_{ASE}\,IL + P_{ASE}\,G\,IL^2 + P_{ASE}\,G^2\,IL^3 + \ldots + P_{ASE}\,G^{N-1}\,IL^N \\ &= P_{ASE}\,IL\left(\frac{1-\left(G\,IL\right)^N}{1-G\,IL}\right) \end{aligned} \tag{4.9}$$

where P_{ASE} is the output ASE power of an amplifier.

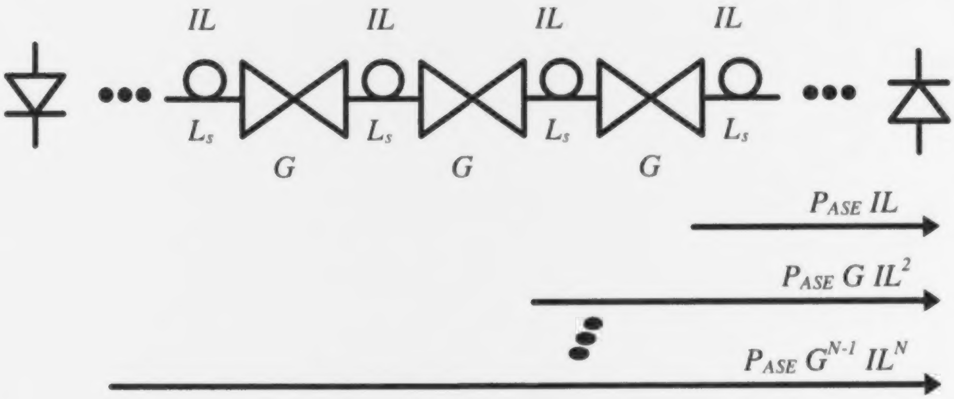

Figure 4.9: An open cascade of *N* amplifiers showing all the contributions to the direct ASE power at the receiver. P_{ASE} is the output ASE power of an amplifier.

4.1.2.2. Added ASE due to SRB

Multi-amplified SRB ASE in systems utilizing one to three amplifiers is first investigated. Based on these results, a generalization will then be made so that the multi-amplified SRB ASE in the *N* open cascade amplifier system can be determined. Figure 4.10 to Figure 4.12 show the SRB events that occur in transmission links utilizing one, two and three in-line amplifiers. In these figures, the subscript *b* denotes backward traveling and the subscripts, 1, 2 and 3, denote the locales of amplifiers. In the one in-line amplifier case, there is only one SRB event, and the SRB of ASE power at the receiver can be easily calculated by multiplying the backward traveling ASE power from the amplifier by the Rayleigh backscattering reflectance, amplifier gain and transmission loss between the amplifier and receiver, giving rise to

$$P_{ASE,SRB} = P_{ASE}\, R_{RB}\, G\, IL \tag{4.10}$$

For the two in-line amplifier case, as shown in Figure 4.11, there is one SRB event generated by the backward traveling ASE from amplifier 1, and two SRB events generated by the ASE from amplifier 2. By adding these three contributions, the SRB ASE power can be calculated as

$$\begin{aligned} P_{ASE,SRB} &= P_{ASE}\, R_{Rb}\, G\, IL + P_{ASE}\, R_{Rb}\, G^3\, IL^3 + P_{ASE}\, R_{Rb}\, G^2\, IL^2 \\ &= P_{ASE}\, R_{Rb}\, G\, IL\left[\left(1+G^2 IL^2\right)+G\, IL\right] \end{aligned} \tag{4.11}$$

For the 3 in-line amplifier case, as Figure 4.12 shows, a total of six SRB events are generated, and the SRB ASE power can be expressed as

$$P_{ASE,SRB} = P_{ASE}\, R_{Rb}\, G\, IL\left[\left(1+G^2 IL^2+G^4 IL^4\right)+G\, IL\left(1+G^2 IL^2\right)+G^2 IL^2\right] \tag{4.12}$$

By proceeding in a similar fashion, the ASE power due to SRB of backward traveling ASE in the *N* open cascade amplifier system can be calculated as

$$\begin{aligned} P_{ASE,SRB} &= P_{ASE}\, R_{Rb}\, G\, IL\left[\begin{matrix}\left(1+(G\, IL)^2+\ldots+(G\, IL)^{2(N-1))}\right)+ \\ (G\, IL)\left(1+(G\, IL)^2+\ldots+(G\, IL)^{2(N-2))}\right)+\ldots+(G\, IL)^{N-1}\end{matrix}\right] \\ &= P_{ASE}\, R_{Rb}\, G\, IL\left(\sum_{i=1}^{N}(G\, IL)^{N-i}\cdot\frac{1-(G\, IL)^{2i}}{1-(G\, IL)^2}\right) \end{aligned} \tag{4.13}$$

This equation indicates clearly that the SRB ASE power increases significantly with the number of amplifiers and the gain-loss product.

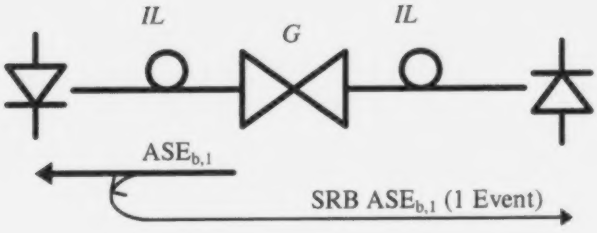
IL
G
IL
$ASE_{b,1}$
SRB $ASE_{b,1}$ (1 Event)

Figure 4.10: SRB ASE event in a transmission link with *one* in-line amplifier.

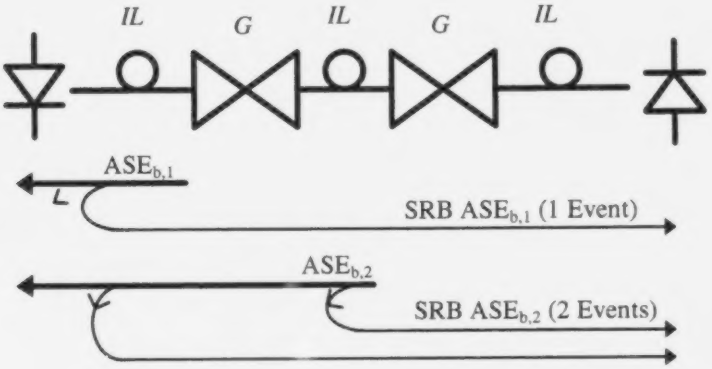
IL
G
IL
G
IL
$ASE_{b,1}$
SRB $ASE_{b,1}$ (1 Event)
$ASE_{b,2}$
SRB $ASE_{b,2}$ (2 Events)

Figure 4.11: All SRB ASE events in a transmission link with *two* in-line amplifiers.

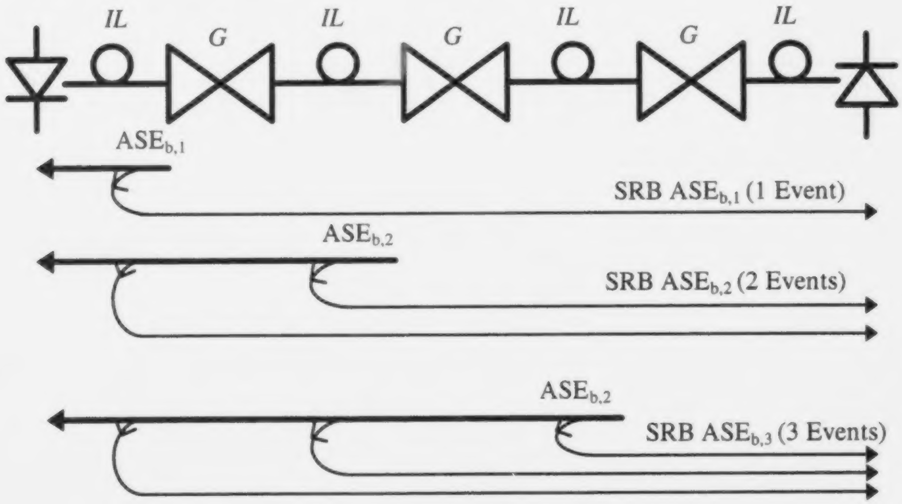
IL
G
IL
G
IL
G
IL
$ASE_{b,1}$
SRB $ASE_{b,1}$ (1 Event)
$ASE_{b,2}$
SRB $ASE_{b,2}$ (2 Events)
$ASE_{b,2}$
SRB $ASE_{b,3}$ (3 Events)

Figure 4.12: All SRB ASE events in a transmission link with *three* in-line amplifiers.

4.1.2.3. Added ASE due to DRB

Multi-amplified DRB ASE in systems utilizing three amplifiers is first investigated. Based on this result, a generalization will subsequently be made so that the multi-amplified DRB ASE in the open cascade amplifier system can be determined as in the previous section. Figure 4.13 shows the total number of DRB ASE events generated in a transmission link employing three in-line amplifiers. In this figure, the subscript f denotes the forward traveling of ASE. The ASE powers, due to DRB of the forward traveling ASE from the 3rd, 2nd and 1st amplifier, can be respectively described as

$$P_{ASE}\, R_{Rb}{}^2\, G^2\, IL\left[\left(1+G^2IL^2+G^4IL^4\right)\right],$$

$$P_{ASE}\, R_{Rb}{}^2\, G^2\, IL\left[G\,IL\left(1+G^2IL^2+G^4IL^4\right)+G\,IL\left(1+G^2IL^2\right)\right] \text{ and}$$

$$P_{ASE}\, R_{Rb}{}^2\, G^2\, IL\left[G^2\,IL^2\left(1+G^2IL^2+G^4IL^4\right)+G^2\,IL^2\left(1+G^2IL^2\right)+G^2\,IL^2\,\right]$$

The summation of these effects yields the total DRB ASE power in this three in-line amplifier system as

$$P_{ASE,DRB} = P_{ASE}\, R_{Rb}{}^2\, G^2\, IL\begin{bmatrix}\left(1+G\,IL+G^2\,IL^2\right)\left(1+G^2IL^2+G^4IL^4\right)+\\ G\,IL\left(1+G\,IL\right)\left(1+G^2IL^2\right)+G^2\,IL^2\end{bmatrix} \tag{4.14}$$

By proceeding in a similar manner for the N open cascade amplifier system, the total ASE power induced by DRB of the forward traveling ASE in such system can be derived as

$$P_{ASE,DRB} = P_{ASE}\, R_{Rb}{}^2\, G^2\, IL\left(\sum_{i=1}^{N}\left(G\,IL\right)^{N-i}\cdot\frac{1-\left(G\,IL\right)^i}{1-\left(G\,IL\right)}\cdot\frac{1-\left(G\,IL\right)^{2i}}{1-\left(G\,IL\right)^2}\right) \tag{4.15}$$

Again, this equation indicates that the DRB ASE power also increases substantially with the number of amplifiers and the gain-loss product.

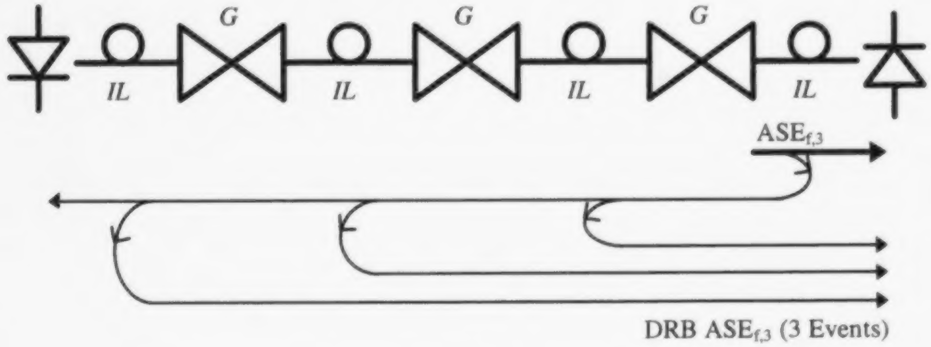
G
G
G
IL
IL
IL
IL
ASE$_{f,3}$
DRB ASE$_{f,3}$ (3 Events)

(a)

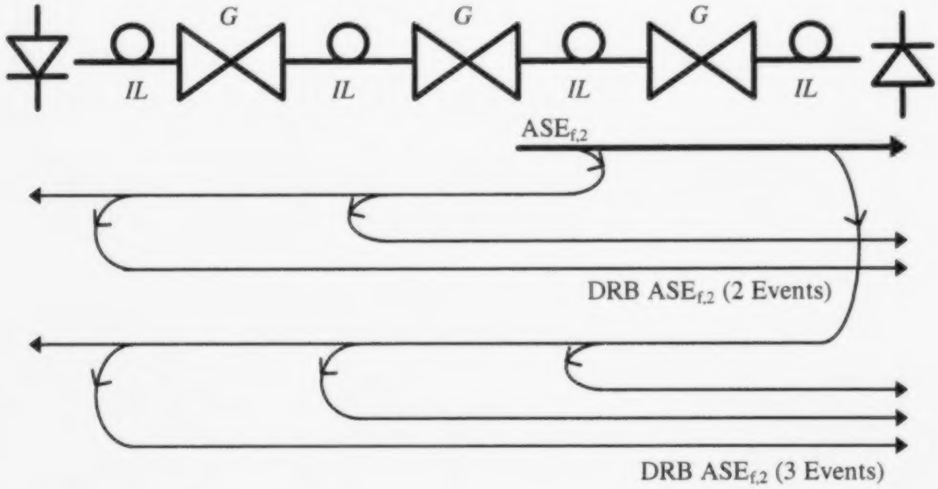
G
G
G
IL
IL
IL
IL
ASE$_{f,2}$
DRB ASE$_{f,2}$ (2 Events)
DRB ASE$_{f,2}$ (3 Events)

(b)

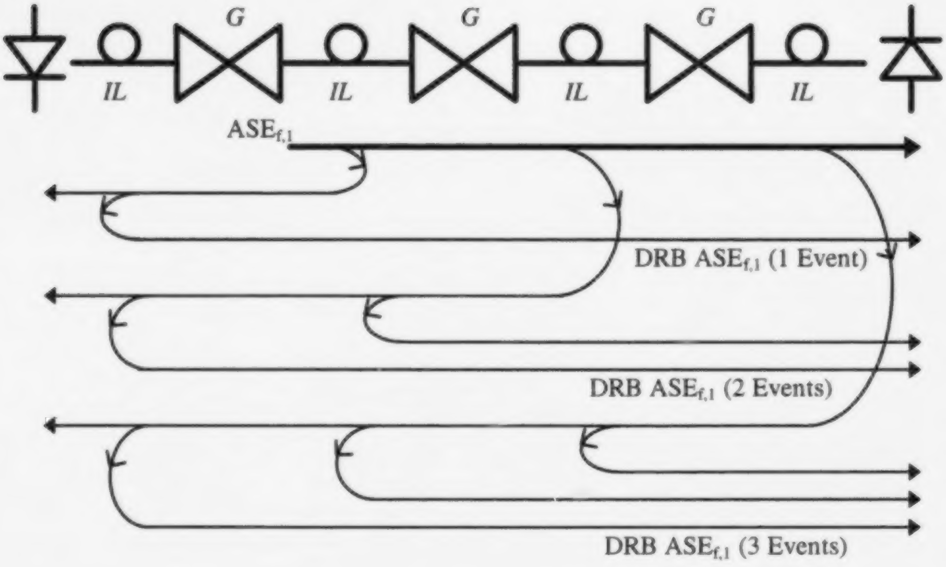
G
G
G
IL
IL
IL
IL
ASE$_{f,1}$
DRB ASE$_{f,1}$ (1 Event)
DRB ASE$_{f,1}$ (2 Events)
DRB ASE$_{f,1}$ (3 Events)

(c)

Figure 4.13: All DRB ASE events in a 3 in-line amplifier transmission link. As shown are the contributions from the (a) 3rd amplifier, (b) 2nd amplifier and (c) 1st amplifier.

4.1.2.4. ASE Power Due to SRB and DRB

By combining Eqn. (4.13) and (4.15), the total induced ASE power from both the multi-amplified SRB and DRB can be readily obtained as

$$P_{ASE,RB} = P_{ASE}\, R_{Rb}\, G\, IL \sum_{i=1}^{N} \left\{ (G\, IL)^{N-i} \cdot \frac{1-(G\, IL)^{2i}}{1-(G\, IL)^{2}} \left(1 + R_{Rb}\, G \frac{1-(G\, IL)^{i}}{1-(G\, IL)} \right) \right\} \tag{4.16}$$

This equation, along with Eqn. (4.8) describing the DRB noise during spaces and marks and Eqn. (4.9) describing the total direct traveling ASE power at the receiver, will be applied later in this section to derive the power penalty expression in order to quantify the degrading impact of Rayleigh backscattering.

4.1.3. Noise Analysis

In an IM-DD digital system with optical fiber amplifiers, the significant noise sources are several. They include the receiver thermal noise, signal to spontaneous beat noise and spontaneous to spontaneous beat noise. Since the shot noises due to the ASE and the signal are much less than the spontaneous to spontaneous beat noise and the signal to spontaneous beat noise [92], these shots noises are ignored. With optical noise equivalent bandwidth B_o and electrical noise equivalent bandwidth B_{re}, the mean square noise currents of the signal to spontaneous beat noise and spontaneous to spontaneous beat noise due to the direct ASE power can be respectively expressed as [71-72]

$$\left\langle i_{sig\_sp,i}{}^2 \right\rangle = 2P_i \, P_{ASE,dir} \, \Re^2 \frac{B_{re}}{B_o} \tag{4.17}$$

and

$$\left\langle i_{sp\_sp}{}^2 \right\rangle = \left(P_{ASE,dir} \right)^2 \Re^2 \frac{B_{re}}{B_o} \tag{4.18}$$

where $P_{ASE,dir}$ is the direct ASE power at the receiver and has been given by (4.9). To determine the receiver sensitivity penalty due to the RB impact, one may first consider the mean square noise currents for spaces and marks, with RB impact neglected. They are respectively given by

$$\begin{aligned} \sigma_0{}^2 &= \left\langle i_{sig\_sp,0}{}^2 \right\rangle + \left\langle i_{sp\_sp}{}^2 \right\rangle + \left\langle i_{th}{}^2 \right\rangle \\ &= 2P_0 \, P_{ASE,dir} \, \Re^2 \frac{B_{re}}{B_o} + \left(P_{ASE,dir} \right)^2 \Re^2 \frac{B_{re}}{B_o} + \left\langle i_{th}{}^2 \right\rangle \end{aligned} \tag{4.19}$$

and

$$\begin{aligned}\sigma_1{}^2 &= \left\langle i_{sig\_sp,1}{}^2 \right\rangle + \left\langle i_{sp\_sp}{}^2 \right\rangle + \left\langle i_{th}{}^2 \right\rangle \\ &= 2P_1\, P_{ASE,dir}\, \Re^2 \frac{B_{re}}{B_o} + \left(P_{ASE,dir}\right)^2 \Re^2 \frac{B_{re}}{B_o} + \left\langle i_{th}{}^2 \right\rangle\end{aligned} \tag{4.20}$$

If the RB impact is taken into account, the received ASE power will be increased and the DRB noise will be added to the receiver. As a result, these noise expressions become

$$\sigma_{0,RB}{}^2 = 2P_0\left(P_{ASE,dir} + P_{ASE,RB}\right)\Re^2 \frac{B_{re}}{B_o} + \left(P_{ASE,dir} + P_{ASE,RB}\right)^2 \Re^2 \frac{B_{re}}{B_o} + \left\langle i_{th}{}^2 \right\rangle + \left\langle i_{DRB,0}{}^2 \right\rangle \tag{4.21}$$

and

$$\sigma_{1,RB}{}^2 = 2P_1\left(P_{ASE,dir} + P_{ASE,RB}\right)\Re^2 \frac{B_{re}}{B_o} + \left(P_{ASE,dir} + P_{ASE,RB}\right)^2 \Re^2 \frac{B_{re}}{B_o} + \left\langle i_{th}{}^2 \right\rangle + \left\langle i_{DRB,1}{}^2 \right\rangle \tag{4.22}$$

It is clear from these equations that the noises are enhanced in the presence of RB; therefore, to restore the original BER, the received signal power has to be increased. The amount of necessary increase in the received optical power, or the power penalty, will be determined as follows.

By approximating the spontaneous to spontaneous beat noise as Gaussian distributed, an assumption which yields only slight over-estimation in receiver sensitivities [72-73], the BER can be determined through the following relation:

$$BER = \frac{1}{Q\sqrt{2\pi}} \exp\left(\frac{-Q^2}{2}\right) \tag{4.23}$$

where Q is the electrical signal to noise current (or voltage) ratios, also known as Personick's Q factors. In obtaining the minimal BER, the Q values during spaces and marks are equated, giving rise to

$$Q = \frac{P_1 \Re - D}{\sigma_1} = \frac{D - P_0 \Re}{\sigma_0} \tag{4.24}$$

where D is the receiver decision threshold. If the impact of RB is included and an increase in the receiver power δP is introduced to restore the same Q value when RB is absent or neglected, the expression for Q becomes

$$Q = \frac{P_1 \delta P \Re - D_{RB}}{\sigma_{1,RB}} = \frac{D_{RB} - P_0 \delta P \Re}{\sigma_{0,RB}} \tag{4.25}$$

where D_{RB} is the new optimal decision threshold in the presence of Rayleigh backscattering. Appendix F shows that when the penalty is modest, by substituting Eqn. (4.17) to (4.22) into (4.24) and (4.25), the power penalty (in decibels) can be expressed as

$$\begin{aligned} \Delta P &= 10\log(\delta P) \\ &= 10\log\left(\frac{P_{ASE,dir} + P_{ASE,RB}}{P_{ASE,dir}}\right) + 10\log\left\{1 - \frac{Q^2}{2}\frac{\left\langle {i_{DRB}}^2\right\rangle}{{P_{re}}^2\Re^2}\frac{d+1}{d-1}\right\}^{-1} \end{aligned} \tag{4.26}$$

where d is the extinction ratio, relating the optical signal powers during spaces and marks as

$$d = \frac{P_1}{P_0} \tag{4.27}$$

Again, in this generic expression, $P_{ASE,dir}$ is the direct travel ASE power and $P_{ASE,RB}$ is the added ASE power by SRB and DRB, and which are respectively given by Eqns. (4.9) and (4.16). Also in this expression, $\left\langle i_{DRB}{}^2 \right\rangle$ is the total mean square DRB noise current at the receiver and has been given by Eqn. (4.7). This expression indicates that the degradation arises from 2 sources. The first is the penalty induced by the added ASE power by SRB and DRB. The second is the penalty induced by the DRB noise, and this penalty increases positively with the Q factor and inversely with the extinction ratio d. Eqn. (4.7), (4.9), (4.16) and (4.26) yield the most important results in the derivation and they will be applied in the following section in order to analyze the performance of open cascade systems. To clarify, they are stated again as follows:

$$\boxed{\left\langle i_{DRB}{}^2 \right\rangle = \frac{10}{9} R_{Rb}{}^2 P_{re}{}^2 \Re^2 G^2 \sum_{i=1}^{N} i\left(G\,IL\right)^{2(N-i)}} \qquad (4.7)$$

$$\boxed{P_{ASE,dir} = P_{ASE}\; IL\left(\frac{1-\left(G\,IL\right)^N}{1-G\,IL}\right)} \qquad (4.9)$$

$$\boxed{P_{ASE,RB} = P_{ASE}\; R_{Rb}\, G\, IL \sum_{i=1}^{N}\left\{\left(G\,IL\right)^{N-i} \cdot \frac{1-\left(G\,IL\right)^{2i}}{1-\left(G\,IL\right)^2}\left(1+R_{Rb}\, G\frac{1-\left(G\,IL\right)^i}{1-\left(G\,IL\right)}\right)\right\}} \qquad (4.16)$$

$$\boxed{\Delta P = 10\log\left(\frac{P_{ASE,dir}+P_{ASE,RB}}{P_{ASE,dir}}\right) + 10\log\left\{1-\frac{Q^2}{2}\,\frac{\left\langle i_{DRB}{}^2\right\rangle}{P_{re}{}^2\Re^2}\,\frac{d+1}{d-1}\right\}^{-1}} \qquad (4.26)$$

Note that by substituting Eqns. (4.9) and (4.16) into the penalty expression (4.26), it can be realized that the P_{ASE} terms are eliminated. Therefore, the penalty expression is independent of the received ASE power, or the noise figures of optical amplifiers.

4.2. Examination of Open Cascade Systems

Here, using the power penalty expressions (4.26), along with (4.7), (4.9) and (4.16), a theoretical study of systems utilizing open cascade amplifiers is presented. First, two kinds of systems are investigated: systems with interamplifier losses being equal to amplifier gains and systems with reciprocals of interamplifier losses being significantly larger than the gains. The former system represents conventional transmission link design, and the latter represents a new design which promises the reduction of multi-amplified double Rayleigh backscattering effects. After the investigation, the inter-amplifier loss and gain constrains are removed, and the end-to-end BER will then be calculated as a function of the inter-amplifier loss and amplifier gain product.

4.2.1. Power Penalty

By setting the interamplifier loss *IL* reciprocally equal to the amplifier gain *G* (i.e. $G\,IL = 1$) for Eqn. (4.7), (4.9) and (4.16), these equations are reduced to

$$P_{ASE,dir} = P_{ASE}\,IL\,N \tag{4.28}$$

$$\left\langle i_{DRB}{}^{2}\right\rangle = \frac{10}{9} R_{Rb}{}^{2} P_{re}{}^{2} \Re^{2} G^{2} \left(\frac{N(N+1)}{2}\right) \tag{4.29}$$

and

$$P_{ASE,RB} = P_{ASE}\,R_{Rb}\,G\,IL\left[\frac{N(N+1)}{2} + R_{Rb}\,G\,\frac{N(N+1)(2N+1)}{6}\right] \tag{4.30}$$

Substituting these equations into the general penalty expression (4.26) yields the penalty for an *N* open cascade amplifier system having interamplifier loss being reciprocally equal to amplifier gain as

$$\Delta P = 10\log\left(1 + R_{Rb}G\frac{N+1}{2} + R_{Rb}{}^2 G^2 \frac{(N+1)(2N+1)}{6}\right) + 10\log\left\{1 - \frac{5}{9}Q^2 R_{Rb}{}^2 G^2 \frac{N(N+1)}{2}\frac{d+1}{d-1}\right\}^{-1} \tag{4.31}$$

Using this equation, Figure 4.14 depicts the calculated power penalties due to DRB of signal, SRB and DRB of ASE, and these Rayleigh backscattering effects as a function of the number of amplifiers in the open cascade. In the calculation, the amplifier gain and interamplifier loss are equal to 17 dB and -17 dB, respectively, and other parameters are as BER = 10^{-14}, R_{Rb} = -33 dB and d = 10. This figures indicates that the degradation comes mainly, but not entirely, from the noise due to the DRB of the signal, and this penalty rises substantially with the number of amplifiers in the cascade.

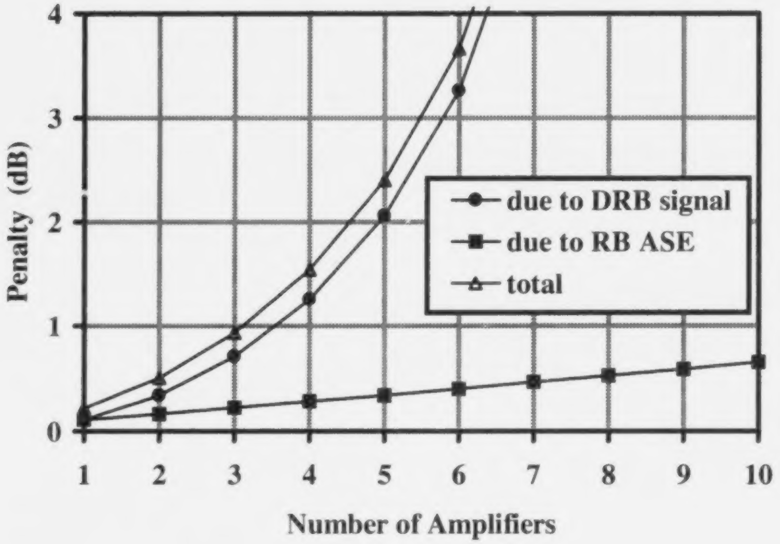

Figure 4.14: Power penalty versus number of amplifiers in an open cascade with $G = 1/IL$ = 17 dB, BER=10^{-14}, R_{Rb}=-33 dB and d = 10.

Now, the gain-loss product in Eqn. (4.7), (4.9), and (4.16) is set at -3 dB (i.e. 0.5), which exemplifies the situation of systems with reciprocal of interamplifier loss being 3 dB greater than amplifier gain. In the following calculation, the number of amplifiers used is limited only to five. This is due to the progressively decreasing signal power as the signal propagates toward the receiver. These newly obtained equations are then substituted into the general penalty expression (4.26) in order to calculate the reduced power penalties with the transmission link engineered in this way. Figure 4.15 depicts these reduced power penalties. Comparing this figure to Figure 4.14 clearly reveals that the penalties, particularly the penalty due to DRB of signal, have been greatly reduced by engineering the amplifier cascade in this way. It is also important to note that when the number of amplifiers is 1 or 2, there is no real advantage to this form of engineering; however, for more than 2 amplifiers, the benefit becomes clear.

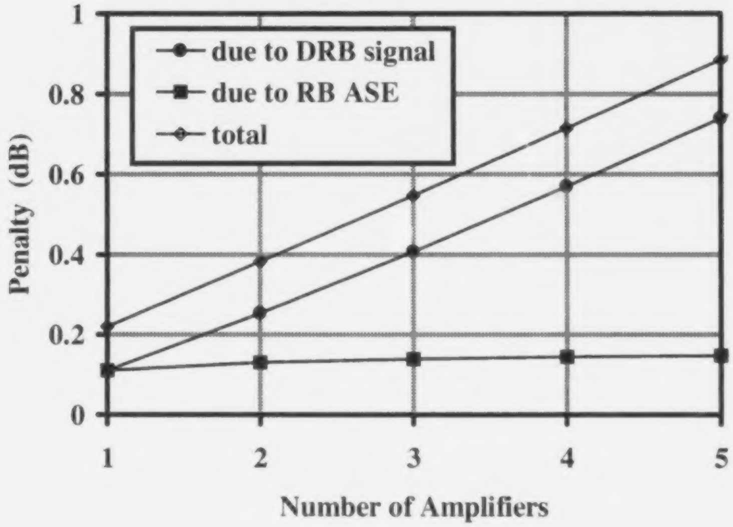

Figure 4.15: Power penalty versus number of amplifiers in an open cascade with $G\ IL = 0.5$, BER=10^{-14}, $G = 17$ dB, R_{Rb}=-33 dB and $d = 10$.

4.2.2. Total Amplifier Gain

Since the above engineering method limits the possible number of in-line amplifiers in transmission link, the total available gain of a chain of in-line amplifiers may also be restricted. In what follows, the total available gain of a chain of in-line amplifiers will be simply abbreviated as the total amplifier gain, and will be calculated by summing each in-line amplifier's gain.

Using Eqn. (4.7), (4.9), (4.16) and (4.26) as in the previous subsection, Figure 4.16 and Figure 4.17 depict the total amplifier gains of the above systems versus the number of amplifiers in the link with the power penalty as a parameter. Again, in these systems, one determines the gain-loss product to be equal to 1, and in the other systems the gain-loss product to be equal to 0.5. Note that the total amplifier gain is calculated as the number of amplifiers times the amplifier gain, and also that the amplifier gain is not fixed, as compared to the previous power penalty calculations, but is determined by applying the penalty expression .

In Figure 4.16, for 0.5 dB penalty when there is one in-line amplifier, the total gain is equal to the sole amplifier gain, which is about 20 dB. If the number of amplifiers employed in link is increased to 10, then each amplifier gain has to be lessened to about 11 dB for the same 0.5 dB penalty. However, the total amplifier gain is enhanced to about 110 dB. If the allowable penalty is increased 2 dB, each amplifier gain can be operated at about 14 dB, and therefore a total of about 140 dB total amplifier gain will be available.

For the case where reciprocal of interamplifier loss is significantly larger than amplifier gain, Figure 4.17 shows that due to the reduced multi-amplified Rayleigh backscattering effects, each amplifier can have a higher gain, which results a total amplifier gain of about 80 dB for 0.5 dB penalty, or more than 90 dB for 2 dB penalty with only five amplifiers in link.

By comparing the results of these two kinds of links, one finds that the operating amplifier gain is lower, but the possible number of amplifiers in the link is larger for the link with the gain-loss product being equal to 1. Nevertheless, both kinds of open cascade links can provide large total amplifier gains, provided that each in-line amplifier has a moderate gain, and these total amplifier gains can be further increased by allowing a modest power penalty.

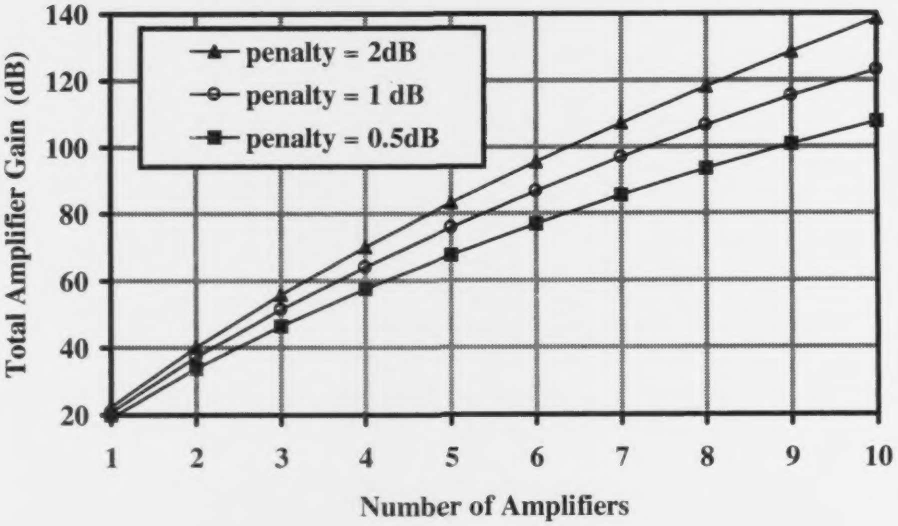

Figure 4.16: Total amplifier gain versus number of amplifiers in link with $G\,IL = 1$. The calculations utilize BER = 10^{-14}, R_{Rb} = -33 dB $d = 10$ and the penalty as a parameter.

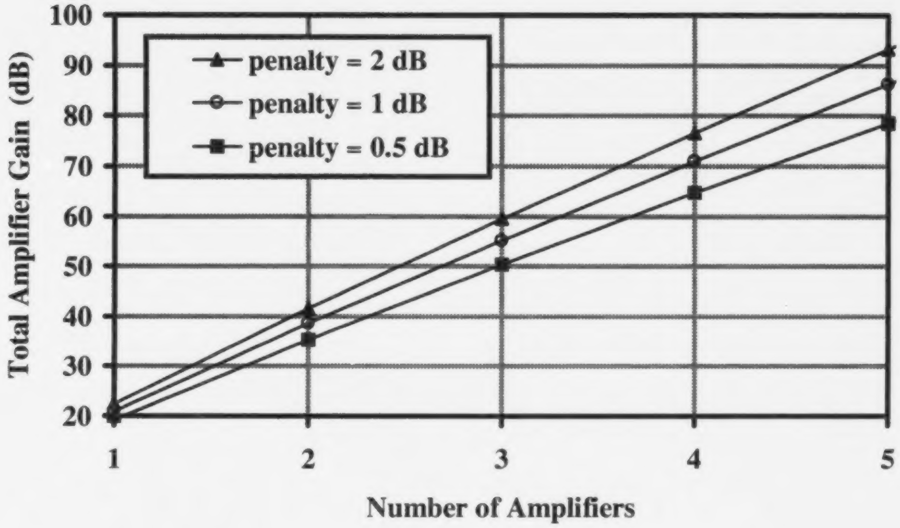

Figure 4.17: Total amplifier gain versus number of amplifiers in link with $G\ IL = 0.5$. The calculations utilize BER = 10^{-14}, $R_{Rb} = -33$ dB, $d = 10$ and the penalty as a parameter.

4.2.3. End-To-End Bit Error Ratio

In the previous section, the relation between the total amplifier gain, number of amplifiers and power penalty due to Rayleigh backscattering has been investigated. However, in order to determine the total loss budget of an open cascade system, knowing the total amplifier gain is not enough because the total loss budget also depends on the optical launched power, the spontaneous emission factors of optical amplifiers, and the sensitivity of the receiver. Here, the total loss budget and the end-to-end BER of an open cascade system in relation to the gain-loss product is studied.

To determine the total loss budget, the penalty expression is not applicable, and in order to calculate the BER, the total noises during spaces and marks and the signal power at the receiver need to be considered. The noises during spaces and marks have been previously given by Eqn. (4.21) and (4.22).

The received signal power for an open cascade system, as depicted in Figure 4.5, can be readily determined as the launched power P_{tx} multiplied by the amplification and attenuation during its propagation toward the receiver:

$$P_{re} = P_{tx}\, G^{N}\, IL^{N+1} \tag{4.32}$$

From Eqn. (4.24), the Q factor can be rewritten as

$$Q = \frac{P_1\Re - P_0\Re}{\sigma_{1,RB} + \sigma_{0,RB}} \tag{4.33}$$

By substituting the noise equations (4.21) and (4.22) into the above equation, and subsequently making P_0 and P_1 in terms of the launched power P_{tx} and extinction ratio d, we obtain the Q factor as a function of the gain-loss product, launched power and extinction ratio. Using this function as well as the BER equation (4.23), the end-to-end system BERs for a 10 Gb/s system with an open cascade of 8 amplifiers are calculated and presented in Figure 4.18. In the calculation, a preamplifier with 20 dB gain is assumed in the receiver, and the parameters used are listed in Table 4.1. 5 dBm launched power is used and could correspond to the output power of a transmitter equipped with an external modulator followed by a post-amplifier. Three interamplifier losses are used, namely 14, 17 and 20 dB, and all amplifiers are assumed to have identical gains. Also shown are the BERs when RB is not present, representing a similar system with isolators in-between amplifiers.

This figure reveals that there exists a minimum BER at a certain value of the amplifier gain in the open cascade system, i.e. as the amplifier gain increases, the BER first decreases, and then rises again after passing through a minimum. This behavior can be explained as follows: when the amplifier gain is small, the thermal noise at the receiver is dominant, and the low detected signal power gives rise to the poor BER. As the amplifier gain increases, the detected signal power increases and so does the total noise power. Since the DRB noise is not significant in this low gain region, the increase in signal power is larger than the increase in the total noise power; therefore, the BER is reduced. As the amplifier gain further increases, the detrimental DRB impact becomes important. Once it has become the dominant noise source in the receiver, the BER increases with the amplifier gain because in this higher gain region, the increase in DRB noise power is larger that the increase in signal power. The larger increase in DRB noise power is due to the fact that the DRB noise is approximately proportional to the quadruple of the amplifier gain, as indicated by Eqn. (4.7), whereas the detected signal power is only proportional to the square of the amplifier gain.

Recall that DRB noise is a form of RIN, and therefore, increasing the launched signal power will not affect the curves on the right hand side in Figure 4.15. However, the curves on the left hand side, which signify thermal noise or signal to spontaneous beat noise domination, will shift to the left by using higher launched power. When the interamplifier loss is equal to 20 dB, no matter how the amplifiers are operated, a low BER cannot be achieved in the open cascade system. However, if the interamplifier loss is reduced to 17 dB, low BERs can be obtained. For a BER target of less than 10^{-14}, each amplifier can be operated at about 15.4 to 16.4 dB, resulting in an amplifier usable range of about 1.0 dB. Thus, for such system, a total of a 153 dB (17 dB x 9) loss budget can be available.

As one further reduces the interamplifier loss to 14 dB, this usable range broadens to roughly 2.7 dB (amplifier gain from 11.7 to 14.4 dB), and a total of a 126 dB (14 dB x 9) loss budget can be obtained. As expected, there is no such upper bound for the amplifier gain in the conventional optically amplified system which employs isolators, as evidenced by the dotted lines in this figure.

To conclude, systems with an open cascade of amplifiers, each operated at a moderate gain, are capable of providing a large transmission budget. Such systems could be an additional option for economic network implementation and growth.

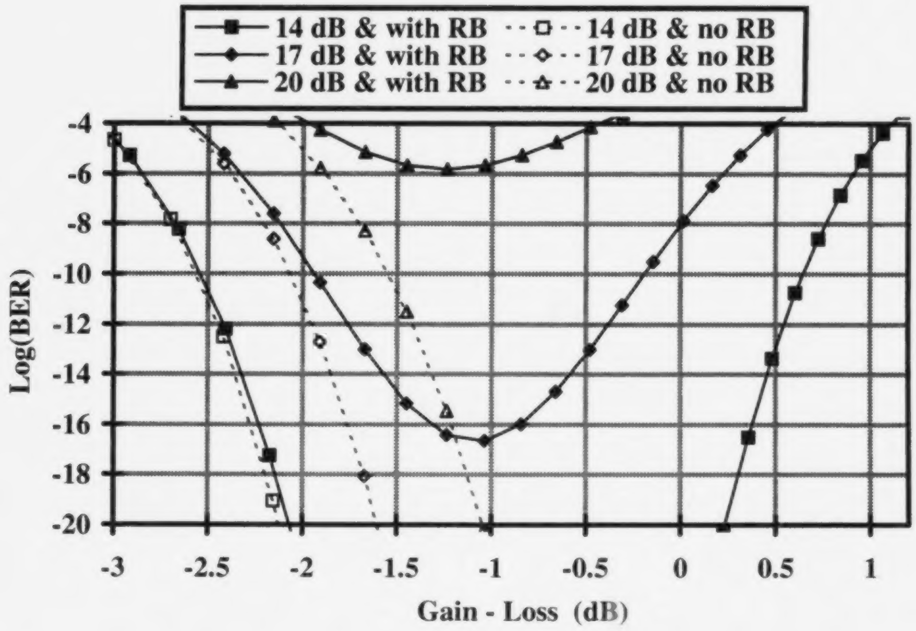

Figure 4.18: BER versus gain-loss product for the system using a cascade of 8 amplifiers, with and without Rayleigh backscattering for interamplifier losses: 14, 17 and 20 dB.

Parameter	Symbol	Value
Launched power	P_{tx}	5 dBm
gain of preamplifier		20 dB
RB reflectance	R_{RB}	-33 dB
Receiver optical noise bandwidth	B_o	1.5x126 GHz (i.e. 1.5 nm)
Receiver electrical noise bandwidth	B_{re}	7 x 10^9 Hz
Front-end thermal noise current density		13 pA/Hz
Spontaneous emission factor	n_{sp}	1.5
Extinction ratio	d	10
Detector responsivity	$\Re$	0.7 A/W

Table 4.1: List of parameter values used in the calculation of the BER.

4.3 Experimental Verification

In this section, the experimental setups and results for verifying the validity of the power penalty expression (4.31) are presented. In the experiments, setups using one to three in-line EDFAs, with and without isolators, have been used. For a fixed BER, by comparing the measured optical powers at the receiver when in-line isolators were not used to the powers when in-line isolators were used, the penalties due to RB impact have been determined. By comparing the measured power penalties to the theoretical values, the validity of the penalty expression has been confirmed. Lastly, end-to-end BER has been measured as a function of the gain-loss product and compared to the theoretical values for verifying the validity of the theoretical studies in Section (4.2.3) and the existence of a minimum BER in the open cascade system.

4.3.1 Experimental Setup

4.3.1.1. Optical Transmitter

The block diagram of the optical transmitter used in the experiments is depicted in Figure 4.19. The laser source was a DFB laser diode with model number NT8L79NA. It was situated in a Prototype 1550 nm Laser/Mach-Zehnder Modulator, and was built by Jason Lamont and David Clegg of Tr*labs*. The source had a lasing wavelength of 1530.8 nm at 20 °C and was chosen because at its lasing wavelength, sufficient power gain could be obtained from our in-house EDFAs for analyzing the RB impact. Recall that RB impact increases significantly with the in-line amplifier gain. This source had an intrinsic RIN of less than -140 dB/Hz over 3 GHz and a laser linewidth (full width half maximum) of 6 MHz.

At the time of conducting these experiments, the Mach-Zehnder modulator inside this prototype was not yet available. In this case, this prototype was utilized only as a continuous-wave laser source and an external modulator was employed. The modulator utilized was a 1x2 electro-optic switch from United Technologies Photonics. A polarization rotator was used to connect the diode output to the modulator. By adjusting the polarization of the diode output, the transparency and electro-optic effect of the modulator could be maximized.

The modulating signal was a Non Return to Zero (NRZ), 2^7-1 Pseudo-Random Bit Sequence (PRBS) at a data rate of OC-48 (i.e. ~2.5 GHz), originating from an HP 70841A Pattern Generator. The comparatively short pattern was used because of the low frequency cutoff of the Mini-Circuit power amplifier, which was required to boost the modulating power for obtaining full switching operation. With the amplifier, the RF power at the modulator was about 27 dBm, which was sufficient for nearly full switching operation [74]. A DC voltage was supplied to bias the modulator and any changes in the DC voltage would vary the extinction ratio of the output signal. Therefore, by altering the voltage slightly, various extinction ratios could be generated. This feature was utilized in the experiments to prove the extinction ratio dependence in the general power penalty expression (4.31).

An optical isolator with better than 50 dB isolation was inserted right after the modulator to eliminate any reflections entering the modulator which would generate additional noises. After the isolator, the net modulated output power to the transmission fiber was about -5 dBm.

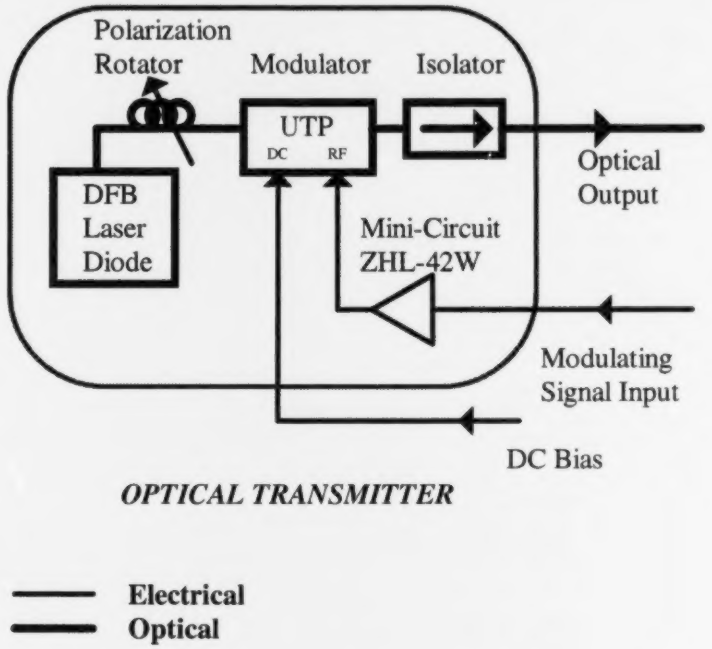
Polarization
Rotator
Modulator
Isolator
UTP
DC
RF
DFB
Laser
Diode
Optical
Output
Mini-Circuit
ZHL-42W
Modulating
Signal Input
DC Bias
OPTICAL TRANSMITTER
Electrical
Optical

Figure 4.19: Block diagram of the optical transmitter used in the experiment.

4.3.1.2. Optical Receiver

The block diagram of the receiver used in the experiments is shown in Figure 4.20. In this receiver, an EDFA with serial number TRL-R0302-004 was used as a preamplifier to increase the receiver's sensitivity. An isolator was situated in front of the EDFA to stop the backward traveling ASE from being coupling into the transmission link. Before photodetection, an optical Bandpass Filter (BPF) was added after the EDFA to filter the out-of-band forward traveling ASE. With the BPF, the spontaneous to spontaneous beat noise was reduced. The photodetection was performed by an OC-192 PIN/Preamp Module from BNR. This module had about 20 dBΩ trans-impedance gain, 10 GHz bandwidth and a very low noise characteristic. A second stage amplifier from Veritech with 10 GHz bandwidth was also utilized so that a sufficiently large signal could be generated for subsequent measurements. Since the amplifier was designed for AC-coupling, a DC block was inserted between the module and the amplifier to remove the

DC from the detected signal and to ensure proper operation. To remove the out-of-band noise, a K&L 2.5 GHz lowpass filter was placed after the amplifier. Note that this optical receiver configuration and the previously described optical transmitter configuration were used for all the experiments discussed in this chapter.

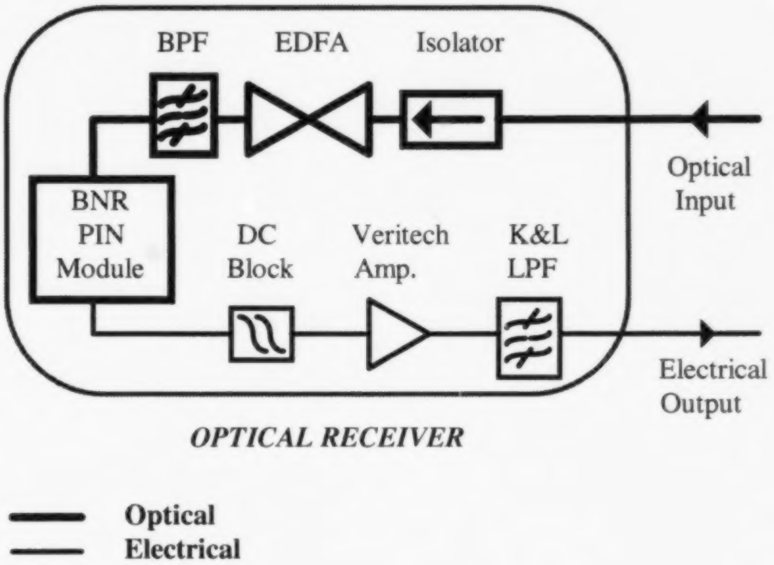
BPF
EDFA
Isolator
Optical Input
BNR PIN Module
DC Block
Veritech Amp.
K&L LPF
Electrical Output
OPTICAL RECEIVER
Optical
Electrical

Figure 4.20: Block diagram of the optical receiver used in the experiment.

4.3.2. Receiver Sensitivity Measurement

Here the back to back receiver sensitivity measurement is discussed. Figure 4.21 shows the sensitivity measurement setup. It utilized the optical transmitter and receiver setups described above. The modulating signal was a 2^7-1, NRZ, PRBS at a data rate of 2.5 Gb/s. The output of the transmitter was connected to the receiver through a JDS 7000 Variable Optical Attenuator (VOA). The VOA had a 90% output port and a 10% output port. The 90% output port was connected to the receiver and the 10% output port was connected to an HP 8153A optical power meter. The exact power ratio of the 90%

port to the 10% port was measured to be 10.2 dB. Therefore, by setting the calibration factor of the power meter to 10.2 dB, the average power to the receiver could be readily read from the power meter.

The output of the receiver was halved through a 6 dB power splitter from Mini-Circuit. One of the split powers was connected to an HP 70004A Error Detector to determine the BER, and the other was connected to an HP 54120B Digitizing Oscilloscope in order to determine the extinction ratio of the signal. The oscilloscope was General Purpose Interface Bus (GBIP)-connected to a Macintosh II Si computer and the data acquisition was performed using a software package called LabVIEW. Using a LabVIEW program and Matlab program, named respectively HP54123T Trace Average and FOCSS, and written by Sheldon Walklin, a Ph. D. student at TR*Labs*, a time-averaged eye diagram of the detected signal could be obtained. Figure 4.22 shows an eye diagram with maximum eye opening. This was achieved by carefully adjusting the DC bias of the electro-optic switch in the transmitter for a minimum BER. This diagram reveals that there was some Intersymbol Interference (ISI) generated in the signal, thereby causing eye closure. To determine the source of ISI contribution, a simple configuration, shown in Figure 4.23, was used to analyze the K&L 2.5 GHz LPF, Veritech 10 GHz amplifier and Mini-Circuit 4.2 GHz amplifier. Figure 4.24 to Figure 4.26 present the eye diagrams when these components were undergoing the test. These diagrams indicate that a significant amount of ISI arose from the Mini-Circuit amplifier. This ISI could explain the eye-closure of the signal. Since this amplifier was used to drive the external modulator in the transmitter, the effective extinction ratio would then be reduced.

By adjusting the VOA, a set of BERs for various received powers was obtained. With these data, the receiver sensitivity was plotted, producing Figure 4.27. Also plotted was the sensitivity of the transmitter when the EDFA, isolator and BPF in Figure 4.19 were removed. This figure clearly shows the benefit of employing EDFA as a preamplifier.

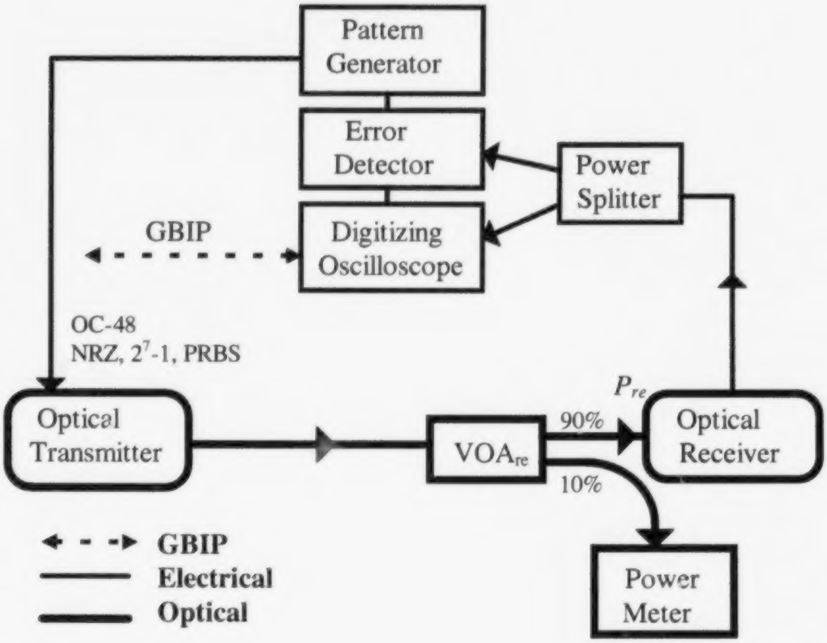
Pattern Generator
Error Detector
Digitizing Oscilloscope
Power Splitter
GBIP
OC-48
NRZ, 2^7-1, PRBS
P_{re}
Optical Transmitter
VOA$_{re}$
90%
10%
Optical Receiver
Power Meter
GBIP
Electrical
Optical

Figure 4.21: Back to back configuration for the receiver sensitivity.

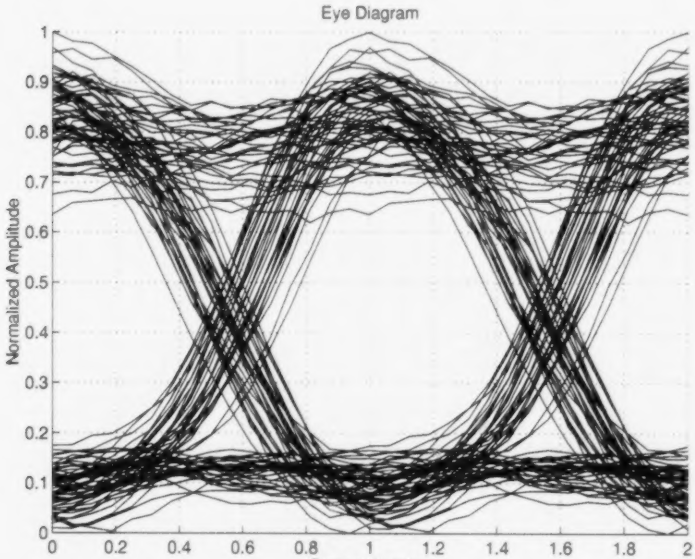

Figure 4.22: Averaged eye diagram of the signal.

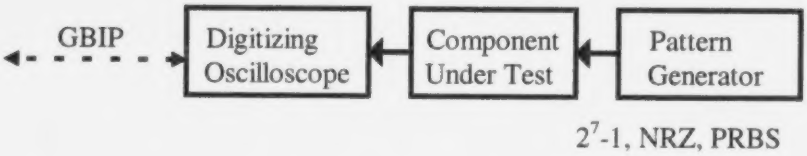
GBIP
Digitizing Oscilloscope
Component Under Test
Pattern Generator
2^7-1, NRZ, PRBS

Figure 4.23: Component ISI measurement configuration.

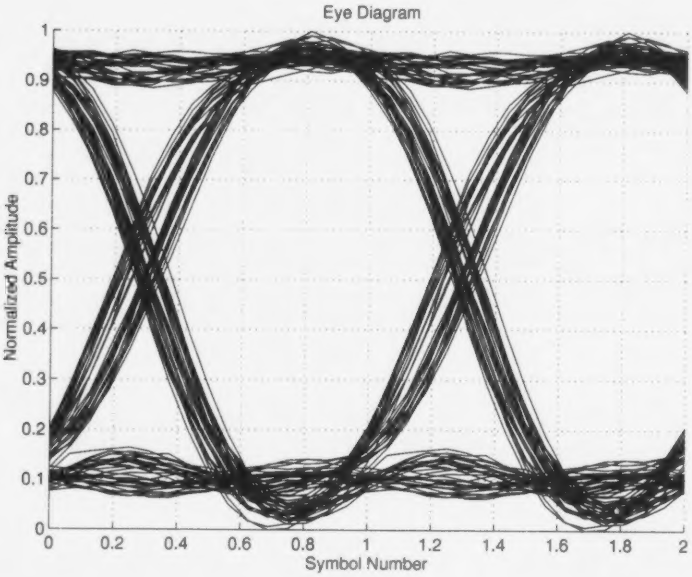

Figure 4.24: Eye diagram for the K&L 2.5 GHz LPF.

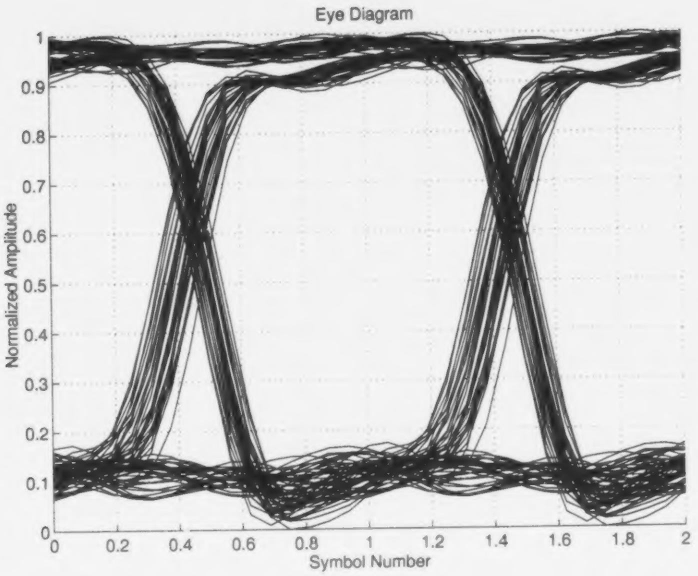

Figure 4.25: Eye diagram for the Veritech amplifier.

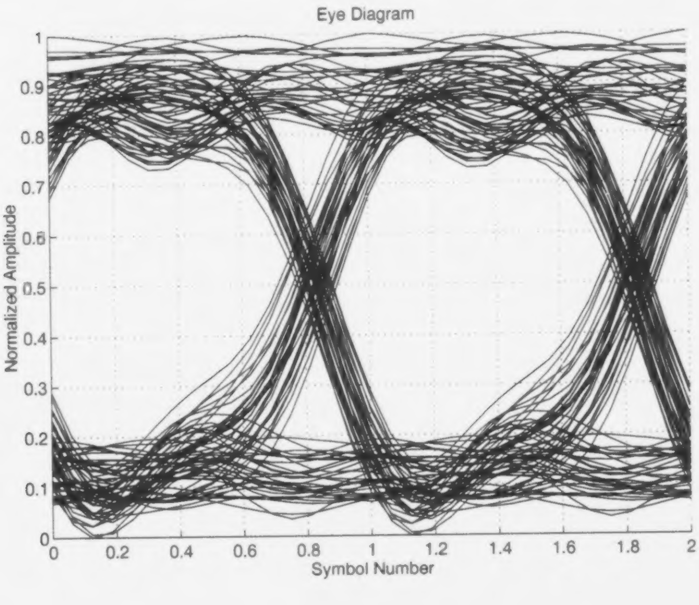

Figure 4.26: Eye diagram for the Mini-Circuit Amplifier.

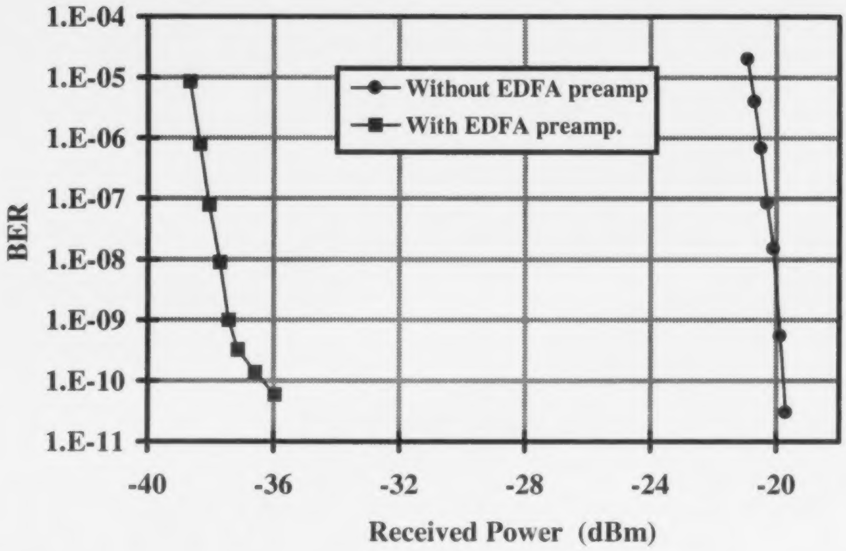

Figure 4.27: Sensitivities of the receivers with and without the EDFA.

4.3.3. Receiver Power Penalty Measurements

Previously, the receiver sensitivity was measured without any transmission fiber and in-line EDFAs. At this time, transmission links with one to three in-line EDFAs were respectively introduced into the setup shown in Figure 4.21 and in each case the receiver sensitivity, which gave a BER of $5x10^{-10}$, was measured as a function of the net EDFA gain. To factor out the ASE in order to measure the signal gain of the EDFA accurately, a 90/10 power splitter, polarization rotator and polarization splitter were employed after each EDFA, as depicted in Figure 4.28. Since the signal had a better than 20 dB polarization extinction ratio, as stated in the specifications, and the ASE is unpolarized, the polarization rotator could be adjusted such that one output of the polarization splitter was maximized and the other was minimized. By subtracting the minimum, which contained only half ASE, from the maximum, which contained the signal plus half the ASE, the net signal power could be determined. The signal gain could also be determined with the knowledge of the component losses. In addition, since the DRB of the signal is almost completely unpolarized, this gain measurement method has the ability to factor out the DRB noise. In this EDFA unit, a BPF was included and was situated in front of the amplifier to prevent the out-of-band singly amplified SRB of ASE from saturating the amplifier.

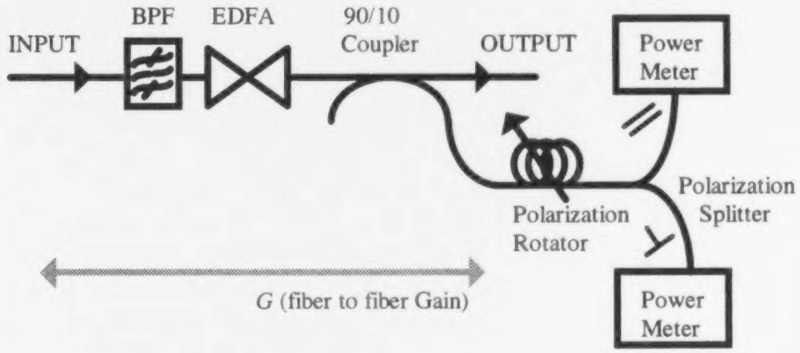

BPF
EDFA
90/10 Coupler
INPUT
OUTPUT
Power Meter
Polarization Rotator
Polarization Splitter
G (fiber to fiber Gain)
Power Meter

Figure 4.28: An EDFA unit with gain measurement capability.

In the one in-line EDFA situation, two different values of extinction ratio were used to confirm its dependence on the penalty expression. After that, measurements of two and three in-line EDFA cases were taken to further verify the number-of-amplifier dependence. In each case, to ensure that the transmission link experienced the worst case of amplified DRB effect, each in-line EDFA was immediately surrounded by at least 10 km of fiber. Also measured were the sensitivities when isolators were placed in front and/or after each EDFA to effectively eliminate the RB impact. Table 4.2 summarizes the fibers used in the experiments, and the fiber were measured using the setup in Appendix B.

Symbol in diagrams	Fiber length (km)	Total Average Fiber Loss (dB/km)	Rayleigh Backreflectance (R_{Rb})
L_1	25	0.223	-32.5 dB
L_2	50	0.244	-33.0 dB
L_3	10	0.219	-32.2 dB
L_4	10	0.232	-32.6 dB
L_5	50	0.243	-33.3 dB
L_6	25	0.218	-32.1 dB

Table 4.2: Summary of fibers used in the experiments.

4.3.3.1. Single In-line EDFA

The setup for one in-line EDFA experiment is shown in Figure 4.29. The EDFA unit, as drawn in Figure 4.28, was surrounded by transmission fibers L_1 and L_2 to generate the amplified RB effects. The EDFA employed in the unit had a serial number of TRL9407-BF450-001. Since deep saturation of the EDFA would limit its available gain, a VOA was placed directly after the transmitter to lower the input power to the EDFA. In this case, by setting the reading of the VOA to 7.6, the input power to the EDFA became -21.5 dBm. A BPF was placed at the end of the transmission fiber (L_2) to filter the out-of-band ASE arriving from the in-line EDFA. This BPF was not placed directly after the in-line EDFA because doing so would reduce the effective gain seen by Rayleigh backscattering. The VOA at the receiver was utilized to adjust the received power and to obtain a BER of $5\text{x}10^{-10}$.

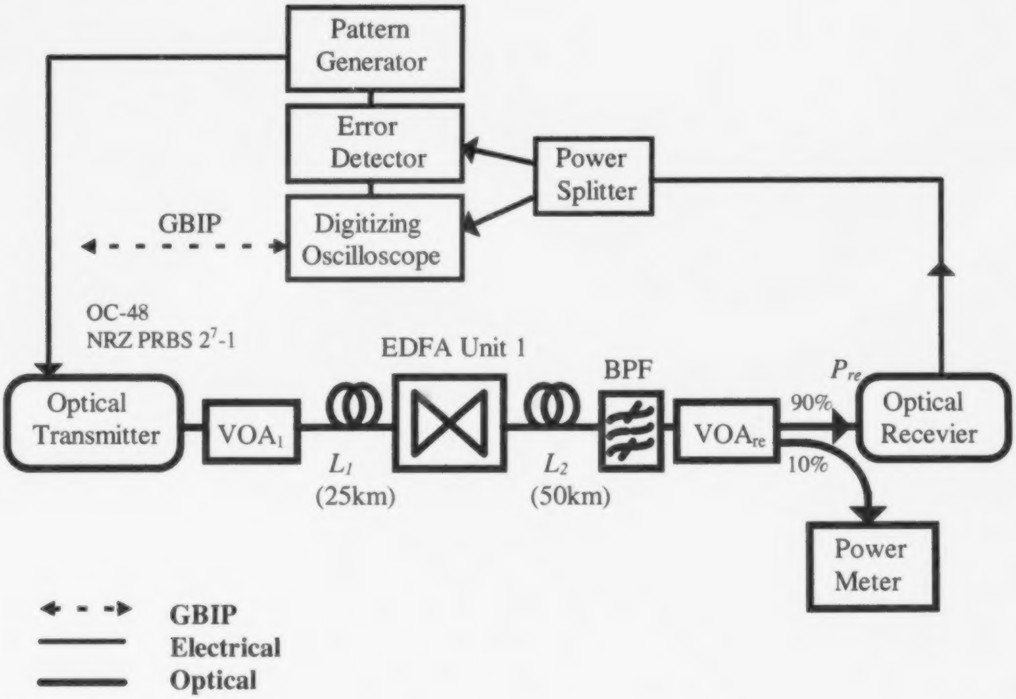
Pattern Generator
Error Detector
Digitizing Oscilloscope
Power Splitter
GBIP
OC-48
NRZ PRBS 2^7-1
EDFA Unit 1
BPF
P_re
Optical Transmitter
VOA_1
L_1 (25km)
L_2 (50km)
VOA_re
90%
10%
Optical Recevier
Power Meter
GBIP
Electrical
Optical

Figure 4.29: The configuration for 1 in-line EDFA experiment.

Table 4.3 shows the required received powers to obtain a BER of approximately 5×10^{-10} for various values of the in-line EDFA gain. The approximation in the BER measurement is due to the difficulty in obtaining exactly 5×10^{-10}. For example, in a thermal noise dominated system which has a BER of 5×10^{-10}, a change of only 0.025 dB in received power yields a change of 1×10^{-10} in the BER.

To verify that most of the received power was contributed from the directly traveling signal, a polarization rotator, followed by a polarization splitter, was inserted prior to the power meter at the receiver when the gain of the in-line EDFA was the largest (i.e. 24.8 dB). Through careful adjustment of the rotator, the maximum difference between the outputs of the polarization splitter proved larger than 13 dB, implying that all the received powers listed in Table 4.3 were essentially contributed from the directly traveling signal.

To measure the required received power for the similar BER ($5x10^{-10}$) without the Rayleigh backsattering impact, an optical isolator replaced the BPF inside the EDFA unit and was inserted directly after the EDFA unit. With this arrangement, the VOA_1 was adjusted to 8.5 in order to retain the same level of input power to the EDFA. Note that it is important to keep the input powers to the EDFA the same because the signal to spontaneous beat noise is dependent of the EDFAs input power. The received powers for a BER of about $5x10^{-10}$ were found to be independent on the amplifier gains, and equal to -37.1 dBm for both low and high amplifier gains. By subtracting -37.1 dBm from the received powers measured previously in the presence of RB, the penalty penalties due to the RB impact were obtained and shown in Table 4.3 as well.

Net Gain G (dB)	Received Power P_{re} (dBm)	BER	Power Penalty ΔP (dB)
14.5	-36.8	4×10^{-10}	0.3
16.6	-36.9	6×10^{-10}	0.2
18.6	-36.6	3×10^{-10}	0.7
20.6	-36.0	8×10^{-10}	1.1
21.9	-34.8	2×10^{-10}	2.3
22.9	-33.8	5×10^{-10}	3.3
23.5	-31.2	4×10^{-10}	5.9
24.3	-29.3	8×10^{-10}	7.8
24.8	-25.3	5×10^{-10}	11.8

Table 4.3: 1 in-line EDFA measurement results.

To calculate the theoretical penalty, the extinction ratio of the signal has to be determined. To determine an extinction ratio, one needs to know the ratio of the AC gain to DC gain of a receiver [75]. Since the gain ratio was unknown in this case, only an approximation of the extinction ratio could be obtained. This was accomplished in the following subsection.

4.3.3.1.1. Approximation to Extinction Ratio

Illustrated below is a way to determine an extinction ratio of an optical signal. Figure 4.30 depicts optical power levels during spaces and marks. The average received optical power can be expressed as

$$P_{re} = \frac{P_1}{2}\left(1+\frac{1}{d}\right) \tag{4.34}$$

By multiplying the responsivity of the photodetector, the detected DC current becomes

$$I_{DC} = \frac{P_1}{2}\left(1+\frac{1}{d}\right)\Re \tag{4.35}$$

For a receiver as shown in Figure 4.31, the detected peak-to-peak voltage can be expressed as

$$V_{p-p} = P_1\left(1-\frac{1}{d}\right)\Re \cdot g_{RF} \cdot R \tag{4.36}$$

where g_{RF} and R is the voltage gain and effective input impedance of the RF amplifier, respectively. Using Eqn. (4.35) and (4.36), we express the extinction ratio as

$$d = \frac{2I_{DC} \cdot g_{RF} \cdot R + V_{p-p}}{2I_{DC} \cdot g_{RF} \cdot R - V_{p-p}} \tag{4.37}$$

Therefore, the extinction ratio can be determined if all the parameters in the right hand side of the last equation can be measured accurately. However, as the eye diagram depicted earlier in Figure 4.22, the measured $V_{p\text{-}p}$ varied from one trace to the other. As a result, Eqn. (4.37) is not applicable in this case.

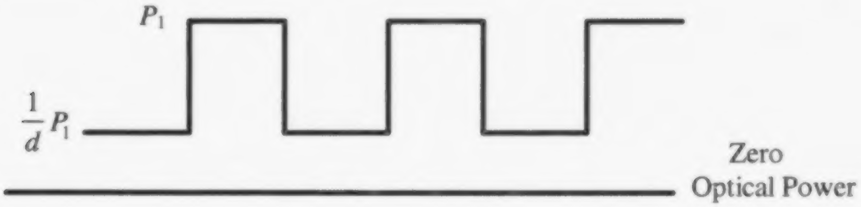

Figure 4.30: Optical signal power levels during spaces and marks.

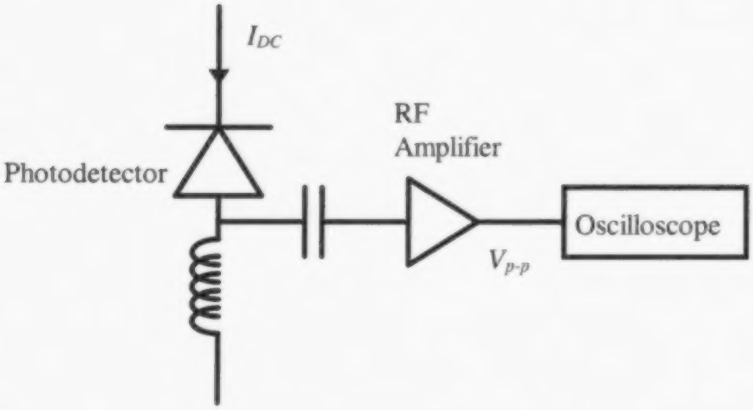

Figure 4.31: An optical receiver.

To approximate an extinction for the detected signal, the eye diagram for the detected signal as shown in Figure 4.32 was used. In this diagram, the highest trace during a space and the lowest trace during a mark contributed the most errors when compared to other traces, due to the smallest eye opening. In addition, with the pattern of the modulating signal being only 2^7-1, these traces occurred once every 127 bits, thereby accounting for most of the observed bit errors. Hence, to a good approximation, these traces could be used as the normalized optical powers during a space and a mark to define the extinction ratio of the signal. If the minimum of the signal outputted from the modulator was assumed to have almost zero optical power as compared to its maximum, the normalized zero point in this eye diagram also corresponded to the true zero optical power point. This assumption was justified because a large modulating power was used to drive the modulator in the experiments [74]. By using the highest and lowest traces respectively as the optical power for a space and a mark, the extinction ratio could be approximately obtained as 3.7.

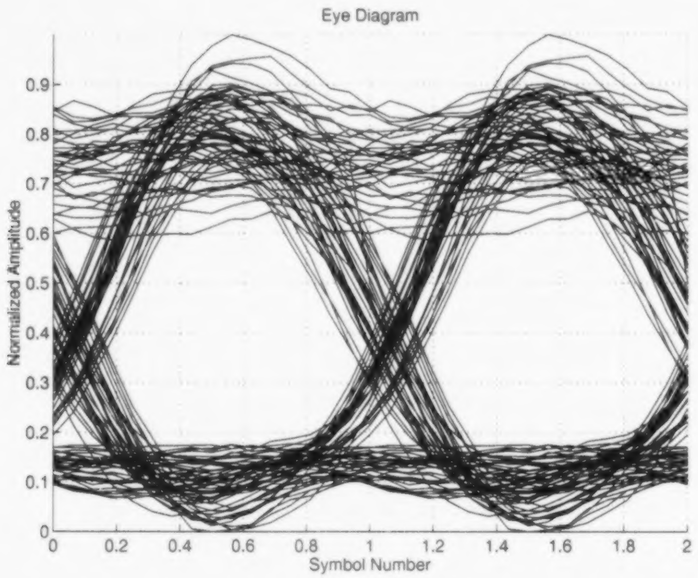

Figure 4.32: Eye diagram for 1 in-line EDFA experiment.

4.3.3.1.2. Theoretical and Experimental Comparison

The previously derived penalty expression (4.31) assumed the presence of connecting fibers with the same Rayleigh backscattering reflectance. However, the fibers used in these experiments did not have this property. To account for this, a simple modification of the expression is required, and which is listed in Table 4.4. Also listed are the parameters used in the calculation of the power penalty. Figure 4.33 depicts the experimental and theoretical penalties for this single in-line EDFA experiment. This clearly demonstrates that the theory agrees closely with the experimental measurements.

R_{RB}^2	$R_{RB\perp 1} R_{RB\perp 2}$
Q	6.1
d	3.7
N	1

Table 4.4: The modification and parameters involved in the calculation of the penalty.

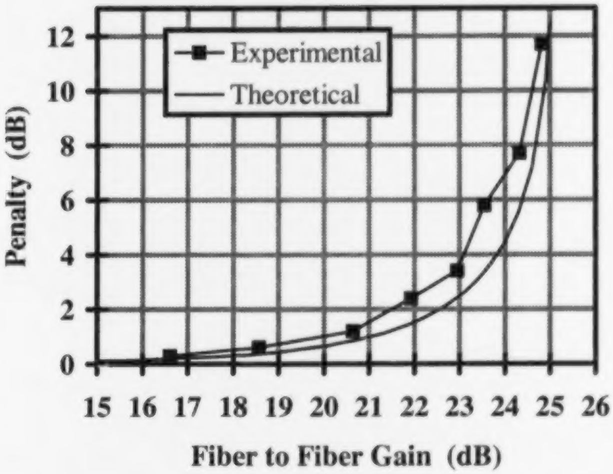

Figure 4.33: The experimental and theoretical penalties versus the in-line EDFA gain.

4.3.3.1.3. Reduced Extinction Ratio

In this experiment, the power penalty was investigated again for the same configuration, as shown in Figure 4.29. In this case, the DC voltage was changed slightly to obtain an eye with a smaller opening. Figure 4.34 shows the eye of the received signal after the DC bias adjustment. The extinction ratio of the eye is approximately equal to 1.8.

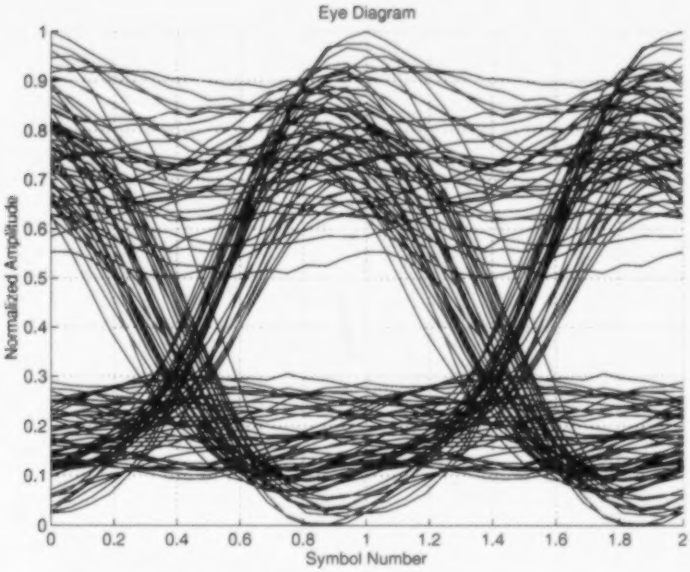

Figure 4.34: Eye of the received signal after adjusting the bias slightly.

By going through the same measurement procedures as utilized previously, a set of required received powers and penalties for various in-line EDFA gains were recorded, as listed in Table 4.5. To calculate the theoretical power penalty as a function of the in-line EDFA gain, the penalty expression, along with Table 4.4 and 1.8 for the extinction ratio, was used. Both the experimental and theoretical values are presented in Figure 4.35. Again, this figure shows agreement between the theoretical and experimental results.

Net Gain *G* (dB)	Received Power P_{re} (dBm)	BER	Power Penalty ΔP (dB)
16.8	-34.8	5 x 10^{-10}	0.4
19.6	-34.7	3 x 10^{-10}	0.5
20.6	-34.2	5 x 10^{-10}	1.0
21.5	-31.9	6 x 10^{-10}	3.3
22.4	-29.3	7 x 10^{-10}	5.9
22.7	-24.5	6 x 10^{-10}	10.7

Table 4.5: 1 in-line EDFA measurement results for the signal with a smaller eye opening.

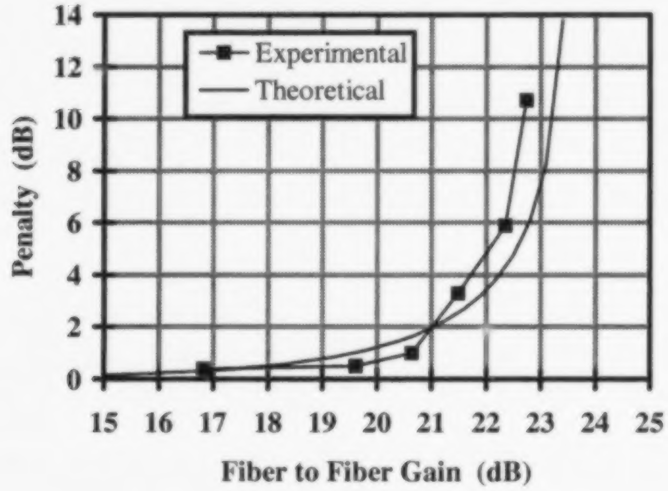

Figure 4.35: Experimental and theoretical power penalties for the signal with a smaller eye opening.

4.3.3.1.4. Discussion of These Experiments

To illustrate the extinction ratio dependence, the experimental and calculated power penalties for the two extinction ratios used in the previously experimental measurements are depicted together in Figure 4.36. Also shown in this figure is the theoretical power penalty versus in-line amplifier gain for an optical signal with a perfect extinction ratio. It can be seen from this figure that extinction ratio has a significant impact on determining the power penalty. In addition, this figure indicates that for the high amplifier gain, the experimental results give a consistently higher penalty than the theoretical calculations. The reason for this discrepancy can be two-fold. First, as Appendix F illustrates, the penalty expression determines the lower bound value, and the deviation from the actual value increases with the amplifier gain. Second, in determining the extinction ratio, the assumption that the normalized zero in the eye diagram corresponds to the detection of the zero optical power will overestimate the real extinction ratio.

Nevertheless, in most practical situations, only a small penalty can be tolerated; therefore the in-line amplifier gain in an open cascade link is restricted only to some moderate value. Note that the more detailed study on the open cascade system was discussed earlier in this chapter. Since the penalty expression closely predicted the experimental results for the two different extinction ratios, particularly for low amplifier gains, the validity of this expression has been experimentally verified for a single in-line amplifier.

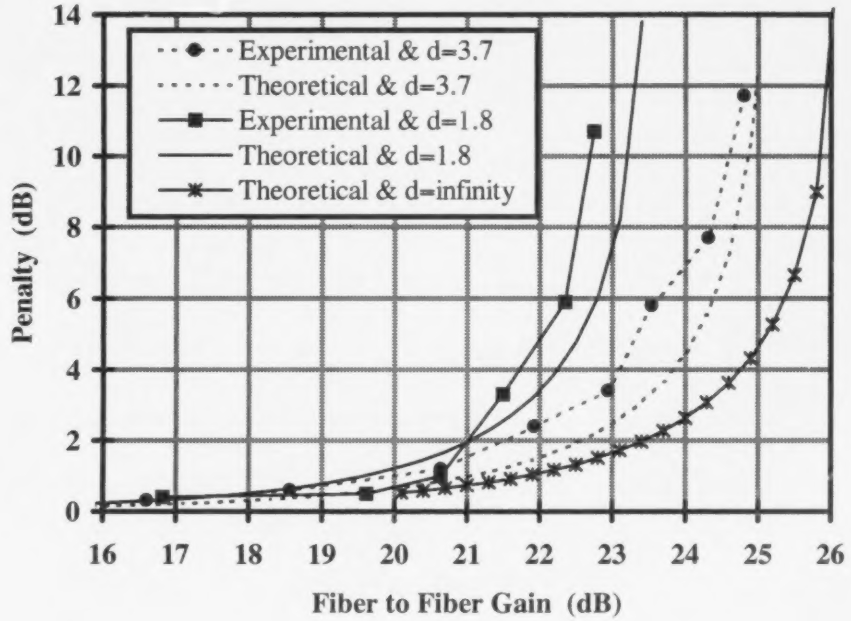

Figure 4.36: Both the experimental and theoretical results for the two extinction ratios.

4.3.3.2. Multiple In-line EDFAs

4.3.3.2.1. Two In-line EDFAs

Figure 4.37 depicts the experimental configuration for a transmission link with an open cascade of two in-line EDFAs. This configuration is similar to that of the single in-line EDFA experiment, except that an EDFA unit, 2 reels of fiber and a VOA have been added. The added EDFA unit, dubbed EDFA unit 2 in the diagram, contained an EDFA with serial number TRL9407-BF450-002, and a polarization rotator, polarization splitter and power meter to measure the signal gain, as illustrated previously in Figure 4.28. The details of the fibers have been previously given in Table 4.2. The VOA_2 between the EDFA units was intended to adjust the transmission loss such that the interamplifier loss could be adjusted to be equal to the amplifier gain. This condition has been applied in the derivation of the penalty expression (4.31).

In this experiment, the VOA_1 was set to 6.1, yielding -20 dBm input power to the first EDFA unit. The measurement procedures for determining the required received power to give a BER of about $5x10^{-10}$ can be briefly described as follows:

a) Set the gain of the EDFA unit 1 to some value *G*.
b) Adjust the VOA_2 such that the total loss of the transmission is also 1/*G*.
c) Adjust the gain of the EDFA unit 2 to *G* as well.
d) Readjust the gain of the EDFA unit 1 to *G* since this gain will change slightly due to the change in ASE level after procedure c and d.
e) Readjust the gain of the EDFA unit 2 since this gain will change slightly due to the change in ASE level after procedure d.
f) Repeat procedures d and e until no noticeable changes occur in the gain.
g) Vary the VOA_{re} attenuation to obtain a BER of approximately $5x10^{-10}$ and record the received power.

By following and repeating these procedures, a series of received powers for various in-line EDFA gains were obtained and are listed in Table 4.6. Note that the listed received power in this table had been proven to contain mostly the forward traveling signal by using the polarization method as discussed previously in Section (4.3.3.1). Also given in this table are the power penalties compared to the isolated EDFA system, in which an optical isolator replaced the BPF inside the EDFA unit 1 and was added right behind the EDFA unit 2. With these isolators, the Rayleigh backscattering effects were essentially eliminated.

Figure 4.38 depicts the eye diagram of the received signal in this experiment, which determines the extinction ratio for the theoretical power penalty. The opening of this eye had been maximized by carefully adjusting the DC bias for a minimum BER at the beginning of the measurement. The extinction ratio in this case was approximately equal to 3.6. By inserting this value into the penalty expression (4.31) and considering the differences in the Rayleigh backscattering reflectance of the fibers given in Table 4.2, the power penalties are calculated and listed in Table 4.6. Figure 4.39 shows these calculated penalties along with the experimental penalties. Again, the theoretical values accurately match the experimental values in this two in-line EDFA experiment; the underestimation of the penalty expression in a high gain region has been addressed earlier in Section (4.3.3.1.4).

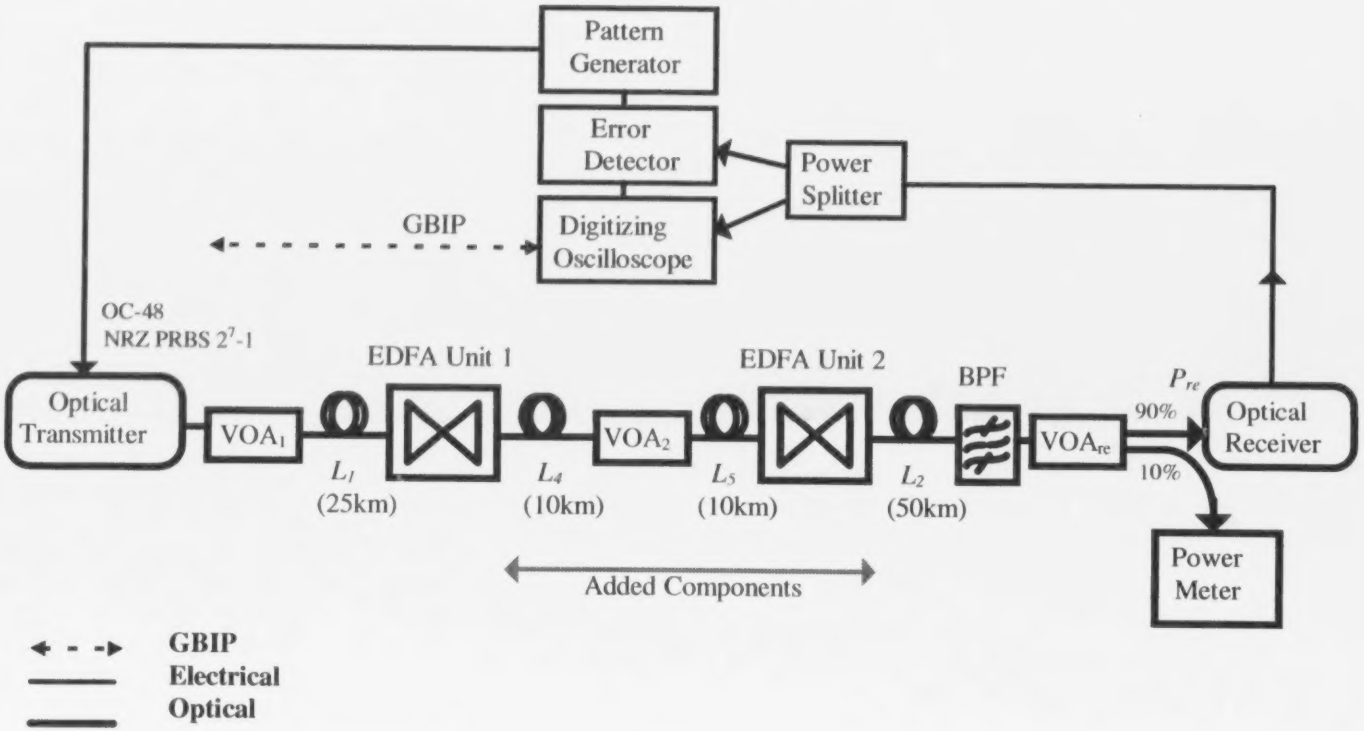
Pattern Generator
Error Detector
Digitizing Oscilloscope
Power Splitter
GBIP
OC-48
NRZ PRBS 2^7-1
Optical Transmitter
VOA_1
EDFA Unit 1
L_1 (25km)
L_4 (10km)
VOA_2
L_5 (10km)
EDFA Unit 2
L_2 (50km)
BPF
VOA_{re}
P_{re}
90%
10%
Optical Receiver
Power Meter
Added Components
GBIP
Electrical
Optical

Figure 4.37: Configuration for 2 in-line EDFA experiment

Net Gain G (dB)	Received Power P_{re} (dBm)	BER	Power Penalty ΔP (dB)
15.6	-36.0	7×10^{-10}	0.6
16.3	-36.1	3×10^{-10}	0.5
17.2	-36.2	5×10^{-10}	0.4
18.3	-35.9	4×10^{-10}	0.7
18.8	-35.4	3×10^{-10}	1.2
19.6	-34.5	5×10^{-10}	1.9
20.7	-33.5	4×10^{-10}	3.1
21.2	-31.7	5×10^{-10}	4.9
21.9	-29.8	3×10^{-10}	6.8
22.6	-26.0	6×10^{-10}	10.6

Table 4.6. Measurement results for the 2 in-line EDFA configuration.

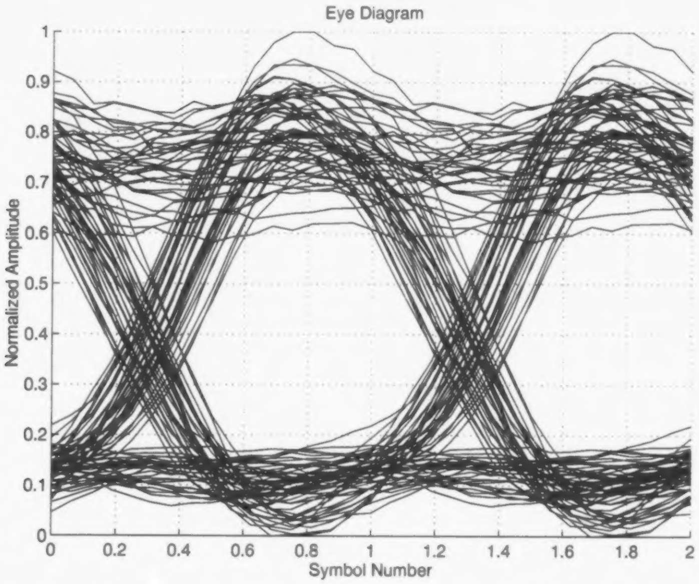

Figure 4.38: Eye diagram of the received signal in the 2 in-line EDFA experiment.

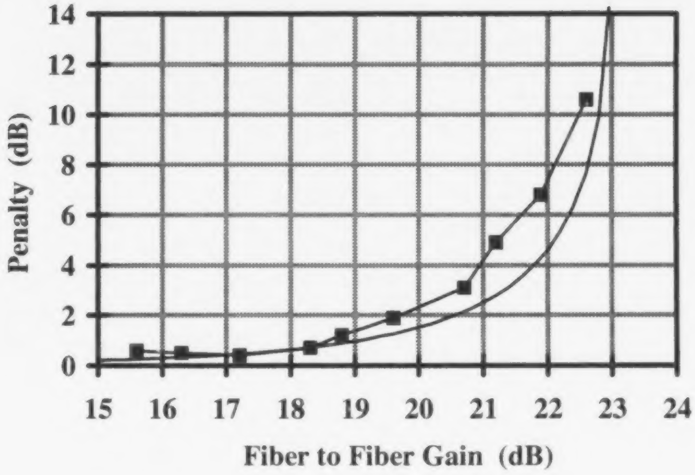

Figure 4.39: Experimental and theoretical results for the 2 in-line EDFA experiment.

4.3.3.2.2. Three In-line EDFAs

Depicted in Figure 4.40 is the configuration for the three in-line EDFA experiment. Compared to the previous configuration for the two in-line EDFA case, another EDFA unit and 2 reels of fiber were added to make up this new arrangement. The newly added unit, as earlier shown in Figure 4.28, contained an EDFA with serial number TRL-R0303-005. Note that, as mentioned before, the VOAs between the EDFA units were to provide the adjustment ability so that the condition of interamplifier loss being equal to amplifier gain could be satisfied.

With this configuration, the input power to the first EDFA unit was -17.6 dBm. The measurement procedures concerning the required received power for a BER of about 5×10^{-10} are logically similar to those concerning the two in-line EDFA case; for purposes of clarification, they are stated as follows.

a) Set the gain of the EDFA unit 1 to some value *G*.

b) Adjust the VOA_1 such that the total loss of the transmission between the unit 1 and unit 2 is 1/*G*.

c) Adjust the gain of the EDFA unit 2 to *G*.

d) Adjust the VOA_2 such that the total loss of the transmission between the unit 2 and unit 3 is 1/*G*.

e) Adjust the gain of the EDFA unit 3 to *G* as well.

f) Readjust the gain of the EDFA unit 2 to *G* since this gain will change slightly due to the change in the ASE level after procedure d and e.

g) Readjust the gain of the EDFA unit 1 to *G* since this gain will change slightly due to the change in the ASE level after procedure b - f.

h) Readjust the gain of the EDFA unit 2 due to the change in the ASE level after procedure g.

i) Readjust the gain of the EDFA unit 3 due to the change in the ASE level after procedure f - h.

j) Repeat procedures f - i until no considerable changes occur in the gain.

k) Vary the VOA_{re} attenuation to obtain a BER of approximately $5x10^{-10}$ and record the received power.

By following and repeating these procedures, a series of received powers for various in-line EDFA gains were obtained, all of which are listed in Table 4.7. Again, the listed received power in this table had been proven, by using the polarization method previously discussed, to contain mostly the forward traveling signal power. Also given in this table are the power penalties in comparison to the isolated EDFA system, in which an optical isolator replaced the BPF inside the EDFA unit 1 and was added directly after the EDFA units 2 and 3. With these isolators, the Rayleigh backscattering effects were basically eliminated.

Concerning the determination of the extinction ratio for the theoretical power penalty, Figure 4.41 depicts the eye diagram of the received signal in this experiment. The opening of this eye had been maximized through careful adjustment of the DC bias in order to obtain minimum BER at the beginning of the measurement. The extinction ratio in this case was approximately equal to 3.3. By inserting this value into the penalty expression (4.31) and considering the differences in the Rayleigh backscattering reflectance of the fibers given in Table 4.2, the power penalty are calculated and listed in Table 4.7. Figure 4.42 compares the experimental measurements with the calculated penalties. Again, the theoretical values correspond accurately with the experimental values in this three in-line EDFA experiment; the underestimation of the penalty expression in the high gain region has been addressed in Section (4.3.3.1.4).

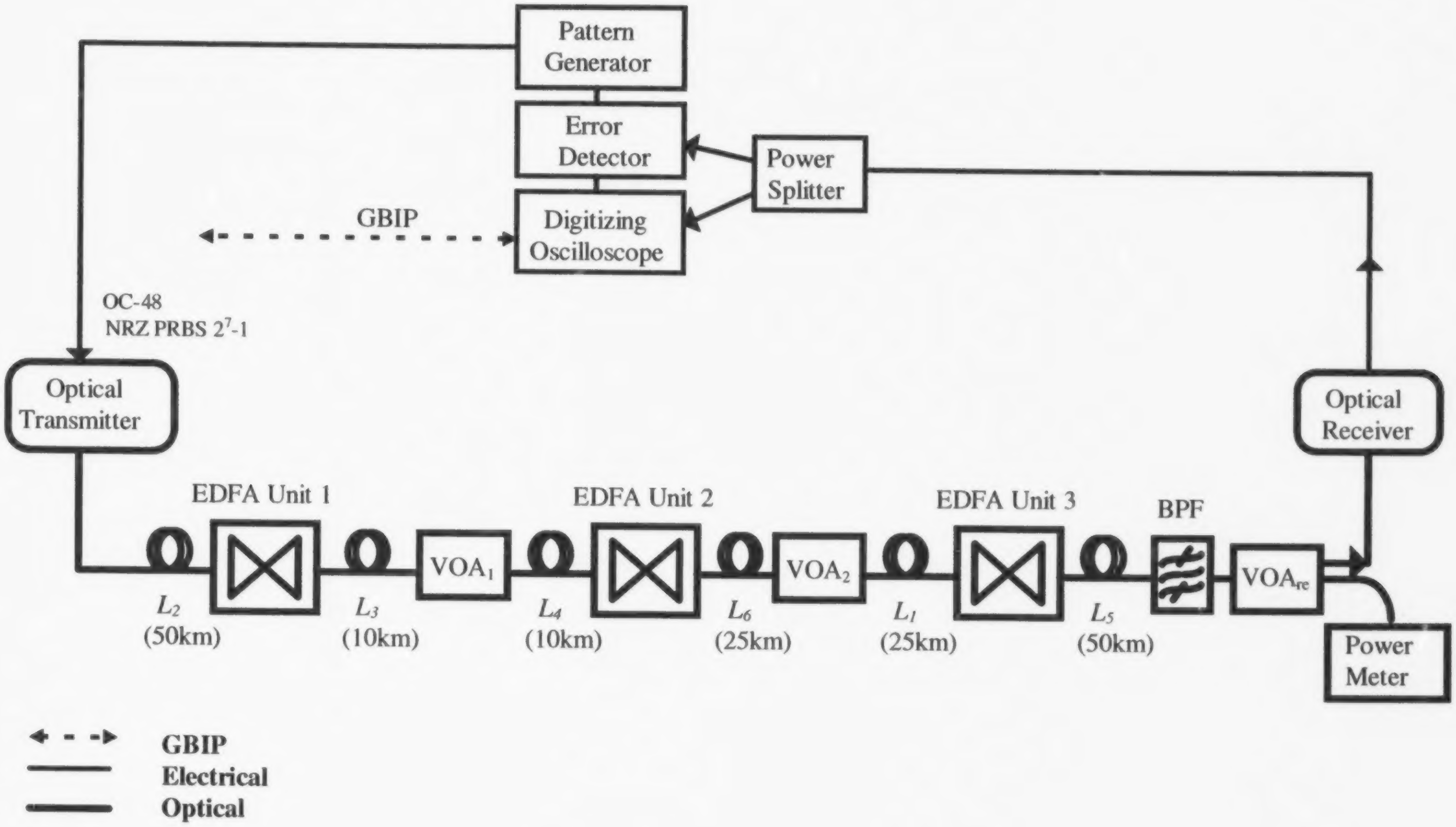

Pattern Generator
Error Detector
Digitizing Oscilloscope
Power Splitter
GBIP
OC-48
NRZ PRBS 2^7-1
Optical Transmitter
Optical Receiver
EDFA Unit 1
EDFA Unit 2
EDFA Unit 3
BPF
VOA$_1$
VOA$_2$
VOA$_{re}$
L_2 (50km)
L_3 (10km)
L_4 (10km)
L_6 (25km)
L_1 (25km)
L_5 (50km)
Power Meter
GBIP
Electrical
Optical

Figure 4.40: Configuration for the 3 in-line EDFA experiment.

Net Gain G (dB)	Received Power P_{re} (dBm)	BER	Power Penalty ΔP (dB)
14.3	-36.3	4×10^{-10}	0.4
15.3	-36.1	4×10^{-10}	0.6
16.3	-35.5	4×10^{-10}	1.2
17.5	-34.5	4×10^{-10}	1.8
19.0	-31.9	4×10^{-10}	4.8
19.9	-28.5	5×10^{-10}	8.2
20.4	-24.5	5×10^{-10}	12.2

Table 4.7: Measurement results for the 3 in-line EDFA configuration.

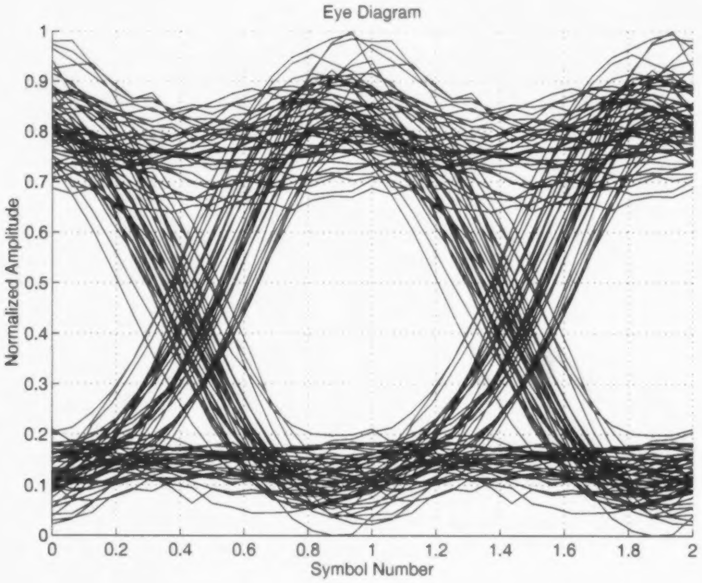

Figure 4.41: Eye diagram of the received signal in the 3 in-line EDFA experiment.

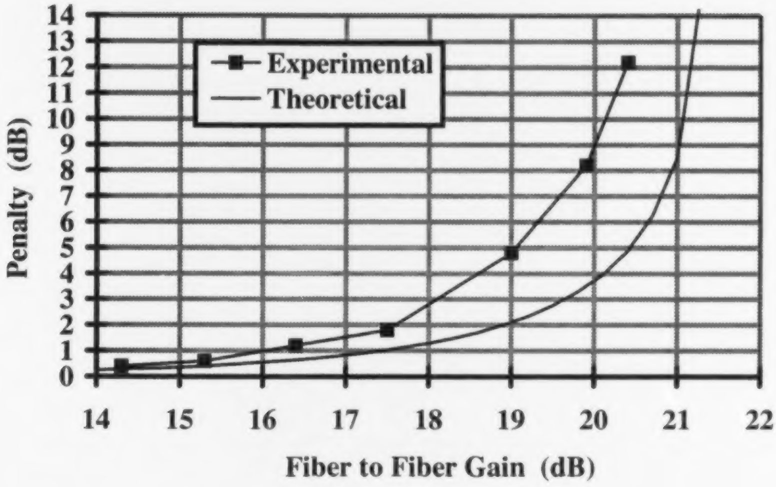

Figure 4.42: Experimental and theoretical results for the 3 in-line EDFA experiment.

4.3.3.2.3. Discussion of These Multiple In-line EDFA Experiments

To illustrate the number-of-amplifier dependence in the penalty expression, the results obtained previously for the single in-line EDFA configuration, and the results for the two and three in-line EDFA configurations, are depicted together in Figure 4.43. Since the allowable penalty in practical systems is only a small amount, and the penalty expression predicted the experimental results for three different numbers of in-line EDFA closely, particularly for low amplifier gains, the number-of-amplifier dependence in this expression has been satisfactorily confirmed. It should be pointed out that the slight decrease in the eye opening for the longer span, as shown in Figure 4.32, Figure 4.38 and Figure 4.41 could be a result of the ISI effect generated by the residual chirp of the UTP switch and fiber dispersion.

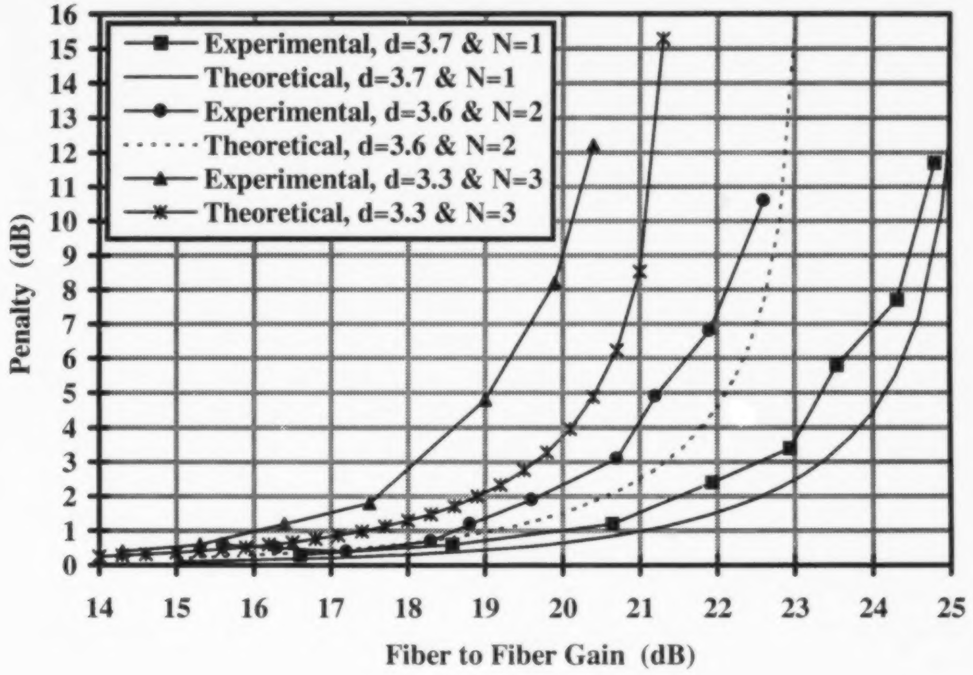

Figure 4.43: Both the experimental and theoretical results for the 1, 2 and 3 in-line amplifier configurations.

4.3.4. End-to-End BER Measurement

In this experiment, the condition of amplifier gain-loss product being equal to 1 was removed, and thus the system BER was measured as a function of this product. By comparing the measured BERs in the open cascade system to the theoretical BERs calculated by considering all the significant noises in the receiver, the previous theoretical studies in Section (4.2.3) has been verified.

The same setup, as shown in Figure 4.40, for the three in-line amplifier system power penalty measurement was utilized in this experimental measurement. The modulating signal was a 2^7-1, NRZ, PRBS at a data rate of 2.5 GHz. Two interamplifier losses were used for the measurement: 18 dB and 20 dB. It should be noted that in the previous procedures the VOA attenuation at the receiver was adjusted to obtain a BER of about

$5x10^{-10}$, but in this experiment, this VOA attenuation was fixed for each interamplifier loss.

In the experiment, when the interamplifier loss was first fixed at 18 dB, BERs at the receiver were recorded for various in-line EDFA gains. For each recorded BER, the gain of each in-line amplifier was adjusted carefully and repeatedly until they were equal. Next, the interamplifier loss was increased to 20 dB, and then a new set of BER values were recorded. Both of these measured BERs as a function of the EDFA gain are depicted in Figure 4.44. Also depicted are the theoretical BER values calculated by considering all the significant noises in the receiver, as discussed in Section (4.2.3) and with the parameters listed in Table 4.2 and Table 4.8. Figure 4.45 depicts the measured and theoretical BERs for the same setup except an isolator replaced the BPF inside the EDFA unit 1 and was added right after the EDFA 2 and 3. Again, with these isolators, the RB effects were virtually eliminated.

Figure 4.44 clearly shows the experimental existence of a minimum BER at a certain value of the amplifier gain in the open cascade system. As confirmed by Figure 4.45, there is no evidence of such behavior in optically amplified isolated systems. It is worth mentioning that when the gain is a few dB less than the loss, the open cascade system is not degraded by the DRB noise, and its BER is determined by the combination of thermal noise, signal to spontaneous beat noise and spontaneous to spontaneous beat noise. Therefore, determination of the theoretical BERs in the low gain region requires the knowledge of the each EDFA's spontaneous emission factor and the optical noise equivalent bandwidth of a chain of optical bandpass filters. and these are difficult to measure accurately. In this case, some practical values for the spontaneous emission factors and optical noise equivalent bandwidth were used to calculate the theoretical BERs, and which are listed in Table 4.8.

On the other hand, when the gain is large, the open cascade system becomes dominated by the DRB noise. As a result, the signal to spontaneous beat noise and spontaneous to spontaneous beat noise can be ignored so that the BER in this high gain region, which is only determined by the DRB noise, can be utilized to verify the theoretical studies discussed earlier in Section (4.2.3). Figure 4.44 shows a reasonably close agreement between the measured BERs and the theoretical BERs. The consistently higher BERs obtained from theory can be explained as follows. In the calculation, an extinction ratio of 3.3 is used, which is the worst case extinction ratio since it was estimated by using the highest and lowest traces in the eye diagram in Section (4.3.3.2.2).

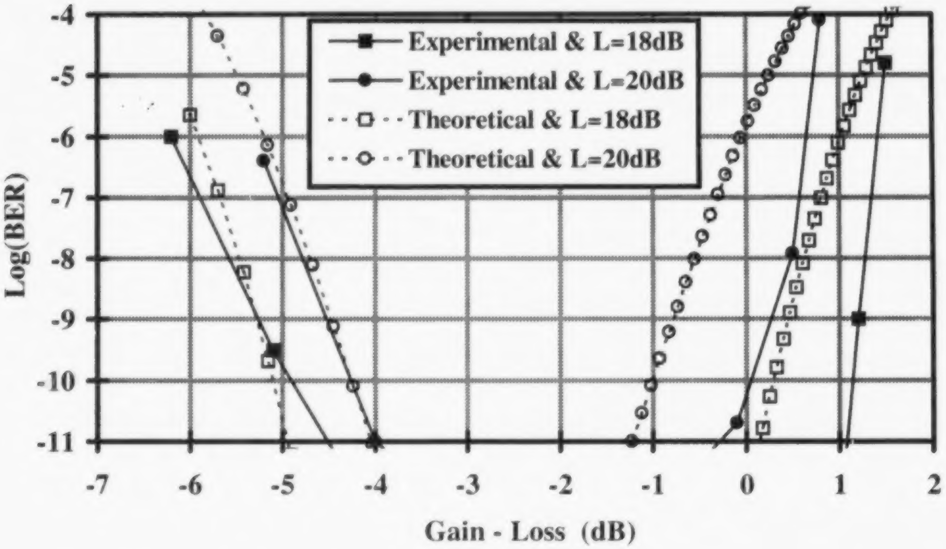

Figure 4.44: Experimental BER on 3 in-line EDFA open cascade systems.

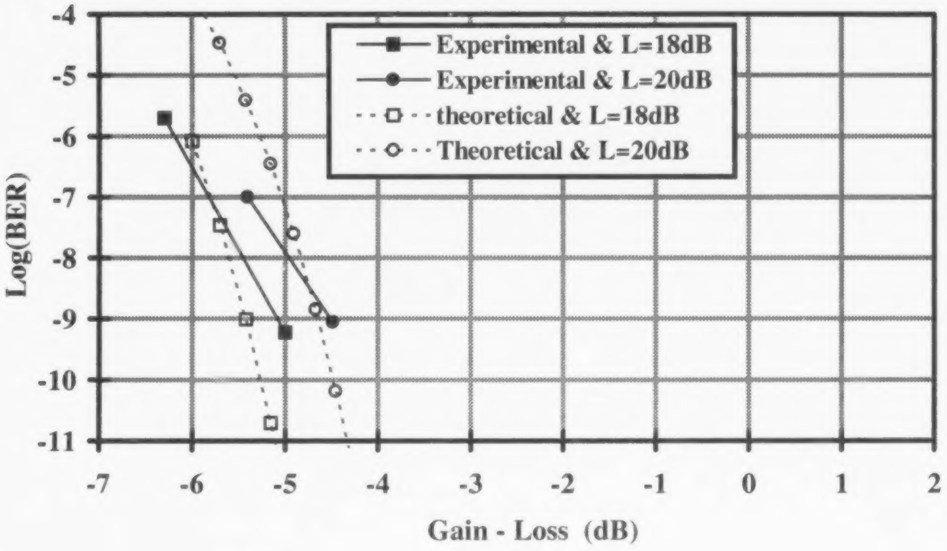

Figure 4.45: Experimental BER on 3 in-line EDFA systems with isolators.

Parameter	Symbol	Value
Optical noise equivalent bandwidth	B_o	1.5x125 GHz (i.e. 1.5 nm)
Spontaneous emission factor	n_{sp}	1.3
Extinction ratio	d	3.3
Electrical noise equivalent bandwidth	B_{re}	2.5 GHz
Gain of preamplifier		20 dB
Interamplifier loss	IL	18 or 20 dB
Number of amplifiers	N	3
Responsivity	$\Re$	0.7
Front-end thermal noise current density		13 pA/Hz

Table 4.8: Parameters involved in the experiment and theoretical calculation.

4.3.5. Experiment Summary

The above experimental results of the one, two and three in-line amplifier measurements demonstrate the validity of the penalty expression for open cascade systems, particularly for modest power penalties. In addition, the theoretical studies on the end-to-end BER in relation to the gain-loss product discussed in Section (4.2.3) has been experimentally confirmed.

4.4 Bi-directional Transmission

Recently, much research has been done on bi-directional transmission systems which use a single fiber [76-80], largely because bi-directional transmission could have great cost-saving potential since the number of fiber links and optical components can be reduced by a factor of two. In addition, by merging upstream and downstream traffic from two separate fiber links into one, a vacant fiber link is left for non-intrusive maintenance or upgrade purposes. This section will discuss different bi-directional system configurations. It includes conventional two fiber link systems, single fiber link systems with special amplifier configurations for eliminating the amplified RB effects and also single fiber link systems employing open cascade amplifiers. As seen earlier, the open cascade systems feasibly provide large system gain for long distance applications. To demonstrate the bi-directionality of open cascade systems, 2 wavelength bi-directional transmission experiments have been performed using open cascade systems. In addition, bi-directional transmission experiments using conventional 2 uni-directional links have been conducted. Both of these experiments will be presented and their results will be compared, based on the number of components required for implementation.

4.4.1 Types of Bi-directional Transmission Systems

4.4.1.1. Two Fiber link Bi-directional

Figure 4.46 depicts a conventional 2 fiber link bi-directional system. In this system, isolators are used to surround the in-line amplifiers so as to eliminate the amplified RB effects. In some situations, it could be more cost-effective to add BPFs to the link in order to filter the out-of-band ASE and to reduce or avoid the gain compression due to ASE accumulation for the higher system gain and lower amplifier noise figure. Since the isolators restrict the transmission direction to one-way, the system demands two links, each with its own amplifiers and isolators as shown, in order for bi-directional transmission to setup. Clearly, such systems necessitate the highest number of components possible for implementation.

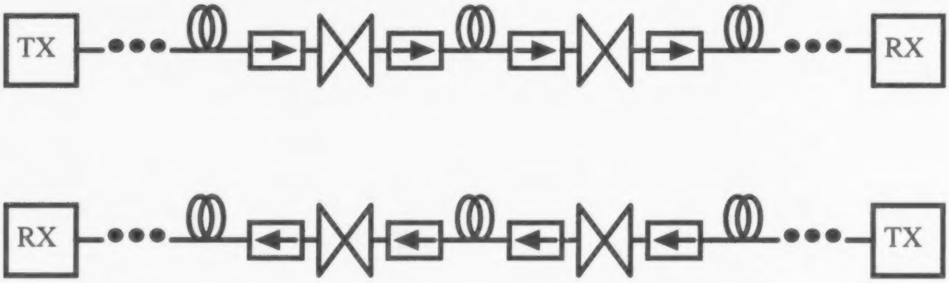

Figure 4.46: Conventional 2 fiber link bi-directional system with isolators in each link.

4.4.1.2. One Fiber Link with Bi-directional Amplifiers

Another kind of bi-directional system which has the ability to reject amplified RB effects is generically shown in Figure 4.47. The shown system employs either optical couplers, circulators or Wavelength Division Multiplexers (WDMs) at the terminal ends in order to combine or separate the signals traveling in the opposite directions. For such a system, only a single transmission fiber link is required, creating the potential for an impact on cost reduction. To compensate for the transmission loss for a longer fiber span, special amplifier configurations can be used. These amplifier configurations should have the ability of amplifying the direct signals at different wavelengths and traveling in opposite directions, but attenuate their respective backscattered signals. Thus, the span can be extended and at the same time, the amplified effects of Rayleigh backscattering can be prevented. Such amplifiers, referred to here as *bi-directional amplifiers*, can be implemented in many ways [77-78].

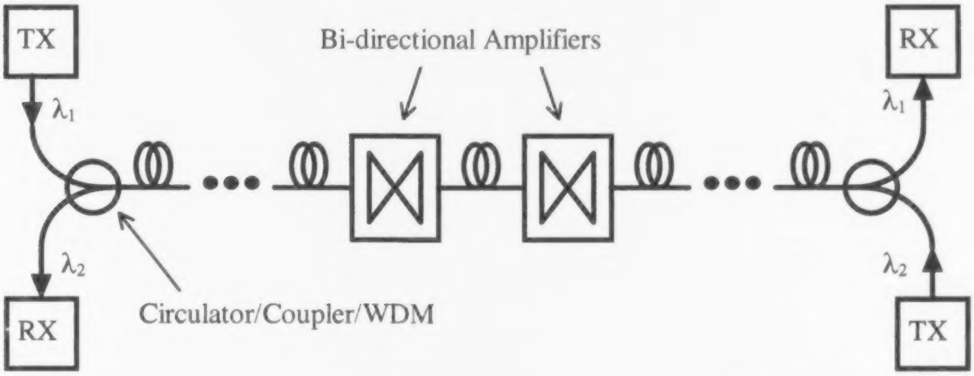

Figure 4.47: 1 fiber link bi-directional system employing bi-directional amplifiers.

At this point, three different modes of bi-directional amplifier implementation will be considered. First, one can create a system with two amplifiers, two circulators, two isolators and 2 BPFs at the signal wavelengths, as depicted in Figure 4.48. This figure reveals that the upstream signal, with a wavelength of λ_1, is routed from port 2 to port 3 of the entrance circulator, and along that path it is amplified and then routed back to the transmission fiber through port 1 to port 2 of the circulator at the rear. Any backscattered signal at this wavelength occurring after the rear circulator traveling to this circulator will be routed from port 2 to port 3 and will be filtered out by the BPF, which has a passband at λ_2. Similarly, the downstream signal, with a wavelength of λ_2, is routed from port 2 to port 3 of the rear circulator, is amplified and is then routed back by the entrance circulator to the transmission fiber. All the backscattering of this signal happened after the entrance circulator will be routed from port 2 to port 3 and be stopped by the BPF, which has a different passband wavelength. Therefore, this kind of amplifier setup has the ability to amplify the directly traveling signal in both upstream and downstream directions but rejects their corresponding backscattering. Since BPFs are situated virtually between amplifiers, this configuration helps reduce the amplifier saturation. Furthermore, by using optical highpass and lowpass filters instead of BPFs and by arranging short wavelength signals in one direction and long wavelength signals in another direction, multiple wavelength bi-directional transmission is also possible with this configuration.

Through a comparison of a single fiber link system, which utilizes this form of bi-directional amplifier setup to a conventional 2 fiber link system with BPFs, it becomes clear that the single fiber link system requires additional 2 circulators but 4 isolators and 1 fiber link less. Currently, the cost for the circulator is still relatively expensive. Once the cost is reduced, this single fiber system could have an impact on reducing the system cost.

It is clear from this figure that one can replace the two circulators with two 50/50 couplers and still maintain the same functionality. The advantage of doing so is cost reduction since the coupler is less expensive than the circulator, but the drawback is the higher loss of the coupler as compared to the circulator.

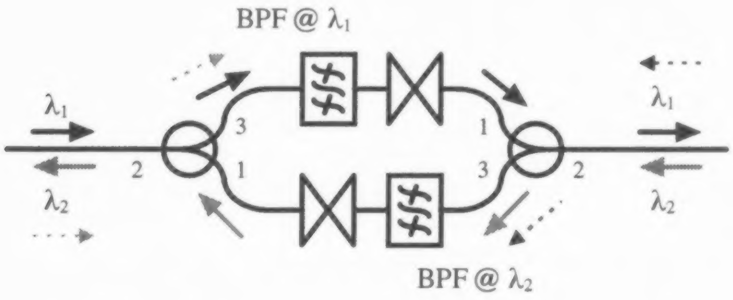

Solid lines - routes of direct signals
Dotted lines - routes of backscattered signals

Figure 4.48: Configuration of a bi-directional amplifier using 2 amplifiers, 2 circulators and 2 BPFs at the signal wavelengths.

The second configuration utilizing 2 amplifiers, 2 WDMs operating at signal wavelengths and 4 isolators, is shown in Figure 4.49. In this configuration, the upstream signal at λ_1 is routed to the upper path by the WDM at the entrance, and routed back by the WDM at the rear to the transmission link after the amplification. Any backscattered signal at this wavelength is routed to the upper path, and is impeded by the isolator. Similar circumstances apply to the downstream signal. Note that similar to BPFs, the WDMs in this configuration also have an effect in the reduction of ASE accumulation.

Presently, JDS Fitel is marketing WDMs that are directional and ideal for such applications. The specified wavelengths are 1533 nm and 1557 nm, each with a transmission bandwidth of ± 3 nm. Use of these directional WDMs infers that there will be no need for the added isolators, thereby simplifying the configuration, as shown in Figure 4.50. With the relatively low cost and adequate performance of these WDM devices, this amplifier configuration can be employed for reducing the bi-directional system implementation cost or for providing an easy and efficient form of maintenance and upgrade. Also, multiple wavelength bi-directional transmission is feasible by using closely spaced wavelength laser sources for further capacity enhancement.

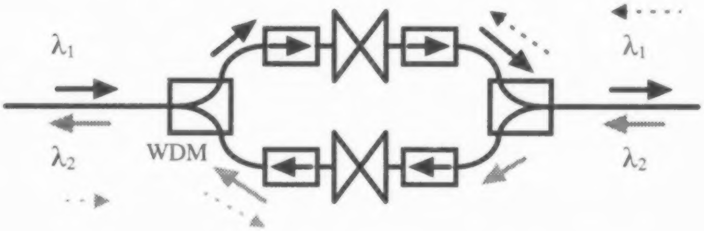

Figure 4.49: Configuration of a bi-directional amplifier using 2 amplifiers, 2 WDMs operating at the signal wavelengths and 4 isolators.

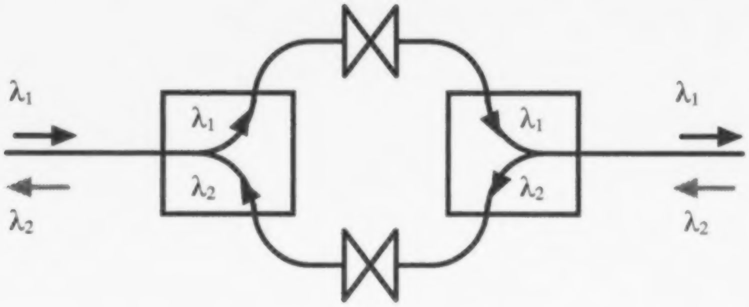

Figure 4.50: Configuration of a bi-directional amplifier using 2 amplifiers, and 2 directional WDMs operating at the signal wavelengths.

Utilizing these directional WDMs, one can even design a more cost-effective bi-directional amplifier. Figure 4.51 depicts this distinct and innovative design [81]. This particular system exploits only 1 amplifier, but 4 directional WDMs. Following the black arrows in this figure one can easily see that the upstream signal λ_1 travels through the amplifier, and any backscattered signal at this wavelength will be rejected by the last WDM. On the other hand, the downstream signal, denoted by the gray arrows, is routed by the WDMs to the input of the amplifier, and after the amplification, is rerouted to the transmission link in its original direction. Again, all the backscattered signal at this wavelength will be stopped by the first WDM.

It becomes clear that both signals travel through the amplifier in the upstream direction, as opposed to those in the previous configurations. Again, closely spaced wavelength sources can be used for multiple wavelength bi-directional transmission. Since this configuration requires only one amplifier and 4 relatively inexpensive WDM devices, the cost of which is much less than a typical fiber amplifier, this configuration can be utilized to reduce the bi-directional system implementation cost significantly, or to provide a means of increasing the capacity of the existing system.

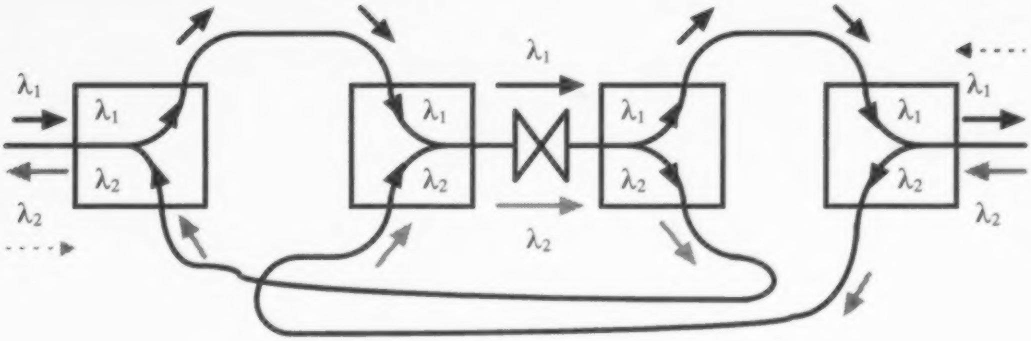

Figure 4.51: Configuration of a bi-directional amplifier using 1 amplifier, and 4 directional WDM devices.

When designing a bi-directional system which employ open cascade amplifiers, each with a moderate gain, as depicted in Figure 4.52, one can quickly recognize that this system needs a minimum number of components for implementation, as compared to the previous configurations. Also, due to the absence of BPFs and WDMs in link, this bi-directional link provides maximum networking flexibility, multiple wavelength transmission, and enables the use of optical time-domain reflectometry, which cannot be used, at least in a straightforward fashion, in all previous configurations discussed above. Due to these benefits, a number of bi-directional experiments on this open cascade system have been conducted and will be discussed in the following subsection.

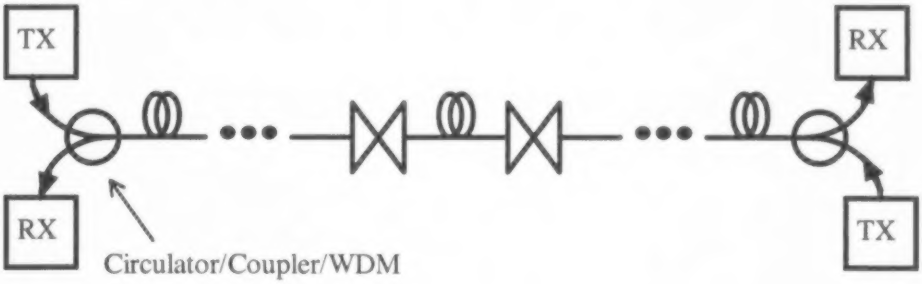

Figure 4.52: Single fiber link bi-directional transmission system employing open cascade amplifiers.

4.4.2 Bi-directional Transmission Experiments

To demonstrate the feasibility of employing open cascade configurations for bi-directional transmission systems, reports are shown of experimental results for a full duplex bi-directional system with a single fiber link and open cascade of up to four EDFAs. In the experiments, the system BER as a function of the link budget was measured. The link budget is defined as the end-to-end total available power budget for the fiber and component losses. For component count comparison, the experimental BER on a conventional system that used two fiber links, each with its own EDFAs and isolators has also been determined.

4.4.2.1. Experimental Arrangement

5 separate 170 km long single fiber bi-directional transmission system configurations have been examined and measured. Note that in the context of what follows, a pre/post amplifier means that the EDFA in question is used both as a preamplifier by the receiver and as a post or power amplifier by the transmitter; this also implies that the length of the fiber between the pre/post amplifier and the transceiver is sufficiently short so that RB effects could be ignored in this part of the link. The transceiver in the context of this writing is a terminal end in which a transmitter, receiver, optical BPF and circulator are situated. The 5 configurations considered are: two and three in-line amplifiers; two pre/post amplifiers; two pre/post amplifiers and one in-line amplifier, and two pre/post and two in-line amplifiers.

In order to ensure that the system experienced the worst case amplified RB effects, each in-line amplifier was surrounded by at least 10 km of fiber. Similarly, the pre/post amplifiers had at least the same amount of fiber on the link side. As an example, Figure 4.53 depicts the experimental configuration for the three in-line EDFA system. The two in-line EDFA configuration is the same except that VOA_2 and $EDFA_3$ are removed and the fibers are redistributed in the link. Similarly, for the pre/post amplifier configurations the first and last EDFAs are placed adjacent to the transceivers.

The transmitter 1 was the analog transmitter discussed and used in chapter 3. It was biased at 30 mA and had a 1543 nm lasing wavelength and a -1 dBm output modulated power, which was measured after the circulator. The transmitter 2 had a lasing wavelength at 1541 nm and -5 dBm modulated power measured after the circulator. Both transmitters were directly modulated by a 622 Mb/s PRBS of pattern length 2^7-1; this short pattern was limited by the low frequency cutoff of the transmitters and receivers. Note that since these signal wavelengths were spaced close together on the relatively flat region of the EDFA gain spectrum, they experienced similar amplification, and thus similar link budgets would be expected.

One common receiver was used and switched between the two terminal ends during the BER measurement. The receiver used was the TR*Labs*/BNR OC-12 Receiver, which had measured sensitivities of -26.3 dBm and -27.0 dBm for the 1543 nm and 1541 transmitters, respectively. BPFs were used in front of the receiver not only to reduce the spontaneous to spontaneous beat noise, but also to reject the backscattering of the opposite traveling signal. The conventional two link bi-directional configuration, to which the bi-directional performance and component count will be compared, is shown in Figure 4.54.

As in previous experiments, all of the fibers used were standard non-dispersion shifted single-mode fibers, possessing the characteristics mentioned earlier in Table 4.2, and all connections between fibers were either fusion splices or ultra low reflection APC connectors with the return loss being better than -60 dB.

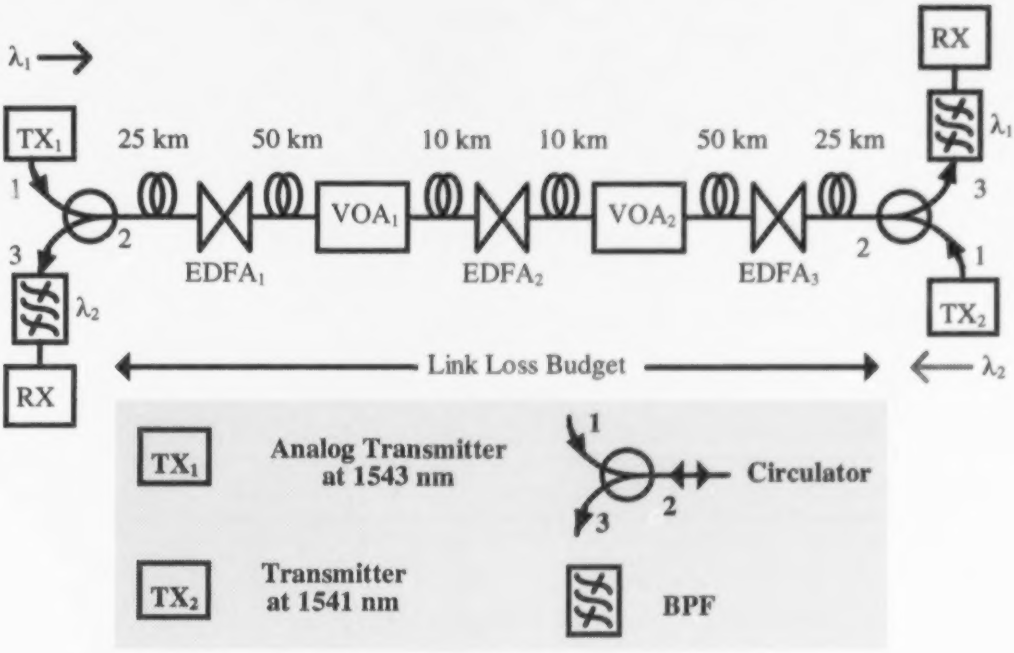
λ1 →
TX1
25 km
50 km
10 km
10 km
50 km
25 km
RX
λ1
1
3
2
VOA1
VOA2
2
3
1
EDFA1
EDFA2
EDFA3
λ2
TX2
RX
Link Loss Budget
← λ2
TX1
Analog Transmitter at 1543 nm
1
Circulator
2
3
TX2
Transmitter at 1541 nm
BPF

Figure 4.53: Full duplex bi-directional transmission with a single fiber link and 3 in-line EDFAs.

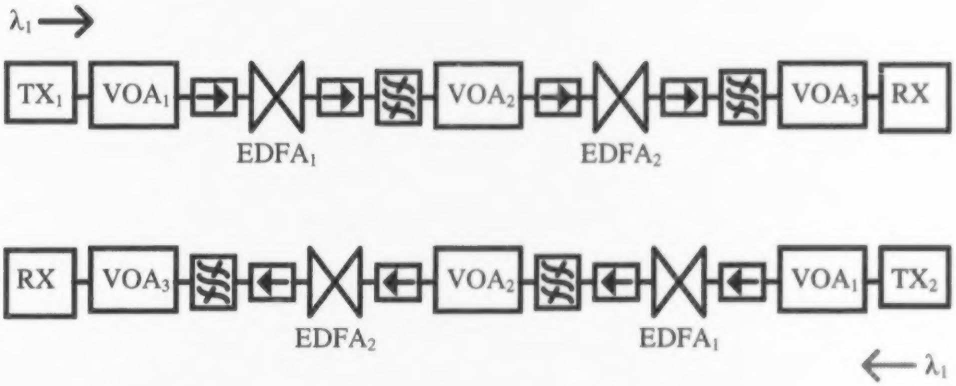
λ1 →
TX1
VOA1
VOA2
VOA3
RX
EDFA1
EDFA2
RX
VOA3
VOA2
VOA1
TX2
EDFA2
EDFA1
← λ1

Figure 4.54: Bi-directional transmission using 2 links and 4 in-line EDFAs.

4.4.2.2. Experimental Results

By adjusting the values of VOAs in each configuration, system BERs as a function of the link budget could be measured. Figure 4.55 presents these measured results, which were obtained in the five open cascade configurations, as well as in one and two in-line EDFA uni-directional link configurations. The link budgets for the 1543 nm transmitter were consistently a few dB higher than the 1541 nm transmitter due to the higher output power of the 1543 nm transmitter. As expected, the results show that the in-line EDFA configuration results in a higher link budget than pre/post configuration with the same number of EDFAs; this is mainly because the pre/post amplifiers are saturated by the transmit signals thereby reducing the operating gains. For this reason, a BER of 10^{-9} for the 1541 nm signal detection in the two pre/post EDFA configuration could just be achieved after the 170 km transmission.

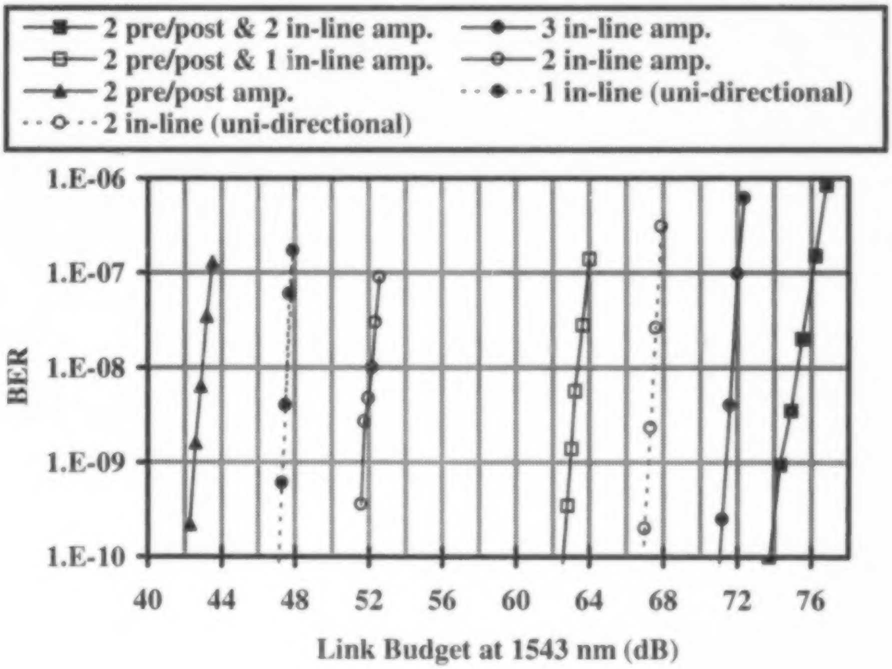

(a)

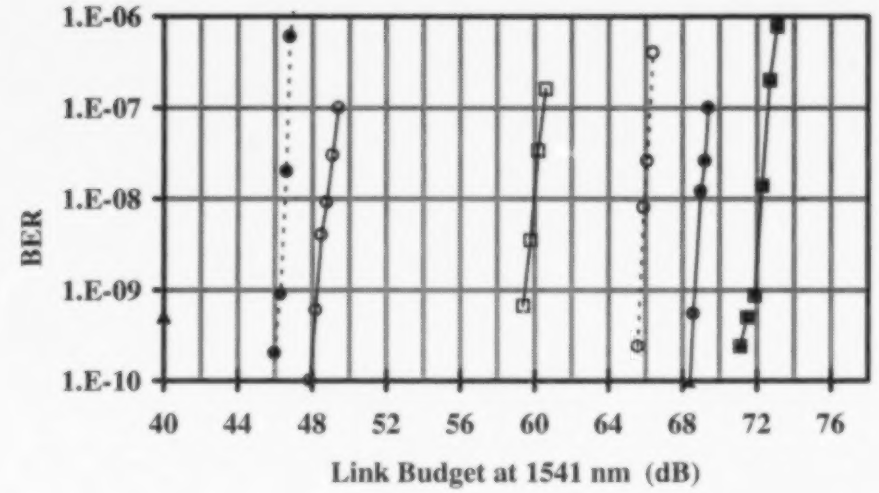

(b)

Figure 4.55: BERs of the different links as a function of the link budget for (a) the 1543 nm and (b) 1541 nm transmitters. Dotted lines denote uni-directional links, and solid lines denote bi-directional links.

Table 4.9 summarizes the results in terms of the link budget for the 1541 nm wavelength and the component count for the various two, three and four amplifier configurations. This wavelength is considered for it has smaller link budgets. These results reveal that for a one-way link loss of about 40 dB, a single two amplifier bi-directional link and two single amplifier uni-directional links will meet a 40 dB loss budget with the same net two-way OC-12 transmission capacity. Both configurations use the same number of EDFAs, but the bi-directional link uses half the fiber and filter, and two circulators as opposed to four isolators. For links with a loss about 60 dB, the loss budget can be satisfied in the bi-directional link configurations relative to the full duplex uni-directional links with one less amplifier, two fewer filters, half the fiber and two circulators against eight isolators.

To conclude these experimental results, in the absence of network operation considerations, have demonstrated that not only are bi-directional open cascade systems feasible for long distance applications, but they also require fewer components to implement, hence allowing one more options for economic network implementation and growth.

EDFA Configuration	Component Count			Link Budget (BER=10^{-9})	
a) Bi-directional	EDFAs	Filters	Circulators	dB	Equivalent fiber length km
2 pre/post, 2 inline	4	2	2	72	306
3 inline	3	2	2	69	293
2 pre/post, 1 inline	3	2	2	60	255
2 inline	2	2	2	48	204
2 pre/post	2	2	2	40	170
b) Unidirectional	EDFAs	Filters	Isolators		
2 links, 2 EDFAs/link	4	4	8	66	2x281
2 links, 1 EDFA/link	2	2	4	46	2x196

Table 4.9: Link budgets and component counts for various bi-directional system configurations.

4.5. Impact of Internal Amplifier Rayleigh Backscattering

Recently, there has been considerable interest in using long distributed Erbium-Doped Fiber (EDF) amplifiers in long-haul transmission systems, mainly due to its low amplified spontaneous emission and applicability to solition transmission [82-86]. In these systems, EDFs are employed not only as an amplifying fiber but also as the transmission medium. By using dispersion shifted EDFs, lossless [83-84] and as well as dispersion free [85-86] transmission using 1550 nm sources have been demonstrated.

Another possible way to implement end-to-end lossless and dispersion free transmission is to utilize a 1310 nm transmitter source along with amplifiers functioning in this wavelength. The key benefit of the 1310 nm system is the exploitation of the zero dispersion characteristic at 1310 nm of the most commonly installed standard fiber throughout the world; for such a system, no dispersion compensation techniques are required. To date, the most promising candidates for providing 1310 nm amplification are the Praseodymium-Doped Fluoride Fiber Amplifiers (PDFFAs), and due to their benefit, there has been a lot of ongoing research work both on analog [64-65,87-88] and high speed digital [89-90] transmissions in the past few years.

In the previous analysis, the effect of Rayleigh backscattering within the fiber amplifiers as depicted in Figure 4.56, was ignored. This is a valid assumption as long as the Rayleigh backscattering coefficient of the amplifying fiber is sufficiently small, such as with EDFAs. However, for systems using fiber amplifiers with high baskscattering coefficients, such as PDFFAs, this RB impact cannot be neglected. Similarly, if one uses long distributed EDFAs, the internal scattering along the full system length also has to be included because distributed EDFs are effectively lossless and long, and hence a considerable amount of RB would be expected. The following section will explore the impact of RB in these systems.

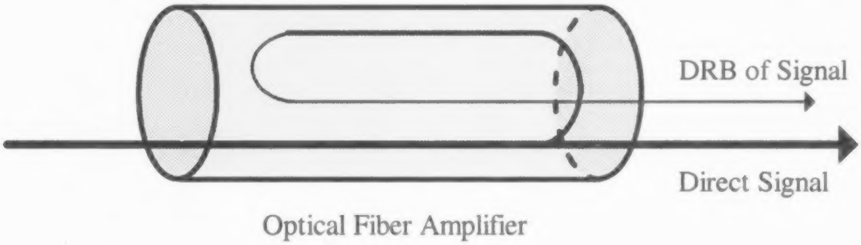

Figure 4.56: Double Rayleigh backscattering of a signal induced inside an optical fiber amplifier.

4.5.1. Penalty Derivation Due to Internal DRB

The DRB noise generated within a "lumped" fiber amplifier is different from that which is generated in a long piece of fiber because the conditions:

a) the fiber loss is small within the coherence length

b) the source field coherence length is relatively short compared to the fiber length given in Section 2.2, may not be satisfied when deriving the DRB noise spectrum, due to short length and large gain coefficient of the amplifier. Here a "lumped" fiber amplifier is referred to as a short fiber amplifier, with a typical length ranging between a few meters to several tens of meters. The failure of conditions (a) and (b) will not result in a closed form expression for the DRB noise spectrum. Nevertheless, one can still calculate the total DRB noise current induced within fiber amplifiers over the receiver bandwidth, and then apply the general power penalty expression (4.26) to characterize this impact on digital IM-DD systems which employ a chain of isolated lumped fiber amplifiers.

Inserting $\tau = 0$ in Eqn. (2.21), the total DRB mean square noise current generated within an amplifier with length L_l can be expressed as

$$\begin{aligned}\left\langle i_{DRB}{}^2 \right\rangle &= \left\langle R_{I_{DRB}}(0) \right\rangle A_{eff}{}^2 \Re^2 \\ &= \lim_{T\to\infty} \frac{1}{T} \int_{-\frac{T}{2}}^{\frac{T}{2}} 2 \left\langle \begin{aligned} &P_{dir}(t, L_l) \cdot \\ &\int_0^{L_l} \int_0^{z_2} P_{dir}\left(t - 2\frac{z_2 - z_1}{v}, L_l \right) \exp\left(\int_{z_1}^{z_2} 2g(z)\,dz \right) dz_1 dz_2 \end{aligned} \right\rangle \alpha_s{}^2 S^2 \Re^2 \, dt \end{aligned} \tag{4.38}$$

where $g(z)$ is the gain coefficient and $P_{dir}(t,L_l)$ is the optical signal power at the output of the amplifier. In expressing the above equation, the following relation has been used:

$$P_{dir}(t, L_l) = \left(\varepsilon_{dir}(t, L_l) \varepsilon_{dir}{}^*(t, L_l) \right) A_{eff} \tag{4.39}$$

As shown similarly in Appendix A, for high speed transmission systems, $P_{dir}(t,L_l)$ inside the double integral in Eqn. (4.38) can be extracted and written as the average optical power P_{re} in order to eliminate the time dependence, yielding

$$\left\langle i_{DRB}{}^2\right\rangle = 2\left(\lim_{T\to\infty}\frac{1}{T}\int_{-\frac{T}{2}}^{\frac{T}{2}}\left\langle P_{dir}(t,L_l)P_{re}\right\rangle dt\right)\cdot\left(\int_0^{L_l}\int_0^{z_2}\exp\left(\int_{z_1}^{z_2}2g(z)dz\right)dz_1dz_2\right)\Re^2\alpha_s{}^2S^2$$
$$= 2P_{re}{}^2\,\Re^2\left(\int_0^{L_l}\int_0^{z_2}\exp\left(\int_{z_1}^{z_2}2g(z)dz\right)dz_1dz_2\right)\alpha_s{}^2S^2 \tag{4.40}$$

By approximating $g(z)$ as the average gain coefficient g_o, the mean square DRB noise current expression becomes

$$\left\langle i_{DRB}{}^2\right\rangle = 2P_{re}{}^2\,\Re^2\left(\int_0^{L_l}\int_0^{z_2}\exp\left(2g_o(z_2-z_1)\right)dz_1dz_2\right)\alpha_s{}^2S^2$$
$$= 2P_{re}{}^2\Re^2\,\frac{e^{2g_oL_l}-2g_oL_l-1}{4g_o{}^2}\alpha_s{}^2S^2 \tag{4.41}$$

Since the square of the gain of a lumped amplifier ($G^2 = e^{2g_oL_l}$) is much larger than $2g_oL_l+1$, the total mean square noise current for a lumped amplifier is given to a good approximation by

$$\left\langle i_{DRB,lump}{}^2\right\rangle = P_{re}{}^2\Re^2\,\frac{G^2}{2g_o{}^2}\alpha_s{}^2S^2 \tag{4.42}$$

Note that polarization is assumed to be preserved within a lumped fiber since the amplifier length is fairly short, and that the subscript *lump* is used to specify lumped amplifiers. For systems using a chain of N lumped fiber amplifiers with isolators surrounding the amplifiers so as to eliminate the multi-amplified RB effects as in the open cascade situation, the total accumulated DRB noise can be expressed as

$$\left\langle i_{DRB,lump}{}^{2}\right\rangle = N\left(P_{re}{}^{2}\Re^{2}\frac{G^{2}}{2g_{o}{}^{2}}\alpha_{s}{}^{2}S^{2}\right) \tag{4.43}$$

On the other hand, for the systems employing a long distributed EDFA as transmission medium where the net loss roughly equals zero [83-84], then by assuming randomly aligned polarization for DRB and by substituting $g_0 \to 0$ into Eqn. (4.41), one obtains the mean square noise current due to DRB for this system as

$$\left\langle i_{DRB,dist}{}^{2}\right\rangle = P_{re}{}^{2}\Re^{2}\frac{L_{l}{}^{2}}{2}\alpha_{s}{}^{2}S^{2} \tag{4.44}$$

where the subscript *dist* denotes the distributed EDFA. It becomes clear from this equation that due to the square of the amplifier length dependence ($L_l{}^2$), the total noise can be lowered by placing isolators in the link in order to break down the total distributed fiber length into N isolated pieces of length L_s. In such a case the total noise becomes

$$\left\langle i_{DRB,dist}{}^{2}\right\rangle = N\left(P_{re}{}^{2}\Re^{2}\frac{L_{s}{}^{2}}{2}\alpha_{s}{}^{2}S^{2}\right) \tag{4.45}$$

Inserting Eqn. (4.43) and (4.45) into the generic penalty expression (4.26) gives the power penalties due to internal DRB for these system as

$$\Delta P_{lump} = 10\log\left\{1-\frac{Q^{2}}{2}N\frac{G^{2}}{2g_{o}{}^{2}}\alpha_{s}{}^{2}S^{2}\frac{d+1}{d-1}\right\}^{-1} \tag{4.46}$$

and

$$\Delta P_{dist} = 10\log\left\{1-\frac{Q^{2}}{2}N\frac{L_{s}{}^{2}}{2}\alpha_{s}{}^{2}S^{2}\frac{d+1}{d-1}\right\}^{-1} \tag{4.47}$$

It should be mentioned that similar to the case of an open cascade of EDFAs, where the DRB noise penalty also involves a term in NG^2, so too here for the lumped amplifiers can one reduce the impact of DRB noise within the amplifiers themselves by designing a system with a larger number of low gain amplifiers. This can readily be accomplished by creating a single amplifier composed of several amplifying fibers with isolators in between. The above theory provides the design criteria for such a system.

4.5.2. Theoretical Results

Three different systems are considered: single-mode fiber systems with either lumped EDFAs or lumped PDFFAs and systems utilizing distributed EDFAs as the transmitting medium. In step-index single-mode fibers, the recapture factor S is related to the Numerical Aperture (NA) through the following approximation [26,28]:

$$S \approx 0.223\frac{n_1^{\,2} - n_2^{\,2}}{n_1^{\,2}} = 0.223\frac{NA^2}{n_1^{\,2}} \tag{4.48}$$

where n_1 and n_2 are the refractive indices of the core and cladding of the fiber. Substituting this equation into Eqn. (4.46), Figure 4.57 presents the calculated power penalty for a BER of 10^{-14} against the number of lumped fiber amplifiers in a link, with the Rayleigh scattering loss coefficient as a parameter. In the calculation, each amplifier is 25 m long and has an internal gain of 25 dB and a NA of 0.2. Also, a 10 dB extinction ratio and a refractive index of 1.5 for the fiber core are assumed. Figure 4.58 presents the penalty for the case in which the NA used in the calculation is increased to 0.4. Since PDFFAs typically have large NA ranging from 0.2 to 0.4 [65,88-90] and the best reported internal scattering loss coefficient ranges from 0.02 dB/m to 0.05 dB/m [65,88-90], these two figures clearly indicate that lower NA and lower scattering loss values need to be achieved before PDFFAs can be used in long concatenation links. It is worth mentioning that since the scattering loss of a fiber has been shown to be reduced with lower NA [91], being able to design PDFFAs with low NA could have an very substantial impact on reducing the internal DRB effect.

Nevertheless, for lumped EDFAs, because the scattering loss coefficient is as small as 0.5 dB/km and because the NA is smaller than 0.2, the DRB contribution from the EDFAs gives a negligible penalty for links with many amplifiers. For example, for an EDFA having a NA of 0.2 and a scattering loss coefficient of 1 dB/km, one could concatenate 250 amplifiers for a penalty caused by the internal DRB impact of less than 0.1 dB.

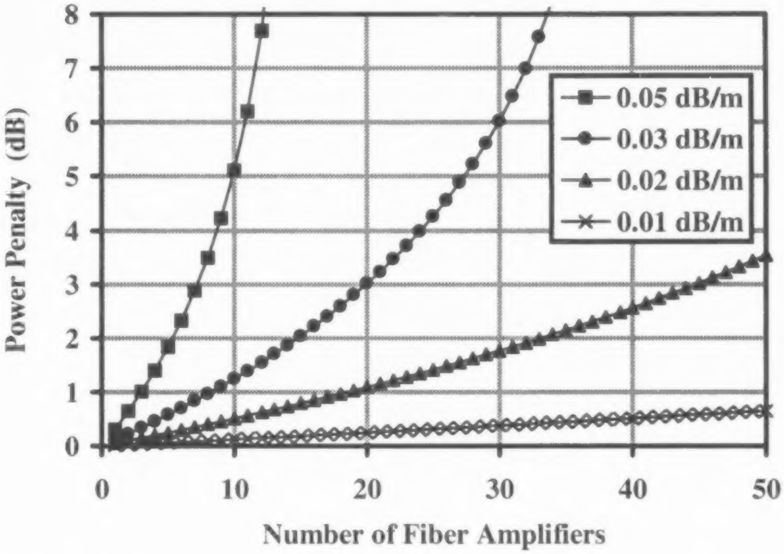

Figure 4.57. Power penalty against number of lumped amplifiers for a BER of 10^{-14}, NA of 0.2 and with the Rayleigh scattering loss coefficient as a parameter.

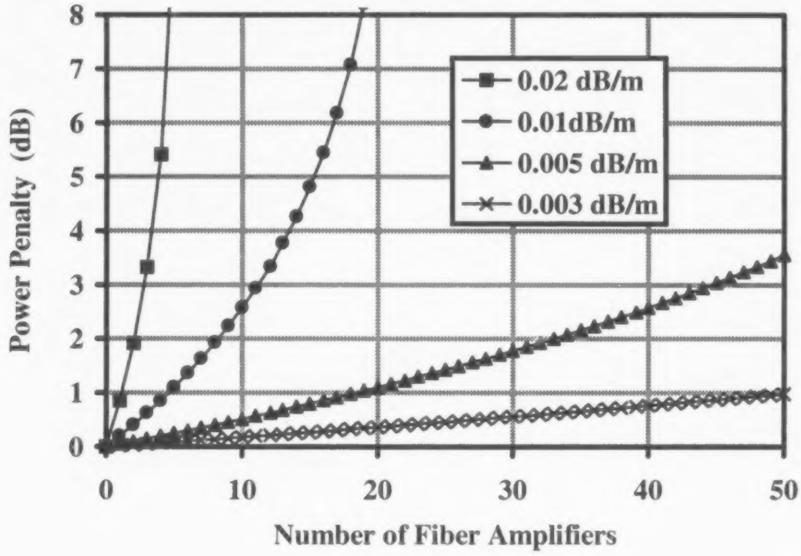

Figure 4.58: Power penalty against number of lumped amplifiers for a BER of 10^{-14}, NA of 0.4 and with the Rayleigh scattering loss coefficient as a parameter.

For distributed EDFA systems, Figure 4.59 shows the calculated isolator spacing, or equivalently, the distributed EDF length, required to achieve a BER of 10^{-14} as a function of the total full system length. It is calculated for a power penalty of 1 dB, extinction ratio of 10 dB and two different Rayleigh backscattering coefficients, which are equivalent to the product of the recapture factor S and Rayleigh scattering coefficient α_s. $S\alpha_s$ = -70 dB/m corresponds to a conventional single-mode fiber, and $S\alpha_s$ = -65 dB/m might be that value associated with a higher level of core doping required for amplification or dispersion shifted fiber design [20]. Figure 4.60 depicts the expected power penalty against isolator spacing for a hypothetical 9000 km long distributed EDFA system. Both of these figures clearly reveal the importance of using small NA and a low scattering coefficient to increase the isolator spacing. The use of short isolator spacing gives rise to two limitations. First, more isolators need to be utilized, thereby increasing transmission loss and system cost. Second, since the optimum pumping scheme for distributed EDFAs is bi-directional pumping [82-83], the constraint on isolator spacing limits the distance between pump stations, and as a result, more pump stations need to be installed.

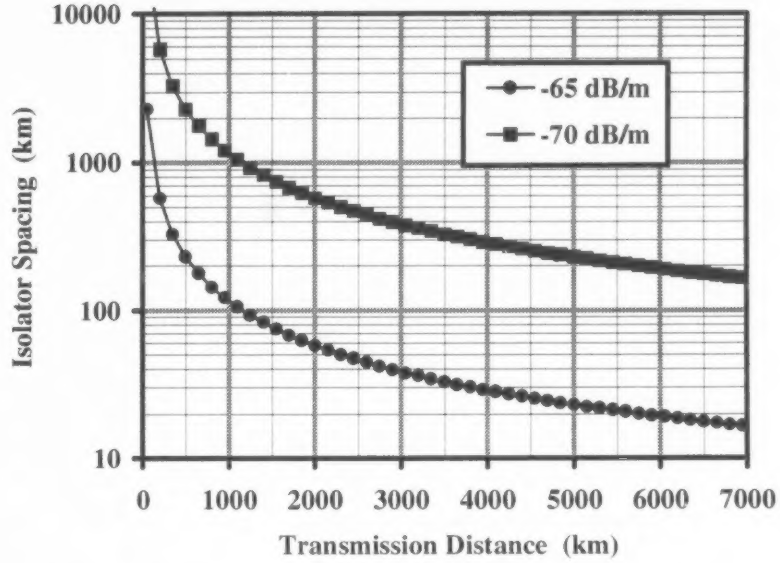

Figure 4.59: Isolator spacing against transmission length for a distributed EDFA system with a BER of 10^{-14}, 1 dB power penalty and two values of Rayleigh backscattering coefficient.

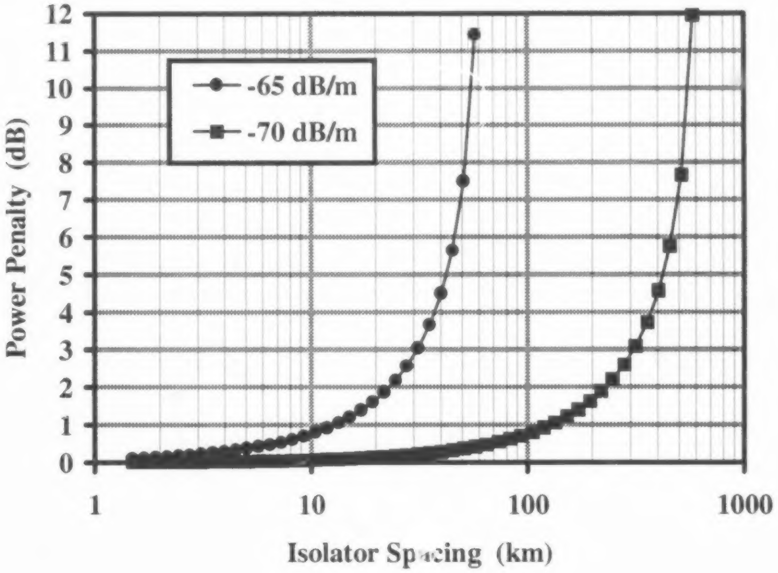

Figure 4.60: Penalty against isolator spacing for a 9000 km distributed EDFA system with a BER of 10^{-14} and two values of Rayleigh backscattering coefficient.

Chapter 5

CONCLUSIONS

In this dissertation, the Rayleigh backscattering impact on transmission performance of various forms of fiber optic transmission systems has been studied. By modeling the scattering coefficient as a delta-correlated circular complex Gaussian random variable a general and accurate expression for the double Raleigh backscattering noise has been derived. This DRB noise expression has been successfully verified in simple experiments using a generic AM-SCM signal generated by direct modulation of a DFB laser.

5.1. Summary of the Results on Analog Systems

The noise expression was then simplified in directly and externally modulated AM-SCM systems to facilitate easier use. In directly modulated systems, it is clear that DRB noise has a Gaussian shape that is much wider than the intrinsic linewidth of the laser, and that this Gaussian shape can be calculated using a simple equation in terms of fiber length, Rayleigh backreflectance, total fiber loss coefficient, rms modulation index, chirping efficiency and bias current.

In externally modulated systems, however, the laser phase fluctuation cannot be ignored and the DRB RIN is clearly composed of a series of Lorentzian laser lineshape noise spectra, centered at DC and subcarrier frequencies, and can be expressed in terms of fiber length, Rayleigh backreflectance, total fiber loss coefficient, laser linewidth and peak modulation of each channel.

Both of these simplified DRB noise expressions have been applied to 1310 nm and 1550 nm systems with and without the use of optical amplifiers to determine their received CNRs. Several characteristics have been generalized from these results:

- DRB noise can be reduced by inserting optical isolators to break up the transmission link.
- DRB noise in 1310 nm systems is about 6 dB higher than that of 1550 nm systems.
- In directly modulated systems, DRB noise spectrum is relatively flat, and it decreases with chirping efficiency. Therefore, systems using laser diodes with large chirping efficiencies can reduce the DRB noise significantly, giving rise to a improvement in CNR.
- In externally modulated systems, DRB noise spectrum, on the other hand, shows a strong frequency dependence. To reduce this dependence, optical sources with either relatively narrow or wide linewidths should be used. Through the use of such sources, the DRB noise in CATV frequency and CNR degradation will also be reduced.
- Both 1310 nm and 1550 nm systems equipped with optical amplifiers have been shown to be capable of extending the system reach and coverage in the presence of DRB by using a higher received power to compensate for the additional noise added from the amplifiers.

5.2. Summary of Results on Digital Systems

The impact of RB on optically amplified IM-DD digital systems has been investigated. To quantify this impact, a generic power penalty expression describing the degrading effects due to the backscattered ASE and signal has been derived, and subsequently verified by a series of OC-48 transmission experiments. The experimental results have confirmed the validity of the expression, particularly for modest penalties. Using this derived expression, it has been demonstrated that open cascade systems are capable of providing large system gain provided that each in-line amplifier has moderate amplifier gain.

In addition, different kinds of bi-directional transmission configurations have been discussed. Bi-directional systems, using bi-directional amplifiers composed of 4 WDMs, as shown in Figure 4.51, prove promising in the areas of system cost reduction and upgrade, in comparison to existing 2 fiber link bi-directional systems. However, open cascade systems still require the minimum number of components to implement, and it has been experimentally confirmed that bi-directional open cascade systems provide similar system power budget but require fewer components, compared to the 2 fiber link bi-directional systems.

In the latter segment of this work, a new penalty expression, accounting for the DRB noise generated inside high scattering fiber amplifiers or distributed fiber amplifiers, has been obtained. Calculated results have shown that for systems that employ lumped EDFAs in long distance transmission applications, the penalty is negligible. However, when employing PDFFAs or distributed EDFAs, due to their relatively large numerical aperture and Rayleigh scattering coefficient, the penalty could be severe.

5.3. Future Research

Future work in the context of bi-directional transmission could comprise detailed investigations of the implementation for open cascade system configurations as well as for other system configurations, such as systems employing one fiber link and WDMs, and systems with two separate fiber links. A insightful comparison could consider the net transmission capacity, link budget and cost concurrently. Furthermore, systems combining various configurations could be of special interest in some particular situations.

Concerning the performance of EDFAs in open cascade and WDM routing environments, further research topics could include a continuation of the extensive computer simulation study, accomplished by former M.Sc. student, Caroline Delisle [93]. Special attention should be given to the effects of amplifier gain compression and variation across the spectrum, as well as noise figure in multiple wavelength bi-directional transmission.

References

[1] Judy, A. F., "Intensity noise from fiber Rayleigh backscatter and mechanical splices", Proceedings of 15th European Conference on Optical Communications., Gothenbury, September 1989, pp. 486-489.

[2] Gimlett, J. L., Young, J., Spicer, R. E., and Cheung, N. K., "Degradations in Gbit/s DFB laser transmission systems due to phase-to-intensity noise conversion by multiple reflection points", Electronics Letters, Vol. 38, No. 7, March 1988, pp. 406-408.

[3] Gimlett, J. L, Iqbal, M. Z., Curtis, L., Cheung, N. K., Righetti, A., Fontana, F., and Grasso, G., "Impact of multiple reflection noise in Gbit/sec lightwave systems with optical fiber amplifiers", Electronics Letters, Vol. 25, No. 20, September 1989, pp. 1393-1394

[4] Gimlett, J. L., and Cheung, N. K., "Effects of phase-to-intensity noise conversion by multiple reflections on gigabit-per-second DFB laser transmission systems", Journal of Lightwave Technology, Vol. 7, No. 1, June 1989, pp. 888-895.

[5] Gimlett, J. L., Iqbal, M. Z., Cheung, N. K., Righetti, A., Fontana, F., and Grasso, G., "Observation of equivalent Rayleigh scattering mirrors on lightwave systems with optical amplifiers," IEEE Photonics Technology Letters, Vol. 2, No. 3, March 1990, pp. 211-213.

[6] Darcie, T. E., Bodeep, G. E., and Saleh, A. A. M., "Fiber-reflection-induced impairments in lightwave AM-VSB CATV system", Journal of Lightwave Technology, Vol. 9, No. 8, August 1991, pp. 991-995.

[7] Wu, S., and Yariv, A., "Theoretical and experimental investigation of conversion of phase noise to intensity noise by Rayleigh scattering in optical fibers", Applied Physics Letters, Vol. 59, No. 10, September 1991, pp. 1156-1158.

[8] Yariv, A., Blauvelt, H., and Wu, S. W., "A reduction of interferometric phase-to-intensity conversion noise in fiber links by large index phase modulation of the optical beam", Journal of Lightwave Technology, Vol. 10, No. 7, July 1992, pp. 978-981.

[9] Blauvelt, H. A., Kwong, N. S., Chen, P. C., and Ury, I., "Optimum range for DFB laser chirp for fiber-optic AM video transmission", Journal of Lightwave technology, Vol. 11, No. 1, January 1993, pp. 55-59.

[10] van der Plaats, J. C., and Willems, F. W., "RIN increase caused by amplified-signal redirected Rayleigh scattering in erbium-doped fibers", OFC'94 Technical Digest, San Jose, WM6, pp. 158-160.

[11] Willems, F. W., van der Plaats, J. C., and DiGiovanni, D. J., "EDFA noise figure degradation caused by amplified signal double Rayleigh scattering in erbium-doped fibers", Electronics Letters, Vol. 30, No. 8, April 1994, 645-646.

[12] Yonetani, H., Ushijima, I., Takada, T., and Shima, K., "Transmission characteristics of DFB laser modules for analog applications", Journal of Lightwave Technology, Vol. 11, No. 1, January 1993, pp. 147-153.

[13] Atlas, D. A., Pidgeon, R., and Little, F., "Rayleigh backscatter effects on 1550-nm CATV distribution systems employing optical amplifiers", Journal of Lightwave Technology, Vol. 13. No. 5, May 1995, pp. 933-946.

[14] Gysel, P., and Staubli, R. K., "Statistical properties of Rayleigh backscattering in single-mode fibers", Journal of Lightwave Technology, Vol. 8, No. 4, April 1990, pp. 561-567.

[15] Gysel, P., and Staubli, R. K., "Spectral properties of Rayleigh backscattered light from single-mode fibers caused by a modulated probe signal", Journal of Lightwave Technology, Vol. 8, No. 12, December 1990, pp. 1972-1990

[16] Staubli, R. K., and Gysel, P., "Statistical properties of single-mode fiber Rayleigh backscattered intensity and resulting detector current", IEEE Transactions on Communications, Vol. 40, No. 6, June 1992, pp. 1091-1096.

[17] Kuwabara, T., Koga, H., Kato, Y., and Mistunaga, Y., "Optical fiber identification using Rayleigh backscattered light", IEEE Photonics technology Letters, Vol. 4, No. 7, July 1992, pp. 751-753.

[18] Chraplyvy, A. R., Marcuse, D., and Tkach, R. W., "Effect of Rayleigh backscattering from optical fibers on DFB laser wavelength", Journal of Lightwave Technology, Vol. LT-4, No. 5, May 1986, pp. 555-559.

[19] Mark, J., Coherent Measuring Technique and Rayleigh Backscatter from Single-Mode Fibers, Electromagnetics Institute, Technical University of Denmark, February 1987, pp. 35-55.

[20] Hensen, S. L., Dybdal, K., and Larsen, C. C., "Gain limit in erbium-doped fiber amplifiers due to internal Rayleigh backscattering", IEEE Photonics technology Letters, Vol. 4, No. 6, June 1992, pp. 559-561.

[21] Zervas, M. N., and Laming, R. I., "Performance limits of erbium-doped-fiber amplifiers due to internal Rayleigh backscattering", OFC'93 Technical Digest, San Jose, ThF1, pp. 178-179.

[22] Keiser, Gerd, Optical Fiber Communications, McGraw Hill, New York, 1991, p. 93.

[23] Miya, T., Terunuma, Y., Hosaka, T., and Miyashita, T., "Ultimate low-loss single-mode fiber at 1550 μm", Electronics Letters, Vol. 15, No. 4, February 1979, pp. 106-108.

[24] Healey, P., "Statistics of Rayleigh backscatter from a single-mode fiber", IEEE Transactions on Communications, Vol. Com-35, No. 2, Februry 1987, pp. 210-213.

[25] Nazarathy, M., Sorin, W. V., Baney, D. M., and Newton, S. A., "Spectral Analysis of optical mixing measurements", Journal of Lightwave Technology, Vol. 7, No. 7, July 1989, pp. 1083-1096.

[26] Nakazawa, M., "Rayleigh backscattering theory for single-mode optical fibers", J. Optical Society of America, Vol. 73, No. 9, September 1983, pp. 1175-1180.

[27] Eickhoff, W., and Ulrich, R., "Statistics of backscattering in single-mode fiber", IOOC-81 Technical Digest, TuK4, pp.76-78.

[28] Brinkmeyer, E., "Analysis of the backscattering method for single-mode optical fibers", J. Optical Society of America, Vol. 70, No. 8, August 1980, pp. 1010-1012.

[29] Thomas J. B., In Introduction to Communication Theory and Systems, Springer-Verlag, New York, 1988, p. 102.

[30] Rowe, H, E., Signals and Noise in Communication Systems, D. Van Nostrand Company, Princeton, 1965, pp. 35-39.

[31] Deventer, M. O., "Polariazation properties of Rayleigh backscattering in single-mode fibers", Journal of Lightwave Technology, Vol. 11, No. 12, December 1993, pp. 1895-1899.

[32] Chiddix, J. A., Vaughan, J. A., and Wolfe, R. W., "The use of fiber optics in cable communications Networks", Journal of Lightwave technology, Vol. 11, No. 1, January 1993, pp. 154-166.

[33] Paff, A., "Hybrid fiber/coax in the public telecommunications infrastructure", IEEE Communications Magazine, April 1995, pp. 40-45.

[34] Foschini, G. J., and Habbab, I. M. I., "Capacity of broadcast channels in the near-future CATV architecture", Journal Lightwave Technology, Vol. 13, N0. 3, March 1995, pp. 507-516.

[35] Lu, X., Darcie, T. E., Bodeep, G. E., Woodward, S. L., and Gnauck, A. H., "Mini-fiber-node hybrid fiber coax networks for two-way broadband access", OFC'96 Technical Digest, San Jose, WI3, pp. 143-144.

[36] Ciciora, W. S., An Overview of Cable Television in the United States, Cable Television Laboratories, Inc., 1990, p. 12.

[37] Couch, L. W., Digital and Analog Communication Systems, 4th edition, Macmillan Publishing Company, New York, 1993, p. 321.

[38] Ovadia, S., Dai, H., Lin, Chinlon, and Anderson, W. T., "Performance of hybrid multichannel AM/256-QAM video lightwave transmission systems", IEEE Photonics Technology Letters, Vol. 7, No. 11, November 1995, pp. 1351-1353.

[39] Lu, X, Bodeep, G. E., and Darice, T. E., "Broad-band AM/VSB/64 QAM cable TV system over hybrid fiber/coax network", IEEE Photonics Technology Letters, Vol. 7, No. 4, April 1995, pp. 330-332.

[40] Pham, K., Conradi, J., Cormack, G., Thomas, B., and Anderson, C. W., "Impact of Noise and nonlinear distortion due to clipping on the BER performance of a 64-QAM signal in hybrid AM-VSB/QAM optical fiber transmission system", Journal of Lightwave Technology, Vol. 13, No. 11, November 1995, pp. 2197-2201.

[41] Kerpez, K. J., "A comparison of QAM and VSB for hybrid fiber/coax digital transmission", IEEE Transactions on Broadcasting, Vol. 41, No. 1, March 1995, pp. 9-15.

[42] Moore, D., "Error Performance of M-ary ASK/VSB in a hybrid AM/VSB-ASK/VSB subcarrier multiplexed CATV systems", TR*Labs* report TR-95-01, February 1995.

[43] Nazarathy, M., Berger, J., Ley, A. J., Levi, I. M., and Kagan, Y., "Progress in externally modulated AM CATV transmission systems", Journal of Lightwave technology, Vol. 11, No. 1, January 1993, pp. 82-105.

[44] Iwai, T., Sato, K., and Suto, K., "Signal distortion and noise in AM-SCM transmission systems employing the feedforward linearized MQW-EA external modulator", Journal of Lightwave technology, Vol. 13, No. 8, August 1995, pp. 1606-1612.

[45] Alameh, K. E., and Minasian, R. A., "Optimization of fiber amplifier SCM lightwave video systems using direct and external modulation", Journal of Lightwave Technology, Vol. 11, No.1, January 1993, pp. 76-81.

[46] Shi, Q., "Asymptotic clipping noise distribution and its impact on M-ary QAM transmission over optical fiber", IEEE Transactions on communications, Vol. 43, No. 6, June 1995, pp. 2077-2084.

[47] Lu, X., Bodeep, G. E., and Darcie, T. E., "Clipping-induced impulse noise and its effect on bit-error performance in AM-VSB/64QAM hybrid lightwave systems", IEEE Photonics Technology Letters, Vol. 6, No. 7, July 1994, pp. 866-868.

[48] Lai, S., Clipping-Induce Impulsive Noise in Directly Modulated Fiber Optic CATV Transmission Systems, University of Alberta, Spring 1996.

[49] NTSC, Recommended Practices, National Cable Television Association, Washington, DC.

[50] Bulow, H., Fritschi, R., Heidemann, R., Junginger, B., Krimmel, H. G., and Otterbach, J., "Analog video distribution system with three cascade 980 nm single-pumped EDFAs and 73 dB power budget", IEEE Photonics Technology Letters, Vol. 4, No. 11, November 1992, pp. 1287-1289.

[51] Yoshinaga, H., Kikushima, K., and Yoneda, E., "Noise properties of cascaded erbium-doped fiber amplifiers in SCM analog video distribution systems", IEICE Transactions on Communications, Vol. E76-B, No. 1, January 1993, pp. 12-19.

[52] Kuo, C. Y., Piehler, D., Gall, C., Kleefeld, J., Nilsson, A., and Middleton, L., "High-performance optically amplified 1550-nm lightwave AM-VSB CATV transport system", OFC'96 Technical Digest, WN2, pp. 196-197.

[53] Muys, W., van der Plaats, J. C., Willems, F. W., Vengsarkar, A. M., Soccolich, C. E., Andrejco, M. J., DiGiovanni., D. J., Peckham, D. W., Kosinski, S. G., and Wysocki, P. F., "Directly modulated AM-VSB lightwave video transmission system using dispersion-compensating fiber and three cascaded EDFAs, providing 50-dB power budget over 38 km of standard single-mode fiber", OFC'96 Technical Digest, WN4, pp. 198-199.

[54] Yoshinaga, H., and Yoneda, Etsugo, "40-channel VSB-AM video transmission through 70 km of high-dispersion fiber by using dispersion-compensating fiber", OFC '95 Technical Digest, TuN6, pp. 66-67.

[55] Petermann, K., Laser Diode Modulation and Noise, Kluwer Academic Publishers, 1988, Chapter 5.

[56] Yoshikuni, Y., Motosugi, G., Kurumada, K., and Ikegami, T., "Optical operation of DFB lasers under chirped pulse transmission", Electronics Letters, Vol. 21, No. 11, May 1985, pp. 476-478.

[57] Heidemann, R., "Investigations on the dominant dispersion penalties", Journal of Lightwave Technology, Vol. 6, No. 11, November 1988, pp. 1693-1697.

[58] Henrique, J. A., da Silva, and O'Reilly, J. J, "System performance implications of laser chirp for long haul high bit rate direct detection optical fiber communications", ICC'88 Technical Digest, pp. 587-592.

[59] Schilling, D., and Taub, H., Principles of Communication Systems, McGraw-Hill, New York, 1986, pp. 159-160.

[60] Saleh, A. A. M., "Fundamental limit on number of channels in subcarrier-multiplexed lightwave CATV system", Electronics Letters, Vol. 25, No. 12, June 1989, pp. 776-777.

[61] Papoulis, A., Probability, Random Variables and Stochastic Processes, McGraw-Hill, New York, 1991, p. 214.

[62] Gysel, H., and Ramachandran, M., "Electrical predistortion to compensate for combined effect of laser chirp and fiber dispersion", Electronics Letters, Vol. 27, No. 5, February 1991, pp. 421-423.

[63] Kuo, C. Y., and Bergmann, E. E., "Low distortion high link budget lightwave CATV transport with amplifier at 1.55 mm", SPIE, Vol. 1786, Fiber Networks for Voice, Video, and Multimedia Services, pp. 190-193.

[64] Yoshinaga, H., Yamada, M., and Shimizu, M., "Fiber transmission of 40-channel VSB-AM video signals by using a praseodymium-doped-fluoride fiber amplifier with direct and external modulation", OFC'95 Technical Digest, TuN5, pp. 65-66.

[65] Nakazato, K., Nishimura, M., Watanabe, C., and Onishi, M., "Performance of Pr-doped fluoride fiber amplifier for multichannel AM-VSB transmission", Optical Amplifiers and Their Applications'93 Postdeadline Paper, PD9-2, pp. 371-374.

[66] Wan, P., and Conradi, J., "Impact of double Rayleigh backscatter noise on digital and analog fiber systems", Journal of Lightwave Technology, Vol. 14, No. 3, March 1996, pp. 288-297.

[67] Olsson, N. A., "Lightwave systems with optical amplifiers", Journal of Lightwave Technology, Vol. 7, No. 7, July 1989, pp. 1071-1082.

[68] Henry, C. H., "Phase noise in semiconductor lasers", Journal of Lightwave Technology, Vol. LT-4, No. 3, March 1986, pp. 298-311.

[69] Woodward, S. L., and Darcie, T. E., "A method for reducing multipath interference noise", IEEE Photonics technology Letters, Vol. 6, No. 3, March 1994, pp. 450-452.

[70] Willems, F. W., Muys, W., and Leong, J. S., "Simultaneous suppression of stimulated Brillouin scattering and interferometric noise in externally modulated lightwave AM-SCM systems", IEEE Photonics Technology Letters, Vol. 6, No. 12, December 1994, pp. 1476-1478.

[71] Barabash, D., and Morris, R., "Semiconductor laser amplifier noise generation", TR*Labs* report TR-89-15, December 1989.

[72] Chan, B., Statistical Properties of EDFAs, University of Alberta, Fall 1995

[73] Lee, J. S., and Shim, C. S., "Bit-error-rate analysis of optically preamplified receivers using an eigenfunction expansion method in optical frequency domain", Journal of Lightwave Technology, Vol. 12, No. 7, July 1994, pp. 1224-1229.

[74] Benterud, K., Fiber Optic Transmission Using OTDM, University of Alberta, Fall 1993, p. 85.

[75] Andersson, P. O., and Akermark, K., "Accurate optical extinction ratio measurements", IEEE Photonics Technology Letters, Vol. 6, No. 11, November 1994, pp. 1356-1358.

[76] Haugen, J., Freeman, J., and Conradi, J., "Bidirectional transmission at 622 Mb/s utilizing erbium-doped fiber amplifiers", IEEE Photonics Technology Letters, Vol. 4, No. 8, August 1992, pp. 913-916.

[77] Farre, F., Bodtker, E., Jacobsen, G., and Stubkjaer, K. E., "Design of bidirectional communication systems with optical amplifiers", IEEE Photonics Technology Letters, Vol. 4, No. 4, April 1993, pp. 425-427

[78] Barnard, C. W., Chrostowaki, J., and Kavehrad, M., "Bidirectional fiber amplifiers", IEEE Photonics Technology Letters, Vol. 4, No. 8, August 1992, pp. 911-913.

[79] Delavaux, J. M. P., Mizuhara, O., Yeates, P. D., and Nguyen, T. V., "10 Gb/s 150-km bidirectional repeaterless optical-fiber transmission", IEEE Photonics Technology Letters, Vol. 7, No. 9, September 1995, pp. 1087-1089.

[80] Wan, P., and Conradi, J., "Comparison of full duplex 622Mb/s bidirectional transmission systems employing an open cascade of erbium doped fiber amplifiers with systems employing isolators", IOOC-95 Technical Digest, ThC3-4, Hong Kong, June 1995, pp. 82-83.

[81] Melle, S., "Optical amplifier systems point to high-capacity, all-optical network applications", Lightwave, March 1996, pp. 34-37.

[82] Rottwitt, K., Bjarklev, A., Hedegaard, P., Lumholt. O., and Rasmussen, T., "Fundamental design of a distributed erbium-doped fiber amplifier for long-distance transmission", Journal of Lightwave Technology, Vol. 10, No. 11, November 1992, pp. 1544-1552.

[83] Tanake, D., Wada, A., Sakai, T., Nozawa, T., and Yamauchi, R., "73.6km attenuation free concatenated fibers doped with distributed erbium", Optical Amplifiers and Their Applications'92 Technical Digest, ThD4, pp. 156-159.

[84] Varming, P., Rottwitt, K., Lester, C., Povlsen, J. H., Newhouse, M. A., and Antos, A. J., “Measurement of signal gain variations on distributed erbium doped fibers”, Electronics Letters, Vol. 31, No. 24, November 1995, pp. 2107-2108.

[85] Tanaka, D., Wada, A., Sakai, T., and Yamauchi, R., “Attenuation free dispersion shifted fiber doped with distributed erbium”, Optical Amplifiers and Their Applications’90 Technical Digest, TuB4, pp. 138-141.

[86] Lester, C., Bertilsson, K., Rottwitt, K., Andrekson, P. A., Newhouse, M. A., and Antos, A. J., “Soliton transmission over more than 90 km using distribution erbium-doped fibers”, Electronics Letters, Vol. 31, No. 3, February 1995, pp. 219-220.

[87] Kikushima, K., Whitley, T., Cooke, R., Stalley, K., and Fake, M., and Lawrence, E., Multichannel FM-TV transmission using an engineered 1.3 μm praseodymium-doped fluoride fiber amplifier”, Electronics Letters, Vol. 30, No. 17, August 1994, pp. 1431-1432.

[88] Yamada, M., Shimizu, M., Yoshinaga, H., Kikushima, K., Kanamori, T., Ohishi, Y., Terunuma, Y., Oikawa, K., and Sudo, S., “Low-noise Pr^{3+}-doped fluoride fiber amplifier”, Electronics Letters, Vol. 31, No. 10, May 1995, 00. 806-807.

[89] Tomita, N., Kimura, K., Suda, H., Shimizu, M., Yamada, M., and Ohishi, Y., “Digital signal transmission experiment using a 1.3 μm-Band Pr^{+3}-doped fluoride fiber amplifier”, IEEE Photonics Technology Letters, Vol. 6, No. 2, February 1994, pp. 258-259.

[90] Whitley, T., “A review of recent system demonstrations incorporating 1.3-μm praseodymium-doped fluoride fiber amplifiers”, Journal of Lightwave Technology, Vol. 13, No. 5, May 1995, pp. 744-760.

[91] Olshansky, R., “Propagation in glass optical waveguides”, Reviews of Modern Physics, Vol. 51, No. 2, April 1979, pp. 341-366.

[92] Steele, R. C., Walker, G. R., and Walker, N. G., “Sensitivity of optically preamplified receivers”, IEEE Photonics Technology Letters, Vol. 3, No. 6, June 1991, pp. 545-547.

[93] Delisle, C., Optical Bidirectional Transmission in Cascaded Erbium-Doped Fibre Amplifiers, University of Alberta, Spring 1995.

Appendix A: Derivation of Eqn. (2.22)

Let $x(t)$ be a fast varying function and $y(t)$ be a slow varying function, then the time-average of the product of these functions for a duration of time T can be approximated by the products of time-averages of these functions as

$$\overline{x(t)\cdot y(t)} \cong \overline{x(t)}\cdot\overline{y(t)} \tag{A.1}$$

or more specifically,

$$\frac{1}{T}\int_0^T x(t)\cdot y(t)\,dt \cong \frac{1}{T}\int_0^T x(t)\,dt\cdot\frac{1}{T}\int_0^T y(t)\,dt \tag{A.2}$$

This can be rewritten as

$$\int_0^T x(t)\cdot y(t)\,dt \cong \frac{1}{T}\int_0^T x(t)\,dt\cdot\int_0^T y(t)\,dt \tag{A.3}$$

Now, invoking the above relation to the inner integral in Eqn. (2.21), in which $\varepsilon_{dir}{}^*(\cdot)\varepsilon_{dir}(\cdot)$ is the fast varying function and $e^{(\cdot)}$ is the slow varying function, yields a new expression for this inner integral as

$$\begin{aligned}&\int_0^{z_2}\varepsilon_{dir}{}^*\left(t-2\frac{z_2-z_1}{v},L\right)\cdot\varepsilon_{dir}\left(t-2\frac{z_2-z_1}{v}+\tau,L\right)e^{-2\alpha(z_2-z_1)}dz_1\\ &\quad=\frac{1}{z_2}\int_0^{z_2}\varepsilon_{dir}{}^*\left(t-2\frac{z_2-z_1}{v},L\right)\varepsilon_{dir}\left(t-2\frac{z_2-z_1}{v}+\tau,L\right)dz_1\cdot\int_0^{z_2}e^{-2\alpha(z_2-z_1)}dz_1\end{aligned} \tag{A.4}$$

Substituting this expression into Eqn. (2.21) gives rise to Eqn. (2.22).

Appendix B: Parameter Measurements

B.1. Rayleigh Backscattering Reflectance

The setup used to measure RB reflectance is shown in Figure B.1.1. The optical power after the Variable Optical Attenuator (VOA) was -6.6 dBm and the power at port 2 of the circulator was -8.3 dBm, which was the incident power on the fiber under measurement. The measured loss from port 2 to port 3 of the circulator was 1.0 dB. The power meter connected to the fiber determined the fiber loss, and the power meter connected to port 3 measured the backscattered power from the fiber.

The measured fiber, which was manufactured by Northern Telecom, was 50 km long fiber and was used in the experiments in Section (3.2). The measured power at the other end of the fiber was -20.0 dBm, meaning that the fiber loss was 11.7 dBm. Also, the backscattered power at port 3 was -42.5 dBm. By removing the fiber, the measured power at port 3 reduced to -60 dBm, which verified that the measured power of -42.5 dBm was due to fiber backreflection. To further confirm that this fiber backreflection was due to Rayleigh backscattering (instead of discrete reflection along the fiber), we reversed the fiber and noticed no change in the power reading. In this case, the Rayleigh backscattering reflectance could be easily determined as -42.5+1+8.3 = -33.2 dB. These measurements were repeated for a 1310 nm laser source to obtain the RB reflectance at this wavelength.

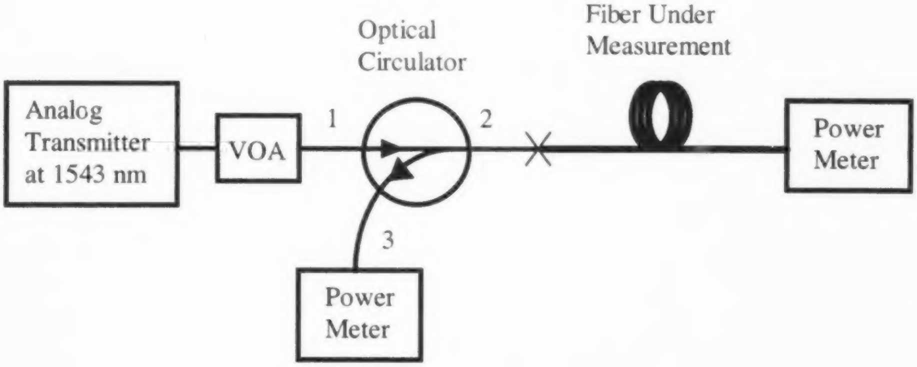

Figure B.1.1: Setup for measuring RB reflectance.

B.2. Laser Linewidth Measurement

The measurement technique used in the experiment was the standard delayed self-homodyne [25]; the setup for this measurement is depicted in Figure B.2.1. The delay path was a 10 km standard single-mode fiber, and which should give a measurement resolution of about 10 kHz. The polarization controller was employed to align the delayed field polarization for maximum mixing efficiency. The optical receiver was a New Focus detector followed by a SHF 90P electrical amplifier, both of which were chosen mainly for their very low cutoff frequencies. Figure B.2.2 depicts the measured beat spectrum and a calculated 14 MHz Lorentzian lineshape. This result clearly shows that the laser linewidth can accurately be described by a 14 MHz Lorentzian lineshape.

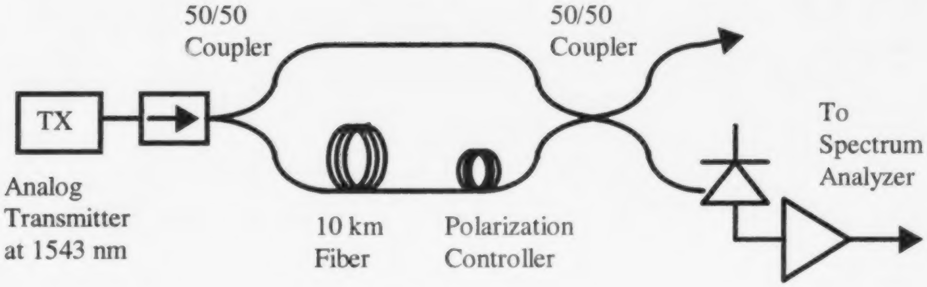
50/50
Coupler
50/50
Coupler
TX
Analog
Transmitter
at 1543 nm
10 km
Fiber
Polarization
Controller
To
Spectrum
Analyzer

Figure. B.2.1: Delayed self-homodyne linewidth measurement setup.

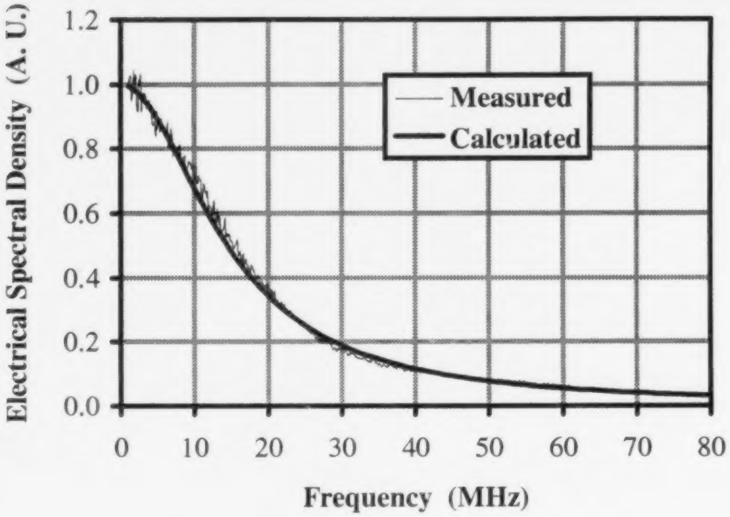

Figure. B.2.2: Measured beat spectrum and a calculated 14 MHz Lorentzian lineshape.

B.3. Laser Chirp Measurement

To measure the chirp efficiency of the DFB laser inside the analog transmitter, the gated delayed self-homodyne technique [25] was employed. The experimental setup was similar to that which was used for linewidth measurement, except that a gated sinusoid signal was applied to modulate the laser. To clarify, the setup is depicted in Figure B.3.1. The gated sinusoid, as generated in Figure B.3.2, switched the laser between two states of operation conditions: one was under CW operation and the other was under sinusoidal modulation. If one chooses the gating period corresponding to the differential delay between two paths, then the setup will effectively function as an optical homodyne system, having a CW local oscillator which mixes with a laser source that is under continuous sinusoidal modulation. With a small amount of chirp, the narrowband FM theory applies, and the mixed spectrum can be described by standard Bessel-function.

In the measurement, the delaying fiber was 10 km long, resulting in approximately a 0.05 ms differential delay. In this case, a 10 kHz square pulse was used as the gating source, and the sinusoid frequency was 100 MHz. The measured spectra for 3 different bias currents were shown in Figure B.3.3. In obtaining these spectra, the peak voltage of the sinusoid was adjusted such that the first null occurred at the fundamental frequency of the sinusoid (i.e. 100 MHz). The bias currents and their corresponding peak voltage levels are listed in Table B.3.1. As seen in the FM theory, the null corresponds to the case for which the Bessel function of the first kind and of the first order $J_l(\beta)$ was equal to zero, more specifically β (the modulation index) equal to 3.83. Since the modulation index can be expressed as

$$\beta = \frac{\Delta f}{f_m} = \frac{\gamma \Delta I}{f_m} \tag{B.3.1}$$

where Δf and f_m are the maximum frequency deviation and sinusoid frequency, respectively, and γ and ΔI are the chirping efficiency and peak modulation current actually seen by the laser diode, respectively, γ can be expressed as

$$\gamma = \frac{\beta f_m}{\Delta I} = \frac{3.83 \cdot 100\,\text{MHz}}{\Delta I} \tag{B.3.2}$$

Note that due to the microstrip circuitry and electrical connections used in the packaging of the optical transmitter, the input modulating signal will be affected before it reaches the laser diode. In this case, we determined ΔI as follows.

We applied a 100 MHz continuous sinusoid with a fixed peak voltage of 1.08 V to the transmitter and initially set the biasing current initially far above threshold such that no clipping occurred. The current was slowly reduced until the second order harmonic dramatically shot up indicating the clipping of the signal. This occurred at a current of 34.6 mA. Since the threshold of the laser was 18.5 mA, the effective peak modulating current was determined to be 16.1 mA. Therefore, a ratio of the input voltage to effective peak modulating current could be established as

$$R = \frac{16.1\text{ mA}}{1.08\text{ V}} = 0.015\frac{\text{A}}{\text{V}} \tag{B.3.3}$$

Using this relation and Eqn. (B.3.2), the effective peak modulating currents for the different sinusoid voltages and chirp efficiencies were determined and listed in Table B.3.1.

Bias Current (mA)	Sinusoid Voltage (mV)	Effective Modulating ΔI (mA)	γ (MHz/mA)
60	102	1.53	250
50	98	1.47	261
30	92	1.38	278

Table B.3.1: Measurement results.

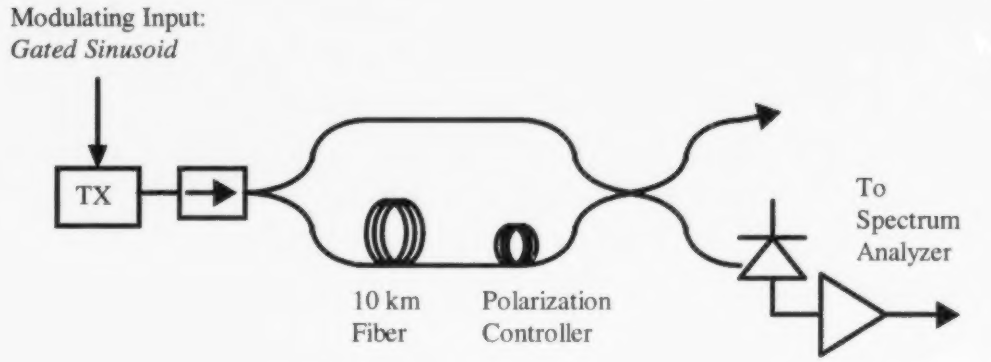
Modulating Input:
Gated Sinusoid
TX
To
Spectrum
Analyzer
10 km
Fiber
Polarization
Controller

Figure. B.3.1: Gated delayed self-homodyne chirp measurement setup.

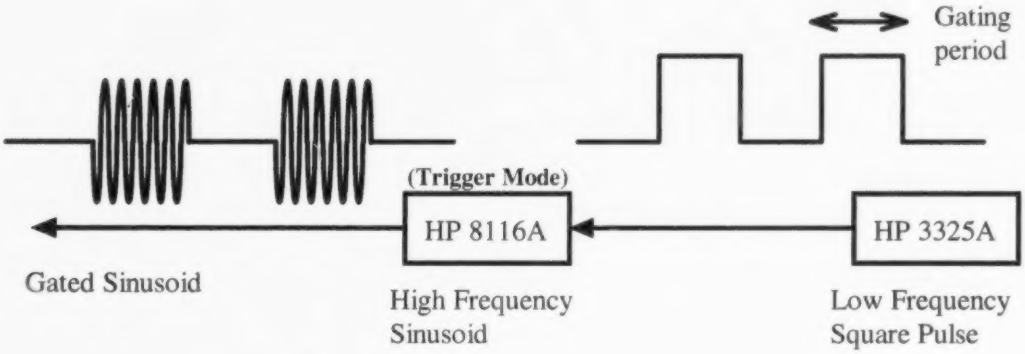
Gating
period
(Trigger Mode)
HP 8116A
HP 3325A
Gated Sinusoid
High Frequency
Sinusoid
Low Frequency
Square Pulse

Figure. B.3.2: A gated sinusoid.

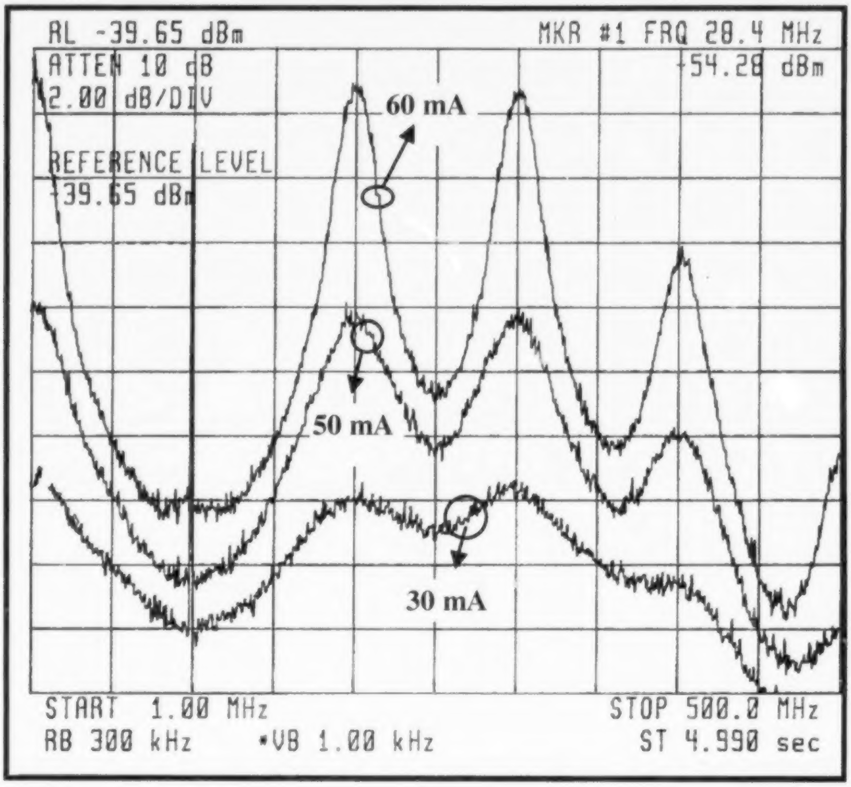

Figure B.3.3: Measured mixed spectra for various bias currents and voltages of the sinusoid. The numbers beside the curves are the bias currents.

Appendix C: Derivation of Eqn. (3.14)

Objective: To show $\overline{\sin\left(2\pi\int_{t}^{t+\tau}\gamma\cdot I_p\cdot m(\zeta)d\zeta\right)}=0$

Proof

$$\overline{\sin\left(2\pi\int_{t}^{t+\tau}\gamma\cdot I_p\cdot m(\zeta)d\zeta\right)}=\frac{1}{T}\int_{-T/2}^{T/2}\sin\left(2\pi\int_{t}^{t+\tau}\gamma\cdot I_p\cdot m(\zeta)d\zeta\right)dt$$
$$=\frac{1}{T}\int_{-T/2}^{T/2}\sin(\phi_{t+\tau}-\phi_t)dt \tag{C.1}$$

where ϕ_t is the total chirp-induced phase change at time t. This phase change will vary around zero and is generically depicted in Figure C.1. A consideration of two cases follows.

Case 1: when $\tau=0$,

$$\frac{1}{T}\int_{-T/2}^{T/2}\sin(\phi_t-\phi_t)dt=\frac{1}{T}\int_{-T/2}^{T/2}0\,dt=0 \tag{C.2}$$

Case 2: Once $\tau\neq 0$, then $\sin(\phi_{t+\tau}-\phi_t)$ varies between 1 and -1 with t. Since the average of the modulating signal is zero in CATV systems, the following relation can be yielded:

$$\frac{1}{T}\int_{-T/2}^{T/2}\sin(\phi_{t+\tau}-\phi_t)dt=0 \tag{C.3}$$

On the other hand, for $\cos(\phi_{t+\tau}-\phi_t)$, when $\tau=0$, $\cos(0)=1$ (instead of 0); therefore its average is also 1, and this average decreases as τ increases and eventually approaches zero when τ exceeds the coherence of the ϕ_t variation. Using the above equations, Eqn. (3.14) can be obtained.

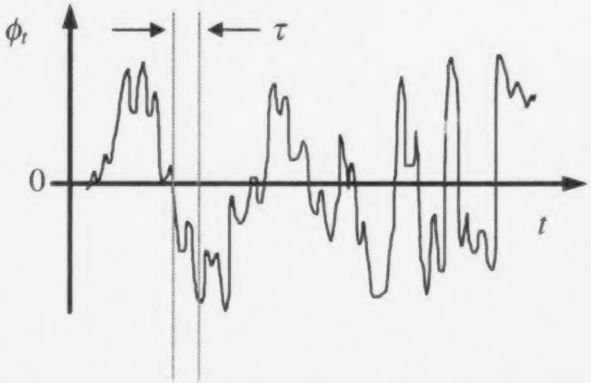

Figure C.1: Time variation of the total phase change due to chirping.

Appendix D: Determination of the Worst CNR Channel

For an external modulated system, the total DRB noise in channel i is given by Eqn. (3.40), as

$$\left\langle i_{DRB,i}{}^{2}\right\rangle = P_{re}{}^{2}\Re^{2}\frac{10}{9}R_{Rb}{}^{2}\left(2\alpha L + e^{-2\alpha L} - 1\right)\frac{2}{\pi}\left[\tan^{-1}\left(\frac{f}{\Delta\nu}\right) + \sum_{k=1}^{N_{ch}}\frac{m_k{}^{2}}{4}\tan^{-1}\left(\frac{f - f_k}{\Delta\nu}\right)\right]_{f_i}^{f_i + 4\text{MHz}} \tag{D.1}$$

From this equation and Figure 3.22, it is clear that noise contributions due to the up-converted spectra (i.e. the second term inside the square bracket) to each channel are the same. Therefore, in determining the most affected channel, these contributions are unimportant and can be ignored. After differentiating Eqn. (D.1) and equating to zero, we obtain

$$0 = \frac{\partial\left\langle i_{DRB,i}{}^{2}\right\rangle}{\partial\Delta\nu} = \frac{\partial}{\partial\Delta\nu}\left\{\left[\tan^{-1}\left(\frac{f_i + 4\text{MHz}}{\Delta\nu}\right) - \tan^{-1}\left(\frac{f_i}{\Delta\nu}\right)\right]\right\}$$

$$0 = \frac{\Delta v}{\Delta v^{2} + \left(f_i + 4\text{MHz}\right)^{2}}\frac{-\left(f_i + 4\text{MHz}\right)}{\Delta v^{2}} + \frac{\Delta v}{\Delta v^{2} + f_i{}^{2}}\frac{f_i}{\Delta v^{2}}$$

$$0 = \left(\left(f_i + 4\text{MHz}\right)f_i - \Delta v^{2}\right) \tag{D.2}$$

Therefore,

$$\Delta v = \sqrt{\left(f_i + 4\text{MHz}\right)f_i} \tag{D.3}$$

Since the sign of the derivative in Eqn. (D.2) changes from positive to negative when Δv increases slightly through $\Delta v = \sqrt{(f_i + 4\text{MHz})f_i}$, $\Delta v = \sqrt{(f_i + 4\text{MHz})f_i}$ will yield a maximum value of the DRB noise given by Eqn. (D.1) or (3.40).

Due to the fact that $f_i + 4\text{MHz}$ and f_i are approximately equal in regards to the CATV frequency allocation,

$$\Delta v = \sqrt{(f_i + 4\text{MHz})f_i} \approx f_i \tag{D.4}$$

is obtained. Thus, the worst affected channel is the one whose has a frequency nearest to the linewidth of the source.

Appendix E: Accounting for the Signal Dependence

The total average DRB noise is given by Eqn. (4.7), and is expressed as

$$\left\langle i_{DRB}{}^2 \right\rangle = \frac{10}{9} R_{Rb}{}^2 P_{re}{}^2 \Re^2 G^2 \sum_{i=1}^{N} i \left(G\,IL \right)^{2(N-i)} \tag{E.1}$$

This equation reveals that the average DRB noise is proportional to the square of the average received direct signal power P_{re}. The square dependence can be explained as follows. The DRB noise is a result of the beating between direct signal field and DRB signal field, which is indeed a distributed sum of the time-delayed versions of a direct signal field, as depicted in Figure E.1. Each of these time-delayed versions is also in proportion to the direct signal field.

For digital systems, it is the DRB noise during spaces and marks which is important. In receiving a space, the DRB signal power is proportional to the average direct signal power P_{re} because of the averaging effect due to the distributed summation, as shown in Figure E.1. Note, however, that the direct signal power is equal to P_0 (power during a space) instead of P_{re}. In receiving a mark, the DRB signal power is still proportional to the average direct signal power P_{re} for the same reason, but the direct signal power is equal to P_1 (power during a mark) in this case. Therefore, intuitively, we can replace $P_{re}{}^2$ in the average DRB noise equation with $P_{re} \cdot P_0$ and $P_{re} \cdot P_1$ respectively for cases of receiving spaces and marks to derive the DRB noises during spaces and marks. The following equation is obtained as a result:

$$\left\langle i_{DRB,i}{}^2 \right\rangle = \frac{10}{9} R_{Rb}{}^2 P_{re} P_i \Re^2 G^2 \sum_{i=1}^{N} i \left(G\,IL \right)^{2(N-i)} \tag{E.1}$$

where P_i is either P_0 or P_1.

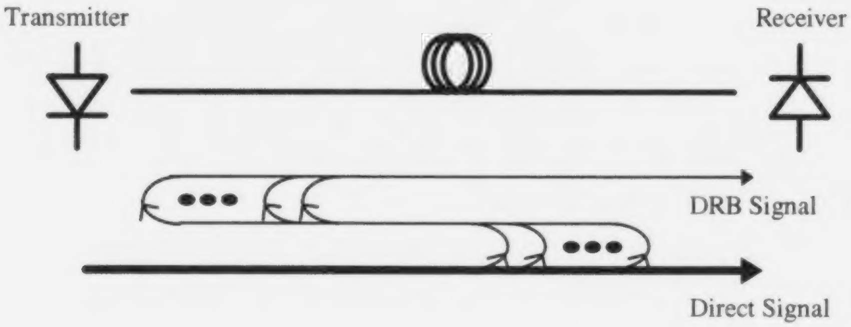
Transmitter
Receiver
DRB Signal
Direct Signal

Figure E.1: Formation of a DRB signal.

Appendix F: Derivation of the Power Penalty

***For the case without RB*:**

During a space, from Eqn. (4.24), and (4.19), we obtain

$$Q = \frac{D - P_0 \Re}{\sigma_0} = \frac{D - P_0 \Re}{\sqrt{2P_0 P_{ASE,dir} \frac{B_{re}}{B_o} \Re^2 + P_{ASE,dir}{}^2 \frac{B_{re}}{B_o} \Re^2 + \left\langle i_{th}{}^2 \right\rangle}} \tag{F.1}$$

Making D as a subject yields

$$D = Q\sqrt{2P_0 P_{ASE,dir} \frac{B_{re}}{B_o} \Re^2 + P_{ASE,dir}{}^2 \frac{B_{re}}{B_o} \Re^2 + \left\langle i_{th}{}^2 \right\rangle} + P_0 \Re \tag{F.2}$$

Similarly, during a mark, we have

$$Q = \frac{P_1 \Re - D}{\sigma_1} = \frac{P_1 \Re - D}{\sqrt{2P_1 P_{ASE,dir} \frac{B_{re}}{B_o} \Re^2 + P_{ASE,dir}{}^2 \frac{B_{re}}{B_o} \Re^2 + \left\langle i_{th}{}^2 \right\rangle}} \tag{F.3}$$

Substituting Eqn. (F.2) into Eqn. (F.3) and then rearranging the equation yields

$$P_{ASE,dir} = \frac{P_1 - P_0}{2Q^2 \frac{B_{re}}{B_o} + 2Q\sqrt{\frac{B_{re}}{B_o} + 2\frac{B_{re}}{B_o}\frac{P_0}{P_{ASE,dir}} + \frac{\left\langle i_{th}{}^2 \right\rangle}{\Re^2 P_{ASE,dir}{}^2}}} \tag{F.4}$$

***For the case with RB*:**

By increasing the received power by δP to keep the Q factor the same, we can express Eqn. (F.2) and (F.3) respectively as

$$D_{RB} = Q\sqrt{\begin{array}{l}2P_0\delta P\left(P_{ASE,dir} + P_{ASE,RB}\right)\dfrac{B_{re}}{B_o}\Re^2 + \\ \left(P_{ASE,dir} + P_{ASE,RB}\right)^2 \dfrac{B_{re}}{B_o}\Re^2 + \left\langle i_{DRB,0}{}^2\right\rangle + \left\langle i_{th}{}^2\right\rangle\end{array}} + P_0\delta P\Re \tag{F.5}$$

and

$$Q = \frac{P_1\delta P\Re - D_{RB}}{\sqrt{\begin{array}{l}2P_1\delta P\left(P_{ASE,dir} + P_{ASE,RB}\right)\dfrac{B_{re}}{B_o}\Re^2 + \\ \left(P_{ASE,dir} + P_{ASE,RB}\right)^2 \dfrac{B_{re}}{B_o}\Re^2 + \left\langle i_{DRB,1}{}^2\right\rangle + \left\langle i_{th}{}^2\right\rangle\end{array}}} \tag{F.6}$$

Substituting Eqn. (F.5) into (F.6) yields

$$\begin{array}{l}Q^2\left(2\dfrac{B_{re}}{B_o}\Re^2\left(P_{ASE,dir} + P_{ASE,RB}\right)\delta P\left(P_1 - P_0\right) + \left\langle i_{DRB,1}{}^2\right\rangle - \left\langle i_{DRB,0}{}^2\right\rangle\right) = \\ \Re^2\delta P^2\left(P_1 - P_0\right)^2 - 2\Re\delta P\left(P_1 - P_0\right)Q\sqrt{\begin{array}{l}2P_0\delta P\left(P_{ASE,dir} + P_{ASE,RB}\right)\dfrac{B_{re}}{B_o}\Re^2 + \\ \left(P_{ASE,dir} + P_{ASE,RB}\right)^2 \dfrac{B_{re}}{B_o}\Re^2 + \left\langle i_{DRB,0}{}^2\right\rangle + \left\langle i_{th}{}^2\right\rangle\end{array}}\end{array} \tag{F.7}$$

Arrangement of the above equation yields

$$P_{ASE,dir}+P_{ASE,RB}=\frac{\delta P(P_1-P_0)-\dfrac{Q^2\left[\langle i_{DRB,1}{}^2\rangle-\langle i_{DRB,0}{}^2\rangle\right]}{\Re^2\delta P(P_1-P_0)}}{2Q^2\dfrac{B_{re}}{B_o}+2Q\sqrt{\dfrac{B_{re}}{B_o}+2\dfrac{B_{re}}{B_o}\dfrac{P_0\delta P}{P_{ASE,dir}+P_{ASE,RB}}+\dfrac{\langle i_{DRB,0}{}^2\rangle+\langle i_{th}{}^2\rangle}{\Re^2\left(P_{ASE,dir}+P_{ASE,RB}\right)^2}}}$$

(F.8)

It becomes clear from Eqn. (F.8) that when the penalty is modest, i.e. when δP and $P_{ASE,RB}$ are small, and when $\langle i_{DRB,0}{}^2\rangle$ is relatively small compared to the other terms in the denominator in Eqn. (F.8), the denominators in Eqn. (F.4) and (F.8) are approximately equal. Therefore, dividing Eqn. (F.8) by Eqn. (F.4) yields

$$\frac{P_{ASE,dir}+P_{ASE,RB}}{P_{ASE,dir}}\le\frac{\delta P(P_1-P_0)-\dfrac{Q^2\left[\langle i_{DRB,1}{}^2\rangle-\langle i_{DRB,0}{}^2\rangle\right]}{\Re^2\delta P(P_1-P_0)}}{P_1-P_0}\qquad\text{(F.9)}$$

Note that the above inequality is due to the neglect of the dominant term δP in the denominator in Eqn. (F.8). By substituting the expressions (4.8) for the DRB noises during a space and mark into Eqn. (F.9), the following equation is obtained:

$$\frac{P_{ASE,dir}+P_{ASE,RB}}{P_{ASE,dir}}\le\frac{\delta P(P_1-P_0)-Q^2\dfrac{10}{9}R_{Rb}{}^2P_{re}G^2\displaystyle\sum_{i=1}^{N}i(G\,IL)^{2(N-1)}}{P_1-P_0}\qquad\text{(F.10)}$$

After substituting the following equations into (F.10):

$$P_1-P_0=P_1\left(1-\frac{1}{d}\right)\qquad\text{(F.11)}$$

and

$$P_{re} = \delta P \frac{P_1 + P_0}{2} = \delta P \frac{P_1\left(1 + \frac{1}{d}\right)}{2} \tag{F.12}$$

we obtain

$$\frac{P_{ASE,dir} + P_{ASE,RB}}{P_{ASE,dir}} \le \delta P - Q^2 \frac{10}{9} R_{Rb}{}^2 G^2 \sum_{i=1}^{N} i(G\,IL)^{2(N-1)} \frac{\delta P}{2} \frac{d+1}{d-1} \tag{F.13}$$

or equivalently

$$\delta P \ge \frac{P_{ASE,dir} + P_{ASE,RB}}{P_{ASE,dir}} \cdot \left(1 - Q^2 \frac{10}{9} R_{Rb}{}^2 G^2 \sum_{i=1}^{N} i(G\,IL)^{2(N-1)} \frac{1}{2} \frac{d+1}{d-1}\right)^{-1} \tag{F.14}$$

From this equation, the penalty ΔP can be expressed (in decibels) as

$$\begin{aligned} \Delta P &\ge 10\log(\delta P) \\ &\ge 10\log\left(\frac{P_{ASE,dir} + P_{ASE,RB}}{P_{ASE,dir}}\right) + 10\log\left(1 - \frac{10}{9} Q^2 R_{Rb}{}^2 G^2 \sum_{i=1}^{N} i(G\,IL)^{2(N-1)} \frac{1}{2} \frac{d+1}{d-1}\right)^{-1} \end{aligned} \tag{F.15}$$

or (from Eqn. 4.7)

$$\Delta P \ge 10\log\left(\frac{P_{ASE,dir} + P_{ASE,RB}}{P_{ASE,dir}}\right) + 10\log\left(1 - \frac{Q^2 \langle i_{DRB}{}^2 \rangle}{2 P_{re}{}^2 \Re^2} \frac{d+1}{d-1}\right)^{-1} \tag{F.16}$$